THE UNIVERSITY
of EDINBURGH

Studying the Synaptome: Insights into ketamine action

Sarah A. Lemprière

Ph.D. Thesis

University of Edinburgh

Centre for Clinical Brain Sciences

2018

Declaration

I declare that this thesis, and the work described herein, is my own unless indicated otherwise and has not been submitted for any other degree.

Sarah Lemprière

September 2018

Acknowledgements

Although it's my name on the cover, there are so many people without whom this work would not have been possible. I would first like to thank my supervisor **Prof. Seth Grant** for providing me with so many valuable opportunities, and for his advice and guidance. I would also like to thank my second supervisor **Dr. Noboru Komiyama** for his continuous support and encouragement, and my thesis committee members **Prof. Peter Kind** and **Dr. Szu-Han Wang** for ensuring I was on track.

I would like to thank **Dr. Jess Nithianantharajah, Dr. Melissa Cizeron and Dr. Fei Zhu** for laying the foundations for this project with their earlier work and for teaching and inspiring me on a personal level, something for which I am so grateful! I would also like to thank **Kathryn Elsegood** for looking after me when I first started in science and for teaching me so much. Thanks also to **Dr Elaine Marshall** and **Ann Ross** for all their help and kind advice. I would like to thank **Alisdair Tullo** for his earlier work on the synaptome mapping pipeline and **Dr. Ricky Qiu** for continuing that, developing the Ensemble analysis method, and for helping me to use it.

I would not have made it to the end of this project without the friendship of those I work alongside. I would like to thank **Jamie Rose** for the comic relief and pictures of puppies, **Cathy Mclaughlin** for being completely wonderful and always understanding, and **Dr. Aimun Jamjoom** for sharing this PhD journey with me and completing the perfect 'lunch crew'. I would like to thank **Dr. Matt Broadhead** for inspiring me early on with his enthusiasm for science, and **Nat O'Neill** for always providing interesting conversation. Thanks also to all the members of the Grant lab, past and present: **Vlad Anton, Edita Bulovaite, Dimitra Koukaroudi, Rhiannon Grant, YK Ko, Dr Max Kratsche, Dr Laura Tomas-Roca and others.**

I would like to thank all my flatmates from the last few years for being such supportive friends: **Christina Thompson-Ross, Hannah Morehead, Ellie Abraham, Maddie Guy and Kim Syme.**

I would like to thank all the members of **Crossroads Church** for being a wonderful family for me in Edinburgh, in particular **Tom & Leigh Ann Fraley and Brian, Rebecca & Reuben Clarke.**

Saving the most important until last, I would like to thank my parents, **Mark and Moira,** and my sister **Beth** for their love and support and for always being proud of me. I would also like to thank the rest of my family for being all-round wonderful: **Gill Brown, the Von Radowitz's, the Frenchies and the Welsbys.** A special thank you goes to my grandmother **Shelia Lemprière,** who inspires me every day.

Finally, I would like to dedicate this thesis to my grandparents who are no longer with us, **Matthew & Dorothy Brown** and **Peter Lemprière.**

List of figures

List of tables

List of abbreviations

2-DG	*2-deoxyglucose*
AMPAr	*α-amino-3-hydroxy-5-methyl-4-isoxzolepropionic acid receptor*
ANOVA	*Analysis of variance*
Arc (Arg3.1)	*Activity-regulated cytoskeleton-associated protein (Activity-regulated gene 3.1)*
BDNF	*Brain-derived neurotrophic factor*
BPRS	*Brief psychiatric rating scale*
CADSS	*Clinician-administered dissociative states scale*
CaMKII	*Ca^{2+}/calmodulin-dependent protein kinase II*
CMS	*Chronic mild stress*
CRE	*cAMP response element*
CREB	*cAMP response element-binding protein*
CTD	*C-terminal domain*
DAPI	*4',6-Diamidino-2-Phenylindole*
DG	*Dentate Gyrus*
DLG	*Disks large homolog*
ECS	*Electroconvulsive seizure*
eEF2	*Eukaryotic translation elongation factor 2*
eGFP	*Enhanced green fluorescent protein*
EM	*Electron microscopy*
EPSC	*Excitatory postsynaptic current*
EPSP	*Excitatory postsynaptic potential*
ERK	*Extracellular signal-regulated kinase*
FRET	*Fluorescence resonance energy transfer microscopy*
FST	*Forced swim test*
GABA	*Gamma-Aminobutyric acid*
GAD67	*Glutamic acid decarboxylase 67*
GTP	*Guanosine triphosphate*
HDRS	*Hamilton depression rating scale*
HFS	*High frequency stimulation*
HNK	*Hydroxynorketamine*
HOM	*Homozygous*
IEG	*Immediate early gene*
kDa	*Kilodalton*
LBD	*Ligand-binding domain*
LH	*Learned helplessness*

LTD	*Long-term depression*
LTP	*Long-term potentiation*
MADRS	*Montgomery-Asberg depression rating scale*
MAGUK	*Membrane-associated guanylate kinase*
MDa	*Megadalton*
MDD	*Major depressive disorder*
MEF2	*Myocyte enhancer factor 2*
mEPSC	*Miniature excitatory postsynaptic current*
mGluR	*Metabotropic glutamate receptor*
mIPSC	*Miniature inhibitory postsynaptic current*
MMSE	*Mini-mental state examination*
MPP	*Medial perforant path*
mRNA	*Messenger RNA*
mTOR	*Mammalian target of rapamycin*
NA	*Numerical aperture*
nm	*Nanometre*
NMDAR	*N-methyl-D-aspartate receptor*
NO	*Nitric oxide*
nNOS	*Neuronal nitric oxide synthase*
NSFT	*Novelty-supressed feeding test*
NTD	*N-terminal domain*
ODNs	*Oligodeoxynucleotides*
OF	*Open-field*
p4E-BP1	*Phosphorylated Eukaryotic translation initiation factor 4E binding protein 1*
pAKT	*Phosphorylated protein kinase B*
PCP	*Phencyclidine*
pERK	*Phosphorylated extracellular signal-regulated kinase*
PFC	*Pre-frontal cortex*
PKA	*Protein kinase A*
PML	*Promyelocytic leukemia*
pmTOR	*Phosphorylated mammalian target of rapamycin*
pp70S6K	*Phosphorylated p70S6 kinase*
PPI	*Prepulse inhibition*
PSD	*Post-synaptic density*
PSD93	*Post-synaptic density protein 93*
PSD95	*Post-synaptic density protein 95*
QIDS-SR	*Quick inventory of depressive symptomatology*
RasGFR1	*Ras-specific guanine nucleotide-releasing factor 1*
SC	*Subcutaneous*
SANS	*Scale for the assessment of negative symptoms*
SAP102	*Synapse-associated protein 102*
SARE	*Synaptic activity-response element*

SEM	*Standard error of the mean*
SNRI	*Serotonin and norepinephrine reuptake inhibitor*
SPT	*Sucrose preference test*
SRF	*Serum response factor*
SSRI	*Selective serotonin reuptake inhibitor*
SynGAP	*Synaptic ras GTPase-activating protein 1*
TMD	*Transmembrane domain*
TrkB	*Tropomyosin receptor kinase B*
TST	*Tail suspension test*
TTX	*Tetrodotoxin*
μm	*Micrometre*
VAS	*Visual analogue scale for intoxication*
VGlut1	*Vesicular glutamate reporter 1*
WT	*Wild-type*
YMRS	*Young mania rating scale*

Abstract

Major depressive disorder (MDD) is a growing health problem. Current treatment options are not always effective and take several weeks of regular administration before an improvement can be seen in symptoms. Sub-anaesthetic doses of ketamine have been found to have antidepressant effects in previously treatment-resistant MDD after just one dose. However, ketamine also produces short term psychosis-like side effects which are undesirable for MDD patients. Ketamine is known to be an NMDA receptor antagonist, binding within the channel pore to block ion flow, however the molecular mechanism(s) underlying its antidepressant and psychosis-like effects are still unclear.

In this thesis several genetically modified mouse lines were used to probe the molecular events involved in ketamine's actions. Firstly, a mouse line in which the c-terminal domain (CTD) of the NMDAR subtype GluN2B had been replaced with that of GluN2A, and a second line in which the opposite replacement had taken place, were used to investigate the role of the CTD in the NMDAR response to ketamine. It was found that the GluN2B CTD is required for the short-term psychosis-like response to a sub-anaesthetic dose of ketamine. This is interesting as the channel pore region, containing the binding site for ketamine, is unaltered in these mutants. Therefore, this finding implicates GluN2B CTD specific intracellular signalling molecules in this action of ketamine and raises the question of whether the CTD itself is able to respond to ketamine binding within the pore to induce signalling changes, perhaps via a conformational change.

Secondly, a mouse line, in which the activity-regulated synaptic protein Arc has been tagged with a fluorescent marker, was used to investigate the response of synapses to both anaesthetic and sub-anaesthetic doses of ketamine. In this experiment tagged Arc protein was visible as punctate accumulations at synapses. A novel method termed 'synaptome mapping' was used to image these accumulations across entire coronal sections and to quantify their number, size and intensity. Using this method alterations to the Arc synaptome map were detected 1h, 6h and 24h following ketamine administration. The two doses used produced different changes to this map, with the sub-anaesthetic antidepressant dose inducing increases in Arc puncta number across many brain regions, whereas the anaesthetic dose induced short term (1h) increases followed by longer term decreases in Arc puncta number. This finding links long-term increases in Arc at the synapse with an antidepressant response to ketamine.

Lay summary

Depression is an illness that affects many people across the globe. Unfortunately, the current treatments are not effective for everyone, they also take several weeks of repeat dosing before they begin to work. Ketamine has been found to have antidepressant effects in these previously treatment resistant patients and is effective after just one dose. Ketamine is an anaesthetic used for various surgical procedures, however, it is specifically low sub-anaesthetic doses which have an antidepressant effect. Ketamine has undesirable psychosis-like side effects which make it unsuitable for use in depressed patients. Therefore, it is important to understand exactly how ketamine is acting on the brain to produce these different effects, in order to design drugs which can be antidepressant without the harmful side effects. The experiments described in this thesis identified two new aspects of ketamine's action at the connections between brain cells (synapses), which may be helpful for this future drug development. The first of these is that low antidepressant doses of ketamine induce increases in the amount of a protein called Arc at synapses. However, high non-antidepressant doses induce a reduction in Arc. This suggests that Arc may contribute to the antidepressant response, and that in the long-term targeting Arc may be a way to induce an antidepressant response. Ketamine is known to bind to and block a receptor, called the NMDA receptor, which is present at synapses. However, it is unclear how ketamine binding to this receptor is able to induce an antidepressant response. The experiments described in this thesis also found that a specific part of that receptor is responsible for the psychosis-like effects of ketamine. This is the part of the receptor which is responsible for linking to signalling inside the cell. The next step for this research will be to find out if the same part of the receptor is responsible for the antidepressant effects of ketamine.

Table of Contents

Chapter 1 Introduction

1.1 The Glutamatergic synapse and the NMDA receptor

1.1.1 Synaptic transmission

The human brain contains approximately 86 billion neurons (Azevedo *et al.*, 2009) that communicate with each other via many more synaptic connections to form large, complex networks. Anatomically, the synapse consists of an axonal terminal of a pre-synaptic neuron, juxtaposed with a dendritic spine of a post-synaptic neuron. The two are separated by a gap of ~20nm (Brady *et al.*, 2005), known as the synaptic cleft. When an electrical impulse travelling along the axon reaches the pre-synaptic terminal it induces the release of neurotransmitters, which travel across the synaptic cleft and bind to receptors on the post-synaptic membrane. The binding of these neurotransmitters either increases (excitatory synapses) or decreases (inhibitory synapses) the likelihood of an action potential firing in the post-synaptic cell, depending on the identity of the neurotransmitters involved. The area of the post-synaptic plasma membrane bordering the synaptic cleft is specialised for the purpose of responding to these neurotransmitters and contains a concentration of scaffolding, signalling and receptor molecules, forming an electron dense area termed the post-synaptic density (PSD). Glutamate is the most common excitatory neurotransmitter in the nervous system. Levels of glutamate are constitutively low in the extracellular space due to the precise regulation of release and reuptake. Release of glutamate from the pre-synaptic terminal, in response to depolarisation, results in a rapid increase in glutamate concentration in the synaptic cleft (Herman & Jahr, 2007; Herman *et al.*, 2011). This glutamate binds to ionotropic glutamate receptors, such as the N-methyl-D-aspartate (NMDA) receptor and α-amino-3-hydroxy-5-methyl-4-isoxzoleproponic acid (AMPA) receptor, positioned on the post-synaptic membrane. The subsequent opening of these ion channels allows an influx of cations into the cell, resulting in the temporary depolarisation of post synaptic membrane potential. These excitatory postsynaptic potentials (EPSPs) increase the probability that the postsynaptic cell will fire an action potential.

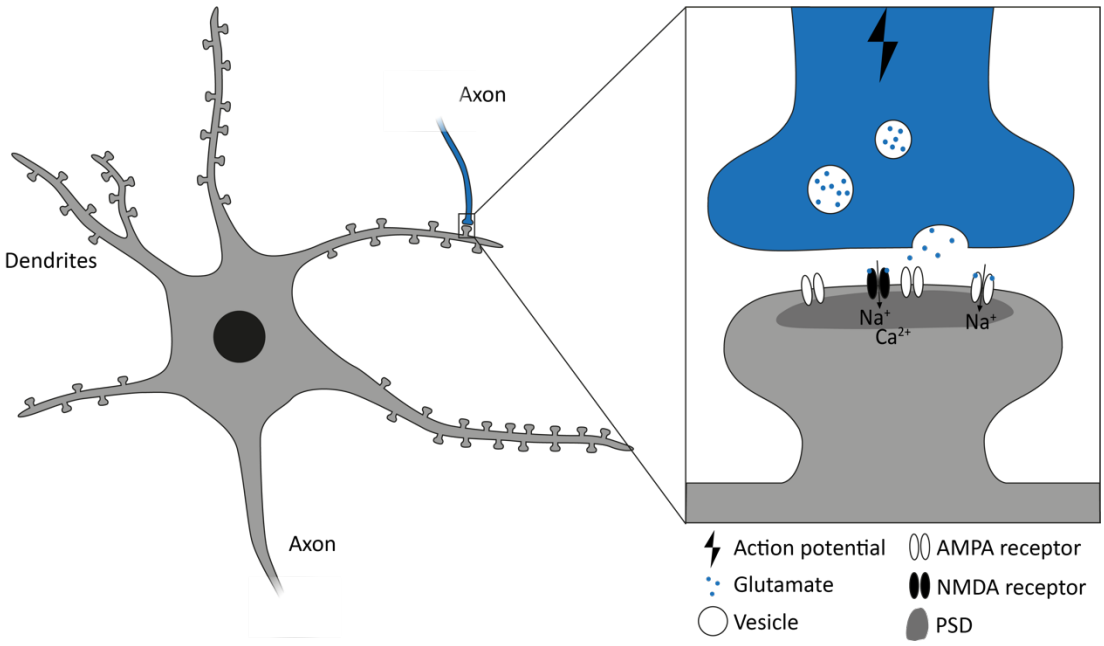

Figure 1 - The glutamatergic synapse

A synapse is the connection between neurons in which the axon terminal of a pre-synaptic neuron (blue) is proximal to the dendritic spine of a post-synaptic neuron (grey). At a glutamatergic synapse the neurotransmitter glutamate is released from the pre-synaptic terminal in response to the arrival of an action potential at the axon terminal. Glutamate then binds to AMPA and NMDA receptors present on the post-synaptic membrane to increase ion flow leading to depolarisation of the post-synaptic neuron. The post-synaptic density (dark grey) borders the synaptic cleft.

1.1.2 Synaptic plasticity

The strength of synaptic connections is highly dynamic. A short period of high frequency stimulation has been found to induce a sustained (hours to days) increase in synaptic strength (Bliss & Lomo, 1973). This is termed long-term potentiation (LTP) and is now known to result from an increase in AMPA receptor delivery to the postsynaptic membrane, alongside structural changes to the dendritic spine, which both increase the probability that the postsynaptic cell will fire an action potential in response to glutamate signalling. Conversely, it was found that a period of low frequency stimulation can induce a long-term depression (LTD) of synaptic strength. Since the identification of these forms of synaptic plasticity, a popular view has been that this relative strengthening and weakening of synaptic connections drives the modification of neuronal networks underlying learning and memory processes. The maintenance of both LTP and LTD requires synthesis of new proteins (Stanton & Sarvey, 1984; Frey *et al.*, 1988; Kauderer & Kandel, 2000), and although many candidate

effector molecules have been identified, many of the mechanisms underlying synaptic plasticity are still to be elucidated.

1.1.3 The NMDA receptor

As mentioned in **section 1.1.1**, the N-Methyl-$_D$-aspartate receptor (NMDAR) is a glutamate-gated cation channel essential for synaptic transmission at excitatory glutamatergic synapses. A unique characteristic of the NMDA receptor is the presence of a voltage-dependent Mg^{2+} block which must be removed by membrane depolarisation of sufficient amplitude and duration before channel opening can take place (Mayer *et al.*, 1984; Nowak *et al.*, 1984). This means that NMDA receptors do not contribute significantly to an EPSP evoked by a single impulse, as the amplitude and duration of depolarisation is not usually significant enough to remove the Mg^{+} block, that kind of fast synaptic transmission is mediated by AMPA receptors. Although there is at least one report of single synaptic events being sufficient to open the NMDAR (Emptage *et al.*, 1999). Multiple impulses in quick succession can increase the amplitude and duration of depolarisation and thus the likelihood of NMDAR activation. Therefore, the NMDAR has been considered a molecular 'coincidence detector', activating only if glutamate is released from a pre-synaptic terminal when there is also sufficient activation of the post-synaptic cell to remove the Mg^{+} block. NMDA receptors also require the binding of a co-agonist Glycine, along with Glutamate, for activation (Johnson & Ascher, 1987; Patneau & Mayer, 1990; Clements & Westbrook, 1991). This 'coincidence detector' characteristic of NMDAR action forms the molecular basis for the paradigm of LTP at synapses. The high Ca^{2+} permeability of NMDARs, as compared with AMPA and kainite receptors (Mayer & Westbrook, 1987), means that channel opening induces an increase in subcellular calcium levels. This activates a host of intracellular signalling cascades, one result of which is LTP-related enhancement of AMPA receptor phosphorylation and trafficking to the postsynaptic membrane. In addition to this, an NMDAR-dependent form of LTD has also been observed (Thiels *et al.*, 1996).

1.1.4 NMDA receptor structure

The NMDAR is a heteromer with subunits consisting of four domains, illustrated in **figure 2**. The n-terminal domain (NTD) contributes to the assembly of subunits and allosteric regulation through interactions with molecules such as Zn^{2+} (Paoletti *et al.*, 2000) or ifenprodil (Williams, 1993). The ligand binding domain (LBD) is proximal to the membrane and contains binding sites for either Glycine, or Glutamate depending on the subunit type (discussed in **section 1.1.5**). The transmembrane domain (TMD) forms the ion channel pore

and consists of three transmembrane helices and a re-entrant loop which lines the pore itself. This loop contains asparagine residues that are essential for Ca^{2+} selectivity and Mg^{+} block (Burnashev *et al.*, 1992). The c-terminal domain (CTD) is involved in guiding receptor trafficking and coupling receptors to specific intracellular signalling and scaffolding molecules (Ryan *et al.*, 2008; Horak & Wenthold, 2009; Frank *et al.*, 2016).

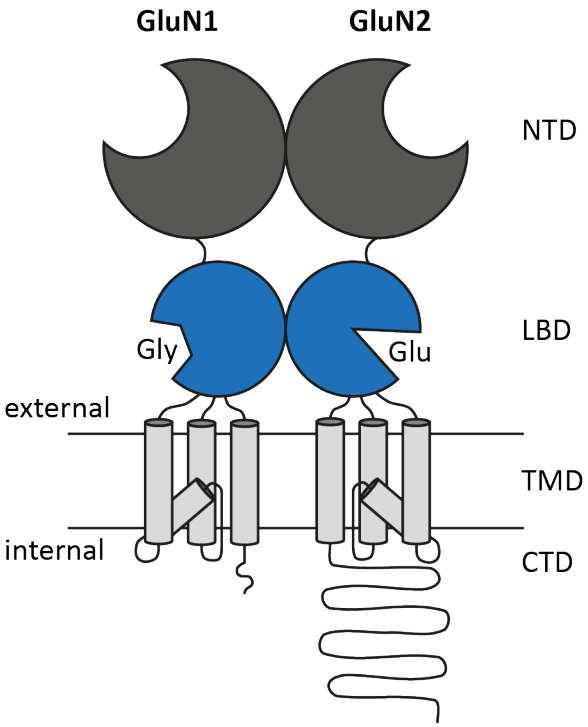

Figure 2 - Structural domains of the NMDA receptor.

NTD = N-terminal domain; LBD = Ligand-binding domain; TMD = Transmembrane domain; CTD = C-terminal domain; Gly = Glycine; Glu = Glutamate.

1.1.5 NMDA receptor subtypes

There are different subtypes of NMDA receptor subunits, which contribute different functional characteristics to the assembled receptor, these are discussed below and summarised in **table 1**. The presence of a GluN1 subunit is essential for receptor assembly and these can combine with either GluN2A-D or GluN3A-B subunits to form a heteromer. The GluN1 subunit family is encoded by a single gene, which can be alternatively spliced to create up to 8 variants (Sugihara *et al.*, 1992; Laurie & Seeburg, 1994; Zukin & Bennett, 1995). The obligatory GluN1 subunit contains the glycine binding site and is essential for receptor assembly and function (Ishii *et al.*, 1993; Scott *et al.*, 2001). There are four GluN2 subunit subtypes (A-D), which contain glutamate binding sites (Laube *et al.*, 1997; Anson *et al.*, 1998). These subtypes arise from separate genes (Monyer *et al.*, 1992) and their identity has a

critical effect on the functional properties of the receptor. Each of the four different GluN2 subtypes has a distinct regional expression pattern within the adult brain. GluN2A is ubiquitously expressed across all brain regions, whereas GluN2B expression is restricted to forebrain only. GluN2C is only found in cerebellum and olfactory bulbs. GluN2D is expressed at low levels, mainly in the diencephalon and telencephalon. (Watanabe *et al.*, 1992; Ishii *et al.*, 1993; Monyer *et al.*, 1994). The canonical NMDAR contains two GluN1 subunits and two GluN2 subunits, most commonly GluN2A or GluN2B. However, tri-heterometic receptors containing two different subtypes of GluN2 have also been identified at the synapse in vivo (Tovar *et al.*, 2013; Hansen *et al.*, 2014). In the adult brain the GluN2A and 2B subtypes are the most widely and highly expressed (Watanabe *et al.*, 1992), and have therefore been the most thoroughly studied to date. The CTD is the most divergent domain between the different GluN2 subtypes (Ryan *et al.*, 2008), enabling them to interact with discrete sets of intracellular signalling molecules. This includes the subtype-specific interactions between the GluN2B CTD and CaMKII, RasGFR1 and SynGAP (Leonard *et al.*, 1999; Strack *et al.*, 2000; Krapivinsky *et al.*, 2003; Kim *et al.*, 2005). All three of these molecules are Ca^{2+} sensitive and

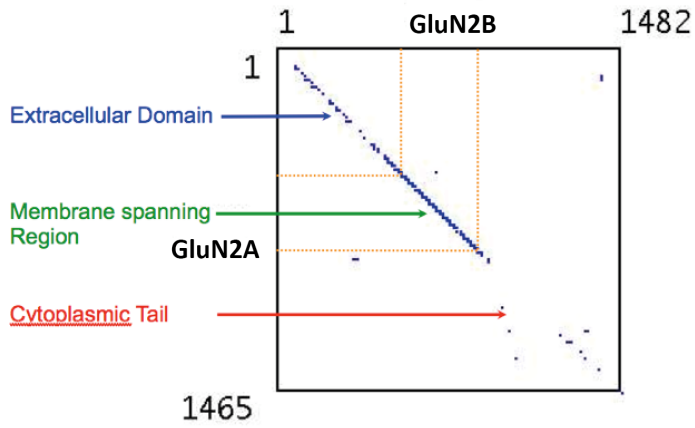

Figure 3 – Dotplot showing sequence homology between GluN2A and GluN2B subunits.

The amino acid sequences of the GluN2A subunit and the GluN2B subunit are compared along the vertical and horizontal axis, respectively. Areas of sequence similarity are denoted by dots. The same amino acid in the same position in both subunits appears as a dot along a diagonal line stretching from top left to bottom right of the dotplot. High levels of sequence homology between GluN2A and GluN2B can be observed in the extracellular domain and the membrane spanning region, in contrast there is divergence between the two subtypes in the cytoplasmic tail region. Figure courtesy of Dr Noboru Komiyama, reproduced with permission.

are involved in plasticity-related changes (Lu *et al.*, 2010; Kristensen *et al.*, 2011). This interaction between CaMKII and GluN2B CTD is essential for LTP, suggesting that proximity

to the NMDAR is important for CaMKII activation (Sanhueza *et al.*, 2011). There are also differences between the NTDs of GluN2 subtypes, allowing a degree of subtype specific allosteric modulation, which has been used experimentally. For example the ifenprodil family of molecules are selective antagonists at GluN2B-containing receptors (Williams, 1993). GluN2A subunits on the other hand, are much more sensitive to blockade of extracellular Zn^{2+} than GluN2B-containing receptors (Paoletti *et al.*, 1997). In addition to this, GluN2 subtypes have differing channel conductance properties. GluN2A and 2B display high conductance channel openings (50pS) with a high Ca^{2+} permeability and sensitivity to Mg^{+}, whereas GluN2C and 2D have a lower conductance (20/40pS), Ca^{2+} permeability and Mg^{+} sensitivity (Monyer *et al.*, 1992; Kuner & Schoepfer, 1996; Schneggenburger, 1996). Subtypes also differ in deactivation speed, with the GluN2A subtype having much faster deactivation than GluN2B, 2C and 2D (Vicini *et al.*, 1998; Wyllie *et al.*, 1998; Gray *et al.*, 2011).

	GluN2A	**GluN2B**	**GluN2C**	**GluN2D**
Expression pattern	Ubiquitous	Forebrain	Cerebellum and olfactory bulbs	Low, diencephalon and telencephalon
Conductance	high	high	low	low
Ca^{2+} permeability	high	high	low	low
CTD interactors		CaMKII, RasGFR1, SynGAP		

Table 1 - Summary of characteristics of NMDA receptor subtypes.

Given these differing properties it can be assumed that different GluN2 subtypes may be involved in different cellular functions. For example, selective blockade of GluN2B-containing receptors with ifenprodil or Ro 25-6981 has been found to abolish induction of LTD but not LTP, suggesting that LTP may be mediated specifically by GluN2A-containing receptors (Liu *et al.*, 2004; Massey *et al.*, 2004). Indeed, there is evidence that the c-terminal domain of GluN2A is required for LTP (Kohr *et al.*, 2003). However, another report found no impairment of LTP by GluN2B- or GluN2A- specific antagonists (Berberich *et al.*, 2005). In addition, GluN2B upregulation has been found to enhance LTP (Tang *et al.*, 1999), and intact LTP has been observed in GluN2A knockout mice, although this could be a compensatory action (Kiyama *et al.*, 1998; Weitlauf *et al.*, 2005). The potential GluN2 subtype-specificity of LTP therefore remains an area of debate, with some concerns about the validity of the pharmacological tools being used to selectively block subtypes (Neyton & Paoletti, 2006).

A popular view has been that GluN2A-containing receptors are localised at synapses, whereas GuN2B-containing receptors are more likely to be found at extra-synaptic sites. This is based on experiments in cultured neurons, in which EPSCs were taken as a measure of synaptic receptor activity, and whole cell currents used to measure activity of extrasynaptic receptors. It was found that block of EPSCs by the GluN2B-specific antagonist ifenprodil was less than the block of whole cell currents. This suggests that the extrasynaptic receptor population is enriched with GluN2B-containing receptors (Tovar & Westbrook, 1999; Martel *et al.*, 2009). Similar findings have been reported in rat cortical slices (Stocca & Vicini, 1998). However, the idea of GluN2B receptors being restricted to extrasynaptic sites is an oversimplification, as there is significant evidence to suggest a functional population of GluN2B receptors at the synapse (Thomas *et al.*, 2006; Harris & Pettit, 2007; Gray *et al.*, 2011; Rauner & Kohr, 2011). For example, when defining synaptic and extrasynaptic NMDAR populations as those that do, or do not, respond to low frequency (0.1Hz) synaptic events respectively, no enrichment of GluN2B receptors in the extracellular compartment was observed (Chen & Diamond, 2002; Clark & Cull-Candy, 2002; Harris & Pettit, 2007). In addition to this, ESPCs are intact in neurons expressing only GluN1/GluN2B-containing receptors (Thomas *et al.*, 2006). There is also a third family of GluN3 NMDA receptor subunits, which consists of the GluN3A & 3B subtypes (Ciabarra *et al.*, 1995; Chatterton *et al.*, 2002). Although these are much rarer than GluN1 & 2, there is a growing body of work investigating their influence on synaptic maturation and pruning (Perez-Otano *et al.*, 2016).

1.1.6 Putative metabotropic action of the NMDAR

The importance of the CTD in NMDA receptor function is highlighted by the finding that animals with a truncation of the GluN2A, 2B or 2C CTD have an identical phenotype to animals with complete deletion of the corresponding subunit, despite the ability to form synaptically activated NMDAR channels being preserved (Sprengel *et al.*, 1998). It is clear that the CTD provides specific binding sites for signalling molecules responding to the influx of Ca^{2+} following channel opening, however, there is also some evidence to suggest that the CTD itself may respond to agonist binding by changing conformation. This would suggest the NMDAR has the potential for metabotropic function. Evidence for this comes from the observation that LTD is still inducible by low-frequency stimulation (LFS) during blockade of the NMDAR ion channel by MK-801. Whereas preventing binding of Glutamate with D-APV prevented induction of LTD (Nabavi *et al.*, 2013). Ion flux-independent NMDAR-dependent LTD has also been described elsewhere (Stein *et al.*, 2015; Carter & Jahr, 2016). In addition

to this, alterations in FRET efficiency between the CTDs of two GluN1 subunits, indicates that in the absence of ion flux there is conformational change of the CTD in response to agonist binding (Dore *et al.*, 2015; Ferreira *et al.*, 2017).

1.1.7 The post-synaptic density and NMDA receptor supercomplexes

It is important to remember that the NMDA receptor is not acting alone at the post-synaptic membrane but that it is interacting with many intracellular signalling and scaffolding molecules within the post-synaptic density (PSD) (Husi *et al.*, 2000; Husi & Grant, 2001). The PSD appears as an electron dense region of plasma membrane situated at the post-synaptic side of the synaptic cleft (Gray, 1959). It is thought to facilitate postsynaptic signalling by regulating receptor localisation such that specific receptors and intracellular interactors are present at the plasma membrane and aligned with the presynaptic active zone, from which neurotransmitters are released (Tang *et al.*, 2016). Mutations in PSD proteins cause over 100 brain diseases (Bayes *et al.*, 2011), highlighting the importance of this structure for normal brain function. Although postsynaptic specialisations are present at both excitatory and inhibitory synapses, the PSD of excitatory synapses is particularly complex. Mass spectrometry of purified PSD preparations has identified between ~400 and ~2000 different proteins present in this structure (Peng *et al.*, 2004; Yoshimura *et al.*, 2004; Collins *et al.*, 2006; Trinidad *et al.*, 2008; Bayes *et al.*, 2011). These include a diverse range of different molecules including scaffolding proteins, receptors and channels, cytoskeletal elements, cell adhesion molecules and intracellular signalling enzymes (Peng *et al.*, 2004). The most abundant of these are CaMKIIa and CaMKIIB, followed by members of the PSD-95 MAGUK family of scaffold molecules and SynGAP, which binds to PSD95. There is also a significant population of glutamate receptors present, with NMDA receptors being more abundant than AMPA receptors (Cheng *et al.*, 2006). It is now known that there are many different subtypes of synapse, containing different combinations of these PSD proteins. Given the sheer number of proteins present at the PSD this raises the potential for a huge number of different synapse types with varying signalling properties. Recent work has confirmed this with large-scale mapping of the scaffold proteins PSD95 and SAP102, identifying a huge diversity in synapse subtypes across previously defined brain regions. In addition to this, new levels of organisation at the level of synapse type were identified within brain regions previously thought to be homogenous (Zhu *et al.*, 2018).

The NMDA receptor is a key structural and functional component of the PSD. The large number of other PSD proteins interacting with the NMDA receptor first became apparent in

the early 2000s (Husi *et al.*, 2000; Husi & Grant, 2001). NMDA receptor activation also changes the phosphorylation status of 127 proteins and 189 phosphopeptides (Coba *et al.*, 2009). Further work has now demonstrated that NMDA receptors are present at the synapse as part of complexes of either ~840kDa or ~1.5MDa. PSD95 and Arc are present in these ~1.5MDa complexes, which also contain other scaffold proteins, ion channels, trans-synaptic adhesion molecules and signalling proteins (Frank *et al.*, 2016). The assembly of these NMDA receptor supercomplexes requires the presence of an intact GluN2B CTD in addition to both PSD95 and PSD93 (Frank *et al.*, 2016). This is strong evidence that proteins at the PSD are assembled into discrete super molecular complexes, rather than one large complex or a more diffuse distributed network. Indeed, as part of the same study 60 different proteins were probed in mouse forebrain synaptoneurosomes and found to be assembled into complexes and supercomplexes of varying sizes, just 13 were also detected in their monomeric form (Frank *et al.*, 2016). Further to this, super resolution imaging methods have enabled the visualisation of discrete 'nanoclusters' of PSD95 molecules assembled within the dendritic spine (Broadhead *et al.*, 2016). A contradictory view had been suggested by previous electron microscopy (EM) work which identified vertical filaments, thought to be PSD95 family molecules, evenly spaced throughout the PSD (Chen *et al.*, 2008). However, in that EM study PSD95 family molecules were identified by their general shape rather than specific labelling.

1.1.8 PSD95 & PSD93

As mentioned, PSD95 and PSD93 are both essential components of the NMDA receptor ~1.5MDa complex, present at the PSD. They are both members of the MAGUK family of scaffold proteins and interact with numerous synaptic proteins including other MAGUK proteins, NMDA receptor subunits, potassium channels and cytoskeletal proteins (Fernandez *et al.*, 2009; Guo *et al.*, 2012). The presence of PSD95 is essential for normal synaptic plasticity and learning and memory function, as PSD95 mutant mice exhibit enhanced LTP and disruption of LTD (Migaud *et al.*, 1998; Carlisle *et al.*, 2008) as well as deficits in spatial learning (Migaud *et al.*, 1998). Interestingly, in these animals NMDA receptors are still localised to the synapse, suggesting that PSD95 is important for the coupling of the NMDA receptor to pathways that control synaptic plasticity, rather than receptor localisation. Mutations in the genes for PSD95 (*DLG4)* and PSD93 *(DLG2)* have been associated with an increased risk of schizophrenia and autism spectrum disorder (Cheng *et al.*, 2006; Walsh *et al.*, 2008; Xing *et al.*, 2016). Interestingly, although there is a large degree of homology between PSD95 and PSD93, they have distinct roles in cognitive processes. PSD95 is essential

even for simple forms of learning, whereas PSD93 is required for more complex cognitive processes (Nithianantharajah *et al.*, 2013).

1.1.9 Summary

The NMDA receptor acts as a 'coincidence detector' at glutamatergic synapses, allowing influx of Ca^{2+} in response to release of glutamate from the pre-synaptic terminal and sufficient depolarisation of the post-synaptic membrane. The post-synaptic density is a highly complex molecular machine composed of complexes and supercomplexes of many different proteins, with many different combinations of these possible. The NMDA receptor is a key element of this machine, assembling large supermolecular complexes via the c-terminal domain of the GluN2B subunit. These complexes contain many signalling molecules that are able to respond to the influx of Ca^{2+} resulting from glutamatergic signalling at the synapse.

1.2 Activity-Regulated Cytoskeleton-Associated Protein (ARC/ARG3.1)

Activity-Regulated Cytoskeleton-Associated protein (Arc), also known as Arg3.1, (hereafter referred to as Arc) is a particularly interesting member of the 1.5MDa complexes described in **section 1.1.8** as it is the product of an immediate early gene, and as such is highly activity-regulated. The *Arc* gene is located on chromosome 8 in the human, chromosome 15 in the mouse, and is conserved across vertebrate species (Lyford *et al.*, 1995). Arc is expressed predominantly in the brain (Link *et al.*, 1995) and is most commonly observed in CaMKII-positive principal neurons (Vazdarjanova *et al.*, 2006), however Arc protein has also been detected in glial cells in the hippocampus (Rodriguez *et al.*, 2008). Its most abundant interacting protein is PSD95 (Frank *et al.*, 2016) and the presence of PSD95 seems to be essential for the synaptic targeting of Arc protein (Fernandez *et.al.*, 2017). There is evidence that Arc mRNA and protein can be specifically targeted to recently-activated synapses (Steward *et al.*, 1998). This provides a method by which composition of the PSD can be specifically altered in response to highly localised changes in activity. At the synapse Arc is thought to alter AMPA receptor endocytosis and F-actin stabilisation, both processes which are involved in synaptic plasticity.

1.2.1 Arc transcription and mRNA transport

First described in 1995 by two independent research groups, *Arc* expression was found to be dramatically increased in brain following electroconvulsive seizure. This activity-induced upregulation was rapid and transient, observed from 30 min to 8 hr post-seizure, and was found to be protein synthesis independent (Link *et al.*, 1995; Lyford *et al.*, 1995; Larsen *et al.*, 2005). These characteristics place Arc as a member of the immediate early gene (IEG) family.

This is a group of genes, including *c-fos* and *zif268*, which are activated rapidly and transiently as a 'first response' to many different cellular stimuli (Sheng & Greenberg, 1990). Although, in contrast to most IEG products *Arc* is not a transcription factor and can be classed as an 'effector' IEG, as its product acts directly to induce a cellular response, see **section 1.2.3** for more information on Arc function. Since those initial seizure experiments carried out in 1995, *Arc* expression has been induced experimentally by a wide variety of stimuli which involve an increase in synaptic activity. These include application of bicuculline or removal of TTX *in vitro* (Shepherd et al., 2006), high frequency stimulation (HFS) of the perforant path input into the hippocampus (Link *et al.*, 1995), microinfusion of BDNF (Ying *et al.*, 2002) and novel environment exploration *in vivo* (Chawla et al., 2005). The complex sequence of events linking synaptic activity to *Arc* expression is still under investigation. However, Arc transcription is induced by activation of NMDARs (Link *et al.*, 1995; Bloomer *et al.*, 2008), mGluRs (Waung *et al.*, 2008), and TrkB receptors (Yasuda *et al.*, 2007). Interestingly, inhibition of AMPARs is also able to increase the degree of Arc expression induced by BDNF (Rao *et al.*, 2006). Downstream of these receptors, activation of the extracellular signal-regulated kinase (ERK) pathway is required for *Arc* transcription (Bluthgen *et al.*, 2017), and this appears to be a key pathway linking synaptic activity with the activation of transcription factors such as CREB and SRF. Several promoter regions, containing response elements for activity-induced transcription factors, have been identified upstream of the Arc open reading frame (ORF). These include a synaptic activity response element (SARE), located ~7kb upstream of *Arc,* which contains binding sites for the transcription factors serum response factor (SRF), myocyte enhancer factor 2 (MEF2) and Ca^{2+}/cAMP-response element binding protein (CREB) (Kawashima *et al.*, 2009; Pintchovski *et al.*, 2009). The presence of this SARE is both necessary and sufficient for synaptic activity-induced transcription of the Arc gene (Kawashima *et al.*, 2009). Activation of CREB, MEF2 and SRF is downstream of Ca^{2+} influx, via ERK signalling in the case of SRF (Esnault *et al.*, 2017), and they have been previously identified as neuronal activity sensors (Robertson *et al.*, 1995; Bito *et al.*, 1996; Flavell & Greenberg, 2008). There is also a "Zeste-like" element at ~1.4kb upstream of the *Arc* transcription initiation site, which mediates activity-induced transcription in a PKA- and ERK-dependent manner (Pintchovski *et al.*, 2009). There are an additional two serum response elements (SREs) at ~1.5kb and ~0.9kb upstream, respectively. These elements were, in fact, the first to be identified, however they were not found to be essential for induction of Arc

transcription by calcium and cAMP (Waltereit *et al.*, 2001). See **figure 4A** for a summary of these promoter regions.

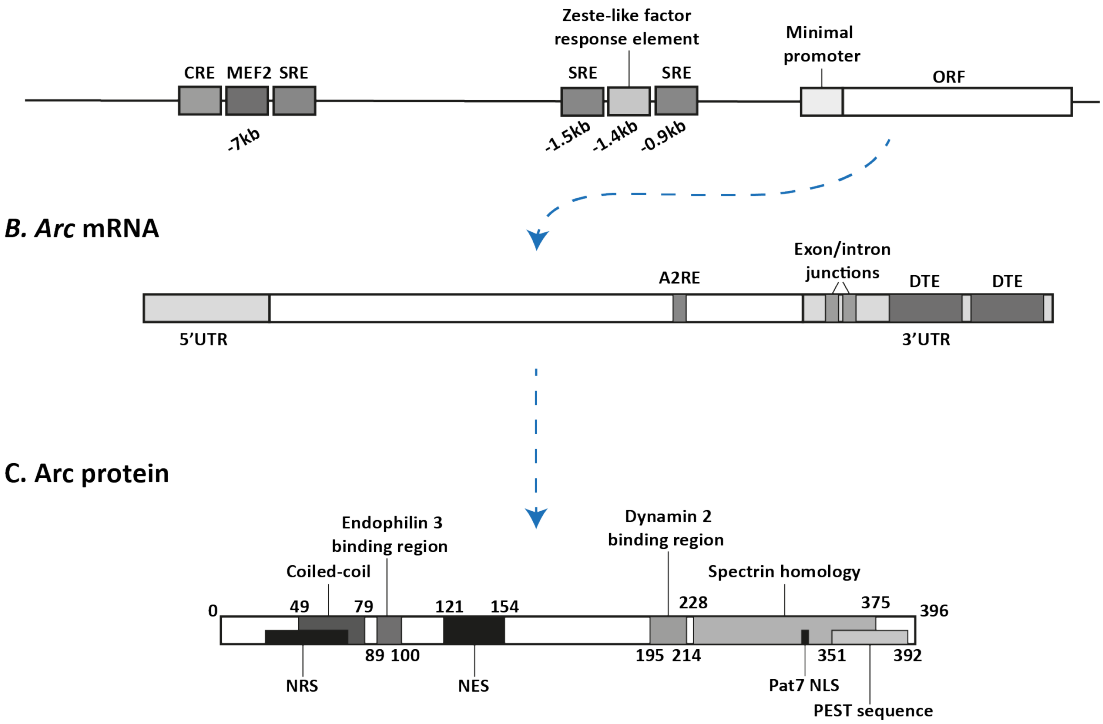

Figure 4 - Schematic diagrams of the Arc gene, mRNA and protein domains of interest.

A. *Arc gene showing regulatory elements upstream of the Arc open reading frame (ORF). CRE = cAMP response element; MEF2 = ; A2RE = A2 response element (Gao et al., 2008); DTE = dendritic targeting element;* ***B.*** *Arc mRNA showing identified functional regions. DTE = Dendritic targeting element;* ***C.*** *Arc protein showing key regions. Arc protein is 396aa in size. NRS = nuclear retention sequence; NES = nuclear export sequence; NLS = nuclear localisation sequence.* ***Adapted from (Bramham et al., 2010).***

Transcription of the *Arc* gene results in the production of mRNA which is transported out of the nucleus and targeted to the dendrites (Link *et al.*, 1995; Lyford *et al.*, 1995; Steward *et al.*, 1998; Wallace *et al.*, 1998), this dendritic transport makes Arc unusual amongst IEGs. Two dendritic targeting elements (DTEs) have been identified within the *Arc* 3' UTR, which are required for this process (Kobayashi *et al.*, 2005). Within the Arc coding region an A2 response element has been identified. This element is the binding site for heterogeneous nuclear ribonucleoprotein (hnRNP), and this binding appears to be required for Arc mRNA transport to dendrites (Gao *et al.*, 2008). See **figure 4B**. What is particularly interesting about Arc is that this transport appears to be not only induced, but specifically guided by recent synaptic activity. This is demonstrated by selective stimulation of the inputs to specific layers

of the dentate gyrus (DG), which is able to induce accumulation of newly synthesised Arc mRNA specifically within the stimulated portion of the dendritic tree (Steward *et al.*, 1998; Shannon *et al.*, 2014). This seems to take place alongside targeted degradation of Arc mRNA in inactive dendritic regions (Farris & Steward, 2010). There is evidence from electron microscopy that this new Arc mRNA is targeted to dendritic spines within the activated layer (Rodriguez *et al.*, 2005). This Arc induction is protein synthesis independent and rapid, with upregulation in the dendrites detected after 1h of stimulation. Interestingly, only high frequency LTP-inducing trains of stimulation are able to induce upregulation of Arc mRNA (Lyford *et al.*, 1995; Steward *et al.*, 1998). This redistribution is dependent upon NMDA receptor activity (Steward & Worley, 2001). Arc mRNA is a target of nonsense-mediated decay (NMD), which limits the number of times a single mRNA can be translated. This process results in a half-life of Arc mRNA in culture of just 47 min (Rao *et al.*, 2006; Giorgi *et al.*, 2007), which enables tight control of Arc protein levels in response to activity. Two introns present in the 3'UTR of the Arc gene make it a target for this kind of regulation (Giorgi *et al.*, 2007).

1.2.1 Arc translation and protein transport

Following transcription, the translation of Arc mRNA is also controlled in an activity-dependent manner. There is evidence that, following HFS, Arc translation can be induced by ERK activation via formation of the eIF4F translation-initiation complex (Panja *et al.*, 2009). mGluR activation is able to induce rapid local translation of pre-existing Arc mRNA in dendrites, which appears to be via phosphorylation of eEF2 (Park *et al.*, 2008; Waung *et al.*, 2008; Bramham *et al.*, 2010). Following targeted stimulation of specific layers of dentate gyrus Arc protein follows the same distribution pattern as mRNA, also showing targeting to activated layers following 2h of stimulation (Steward *et al.*, 1998; Farris & Steward, 2010). Local translation of Arc in dendrites within 15s of glutamate stimulation has since been observed in real time (Na *et al.*, 2016). At the synapse Arc interacts with PSD95 (Fernandez *et al.*, 2009) to form part of the ~1.5MDa NMDAR super complexes previously described (Frank *et al.*, 2016). The interaction of Arc with PSD95 seems to be essential for Arc's presence at the synapse (Fernandez *et al.*, 2017). Although Arc protein is considered to be present predominantly at the post synaptic side of the synapse, there are reports from electron microscopy of Arc labelling in axon terminals (Rodriguez *et al.*, 2005). Although Arc is an 'effector' IEG rather than a transcription factor, localisation of Arc protein to the nucleus has also been observed in vivo and in vitro (Irie *et al.*, 2000; Bloomer *et al.*, 2007; Korb *et al.*, 2013). It seems that Arc localisation to the nucleus can be induced by activity, such as that

induced in the hippocampus by novel environment exploration. A Pat7 nuclear localisation signal (NLS) was identified at amino acids 331-335 of the Arc protein, which appears to be responsible for the active targeting of Arc to the nucleus. A region towards the n terminus, between amino acids 29 and 68, was also identified as a nuclear retention signal (NRS), keeping Arc in the nucleus. In the absence of this NLS a nuclear export signal (NES), identified between amino acids 121 and 154, appears to induce export out of the nucleus into the cytoplasm (Korb *et al.*, 2013). These regions are illustrated in **figure 4C**. Recently, a study, in which purified Arc preparations were analysed with EM, found evidence that Arc protein forms oligomeric structures similar to virus-like capsids (Pastuzyn *et al.*, 2018). Although it is not known whether this takes place in neurons. Further to this, recent evidence also suggests that Arc protein and mRNA can be released by neurons in extracellular vesicles in response to activity and can then be taken up by other neighbouring cells (Pastuzyn *et al.*, 2018).

1.2.2 Arc function

This precise activity-regulated control of Arc levels, coupled with its targeting to recently-activated synapses, suggests a potential role in the process of synaptic plasticity thought to underlie memory formation. Accordingly, knockout of Arc has been reported to result in the inability to form long term memory in fear conditioning, conditioned taste aversion and long-term object-recognition tasks (Plath *et al.*, 2006; Ploski *et al.*, 2008). Interestingly Arc knockout did not seem to affect task acquisition or short term memory (Plath *et al.*, 2006). Infusion of Arc antisense oligodeoxynucleotides (ODNs) into the hippocampus prior to, or immediately after, training in a Morris water maze task can inhibit recall 2 days later. However, infusion at 8h post-training did not affect recall, suggesting a critical period during which Arc is required for memory consolidation (Guzowski *et al.*, 2000). This does not seem to be specific to the hippocampus as infusion of Arc antisense ODNs into the lateral amygdala prior to fear conditioning training can impair recall at 24h (Ploski *et al.*, 2008). Knockout or knockdown of Arc has also been found to impair synaptic plasticity responses. Arc knockout mice display an enhanced early phase but an impaired late phase of LTP in the Dentate Gyrus. These mice also had an impaired maintenance of LTD (Plath *et al.*, 2006). These effects were not specific to the hippocampus, as cerebellar Purkinje cell cultures from Arc knockout animals also display a block of late phase LTD (Smith-Hicks *et al.*, 2010). Block of Arc expression specifically in the hippocampus with the use of *Arc* antisense ODNs produced similar results, LTP maintenance was blocked without affecting induction (Guzowski *et al.*, 2000). Interestingly, infusion of Arc antisense ODNs 2h but not 4h after HFS was able to

reverse ongoing LTP, suggesting a critical window of Arc involvement in LTP consolidation. Arc AS treatment in the absence of HFS had no effect on basal synaptic transmission (Messaoudi *et al.*, 2007). The exact way in which Arc is involved in these two opposing forms of synaptic potentiation is unclear. The highly-regulated, rapid targeting of Arc protein to recently-activated synapses indicates that it could be acting as a short-term tag, marking synapses for modification by other effector molecules (Frey & Morris, 1997; Okuno *et al.*, 2012). Arc does interact with the Actin cytoskeleton, this was reported as early as 1995 when it was found that Arc co-sediments with F-Actin (Lyford *et al.*, 1995). Consolidation of LTP is thought to involve expansion of the PSD and dendritic spine, mediated at least in part by Actin polymerisation (Fukazawa *et al.*, 2003; Matsuzaki *et al.*, 2004). Infusion of Arc AS ODNs 2 h post-HFS of the MPP prevented the increase in phallodin staining in the DG usually associated with LTP-induced increase in F-actin stabilisation at spines. Application of an F-actin stabiliser prevented Arc AS ODNs from inhibiting LTP maintenance, suggesting that Arc may be acting via F-actin to promote LTP consolidation (Messaoudi *et al.*, 2007).

There is also considerable evidence that Arc is able to modulate surface AMPA receptor levels to alter synaptic strength. Arc expression reduces surface levels of GluR1, which is dependent upon Arc binding to the endocytic proteins Dynamin and Endophilin (Chowdhury *et al.*, 2006; Rial Verde *et al.*, 2006). Binding domains for endophilin 3 and dynamin 2 have been identified in the Arc protein sequence, see **figure 4C** (Chowdhury *et al.*, 2006). Arc knockout animals display a ~2-fold increase in surface GluR1 and rate of endocytosis is also lower than that of wild-type, despite such large surface numbers. This can be rescued by transfection of Arc (Chowdhury *et al.*, 2006). Knockdown of Arc expression in cultured hippocampal neurons also produced a slight increase in surface GluR1 levels, which was accompanied by increased mEPSC amplitude (Waung *et al.*, 2008). This suggests that increases in Arc protein can reduce synaptic strength by increasing AMPA receptor endocytosis. In these experiments total GluR1 levels were also decreased, suggesting Arc is able to affect transcription, translation or degradation of GluR1 more globally. This was not a general reduction of all glutamate receptors as NR1 levels actually increased slightly following Arc expression (Chowdhury *et al.*, 2006). This effect of Arc on AMPA receptor levels has been suggested as a mechanism by which Arc may affect LTD. In fact, induction of mGluR-dependent LTD appears to require local translation of Arc in the dendrites. This increase in dendritic Arc levels is rapid and is detectable <10 min after mGluR activation (Park *et al.*, 2008; Waung *et al.*, 2008; Jakkamsetti *et al.*, 2013).

It has been suggested that Arc levels provide a marker of activity at the level of the neuron to guide homeostatic scaling responses. Homeostatic scaling is the process by which synaptic strength is globally reduced or increased across the cell, in a manner which preserves the relative differences in strength between individual synapses. This process is induced by chronic activity or inactivity and is thought to prevent extreme strengthening or weakening of synapses, which could saturate a neuron's capacity for synaptic plasticity (Moser *et al.*, 1998; O'Brien *et al.*, 1998; Turrigiano *et al.*, 1998). Chronic blockade (TTX) or stimulation (Bicuculline) of activity in hippocampal neuronal cultures induces a decrease or increase in Arc protein expression, respectively. Arc knockout blocks the homeostatic scaling of surface GluR1 and synaptic strength by both chronic TTX and chronic Bicuculline. Arc overexpression was also found to block the homeostatic upregulation of GluR1 usually observed following chronic inactivity (Shepherd *et al.*, 2006). This suggests a simple system in which Arc levels provide a marker of the recent state of activity in a neuron and results in the global up- or down-scaling of synaptic strength in response.

The specific function of Arc in the nucleus is still unclear, as it has no known DNA binding regions. However, one line of evidence has shown that nuclear Arc is able to decrease GluA1 transcription via an indirect action on the cyclic AMP response elements (CREs) in its promoter (Korb *et al.*, 2013). Arc forms discrete puncta in the nuclei of hippocampal neurons, which co-localise with PML-nuclear bodies (Bloomer *et al.*, 2007). Interestingly, Arc expression in response to activity upregulates PML expression and this upregulation is both essential for GluA1 transcriptional repression, but also sufficient to induce it in the absence of any change in Arc (Korb *et al.*, 2013). This suggests that Arc may act indirectly via upregulation of PML to reduce GluA1 levels in response to activity, this could form part of the homeostatic response already described.

1.2.3 Arc as a marker of neuronal activity

The activity-regulated nature of Arc expression has led to its use as a marker of recently activated neurons. Fluorescent constructs placed under the control of the Arc promoter have been used to identify neurons activated during fear conditioning (Vousden *et al.*, 2015; Cho *et al.*, 2016), novel environment exposure (Jakkamsetti *et al.*, 2013), motor (rotarod) learning (Cao *et al.*, 2015) and light deprivation/exposure (Wang *et al.*, 2006). In-situ hybridisation and immunohistochemistry have also identified increases in endogenous Arc mRNA and protein respectively, following a vast array of behavioural stimulation protocols. This includes an immediate increase in Arc mRNA in the hippocampus following 5 min of novel

environment exposure (Guzowski *et al.*, 1999; Chawla *et al.*, 2005), followed by an increase in protein levels as early as 30min post-exploration (Ramirez-Amaya *et al.*, 2005).

1.2.4 Arc Summary

In summary, Arc is a highly dynamic, activity-regulated member of the NMDAR supercomplex present at the PSD. It is both targeted to recently-activated synapses, and able to modify the strength of those synapses via increasing AMPA receptor endocytosis or interactions with the cytoskeleton. Arc is also present in the nucleus and can influence GluA1 transcription. Precise control of Arc levels is important for maintenance of LTP, LTD and long-term memory. However, several aspects of Arc regulation and function still remain to be elucidated, including the molecular mechanism by which it is able to facilitate opposing forms of synaptic plasticity.

1.3 Ketamine

1.3.1 Ketamine-induced psychological effects

Ketamine was synthesised in 1962 and was intended as a safer derivative of the anaesthetic Phencyclidine (PCP) which produces severe hallucinogenic side effects. A subsequent study on volunteer prisoners found ketamine to have similar pharmacologic effects to PCP but with shorter duration (Domino, 1984). Ketamine can be described as a dissociative anaesthetic and still produces some of the adverse reactions reported with PCP including hallucinations, blurred vision, delirium, floating sensations, and vivid dreams, although with less frequency (Domino, 1984; Frohlich & Van Horn, 2014). It is this hallucinogenic ability that has led to ketamine's use as a drug of abuse (Dotson *et al.*, 1995). However, it is still used worldwide in clinical practice as it has several beneficial characteristics as an anaesthetic, including a reduced risk of airway collapse or cardiovascular depression (Haas & Harper, 1992).

1.3.1.1 Psychotomimetic effects of ketamine in humans

The effect of sub-anaesthetic doses of ketamine on mental state has been the subject of several studies, the results of which are summarised in **table 2**. The picture emerging from this body of work is that at low doses ketamine is often able to induce perceptual distortions, but that the complex hallucinations associated with emergence from anaesthesia are less common. Also frequently observed, is an increased score on the clinician-reported Brief Psychiatric Rating Scale (BPRS) and the Clinician Administered Dissociative States Scale (CADSS). These scales provide a measure of symptoms including hallucinations, suspiciousness, hostility and dissociative states. Many of the symptoms reported in these studies mimic those of schizophrenic patients, in fact ketamine has been used previously as

an experimental model of schizophrenia (Frohlich & Van Horn, 2014) and exacerbates pre-existing positive symptoms when given to schizophrenia patients (Lahti *et al.*, 1995). Several studies have found these ketamine-induced symptoms to be sensitive to the actions of the antipsychotics Haloperidol (Krystal *et al.*, 1999), LY354740 (Krystal *et al.*, 2005) and Clozapine (Malhotra *et al.*, 1997). Effects on cognitive ability and memory function have also been reported (**table 2**). All of the reported psychosis-like effects are detectable soon after commencement of ketamine infusion and last only briefly (<15 min) after cessation of infusion. Given the serum half-life of ketamine, which is ~11 min in the human (Wieber *et al.*, 1975) it appears that these psychotomimetic effects are an acute response to the presence of the drug and are not a sign of lasting alterations to mental state. Although there is some evidence that long-term recreational use can increase incidence of dissociative and delusional symptoms during drug-free periods, this is rare (Morgan *et al.*, 2010).

	Ketamine dose	Self-reported perceptual distortions	Clinician-reported psychiatric measures	Cognition & memory tests	other
(Ghoneim *et al.*, 1985)	0.25, 0.5 mg/kg	yes	N/A	↓immediate recall	N/A
(Krystal *et al.*, 1994)	0.1, 0.5 mg/kg	yes	↑BPRS score ↑CADSS score	↓verbal fluency & vigilance - MMSE	N/A
(Breier *et al.*, 1997)	0.12 bolus, 0.65 mg/kg over 1 h	N/A	↑BPRS score	N/A	N/A
(van Berckel *et al.*, 1998)	0.3 mg/kg	yes	↑BPRS score	N/A	- PPI
(Newcomer *et al.*, 1999)	Plasma target 150, 45, 13.5 ng/ml	N/A	↑BPRS score ↑SANS score	↓verbal declarative memory - all other	N/A
(Lahti *et al.*, 2001)	0.1-0.5 mg/kg	N/A	↑BPRS score (psychosis & withdrawal subscales)	N/A	N/A
(Abel *et al.*, 2003)	0.23 loading dose, then 0.5 mg/kg over 45 min	N/A	↑BPRS score ↑CADSS score	↓ Category Instance generation ↓backwards digit span - MMSE score - verbal fluency	↑PPI
(Pomarol-Clotet *et al.*, 2006)	Plasma target 100, 200ng/ml	yes	↑CADSS score	N/A	N/A
(Moore *et al.*, 2011)	Plasma target 100, 200ng/ml	N/A	N/A	N/A	↑action-effect binding

Table 2 - Summary of current literature on effect of sub-anaesthetic doses of ketamine on mental state in healthy volunteers.

↑ = sig. increase, ↓ = sig. decrease, - = no change from placebo control. BPRS = Brief Psychiatric Rating Scale. SANS = Scale for the Assessment of Negative Symptoms. CADSS = Clinician Administered Dissociative States Scale. MMSE = Mini Mental State Examination.

1.3.1.2 Antidepressant effects of ketamine in humans

Further to its anaesthetic and psychotomimetic effects, there is now evidence that at low doses ketamine can produce an antidepressant effect in patients with treatment-resistant Major Depressive Disorder (MDD). Several studies have found 0.5 mg/kg ketamine infusion to significantly reduce scores on the Hamilton (HDRS) and Montgomery-Asberg Depression Rating Scales (MADRS), as compared with placebo. Please see **table 3** for a summary of the literature. What is interesting is that the time of onset of this antidepressant effect of ketamine is usually later than the psychotomimetic effects described above. In fact, many studies into the antidepressant effects of ketamine also assessed psychosis-like symptoms with the BPRS, CADSS or VAS (Berman *et al.*, 2000; Zarate *et al.*, 2006; aan het Rot *et al.*, 2010). In these studies, psychosis-like symptoms were transiently increased during infusion but returned to baseline soon after cessation, whereas an antidepressant effect was not detected until ~3-4 h post-infusion. This is with the exception of (Diazgranados *et al.*, 2010) in which the onset of antidepressant effects was more rapid (at cessation of infusion), however this study also involved concomitant use of lithium or valproate. The picture from studies administering ketamine alone suggests that, rather than being a direct result of the presence of ketamine in the brain, these delayed antidepressant effects may be produced by a downstream alteration in brain function. Conventional antidepressant drugs, such as SSRIs are not effective after one dose and can take weeks of daily administration before an improvement in symptoms can be seen. This relatively rapid-onset, but long-lasting, effect of a single dose of ketamine is therefore a promising observation in the search for more optimal antidepressant treatments.

	Ketamine dose	Clinician administered tests	Time point of change (post-infusion start)
(Berman *et al.*, 2000)	0.5 mg/kg over 40 min	↓HDRS score	240 min – 72 h
		↑BPRS score* ↑VAS "high" score*	10 & 40 min
(Zarate *et al.*, 2006)	0.5 mg/kg over 40 min	↓HDRS score	110 min – 7 days
		↑BPRS score* ↑YMRS score*	40 min
(aan het Rot *et al.*, 2010)	0.5 mg/kg over 40 min	↓MADRS score ↓QIDS-SR score	4 h
		↑CADSS score*	0-40 min
(Diazgranados *et al.*, 2010)[a]	0.5 mg/kg over 40 min (N.B concomitant use of lithium or valproate)	↓MADRS score ↓HDRS score ↓BDI score	40 min – 3 days
		↑YMRS score* ↑BPRS score* ↑CADSS score*	40 min
(Murrough *et al.*, 2013)	0.5 mg/kg over 40 min	↓MADRS score	24 h

Table 3 - Summary of current literature on antidepressant effect of sub-anaesthetic doses of ketamine in MDD patients.

*↑ = sig. increase, ↓ = sig. decrease from placebo control. * = test for psychosis-like symptoms. Three studies were excluded from this summary on the basis that they were open-label with no placebo (Price et al., 2009; DiazGranados et al., 2010; Ibrahim et al., 2011). HDRS = Hamilton Depression Rating Scale. MADRS = Montgomery-Asberg Depression Rating Scale. QIDS-SR = Quick Inventory of Depressive Symptoms. BPRS = Brief Psychiatric Rating Scale. VAS "high" = Visual Analog Scale for intoxication "high". YMRS = Young Mania Rating Score.*

1.3.2 Ketamine-induced behaviour in mice

Given the promising antidepressant effects, and worrying psychotomimetic effects, of ketamine observed in humans it has become increasingly important to understand the underlying molecular changes involved. Therefore, much work has focussed on modelling ketamine-induced psychotomimetic and antidepressant effects in laboratory animals. Here I discuss the current evidence for ketamine's effect on rodent behavioural measures, intended to model the described human responses. Interestingly, much of our current knowledge comes from investigations into the possible use of ketamine as an animal model for schizophrenia research.

1.3.2.1 'Psychotomimetic' effects of ketamine in rodents

Sub-anaesthetic doses of ketamine induce increased locomotion in mice, as measured by recording the distance travelled by the animals in an open field arena (Irifune *et al.*, 1991; Imre *et al.*, 2006; Chatterjee *et al.*, 2011). Ketamine-induced hyper-locomotion can be attenuated by antipsychotic drugs (Irifune *et al.*, 1991; Chatterjee *et al.*, 2011) therefore, this measure has been taken as having translational relevance to the ketamine-induced schizophrenia-like effects described in **section 1.3.1.1**. This effect is short-lived, for example administration of 10mg/kg ketamine induces an increase in locomotion at 10 & 20 min post-administration but returns to control levels by 30 min (Irifune *et al.*, 1991). The serum half-life of ketamine in laboratory mice is ~13 min (Maxwell *et al.*, 2006) and a 30mg/kg dose has been found to clear from the brain in <1h (Lord *et al.*, 2013). This timing suggests that, as with the psychosis-like symptoms in humans, ketamine-induced hyper-locomotion is an acute response to the presence of ketamine rather than a more permanent alteration to behaviour. The hyper-locomotive response to ketamine is dose-dependent, with higher doses producing a longer-lasting increase in locomotion (Irifune *et al.*, 1991; Danysz *et al.*, 1994).

1.3.2.2 'Antidepressant' effects of ketamine in rodents

Several different kinds of tests have been developed to assess depressive-like phenotypes in rodents. The most commonly used are the Tail Suspension Test (TST) and Forced Swim Test (FST). These tests are designed to measure the degree of 'behavioural despair' of an animal when it is placed in an uncomfortable situation which it cannot escape from. The amount of time spent not trying to escape from that situation, defined by a lack of movement (immobility time), is taken as a measure of 'behavioural despair'. An increased immobility time is an indicator of reduced attempts to escape from that situation and is considered a

depressive phenotype. In the novelty-supressed feeding test (NSFT) a food pellet is placed in the centre of a novel environment and the latency of the animal to begin feeding on that pellet is recorded. Increased latency to feed is considered a sign of increased anxiety. In the sucrose preference test (SPT) the innate preference of rodents for sucrose water over regular water is used. Absence of that preference is considered an indicator of anhedonia. A depressive phenotype in any of these tests can be rescued by various different antidepressant medications, which are themselves effective in depressed patients (Bodnoff *et al.*, 1988; Cryan *et al.*, 2005; Pollak *et al.*, 2010; Powell *et al.*, 2012).

Table 4 summarises the current literature on the effect of different doses of ketamine on the outcomes of these tests. The picture that emerges from these studies is that sub anaesthetic doses of ketamine are able to induce an antidepressant-like effect which has been reported as early as 30min and can last up to 7 days post-administration. This rapid onset is interesting given the repeated dosing required for SSRIs to become effective. Indeed, several studies have directly compared SSRI and ketamine efficacy in rodent models, confirming the absence of an acute antidepressant effect of SSRIs (Autry *et al.*, 2011; Zanos *et al.*, 2016). Given the ~13 min half-life of ketamine (Maxwell *et al.*, 2006), it is clear that antidepressant effects are lasting beyond the presence of the drug in the brain. This suggests that the transient presence of ketamine is sufficient to induce lasting changes in brain function. What is particularly interesting is the dose-response relationship that emerges from this large body of data. It seems that an antidepressant response to ketamine is restricted to low, sub-anaesthetic doses, with the same effect not observed following higher doses. For example in rats 10mg/kg, but not 80mg/kg, ketamine was able to induce a decrease in FST immobility time (Li *et al.*, 2010). Similar results have been reported by others (Zanos *et al.*, 2016).

However, there are some limitations to the current literature on this topic. There is the possibility that the short term hyper-locomotive response to ketamine, described in **section 1.3.2.1**, could affect the early measurements of immobility in the FST and TST. However, most papers included data showing that general locomotion was not altered at the dose and time point at which the TST or FST was carried out. Those which report an effect in the FST or TST at a dose and time point when hyper-locomotion would be expected (Irifune *et al.*, 1991), but did not specifically test for it, have been highlighted with an asterisk in **table 4**. Regardless of the exact onset time it is clear that the antidepressant effect of ketamine in rodents is more rapid than that of SSRIs. Questions have been raised over the relevance of

'antidepressant' responses in rodent models to clinical outcomes in human patients (Pollak *et al.*, 2010). However, in this case there is supporting data from patient studies, so this is not a significant concern. Several published reports failed to find an effect of ketamine in the FST at doses and time-points previously reported to be effective, in general negative results are less likely to be published, suggesting a potential lack of reproducibility (Popik *et al.*, 2008; Bechtholt-Gompf *et al.*, 2011; Chatterjee *et al.*, 2011). This is not uncommon with rodent tests of depressive phenotypes, as these tests can be affected by various biological factors which complicate comparison across studies (Bogdanova *et al.*, 2013). Again, when viewed alongside the patient data this variability is less of a concern.

	Species/Strain	Ketamine dose	Behavioural alterations	Time post-administration
(Mantovani *et al.*, 2003)	Ms/Male Swiss	0.1mg/kg	↓ immobility time FST	30 min
(Rosa *et al.*, 2003)	Ms/Swiss	5mg/kg	↓ immobility time FST	30 min*
(Hayase *et al.*, 2006)	Ms/ICR	30 & 100mg/kg	↑ time until immobility FST No change in activity FST	60 & 120 min
(Garcia *et al.*, 2008)	Rt/Male Wistar	5, 10 & 15mg/kg	↓ immobility time FST (10 & 15 mg/kg only)	60 min
(Popik *et al.*, 2008)	Ms/Male Albino Swiss	1.25, 2.5, 5 10, 50, 160mg/kg	No effect in FST (except ↓) immobility 50mg/kg 40min)	40 min*, 1 week & 2 weeks
(Cruz *et al.*, 2009)	Ms/Male Swiss	12.5, 25 & 50mg/kg (6.25mg/kg no effect)	↓ immobility time FST ↓ immobility time TST (50mg/kg only)	30 min*
(Ghasemi *et al.*, 2010)	Ms/Male NMRI	2 & 5 mg/kg (0.5 & 1 mg/kg no effect)	↓ immobility time FST	45 min
(Li *et al.*, 2010)	Rt/Male Sprague-Dawley	10 & 80 mg/kg	↓ immobility time FST (10mg/kg only)	24h
(Autry *et al.*, 2011)	Ms/C57BL/6	3 mg/kg	↓ immobility time FST	30min – 7 days
(Bechtholt-Gompf *et al.*, 2011)	Ms/CD-1 Ms/Balb/cJ	0.5, 2.5, 12.5, 40, 80, 160 mg/kg	No effect in FST (except ↓ immobility 160mg/kg, 1h)	1h* & 7 days
(Beurel *et al.*, 2011)	-	10mg/kg	↓ latency to escape LH	24 h
(Chatterjee *et al.*, 2011)	Ms/Male Swiss	100mg/kg	No effect in FST (↑ immobility after 10 x daily 100mg/kg)	24 h
(Koike *et al.*, 2011)	Ms/Male ICR	30mg/kg (3 & 10mg/g no effect)	↓ immobility time TST	30 min & 72 h
(Tizabi *et al.*, 2012)	Rt/Female Kyoto	0.5, 2.5, & 5 mg/kg	↓ immobility time FST (2.5 & 5 mg/kg only @ 30 min, 5 only @ 7 days)	30 min & 7days

(Koike *et al.*, 2013)	Ms/Male ICR Ms/Male C57BL/6J	30mg/kg	↓ immobility time TST, ↓ latency to feed NSFT	30 min & 24 h
(Walker *et al.*, 2013)	Ms/Male CD-1 Ms/Male C57BL/6J	6mg/kg	↓ immobility time FST, ↑ sucrose preference SPT	18 h & 28 h
(Zhou *et al.*, 2014)	Rt/Male Wistar	10mg/kg	↓ immobility time FST	30 min*
(Wang *et al.*, 2015)	Rt/Male Wistar	10mg/kg	↓ immobility time FST ↓ latency to feed NSFT	0.5h-4h
(Zanos *et al.*, 2016)		1, 3, 10, 30, 50 mg/kg	↓ immobility time FST (10 & 30 mg/kg @ 1h, 10mg/kg @ 24h)	30 min & 24h

Table 4 – Summary of current literature on antidepressant-like effect of ketamine in mouse.

*TST = Tail Suspension Test; NSFT = Novelty Supressed Feeding Test; FST = Forced Swim Test; SPT = Sucrose Preference Test; * = lack of locomotion test when reduction in immobility reported within potential hyper-locomotion window.*

1.3.3 Effect of ketamine on memory performance

In addition to its psychosis-like and antidepressant effects, acute low-dose ketamine administration has been found to impair both the encoding and retrieval of episodic memory in humans (Ghoneim *et al.*, 1985; Krystal *et al.*, 1994; Newcomer *et al.*, 1999; Hetem *et al.*, 2000). In rodents 1mg/kg and 3mg/kg doses of ketamine, administered 20 min prior to or immediately after a 'training' session were able to impair novel object recognition during testing 60 min later (Pitsikas & Boultadakis, 2009). Ketamine was also found to impair retrieval of a social recognition memory at 10mg/kg (Gao *et al.*, 2009). The literature on the effect of ketamine administration on working memory in humans is inconsistent (Morgan & Curran, 2006). However, in rodents a deficit in working memory has been observed immediately (~5 min) following low dose (>10mg/kg) ketamine administration (Smith *et al.*, 2011).

1.3.4 Molecular mechanism of ketamine

1.3.4.1 Ketamine as an NMDA receptor antagonist

The primary action of ketamine is as a non-competitive NMDA receptor antagonist. This action is common to dissociative anaesthetic agents including nitrous oxide, dextromethorphan, and PCP (Absalom & Menon, 2010). Ketamine binds within the NMDA

receptor channel pore to block ion flux. This blockade requires an open channel to allow ketamine access to the binding site (Macdonald *et al.*, 1987; Zeilhofer *et al.*, 1992). NMDAR blockade by ketamine is also voltage dependent, increasing with membrane depolarisation (Halliwell *et al.*, 1989; Zeilhofer *et al.*, 1992). Although ketamine's action at the NMDA receptor has been well documented, and is considered to be responsible for the acute anaesthetic effect that ketamine has (Anis *et al.*, 1983; Daniell, 1990; Sato *et al.*, 2004), the molecular mechanisms downstream from receptor blockade are still under investigation. This is particularly important when it comes to understanding the long-lasting antidepressant effects of ketamine, which are known to continue long after the drug has been metabolised. What is interesting to note, is that the psychological effects of ketamine take place at sub-anaesthetic doses, where it is estimated that brain concentrations of the drug would be in the low micromolecular range (Hartvig *et al.*, 1995; Zorumski *et al.*, 2016). At this concentration ketamine is likely to be inhibiting <50% of NMDA receptors, leaving a significant portion unaffected (Dravid *et al.*, 2007; Kotermanski *et al.*, 2009; Zorumski *et al.*, 2016) . There is still debate over whether different NMDA receptor subtypes have different sensitivities to ketamine blockade. An initial study in Xenopus oocytes found similar sensitivity to ketamine blockade across subtypes (Yamakura *et al.*, 1993). However, following this, a study in HEK cells found that at physiological levels of Mg^{2+} differing sensitivities to ketamine are detectable between the subtypes. In this experiment the most sensitive subtype was GluN2C, followed by GluN2D, GluN2A and GluN2B were the least sensitive and were almost indistinguishable from one another (Kotermanski & Johnson, 2009). The impact *in vivo* of any preference of ketamine to block one NMDAR subtype over another will be highly dependent upon the extracellular concentration of ketamine present in the brain following administration. This can be a difficult value to calculate with accuracy and has led to some debate over the likely contribution of individual NMDAR subtypes to behavioural outcomes of ketamine action (Khlestova *et al.*, 2016).

1.3.4.2 Ketamine increases synaptic protein levels

Sub-anaesthetic doses of ketamine have been found to induce long term increases in synaptic protein levels. 10mg/kg ketamine is able to increase levels of Synapsin I, PSD95 and GluR1 in synaptoneurosomes of prefrontal cortex (PFC). This increase was observed at 2 - 72h post-administration, a timeline which coordinates with the antidepressant effects of this dose of ketamine. An increase in Arc was also observed in this preparation but this effect was only detectable at 1 - 2h post-administration, making it more rapid and relatively transient.

Another study replicated this increase in Arc and found it to be sensitive to treatment with the protein synthesis blocker anisomycin (Autry *et al.*, 2011). An increase in spine density in the PFC at 24h post ketamine administration was also observed (Li *et al.*, 2010). Similar increases in Synapsin I, PSD95 and GluR1 have been observed after administration of 30mg/kg ketamine (Tang *et al.*, 2015). Rapid new protein synthesis is required for both the rapid (30 min) and long-lasting (24h) antidepressant effect of ketamine, as both can be blocked by a single administration of anisomycin 30min prior to ketamine administration (Autry *et al.*, 2011).

1.3.4.3 Ketamine activates mTOR signalling

Prior to this synaptic effect, a transient increase in members of the mTOR signalling cascade has been observed. 30min - 1h following 10mg/kg ketamine administration, levels of p4E-BP1, pmTOR and pp70S6K are elevated in PFC synaptoneurosome preparations (Li *et al.*, 2010). A separate report found increased leves of p4E-BP1 and pp70S6K 2 days after a 30mg/kg dose of ketamine, pmTOR levels were unaltered at this timepoint (Tang *et al.*, 2015). Activation of mTOR signalling positively controls protein synthesis, and blockade of mTOR activity with rapamycin prevents ketamine-induced upregulation of synaptic proteins as well as the antidepressant response (Laplante & Sabatini, 2009; Li *et al.*, 2010). Interestingly, the increase in mTOR signalling is not observed following a higher dose (80mg/kg). This dose-dependency correlates with that of the antidepressant effect of ketamine which was also detected at 10mg/kg, but not 80mg/kg (Li *et al.*, 2010). The increase in p70S6K phosphorylation is not specific to the PFC, as a similar result was observed in western blot from hippocampus (Harraz *et al.*, 2016). Levels of the GTP binding protein Rheb, an upstream regulator of mTOR activity, are also increased following ketamine administration. Interestingly, the GluN2B selective inhibitor CERC301 was able to mimic the effects of ketamine on both Rheb and pp70S6K levels but the NMDA receptor antagonist memantine had no effect (Harraz *et al.*, 2016). Upstream of mTOR signalling, ketamine is able to reverse CMS-induced reductions in pAKT and pERK (Tang *et al.*, 2015). This seems to be required for ketamine action as inhibitors of ERK are able to prevent the ketamine-induced antidepressant response (Li *et al.*, 2010; Reus *et al.*, 2014). Further upstream of ERK, BDNF signalling via TrkB receptors has also been implicated in ketamine action. BDNF knockout mice do not display an antidepressant response to ketamine or MK801, the same result was seen in TrkB knockout mice. Both BDNF levels and TrkB activation are transiently increased after ketamine administration (Autry *et al.*, 2011). BDNF is released from the postsynaptic

membrane in response to neuronal activity and acts via surface TrkB receptors to stimulate signalling cascades including ERK (Numakawa *et al.*, 2010). Overall, it is clear that upregulation of synaptic proteins, triggered by activation of ERK/mTOR is taking place in response to sub anaesthetic doses of ketamine. This kind of cellular response usually takes place following increases in neuronal activity (Ghosh & Greenberg, 1995; Sweatt, 2001; Krapivinsky *et al.*, 2003).

1.3.4.4 Ketamine induces glutamate release

There is evidence that subanaesthetic doses of ketamine are able to induce glutamate release and increase neuronal activity in the PFC. 10, 20 & 30mg/kg ketamine all increase glutamate outflow in the PFC. This effect was observed 40-100min post-administration with 30mg/kg producing the longest lasting increase. However, an anaesthetic dose (200mg/kg) actually decreased glutamate outflow 20 – 80 min post-administration. An intermediate dose (50mg/kg) had no lasting effect (Moghaddam *et al.*, 1997). Similar results have been reported by others (Chowdhury *et al.*, 2012; Stone *et al.*, 2012). This is interesting given the similar lack of antidepressant effects at anaesthetic doses. Glutamate increase seems to be functionally required for ketamine-induced psychotomimetic effects in humans, and the severity of psychotomimetic symptoms is positively correlated with glutamate levels (Anand *et al.*, 2000; Krystal *et al.*, 2005; Stone *et al.*, 2012). An increase in neuronal activity as measured by c-fos levels has also been observed in several brain regions (Imre *et al.*, 2006).

1.3.4.5 The indirect 'disinhibition' hypothesis of ketamine action

It is still unclear how ketamine is able to boost neuronal activity given its NMDAr antagonist properties, however, several hypotheses have recently been proposed. These include the suggestion that at low doses ketamine could act preferentially at NMDARs on inhibitory interneurons, thus releasing primary glutamatergic neurons from that inhibition and leading to increased activity. This has been termed the disinhibition hypothesis of ketamine action, and has been discussed in several review articles (Seamans, 2008; Miller *et al.*, 2016; Wohleb *et al.*, 2017). One line of evidence supporting this hypothesis is the observation that 30mg/kg ketamine administration is able to preferentially reduce the firing rate of a subpopulation of putative inhibitory interneurons in the orbitofrontal cortex (Quirk *et al.*, 2009). In this study neuronal populations were defined by their extracellular waveform and spike train characteristics. In culture ketamine was able to decrease GAD67, the enzyme responsible for the majority of GABA synthesis, in Parvalbumin positive interneurons (Kinney *et al.*, 2006). These results have been replicated in the PFC of rats following 2 days of ketamine injection,

in addition to a reduction in GAD67 immunoreactivity, there was a 20% reduction in mIPSCs which were confirmed as GABA mediated currents via blockade with bicuculline (Zhang *et al.*, 2008). However, a requirement for this reduction in inhibitory activity for antidepressant responses has yet to be established. Neither knockout of NMDArs in interneurons nor administration of GABA antagonists has been able to mimic and/or occlude the antidepressant response of ketamine (Autry *et al.*, 2011; Pozzi *et al.*, 2014). This 'disinhibition' hypothesis does go some way towards explaining the unusual dose-dependency of the ketamine response, as at high (anaesthetic) doses any preference for ketamine to bind to certain subpopulations of NMDARs would likely be inconsequential.

1.3.4.6 GluN2B specific actions of ketamine

There is growing evidence that ketamine's antidepressant effects may be mediated specifically by GluN2B containing NMDA receptors. Administration GluN2B-selective antagonists are able to mimic both the antidepressant actions of ketamine in humans and rodents, and the increases in mTOR signalling and synaptic protein synthesis (Preskorn *et al.*, 2008; Li *et al.*, 2010; Lima-Ojeda *et al.*, 2013; Miller *et al.*, 2014). This seems to be via a direct effect on pyramidal neurons, as removal of NMDA receptors from inhibitory interneurons did not alter the behavioural response to GluN2B-specific antagonist Ro 25-6981 (Kiselycznyk *et al.*, 2015). This is interesting as GluN2B is considered to play a role in homeostatic plasticity via its specific interactions with CAMKII and SynGAP. Blockade of action potentials with TTX induces a homeostatic response in which mTOR signalling and protein synthesis are upregulated and mEPSC amplitude is increased. This acute homeostatic response was mimicked and occluded in a mouse line in which GluN2B subunits have been replaced with GluN2A, leaving total surface NMDAr levels unchanged (Wang *et al.*, 2011). A preferential action of ketamine on pyramidal cell GluN2B-containing NMDArs could therefore elicit a homeostatic-like response including mTOR signalling, synaptic protein synthesis and synaptogenesis. Again this could explain the dose dependent nature of ketamine action, as at high doses this preference may be inconsequential. The most compelling evidence for this hypothesis so far comes from a mouse line in which GluN2B has been selectively removed from the principal neurons of the neocortex. Ketamine-induced antidepressant effects, increased excitatory synaptic transmission and increased protein synthesis are all mimicked and occluded in these mice (Miller *et al.*, 2014). Ketamine does not bind preferentially to GluN2B-containing receptors over the other NMDAR subtypes (Kotermanski & Johnson, 2009), so it is unclear how a specific GluN2B action would arise. Again, a high dose of

ketamine would be likely to mask any preferential action via GluN2B, fitting with the previously-described dose-response relationship.

1.3.4.7 NMDAr blockade-induced protein translation via eEF2 dephosphorylation

eEF2 is a signalling molecule thought to act as a biochemical sensor. Action potential-mediated network activity maintains eEF2 in a relatively dephosphorylated (active) state, whereas the spontaneous activity promotes phosphorylation (inactivation) (Sutton *et al.*, 2007). Dephosphorylation of eEF2 has been found to augment protein synthesis (Sutton *et al.*, 2007). It has been suggested that ketamine would block this resting NMDAr activity, attenuating phosphorylation of eEF2 and promoting local protein translation (Autry *et al.*, 2011). In support of this hypothesis ketamine is able to decrease NMDA-mEPSCs and eEF2 phosphorylation in vitro. Decreased eEF2 phosphorylation was also detected 30 min post-ketamine administration in vivo in hippocampus, but not in cortex (Autry *et al.*, 2011). Interestingly, ambient glutamate has been found to produce a tonic current via GluN2B-containing NMDA receptors (Miller *et al.*, 2014). This suggests that part of the GluN2B specific ketamine action described in **section 1.3.4.6** could be due to reduced phosphorylation of eEF2 in response to blockade of this tonic current (Miller *et al.*, 2016).

1.3.4.8 Ketamine metabolites as effectors of the antidepressant response

A recent hypothesis suggests that it is not ketamine, but one of its metabolic products that is inducing an antidepressant effect. This is interesting given that the onset of antidepressant action seems to be taking place after ketamine metabolism. Most metabolites of ketamine, other than norketamine, do not induce anaesthesia and have therefore been previously considered clinically inactive (Leung & Baillie, 1986). However, recent evidence has shown that administration of the (2R,6R)-hydroxynorketamine (HNK) metabolite induces a potent antidepressant action. In addition to this, a form of ketamine with inhibited metabolism to (2S,6S;2R,6R)-HNK failed to induce antidepressant effects in the FST or LH (Zanos *et al.*, 2016). This challenges the widely-held view that NMDAr antagonism underlies ketamine action, as (2R,6R)-HNK does not bind or inhibit NMDA receptors. Indeed, the antidepressant action of (2R,6R)-HNK required the acute activation of AMPA receptors. The effects of (2R,6R)-HNK lasted beyond the presence of detectable levels in brain, and both ketamine and (2R,6R)-HNK increased AMPA receptor levels 24h post-administration (Zanos *et al.*, 2016). This suggests again that the brief presence of the drug is able to initiate long lasting alterations in synaptic strength and/or number. Interestingly, (2R,6R)-HNK seems to lack the dissociative side

effects of ketamine as it has no anaesthetic properties, and does not affect locomotion or coordination in rodents (Leung & Baillie, 1986; Zanos *et al.*, 2016). These new findings are exciting, but considering the evidence described in **section 1.3.4.6** detailing the importance of the GluN2B-containing NMDAR, it may be too soon to rule out a role of the NMDA action of ketamine in its antidepressant effects, as some have suggested. Several recent letters and reviews discuss these two hypotheses in detail (Miller *et al.*, 2016; Collingridge *et al.*, 2017; Zanos *et al.*, 2017).

1.3.4.9 Non-NMDAr targets of ketamine

The idea that ketamine may be acting via targets other than the NMDA receptor is not new. A finding often cited in support of a non-NMDAr target is that (S)-ketamine is a more potent inhibitor of NMDARs, but (R)-ketamine has a more potent antidepressant effect. However, as described in **sections 1.3.2 & 1.3.4.3**, it may be that a low level of NMDAr antagonism is required for antidepressant action rather than widespread blockade. Further to this, MK801, an NMDAr antagonist which lacks ketamine's additional targets, also lacks a long term antidepressant action although it is able to induce a short term effect (Maeng *et al.*, 2008). However, MK801 also has a different affinity for NMDA receptors which could also account for this discrepancy (Wong *et al.*, 1986; Berman & Murray, 1996).

Several other receptor targets for ketamine have been identified. At high doses it is able to inhibit nicotinic and muscarinic acetylcholine receptors, however, its affinity for these receptors is much lower than that for the NMDAr (Durieux, 1995; Yamakura *et al.*, 2000). Ketamine is also able to bind opioid (Smith *et al.*, 1987), dopamine D_2 and serotonin 5-HT_2 receptors (Yamakura *et al.*, 2000; Kapur & Seeman, 2002; Seeman *et al.*, 2005). There is evidence that ketamine can block voltage-gated sodium channels, and that this results in a local anaesthetic effect (Wagner *et al.*, 2001). The identification of these other receptor targets certainly highlights the complexity of ketamine's pharmacological profile and should inform the interpretation of future investigations into its molecular mechanism of action.

1.3.5 Summary

It is clear that there is now a large body of work detailing the effects of ketamine on both human and rodent measures of psychosis and depression. The picture that emerges from this work is one of a short-term psychotomimetic response to sub-anaesthetic ketamine doses, followed by a long-lasting antidepressant response. This antidepressant response outlasts the presence of ketamine in the brain and therefore is likely caused by a downstream effect of transient ketamine action. It also appears to be specifically triggered by low, sub-

anaesthetic, doses. However, despite much effort, the mechanism of action of these distinct psychological responses is still largely unknown. There is evidence for a specific role of the GluN2B subtype of the NMDAR, and the suggestion that ketamine could be acting primarily on inhibitory interneurons to indirectly increase activity of principal excitatory neurons. Ketamine is able to induce increases in glutamate release, activation of mTOR and ERK signalling, and upregulation of synaptic proteins. Both the glutamate release and activation of intracellular signalling is specific to low sub-anaesthetic doses, similar to the dose-response of ketamine's antidepressant effect. Understanding better the molecular events underlying ketamine's different psychological effects will be crucial piece of the puzzle to complete if we are to harness the powerful antidepressant properties of this drug in a safe manner.

1.4 Summary and thesis aims

In conclusion, there are several outstanding questions regarding the molecular mechanism of ketamine's action which the work in this thesis aims to address. As explained above, there is evidence that the antidepressant effect of ketamine is mediated specifically by the GluN2B NMDAR subunit, however, there is no reported specificity of ketamine binding to that subunit. The first aim of this thesis is to investigate this question by establishing which part of the GluN2B subunit is responsible for mediating ketamine's action, is it the channel pore region of GluN2B which is required? Or is it the intracellular c-terminal domain? Further to this, low dose ketamine has been found to induce upregulation of synaptic proteins including Arc and PSD95. However, it is not yet clear whether this is specific to sub-anaesthetic doses, as is the case with ketamine's antidepressant effect. Additionally, a detailed investigation into which brain regions are involved in this synaptic response has not yet been carried out. Therefore, the second aim of this thesis is to investigate the changes in Arc and PSD95 levels at the synapse following sub-anaesthetic and anaesthetic doses of ketamine, across multiple brain regions.

Chapter 2 Materials and Methods

2.1 Animals

All experiments were carried out in accordance with UK animals (Scientific Procedures) Act, 1986 and all procedures were approved by the British home office inspectorate.

2.1.1 The Arc^{VENUS} mouse line

The Arc-venus mouse line was engineered by Dr. Fei Zhu under the supervision of Dr. Noboru H. Komiyama and Prof. Seth G.N. Grant. Full details of the generation and characterisation of this line can be found in her PhD thesis. Briefly, a targeting vector was generated, containing the coding sequence for the Venus form of the yellow fluorescent protein flanked by two homology arms for the *Arc* gene. This vector was designed to insert the Venus sequence into the Arc open reading frame and before its stop codon. Mouse embryonic stem cells were targeted with this vector, correctly targeted ES cells were injected into mouse blastocysts to create chimeric mice. F1 generation heterozygotes were crossed with a cre-deleter mouse to remove the LoxP flanked neo cassette. Progeny were backcrossed on to C57BL/6J mice to establish a working colony, which was bred to homozygosity.

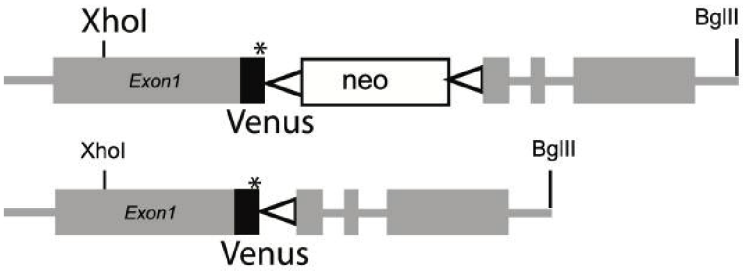

Figure 5 - Generation of Arc-Venus mouse line.

*Schematic illustrations of the targeted genomic Arc locus. The Arc allele was targeted with the Venus (YFP) sequence inserted into its open reading frame and before its stop codon by homologous recombination. neo^r: neomycin-resistance gene. * = stop codon of the coding sequence.* ***Figure and legend reproduced, with permission, from (Fernandez et al., 2017).***

2.1.2 PSD95-eGFP line

The PSD95-eGFP mouse line was engineered by Dr. Fei Zhu under the supervision of Dr. Noboru H. Komiyama and Prof. Seth G.N. Grant. Full details of the generation and characterisation of this line can be found in her PhD thesis and now published (Zhu *et al.*, 2018). Briefly, a targeting vector was generated, containing the enhanced green fluorescent protein (eGFP) coding sequence flanked by two homology arms for the gene encoding the PSD95 protein (*Dlg4*). Mouse embryonic stem cells were targeted with this vector, correctly targeted ES cells were injected into mouse blastocysts to create chimeric mice. F1 generation

heterozygotes were crossed with a cre-deleter mouse to remove the LoxP flanked neo cassette. Progeny were backcrossed on to C57BL/6J mice to establish a working colony, which was bred to homozygosity.

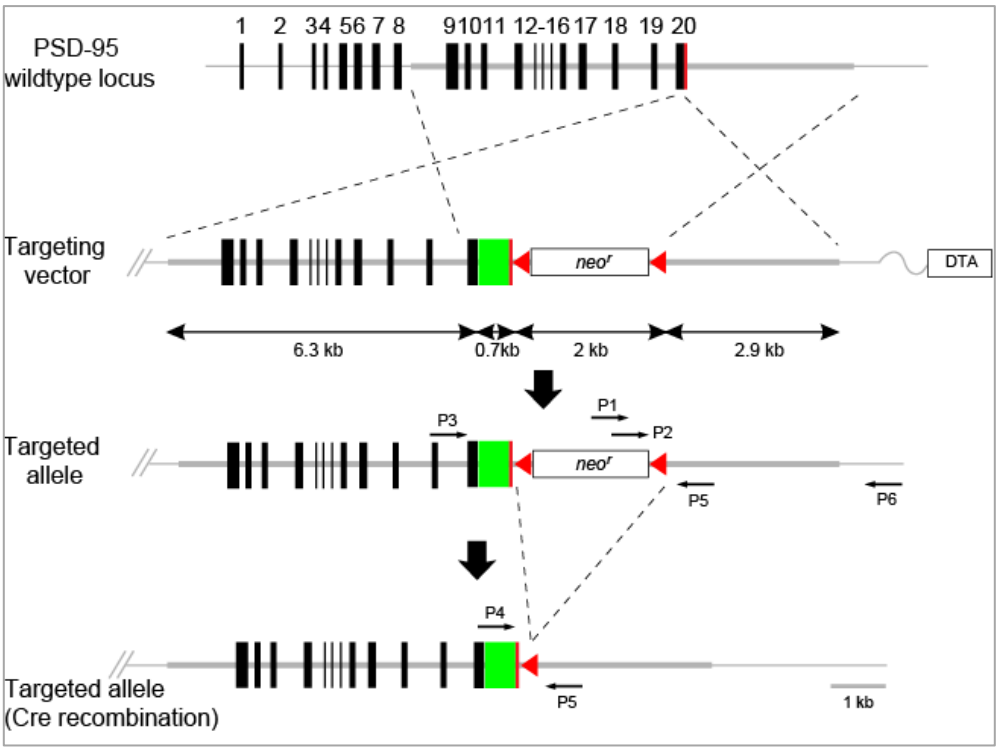

Figure 6 - Generation of PSD95-eGFP mouse line.

Schematic illustrations of the targeted genomic PSD-95 locus. The PSD-95 allele was targeted with the EGFP sequence inserted into its open reading frame and before its stop codon by homologous recombination. Recombination events are shown by dashed lines. neo^r: neomycin-resistance gene; DTA: diphtheria toxin gene. ***Figure and legend reproduced, with permission, from Dr. Fei Zhu PhD thesis.***

2.1.3 GluN2B-2A and GluN2A-2B swap lines

These two complementary mouse lines were engineered by Dr. Noboru H. Komiyama and have been previously published (Ryan *et al.*, 2013). In summary, the exons encoding the c-terminal domains (CTDs) of the GluN2A and GluN2B NMDA receptor subunits were exchanged. The CTDs of GluN2A and GluN2B are encoded by the terminal exons of their respective genes and the initial amino acid sequence encoded by these terminal exons is identical. For the GluN2A$^{2B(CTR)}$ line a targeting construct was designed to replace GluN2A exon 12 with that of GluN2B. For the GluN2B$^{2A(CTD)}$ line a targeting construct was designed to replace GluN2B exon 12 with that of GluN2A. Mouse embryonic stem cells were targeted with these vectors, correctly targeted ES cells were injected into mouse blastocysts to create

chimeric mice. F1 progeny were backcrossed on to C57BL/6J mice to establish a working colony, which was bred to homozygosity.

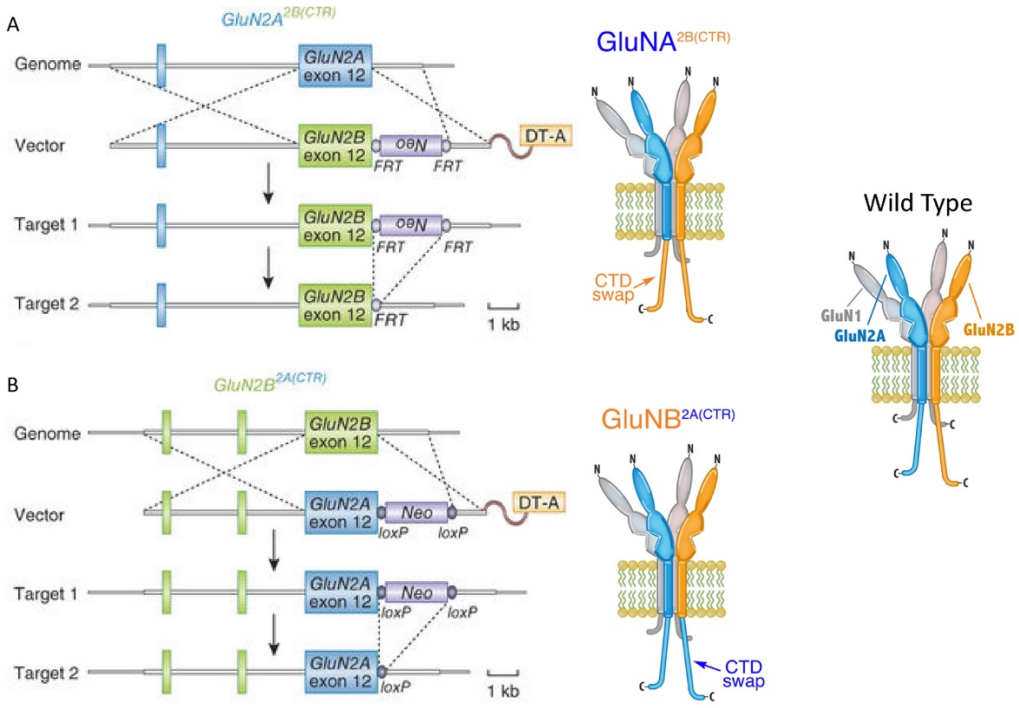

Figure 7 – Generation of GluN2A$^{2B(CTR)}$ and GluN2B$^{2A(CTR)}$ mouse lines.

The GluN2A$^{2B(CTR)}$ allele encodes a chimeric GluN2A subunit consisting of GluN2A extracellular and transmembrane regions and the GluN2B CTD. The terminal GluN2A exon that encodes the CTD was replaced with the paralogous sequence from GluN2B (target 1). The FRT-flanked Neo selection cassette was placed in the GluN2A 3' UTR and was removed by crossing GluN2A$^{2B(CTR)/+}$ mice with CAG-FLP recombinase transgenic mice (target 2). ***B.*** *The GluN2B$^{2A(CTR)}$ allele encodes a chimeric GluN2B subunit consisting of a GluN2B extracellular and transmembrane regions and the GluN2A CTD. The terminal GluN2B exon that encodes the CTD was replaced with the paralogous sequence from GluN2A (target 1). The loxP-flanked Neo selection cassette was placed in the GluN2B 3' UTR and was removed by crossing GluN2B$^{2A(CTR)/+}$ mice with CMV-Cre recombinase transgenic mice (target 2).* ***A & B and corresponding legend reproduced, with permission, from (Ryan et al., 2013)***

2.1.4 PSD93 knockout line

The PSD93 knockout line of mice was generated by the laboratory of David Bredt and has been previously published (McGee *et al.*, 2001). Details of the characterisation of this line can also be found on the genes2cognition.org database. Briefly, a targeting construct was designed to replace the exon containing most of the second PDZ domain of PSD93 with neomycin, this construct was flanked on two sides by a total of 8.5kb genomic DNA. Mouse embryonic stem cells were targeted with this vector. Correctly targeted ES cells were injected

into mouse blastocysts to create chimeric mice. These mice were then bred to produce animals homozygous mutant animals which lack the PSD93 protein (McGee *et al.*, 2001).

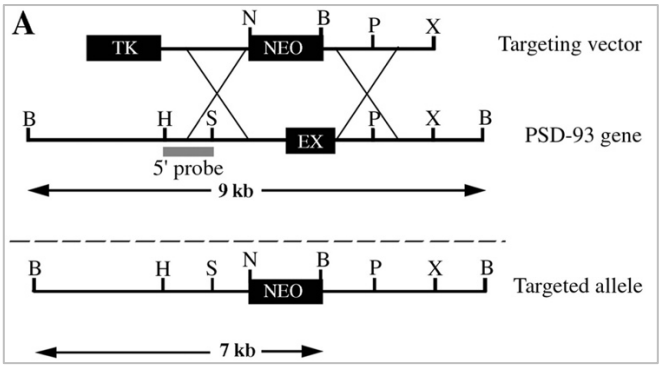

Figure 8 - Targeted disruption of PSD93.

Restriction maps of the pTK/NEO targeting vector, the native PSD-93 gene, and the properly targeted deletion locus are shown. Recombination (shown as large Xs) between the targeting vector and the wild-type locus produced the targeted allele. A BamHI site was engineered into the 3 end of the Neo cassette of the targeting vector to facilitate genotyping. B, BamHI; H, HindIII; N, NheI; P, PstI; S, SacI; X, XbaI. ***Figure and legend from (McGee et al., 2001).***

2.1.5 PSD95 knockout line

The PSD95 knockout line of mice was generated by Margaret Arbuckle and Seth Grant and has been previously published (Yao *et al.*, 2004; Abbas *et al.*, 2009). Details of the generation and characterisation of this line can also be found on the genes2cognition.org database. Mouse embryonic stem cells were targeted with a vector containing 5.2kb and 5kb of flanking genomic DNA. This was inserted in frame into exon 13 of the PSD95 encoding gene (*Dlg4*) with *neomycin/tk* cassette. Correctly targeted ES cells were injected into C57BL/6 blastocysts to create chimeric mice. F1 progeny were backcrossed on to C57BL/6J mice to establish a working colony, which was bred to homozygosity. This insertion of a premature stop codon resulted in the deletion of the area coding for the GK domain of the protein. This caused a near complete absence of PSD95 mRNA and no detectable levels of PSD95 protein in homozygous animals (Yao *et al.*, 2004).

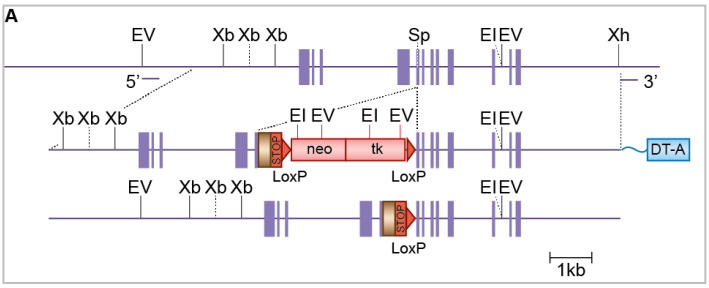

Figure 9 - Targeted mutation of the PSD95 gene.

PSD-95 genomic DNA with restriction enzyme sites (EI, EcoRI; EV, EcoRV; Sp, SpeI; Xb, XbaI; Xh, XhoI.); boxes, exons. With integrated targeting vector (middle) and targeted locus (bottom). tk, thymidine kinase gene; neo, neomycin resistance gene; HA, haemaglutinin epitope tag; STOP, stop codon; arrowheads, loxP sites; DT-A, Diptheria toxin A based vector. ***Figure and legend reproduced, with permission, from genes2cognition.org database.***

2.2 Behavioural paradigms

2.2.1 Open-field testing of ketamine behaviour

For all open-field experiments described below an empty arena of 50cm x 50cm x 25cm was used. At the beginning of each exploration session mice were placed into the centre of the arena and allowed to move freely with the experimenter hidden from their view for the duration of the recording. Movement of the animal was tracked by a ceiling-mounted camera connected to a computer with AnyMaze software (Stoelting Co.). Distance travelled by the animal per 5 min testing period was exported from this software and used for analysis.

2.2.2 Pilot study – Wild-type animals

All mice were 3-month-old C57BL6J males sourced from Charles River (Margate, Kent, UK). Mice were given 7 days to habituate to the animal facility and were then handled by the experimenter briefly once a day for 3 days prior to the start of the experiment. Mice were tested in groups of 4-5 per day in a rolling schedule. On day 1 of this protocol mice were brought into the testing room in home cages and given 30 minutes to acclimatize to the new environment. Mice were then individually placed in the open field (OF) arena and allowed to freely explore for 10 minutes. Mice were then placed back in their home cage and remained in the testing room for an hour before being placed back in the OF for another 10-minute habituation session. Mice were then placed back in their home cage and returned to their housing room. On day 2 of the protocol, mice were brought into the same testing room and again given 30 minutes to acclimatise. Each mouse was then placed back in the same OF arena for 5 minutes of baseline measurements to be taken, before being removed from the OF and given a subcutaneous (SC) injection of either sterile saline or 10mg/kg ketamine

(Vetalar) administered at 10ml/kg or brief handling (naïve control), before being placed immediately back in the OF for a further 55 minutes. Throughout this thesis, Ketamine refers to Vetalar, a ketamine hydrochloride injection manufactured by Boehringer Ingelheim and used regularly in veterinary practice. This is provided in sterile vials at a concentration of 100mg/ml and was diluted in sterile physiological saline (Sodium Chloride 0.9%, provided in vials from Hameln Pharmaceuticals). Please see **figure 10** for a timeline of this protocol, and **table 5** for group sizes. Experimenter was blinded to treatment, with the exception of the naïve control. Animals were culled after removal from the arena.

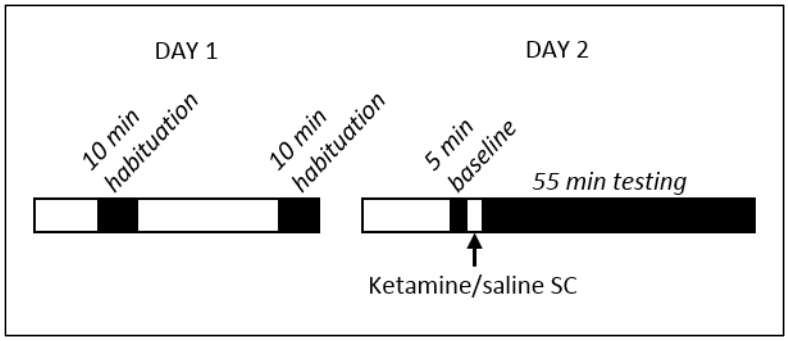

Figure 10 - Timeline of ketamine locomotion pilot study protocol.

Empty boxes represent time spent in home cage in testing room filled boxes represent time spent in open field arena.

2.2.2.1 Main study – GluN2B-2A, GluN2A-2B, PSD95KO & PSD93KO mutants

Mice were briefly handled by the experimenter for 3 (GluN2A-2B, PSD93KO) or 6 days (all other cohorts) prior to experimental day and were tested in groups of 3-4 per day in a rolling schedule. On day 1 of this protocol mice were brought into the testing room and given 30 minutes to acclimatize to the new environment. Mice were then individually placed in the open field (OF) arena and allowed to freely explore for 10 minutes. Mice were then placed back in their home cage and kept in the testing room for an hour before each being placed back in the OF for another 10 min habituation session. Mice were then placed back in their home cage and returned to their housing room. On day 2 of the protocol, mice were brought into the same testing room and given 30 minutes to acclimatise to the room. Each mouse was then placed back in the same OF arena for 15 minutes of baseline measurements to be taken, the mouse was then removed from the OF and given a subcutaneous (SC) injection of either sterile saline or 10mg/kg Vetalar administered at 10ml/kg, before being placed immediately back in the OF for a further 45 minutes. Please see **figure 11** for summary of protocol and **table 5** for information on group sizes.

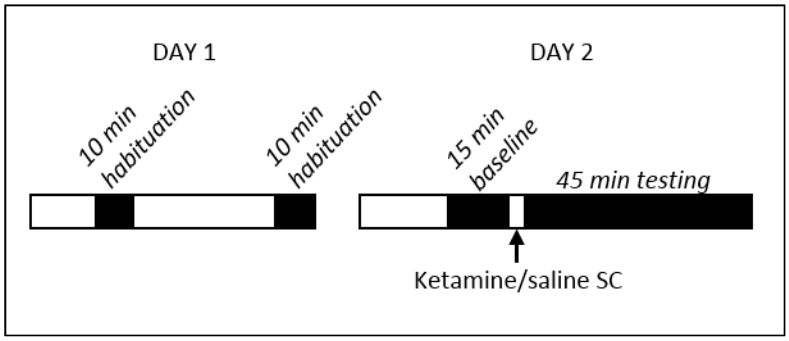

Figure 11 - Timeline of ketamine locomotion mutant study protocol

Empty boxes represent time spent in home cage in testing room filled boxes represent time spent in open field arena.

	Pilot	**GluN2B$^{2A(CTR)}$**		**GluN2A$^{2B(CTR)}$**		**PSD-93 KO**		**PSD-95 KO**		
	WT	WT	HOM	WT	HOM	WT	HOM	WT	HET	HOM
Saline	6	6	6			5	6			
Ketamine	6	9	9	12	12	7	7	11	8	11
Naïve	6									

Table 5 - Animal numbers per genotype and treatment group in ketamine locomotion experiments.

WT = wild-type animal, HET = animal heterozygous for knockout or swap mutation, HOM = animal homozygous for knockout or swap mutation. Grey boxes indicate that a group was omitted from this experiment. Saline control groups were omitted in the case of the GluN2A-2B and PSD-95 knockout experiments, this was due to limited availability of animals of the correct genotype.

2.2.2.2 Forced-swim testing of ketamine behaviour

6 mice (3m,3f) were treated with 10mg/kg ketamine administered as 10ml/kg SC. A further 6 mice (3m,3f) were treated with saline as a control, administered at 10ml/kg SC (**table 6**). 24 hours later mice were tested in the forced swim test. Mice were C57/BL6, 4-5mo. FST apparatus consisted of two plastic cylinders 25.5cm tall with a diameter of 14cm, containing water to a depth of 10cm and maintained at a temperature of 23-25°C (**figure 12**). Two animals were tested simultaneously and were separated from each other and the experimenter by opaque dividers. Each pair consisted of one saline and one ketamine-treated mouse. The test was carried out on one day in a quiet room with consistent light levels. The experimenter performing the FST was blinded to the treatments received. Mice were placed in the water for 6min and videos were recorded for scoring later. Only the last 4 min of each video was used for scoring. The videos were randomised and the experimenter

was blinded to the identity of each video. The criteria for immobility scoring was defined as the mouse remaining completely still, other than slight twitching or small involuntary movements as required to remain upright.

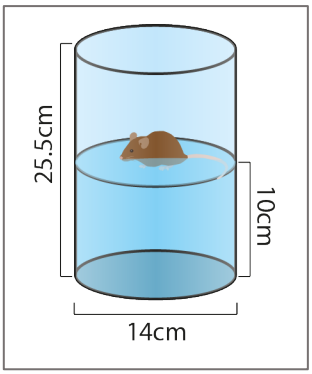

Figure 12 - Diagram of forced swim test apparatus.

	Pilot	**Pilot 2**
	WT	WT
Saline	6	3
Ketamine	6	3

Table 6 – Summary of animal numbers used in the FST pilot experiments.

2.3 Synaptome mapping

For the basal Arc synaptome map described in **section 4.3** $Arc^{VENUS/VENUS}$ mice were taken from their home cages and culled and processed as is described in **section 2.3.1** onwards. For the ketamine Arc and PSD95 synaptome mapping described in **sections 4.4-4.5** groups of animals were treated with either 100mg/kg ketamine (high dose) 10mg/kg ketamine (low dose) or sterile saline, all administered via a subcutaneous route at 10ml/kg. Mice were returned to their home cages following administration. At 1h, 6h or 24h animals were sacrificed and brains processed as described in **section 2.3.1** onwards. Please see **table 7** for group sizes. Ketamine treatment, perfusion and brain freezing for ketamine synaptome mapping was carried out by Dr Jess Nithianantharajah.

	1h			**6h**			**24h**		
	saline	Low	High	saline	Low	High	saline	Low	High
Arc-Venus	5	4	4	5	5	4	5	5	5
PSD95-eGFP							5	4	4

Table 7 - Animal numbers per treatment group and time point in ketamine synaptome mapping experiments.

2.3.1 Transcardial perfusion and freezing of samples

Mice were anaesthetised in by intraperitoneal (IP) injection of 0.1 mL of 20% pentobarbital sodium (Euthatal, Merial animal health Ltd.) Animals were placed back in their cage until unconscious, after which they were transported in the cage to a procedure room for

perfusion. When no responses were observed from pinching toes or tail, two tail samples were taken for PCR genotyping. The mouse was then pinned down on a cork surface and the thorax was opened to expose the heart. A small incision was made in the right atrium and 10mL of cold phosphate buffered saline (PBS, Fisher Scientific), followed by 10mL of cold 4% paraformaldehyde (PFZ, Alfa Aesar 16%, diluted 1:4 in PBS), was injected into the left ventricle. The brain was then dissected out and post-fixed in 4% PFA at 4°C for 3-4h. Brains were cryoprotected by incubation in 30% sucrose (VWR chemicals, w/v in PBS) at 4°C for 72h. Brains were then prepared for embedding by incubation in a 50:50 solution of optimal cutting temperature (OCT) medium (VWR international) and 30% sucrose for 1h at 4°C. Following this, brains were embedded in a plastic mould (Sigma-aldrich) containing OCT and immediately frozen in a container of isopentane (Sigma-Aldrich) placed in liquid nitrogen. Once frozen, brains were stored at -80°C. Brains were protected from the light as much as possible throughout the processing steps detailed above.

2.3.2 Cryosectioning

18µm thick coronal sections were cut with a cryostat (NX70 Thermo Fisher) and directly mounted on glass superfrost plus microscopy slides (Thermo Scientific). A drop of PBS was applied to each slide before collection of the section. The atlas used to guide sectioning was 'The Mouse Brain in Stereotaxic coordinates' by G. Paxinos and K. B. J. Franklin. Slides were then left to dry overnight at room temperature, during which time they were protected from light. Slides were then stored at -80°C. Some PSD95-eGFP samples were sectioned by Jamie Rose and Ellie Tuck.

2.3.3 Immunohistochemistry

Brain sections were first rinsed for 5 min in PBS. A PAP pen was then used to form a hydrophobic barrier encircling each brain section. For each incubation 50µl of solution was applied to each section, sections were kept in a dark, damp chamber throughout. Sections were incubated with blocking solution consisting of tris buffered saline (TBS, Fisher Scientific) containing 5% bovine serum albumin (BSA, Sigma-Aldrich) and 0.2% triton-X (Sigma-Aldrich) for 2 hours. Sections were then incubated with the same blocking solution containing a primary antibody against VGlut1 (cat no. 75-066, Neuromab), at a concentration of 1:250, overnight at 4°C. This was followed by 3x 10min washes with TBS containing 0.2% triton-X. Sections were then incubated with blocking solution containing an anti-mouse IGg1 Alexa Fluor 555 secondary antibody (cat no. A21127, ThermoFisher Scientific) at a concentration of 1:500, and 4',6-diamidino-2-phenylindole (DAPI, Sigma-Aldrich) at a concentration of 1:1000,

for 1 hour at room temperature. This was followed by 3x 10 min washes of TBS containing 0.2% triton-X, a final 10 min wash of TBS only was then carried out and coverslips were applied as described in **section 2.4.5**.

2.3.4 Preparation of Mowiol mounting medium

Mowiol was prepared by dissolving 96g of glycerol (Sigma-Aldrich, BioXtra >99%) and 38.4g Mowiol (Calbiochem) into 192 mL 0.2M Tris buffer (pH8.5) and 96 mL milliQ water (18.2MΩ) by heating to 50°C until clear. This solution was then centrifuged at 8,500 rpm for 15 min at 4°C, supernatant was collected and 2.5% DABCO (1,4-Diazabicyclo[2.2.2]octane, Sigma-Aldrich) added to prevent photobleaching.

2.3.5 Application of coverslips

Slides were removed from the freezer and allowed to dry for 1hr at room temperature, in the dark. Slides were then rinsed in PBS for 5 min, following which 10µl of Mowiol mounting media (see 2.6.3) was applied to each brain section. Each section was covered with a 13mm diameter round cover glass, thickness No. 1,5 (VWR International). Slides were left overnight at room temperature, in the dark, to allow the mounting media to 'cure'.

2.3.6 Spinning disk confocal Imaging

For synaptome mapping whole coronal sections were imaged with the Revolution XDi spinning disk microscopy (SDM) system from Andor technology. The use of this system for synaptome mapping was pioneered by Dr. Melissa Cizeron and full details can be found in her PhD thesis. Briefly the Revolution XDi system uses CSU-X1 which has a 50µm pinhole, and an Andor iXon Ultra monochrome back-illuminated EMCCD camera for detection. Images generated by this system are 16 bit depth and 512 x 512 pixels. Pixel size is 84nm. An Olympus uPlanSAPO 100X oil immersion lens (NA 1.4) was used for all image acquisition. Please see **table 8** for details on lasers and filters used for individual datasets.

Dataset	Laser line	Laser power	Exposure time	Emission filter	Frame averaging	EMCCD gain
Arc-Venus basal map	515nm	40%	120ms	540/30	2	250
Arc-Venus ketamine	488nm	10%	70ms	525/50	4	250
PSD-95 eGFP ketamine	488nm	60%	50ms	525/50	2	250
Arc-Venus with VGlut1 staining	515nm	40%	120ms	540/30	2	250
	561nm	40%	55ms		2	250
Arc-Venus with DAPI staining	488nm	40%	120ms	525/50	2	250
	405nm	18%	55ms	452/45	2	250

Table 8 - Spinning disk confocal microscope aquisition settings used for synaptome mapping datasets.

For synaptome mapping the SDM was set up to acquire sequential images across a rectangular grid with 0% overlap between adjacent tiles. The grid was defined by the user and covered the whole brain section. A small number (~4) of reference focus points were applied to the grid manually to create a map, from which the optimal focal plane for the intermediate tiles was calculated by the system and automatically applied during image acquisition. No z stack was taken. For imaging of VGlut1 and DAPI staining the SDM was used to take individual tile images. Three images were taken per target brain region per mouse.

2.3.7 Image analysis and quantification

The Ensemble method of puncta segmentation and quantification, which was applied to the Arc-Venus and PSD95-eGFP synaptome mapping datasets described in this thesis, was developed by Dr. Zhen Qiu and Melissa Cizeron. It is not related to the Ensembl Genome Browser. Full details and validation of the method can be found in Melissa's thesis and the first data generated using this method was recently published (Zhu *et al.*, 2018). All of the below puncta detection, characterisation and mapping functions were carried out by code written by Dr Zhen Qiu in either Matlab or Python, which was run either by Dr Zhen Qiu or Sarah Lemprière. Credit also goes to Alistair Tullo for work on earlier versions of the synaptome mapping pipeline.

2.3.7.1 Delineations

The grid of tiled images acquired by the SDM was manually segmented into defined anatomical regions of interest to enable informative analysis of the puncta detection data. First, a Matlab script written by Dr. Zhen Qiu was used to produce a low resolution overview

of each acquired grid, generated by downsizing the individual tile images by a factor of 16. These TIFFs were then stitched together using the grid dimensions present in the metadata (see **appendix 9** for Matlab script). These overview stitched images were then opened in Fiji/ImageJ. Image J is a public domain image processing program and can be downloaded for free (https://imagej.nih.gov/ij/download.html). Fiji is a version of ImageJ which comes pre-loaded with plugins for scientific image analysis and is also freely available (https://imagej.net/Fiji/Downloads). The 'polygon selection' tool was then used to delineate the borders of individual anatomical regions contained in the brain section as defined by the Allen Mouse Brain Atlas (http://mouse.brain-map.org). Each region was then added as a region of interest in the Fiji ROI manager and all regions for one brain section were saved as a zip file for use in generation of the synapse maps.

2.3.7.2 Generation of training set and manual punctum counting

The Ensemble method first requires the generation of a training set of images, which are a subset of the total dataset to be analysed. These were randomly selected by Dr Zhen Qiu, from a combination of brain regions and sections representative of the range of synaptic characteristics present in the dataset as a whole. This was carried out separately for the Arc-Venus dataset and the PSD95-eGFP dataset. The 'Cell Counter' plugin for Fiji, built by Kurt De Vos (https://imagej.nih.gov/ij/plugins/cell-counter.html), was used to record the coordinates of puncta within each of the training set images, as defined by the individual observer. The Arc-Venus basal training set was counted independently by 4 individuals, these were Dimitra Koukaroudi, Malik Yousuf, Alexander Gunn and Sarah Lemprière. The Arc-Venus ketamine training set was counted independently by 3 individuals, these were Ellie Tuck, Jess Nithianantharajah and Sarah Lemprière. The PSD95-eGFP training set (288 images) was counted by Dr Melissa Cizeron, Vlad Anto and Andreii Kolesnyk.

2.3.7.3 Generation of Synaptic puncta detection parameters

This set of training images, with their accompanying puncta coordinates, were then used to train an algorithm designed to select a set of puncta detection parameters. This method differs from previously used image analysis methods in that it uses several different filters or thresholds and intelligently combines the thousands of detection results. The combination of thresholds/filters and other parameters are trained automatically by a machine learning algorithm, called ensemble learning, to produce a detection result as close as possible to the manual detection carried out on the training image set. This method of parameter selection was designed and carried out by Dr Zhen Qiu. One set of parameters was chosen for each

Arc-Venus training set (488nm and 515nm acquisition) and one for the PSD95-eGFP training set. The PSD95-eGFP parameters were determined from a training set drawn from Dr Melissa Cizeron's data and had previously been used to analyse the data in her thesis and in the recent publication (Zhu *et al.*, 2018). Those, and the chosen Arc-Venus parameters, were then used to detect puncta in the datasets presented in this thesis, using the pipeline described below.

2.3.7.4 Generation of synapse maps

The puncta detection parameters determined by the manual counting described above were then applied to entire SDM datasets using code written by Dr Zhen Qiu. This code also segmented puncta and determined their mean pixel intensity and overall size. The steps involved in this process are summarised below and in **figure 13**.

Step 1: Puncta segmentation

Prior to segmentation the 512 x 512 pixel tiles acquired by the SDM were each split up into 4 smaller tiles of 256 x 256 pixels. The puncta detection parameters were then applied to each tile and the characteristics of the detected fluorescent puncta, such as their size, shape and fluorescence intensity were quantified. In order to do this the 9 pixels with the highest intensity were identified for each punctum, an average intensity of these 9 was calculated and the edge of the punctum was defined by the first pixels to fall below a certain percentage of that maximum intensity level. For the datasets presented here that percentage was 15%. Once the boundaries of each punctum were defined, the mean intensity and the size of each punctum was calculated. The mean intensity value is the average intensity of all pixels contained within the punctum. The size value is the number of pixels contained within the punctum. A text file containing the coordinates of each individual punctum along with its characteristics was generated for each 256 x 256 pixel sub tile.

Step 2: Generation of a 3D array 'Stat_Sum' image

The text files generated in step 1 were then translated into a 3D array in which each pixel represents one sub-tile. In this array x and y are the coordinates of the sub-tile and each measurement (Puncta number, size and intensity) is represented at a different z level. The value for the pixels within this array are determined by the sum of the given measurement for all puncta within the sub-tile represented. The mean value per sub-tile was then calculated by dividing this sum by the number of puncta detected within that sub-tile.

Step 3: Generation of binary masks

The .zip files containing the manually delineated regions were then converted into a set of binary masks, one per region.

Step 4: Generation of the regional values 'Stat_Region'

The binary masks were then applied to the 'Stat_Sum' array to determine which sub-tiles were contained within a given region. A median value was then calculated for each measurement, for each delineated region. These were exported as a Microsoft Excel file and used for analysis.

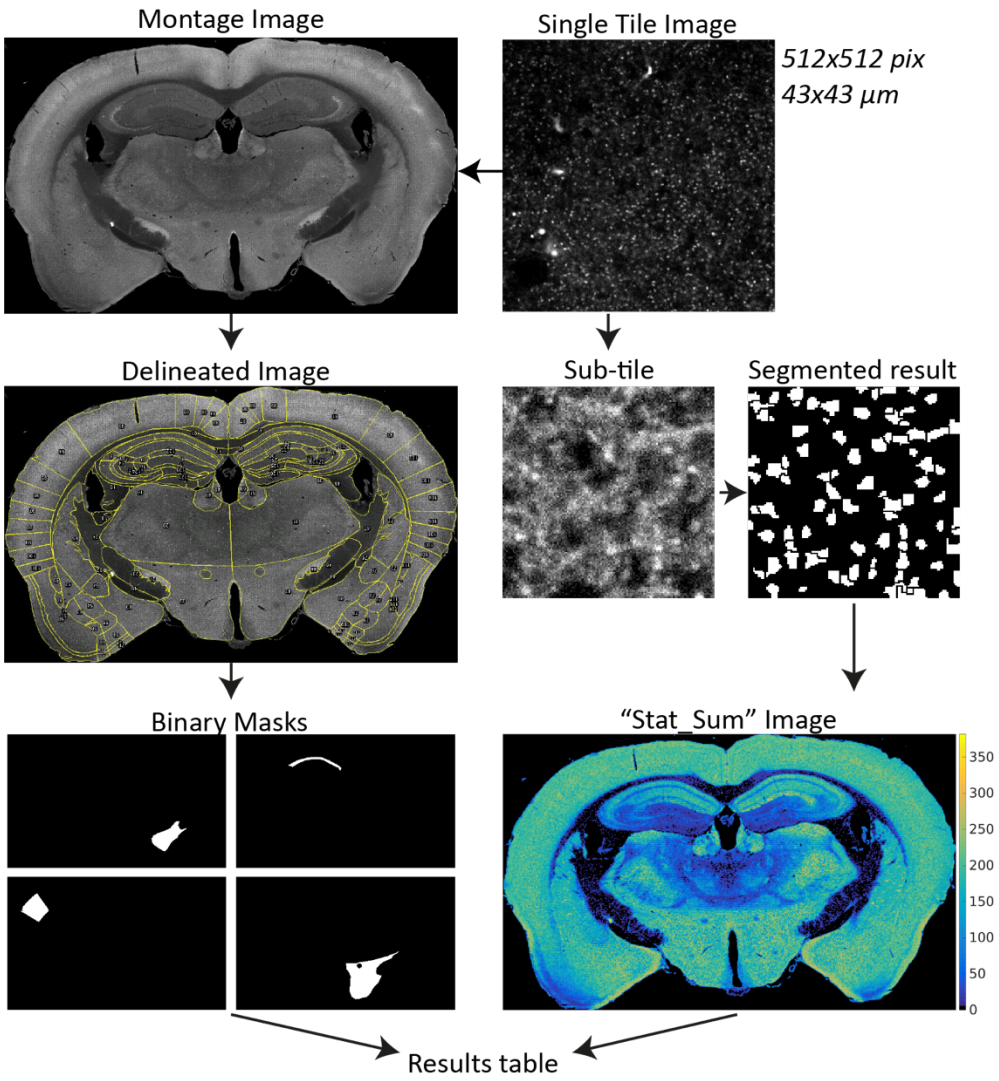

	A	B	C	D
1	region	count_for_stats	area	mean
2	main_RoiSet_Montage_GGV430_sHC_BASALMAP_28_20170829_115812_alv_L	1	10.5	3907.5
3	main_RoiSet_Montage_GGV430_sHC_BASALMAP_28_20170829_115812_alv_R	2	12.21111	4581.875
4	main_RoiSet_Montage_GGV430_sHC_BASALMAP_28_20170829_115812_AUDd_L	161	13.3271	9524.632
5	main_RoiSet_Montage_GGV430_sHC_BASALMAP_28_20170829_115812_AUDd_L1_L	188	13.1725	9981.862
6	main_RoiSet_Montage_GGV430_sHC_BASALMAP_28_20170829_115812_AUDd_L1_R	247.5	12.61717	10306.98
7	main_RoiSet_Montage_GGV430_sHC_BASALMAP_28_20170829_115812_AUDd_L23_L	193	13.76536	10458.79
8	main_RoiSet_Montage_GGV430_sHC_BASALMAP_28_20170829_115812_AUDd_L23_R	234.5	13.06112	10621.7
9	main_RoiSet_Montage_GGV430_sHC_BASALMAP_28_20170829_115812_AUDd_L4_L	184.5	13.45056	10724.16
10	main_RoiSet_Montage_GGV430_sHC_BASALMAP_28_20170829_115812_AUDd_L4_R	237.5	12.85098	11444.49
11	main_RoiSet_Montage_GGV430_sHC_BASALMAP_28_20170829_115812_AUDd_L5_L	144	13.33112	8896.005
12	main_RoiSet_Montage_GGV430_sHC_BASALMAP_28_20170829_115812_AUDd_L5_R	181	12.82294	10059.32
13	main_RoiSet_Montage_GGV430_sHC_BASALMAP_28_20170829_115812_AUDd_L6a_L	142.5	12.82104	8160.513
14	main_RoiSet_Montage_GGV430_sHC_BASALMAP_28_20170829_115812_AUDd_L6a_R	179	12.43455	9828.065
15	main_RoiSet_Montage_GGV430_sHC_BASALMAP_28_20170829_115812_AUDd_L6b_L	41	13.24138	6217.127
16	main_RoiSet_Montage_GGV430_sHC_BASALMAP_28_20170829_115812_AUDd_L6b_R	85	12.4876	7564.934
17	main_RoiSet_Montage_GGV430_sHC_BASALMAP_28_20170829_115812_AUDd_R	200	12.71419	10294.3
18	main_RoiSet_Montage_GGV430_sHC_BASALMAP_28_20170829_115812_AUDp_L	150	13.4381	9127.845
19	main_RoiSet_Montage_GGV430_sHC_BASALMAP_28_20170829_115812_AUDp_L1_L	172.5	13.17342	9655.299
20	main_RoiSet_Montage_GGV430_sHC_BASALMAP_28_20170829_115812_AUDp_L1_R	226	12.86283	9609.011
21	main_RoiSet_Montage_GGV430_sHC_BASALMAP_28_20170829_115812_AUDp_L23_L	167	13.88205	10032.32
22	main_RoiSet_Montage_GGV430_sHC_BASALMAP_28_20170829_115812_AUDp_L23_R	214	13.24375	10470.87
23	main_RoiSet_Montage_GGV430_sHC_BASALMAP_28_20170829_115812_AUDp_L4_L	171	13.48214	10697.15
24	main_RoiSet_Montage_GGV430_sHC_BASALMAP_28_20170829_115812_AUDp_L4_R	222.5	12.98505	11243
25	main_RoiSet_Montage_GGV430_sHC_BASALMAP_28_20170829_115812_AUDp_L5_L	132	13.51724	8711.429

Figure 13 - Schematic diagram of image analysis pipeline

2.3.7.5 Analysis of VGlut1 and DAPI staining

For VGlut1 and DAPI staining images synaptome mapping was not carried out. One of three mice imaged was selected as representative of the group, representative images were selected from that mouse for visual presentation in this thesis.

2.4 Statistical analysis

2.4.1 Analysis of behavioural testing data

Each behavioural testing dataset consisted of two or more treatment/genotype groups and 16 time periods. In order to compare between treatment/genotype groups at each individual time period ordinary two-way ANOVAs were used. These were followed by the appropriate post-hoc multiple comparisons testing for the number of treatment/genotype groups being compared. For a two-group comparison (e.g. **figure 17A**) Sidak's multiple comparisons test was used, for more than two groups (e.g. **figure 16A)** Tukey's multiple comparisons test was used. In the case of multiple groups being compared to one control group (e.g**. figure 18A)** Dunnett's multiple comparisons test was used.

In addition to this comparison of all 16 time periods, the total distance travelled during the first 15 min post-administration was compared between treatment/genotype groups. All datasets were found to be normally distributed with the Shapiro-Wilk test of normality. For datasets with only two treatment/genotype groups an unpaired t-test was carried out. For datasets with more than two treatment/genotype groups an ordinary one-way ANOVA was carried out, followed by Tukey's multiple comparisons test. All tests were carried out using the Prism statistical package (GraphPad Software, San Diego).

2.4.2 Analysis of synaptome mapping data

For the basal Arc synaptome map presented in **section 4.4** of this thesis a two-way ANOVA, followed by Sidak's multiple comparisons was used to test for a significant difference between the left and right hemispheres in the 7 main anatomical regions. As no significant difference in puncta density, size or intensity was identified between hemispheres in the basal Arc map, for the ketamine synaptome mapping data an average value of both hemispheres was calculated for each of the anatomical regions in each mouse.

For the ketamine synaptome mapping experiments, presented in **sections 4.6 & 4.7,** multiple t-tests, one per brain region, were used to compare the saline group to each of the treatment groups. In this analysis no correction for multiple comparisons was used, therefore increasing the likelihood of false positives. However, a form of correction was implemented in the interpretation of these results by focusing on clusters of significantly-affected regions within a common anatomical area. If several related regions are changing together this reduces the chance of the individual results being false positives. A common form of correction for multiple comparisons is the Bonferroni correction, in order to reduce the likelihood of false positives this correction is carried out by testing each individual hypothesis with a higher

significance threshold. The corrected threshold is calculated by dividing the original threshold (usually p<0.05) by the number of comparisons, in the case of the synaptome data this is 86, one comparison per brain regions. Applying the Bonferroni correction to this data would change the critical p value from the usual p<0.05 to p<0.00056. Therefore, regions with p values of >0.00056 and not surrounded by significant changes in one or more anatomically-related regions will not be discussed.

The Cohen's d effect size of the change in synaptome map properties from saline control, to either the high- or low- ketamine dose groups was calculated for each region using the equation below:

$$d = \frac{\bar{x}_1 - \bar{x}_2}{s}.$$

Where *x* is the mean and *s*, the pooled standard deviation, is defined as:

$$s = \sqrt{\frac{(n_1 - 1)s_1^2 + (n_2 - 1)s_2^2}{n_1 + n_2 - 2}}$$

This gives a number based on the number of standard deviations which separate the means of the two groups. The more SDs between the means, the larger the Cohen's d value. A positive value is an increase from the control group and a negative value is a decrease from the control group. For the ketamine synaptome data these Cohen's d values were presented on a colour scale with positive values on a white-red scale and negative values on a white-blue scale. Please see **appendix 17** for visual examples of the spread of data points resulting in different effect size values.

Chapter 3 Ketamine-induced behaviour in PSD protein mutant mice

3.1 Introduction

Ketamine has both short-term psychotomimetic, and long-term antidepressant, effects in humans and in rodent models. In rodent models, the short-term psychotomimetic effects have been studied by observing the behaviour of animals in an open field arena immediately after ketamine administration. Transient hyper-locomotion following administration of a sub-anaesthetic dose of ketamine has been reported (Irifune *et al.*, 1991) and this response is reduced by treatment with antipsychotic medication (Irifune *et al.*, 1998; Chatterjee *et al.*, 2011). The hyper-locomotive response in rodents is thought to be a correlate of the short-term psychotomimetic response observed in human subjects (Zarate *et al.*, 2006), which can include psychomotor agitation (Domino, 1984). The long-term antidepressant effects of ketamine have been frequently assessed in rodents using behavioural despair paradigms (Rosa *et al.*, 2003; Autry *et al.*, 2011), in which an animal is placed in an uncomfortable situation and the time spent immobile, or not trying to escape, is recorded. Decreased immobility time is taken as evidence of antidepressant action and can be induced by existing antidepressant medications (Cryan *et al.*, 2005; Pollak *et al.*, 2010). In the case of sub-anaesthetic does of ketamine, a reduction in immobility time has been reported from 30 min to 7 days post-administration (Autry *et al.*, 2011; Tizabi *et al.*, 2012).

Although its primary action is thought to be NMDA receptor antagonism, the molecular mechanism(s) underlying ketamine's effects are still unclear. Recent evidence has strongly implicated GluN2B-containing NMDA receptors in ketamine's antidepressant action (Miller *et al.*, 2014). However, ketamine appears to bind to both GluN2A- and GluN2B-containing receptors with the same affinity (Yamakura *et al.*, 1993; Kotermanski & Johnson, 2009), it is therefore unclear how this specificity is arising. The amino acid sequences of the GluN2A and 2B subunits are highly similar, with the exception of the c-terminal domain (CTD) (Ryan *et al.*, 2008). The sequence divergence in the CTD of these two subunits results in a specific set of intracellular interactors for each. For example, the GluN2B CTD interacts specifically with CaMKII, RasGFR1 and SynGAP (Leonard *et al.*, 1999; Strack *et al.*, 2000; Krapivinsky *et al.*, 2003; Kim *et al.*, 2005). The GluN2B CTD is also specifically required, in combination with PSD95 and PSD93, for assembly of the 1.5MDa supercomplexes found at the PSD. Absence of any one of these three elements prevents formation of the supercomplex (Frank *et al.*, 2016). Several members of the NMDAR supercomplex have also been found to be upregulated following ketamine administration, these include PSD95 and Arc (Li *et al.*, 2010). This divergence of the CTD between GluN2A and 2B, and the specific role of the GluN2B CTD

in forming supercomplexes, raises the question of whether the reported GluN2B specificity of the ketamine response could be explained by a specific action of its CTD. **The aim of the experiments described in this chapter therefore, was to establish whether the CTD of the GluN2B subunit is functionally important for the action of ketamine, and whether this is due to its role in assembling the 1.5MDa supercomplex at the PSD.** In order to achieve this, the short-term hyper-locomotive response to ketamine was assessed in several mouse lines, each containing mutations in one of the proteins of interest.

3.2 Summary of methods used in this chapter

3.2.1 Animals

In order to dissect out the role of the GluN2B c-terminal domain in ketamine action, independent from that of its ligand-binding or transmembrane domains, two complementary mutant mouse lines were used. The GluN2B$^{2A(CTR)}$ line contains a replacement of the GluN2B CTD with the CTD of the GluN2A subunit. The GluN2A$^{2B(CTR)}$ line contains the inverse: a replacement of the GluN2A CTD with that of the GluN2B subunit. This genetic manipulation leaves the remaining domains of the receptor unchanged. These animals show no alteration in total amount of the modified subunit and display normal synaptic NMDA current and AMPA/NMDA ratio, suggesting that synaptic localisation of these receptors is not altered by the CTD replacement (Martel *et al.*, 2012; Ryan *et al.*, 2013).

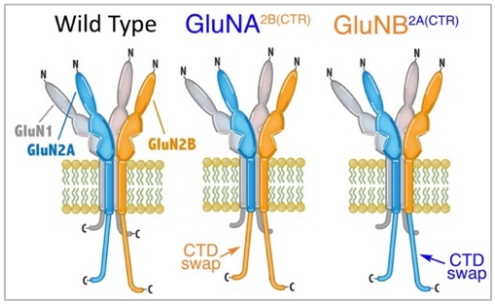

Figure 14 - Schematic diagram showing the replacement of c-terminal domains in GluN2A$^{2B(CTR)}$ and GluN2B$^{2a(CTR)}$ mutants.

In order to investigate the roles of PSD95 and PSD93 in the action of ketamine, two knockout mouse lines were used. The PSD95 knockout line contains a deletion of the part of the gene encoding the GK domain of the protein. This results in near complete absence of PSD95 mRNA, through nonsense-mediated decay, and no detectable protein in homozygous animals (Yao *et al.*, 2004; Abbas *et al.*, 2009). In the PSD93 knockout line the exon containing PDZ domain 2 has been removed, this results in disruption of the gene and the absence of PSD93 protein in homozygous animals (McGee *et al.*, 2001).

3.2.2 Ketamine-induced hyper-locomotion

For the pilot open-field locomotion study 3-month-old C57BL6J males were sourced from Charles River (Margate, Kent, UK). Animals were habituated to the open field (OF) arena during two 10 min exploration sessions the day before the experimental day. On the experimental day animals were given a 5-minute acclimatisation period in the arena. Ketamine (10mg/kg at 10ml/kg) or saline (10mg/kg) was administered via subcutaneous (SC) injection and animals were immediately placed back in the arena for a 55 min testing period. A naïve control group was also included, animals in this group were briefly removed from the open field arena after the acclimatisation period before being placed back in for the testing period. All groups in the pilot study contained 6 animals. For the subsequent open-field locomotion experiments GluN2B$^{2A(CTR)}$, GluN2A$^{2B(CTR)}$, PSD95 knockout and PSD93 knockout animals were bred to homozygosity. For the PSD95 knockout experiment a group of animals heterozygous for the mutation were also used. Wild-type controls were also sourced from the same colonies. These experiments followed a similar format to the pilot study: two habituation sessions of 10 min each were carried out the day before the experiment. However, on the experimental day the acclimatisation period was extended to 15 min. As before, ketamine (10mg/kg at 10ml/kg) or saline (10ml/kg) was then administered via SC injection. The testing period began immediately after injection and lasted 45 min. During all periods in the open-field arena movement of the animal was tracked by a ceiling-mounted camera connected to a computer with AnyMaze software (Stoelting Co.). Distance travelled by the animal per 5 min testing period was exported from this software and used for analysis. For this study the group sizes varied depending on the mutant line, for PSD95 knockout and GluN2A$^{2B(CTR)}$ swap animals a saline control group was omitted due to lack of available animals see **table 5 in chapter 2.**

3.2.3 Ketamine-induced 'antidepressant effects'

For the first forced swim test pilot study, 4-5-month-old wild-type C57BL6J mice were sourced from an in-house colony. 10mg/kg ketamine or saline was administered at a volume of 10ml/kg via SC injection; 6 animals were included in each treatment group. Animals were briefly handled for several days prior to the experimental day to acclimatise them to the experimenter. 24h following administration animals were placed in a plastic cylinder containing water to a depth of 10cm, meaning they could not reach the base of the cylinder and had to float or swim. Mice remained in the water for 6 min, during which their behaviour was recorded with a fixed camera. The last 4 mins of each video was scored in a blinded

fashion for time spent immobile. For the second pilot study the protocol was adapted as follows. Injection volume was reduced to 5ml/kg maintaining final dosage at 10mg/kg, this was with the aim of increasing the efficiency of dose delivery. The depth of water was increased to 20cm. Steps were also taken to decrease the stress of the animals by handling them more frequently prior to the experimental day. This second pilot study was carried out by Victoria Hohendorf, an undergraduate student, under the supervision of Dr Szu-Han Wang and Sarah Lemprière.

3.2.4 Statistical analyses

The statistical tests used varied depending upon the nature of the dataset and are described in the legend of each figure. All tests were carried out using the Prism statistical package (GraphPad Software, San Diego).

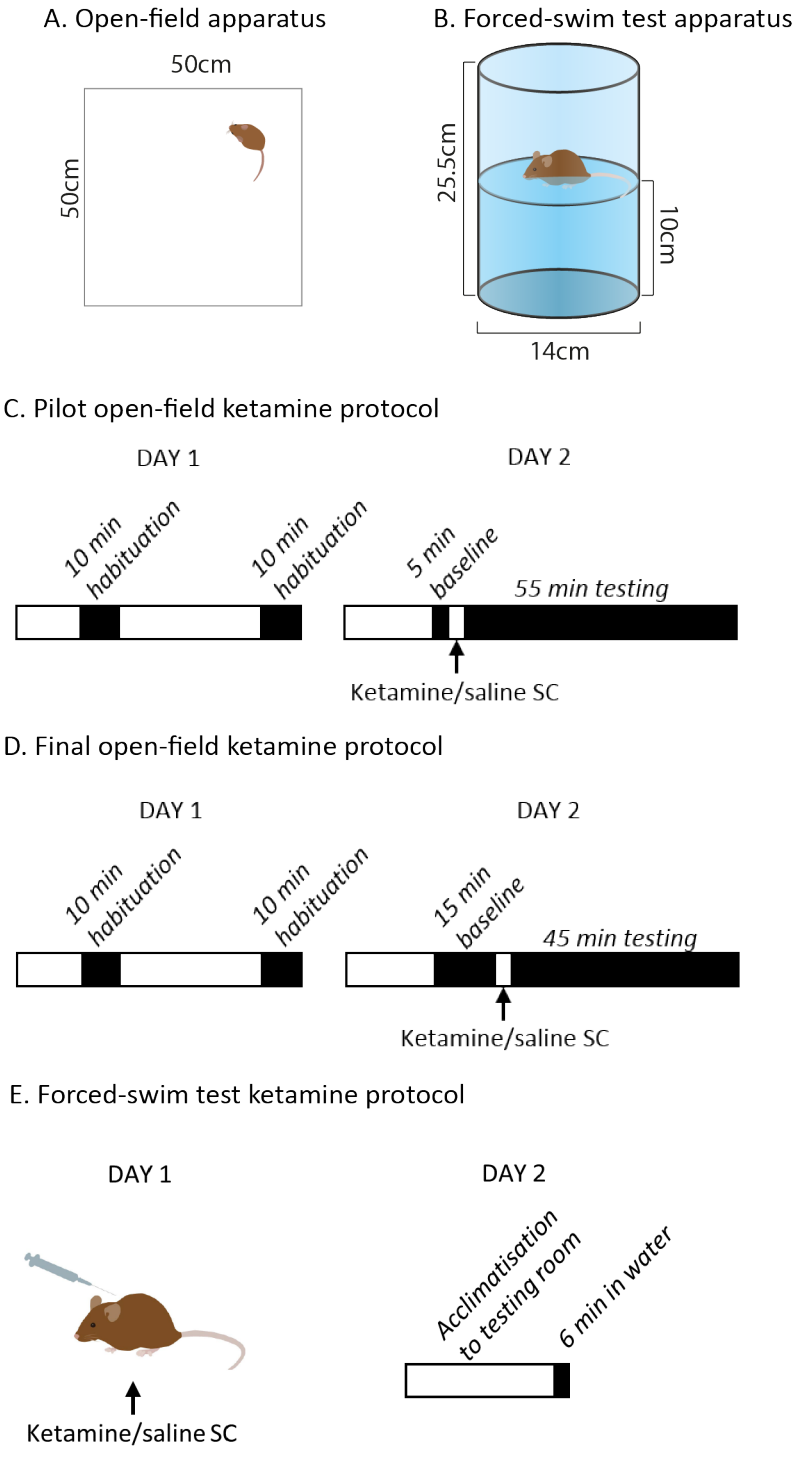

Figure 15 - Summary diagram of ketamine behavioural testing apparatus and protocols.

(Continued on following page) A. *Open-field apparatus used for ketamine-induced hyper-locomotion testing. Open-field arena measured 50cm x 50cm and the walls were 25cm high. Movement of mice was tracked by a ceiling mounted camera. Coat colour of all mice was black, open field arena was constructed from white plexiglass.* ***B.*** *Forced-swim test apparatus used for testing of ketamine-induced antidepressant effects. Animals were placed in a clear cylinder filled with water to a depth of 10cm, kept at a temperature of 23-25°C. Movement of*

the animals was recorded by a tripod mounted camera recording a side view of the cylinder. ***C.*** *Pilot open-field ketamine protocol. Day one contained two 10 min habituation sessions in the open field arena, separated by 1h rest in the home cage. Day 2 contained one 5 min baseline recording session, followed immediately by SC administration of ketamine of saline, and a further 55 min recording session.* ***D.*** *Final open-field ketamine protocol. Day 1 contained two 10 min habituation sessions in the open field arena, separated by a 1h rest period in the home cage. Day 2 contained one 15 min baseline recording session, followed immediately by SC administration of ketamine or saline, and a further 45 min testing session.* ***E.*** *Forced-swim test ketamine protocol. Administration of ketamine or saline was carried out on day 1. On day 2, 24h post-administration, animals were tested in the forced-swim test for 6 min. The last 4 min of the testing session was used for scoring.*

3.3 Ketamine-induced hyper-locomotion results

3.3.1 Pilot study

In this protocol two habituation sessions were used to enable the animal to acclimatise to the OF arena prior to the testing day. During these two habituation sessions the average distance travelled by all groups gradually decreased as mice became more familiar with the environment and reduced their exploratory behaviour. Mean distance travelled decreased significantly from 18.55m during the first 5 min of to 10.34m during the final 5 min of habituation ($p<0.0001$, **figure 16B**). This response to repeated OF exposures is well documented (Bolivar *et al.*, 2000). In the ketamine-treated group there is then a significant increase in distance travelled at 5, 10 and 15 min post-administration, as compared with either the saline-treated or naïve groups (**figure 16A**. KET vs SAL: 5 min $p<0.0001$, 10 min $p<0.0001$, 15 min $p<0.0001$). This reaches a peak during the 5-10 min post-administration at which point there is a 137% increase in mean distance travelled from the 5 min 'baseline' period immediately preceding ketamine administration (BL = 12.87m, 5-10 min post-administration = 30.54m). This time course of hyper-locomotion is consistent with published findings, where 10mg/kg ketamine induced an increase in locomotion during the 0-10 min post-administration, but was close to baseline during the 10-20 min period (Irifune *et al.*, 1991). Based upon this evidence, for the remaining open-field experiments presented here I have defined the 'ketamine response window' as the 15 min immediately following ketamine administration. **Figure 16C** shows a significant increase in total distance travelled during the ketamine response window in the ketamine-treated group (KET v SAL $p = 0.0002$, KET v NAÏVE $p = 0.0004$, SAL v NAÏVE $p = 0.9336$).

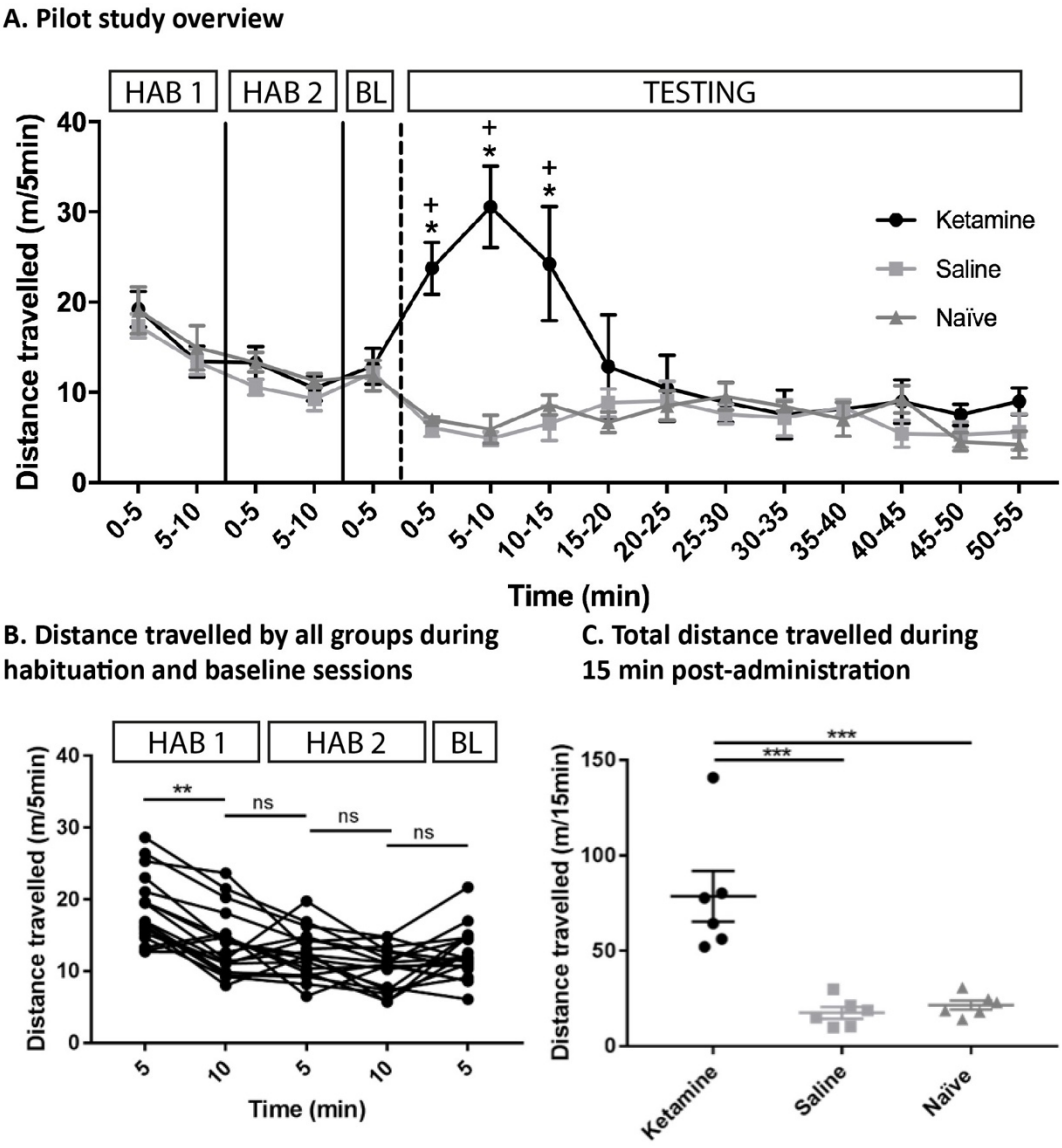

Figure 16 - Ketamine-induced changes in locomotion in wild-type C57BL6 mice.

A*. Distance travelled in open-field arena per 5 min segment across all open field sessions. Data points = mean, error bars = standard error of the mean (SEM). * = p<0.0001 KET vs SAL, + = p<0.0001 KET vs NAÏVE, two-way ANOVA with Tukey's multiple comparisons test.* ***B****. distance travelled by individual mice per 5 min during habituation and baseline sessions. Data points = individual animals. All treatment groups pooled. ns = p>0.05, ** = p<0.01, one-way ANOVA with Bonferroni multiple comparisons test* ***C****. Distance travelled in open-field arena during the 15 min immediately following ketamine administration. Data points = individual animals, error bars = SEM. *** = p<0.001, one-way ANOVA with Tukey's multiple comparisons test. N = 6 animals per group. HAB = habituation session, BL = Baseline session.*

3.3.2 GluN2B-2A & GluN2B-2A swap mutants

Here, two complementary genetically modified mouse lines were used, in the first of which ($GluN2B^{2A(CTR)}$) the CTD of the GluN2B NMDA receptor subunit has been replaced with that of the GluN2A subunit, leaving the other receptor domains unchanged. $GluN2B^{2A(CTR)}$ animals

travelled further than wild-type during the second habituation session, and the first 10 min of the baseline session (GDL vs WT: HAB2 0-5 min p = 0.0005, HAB2 5-10 min p = 0.04, BL 0-5 min p < 0.0001, BL 5-10 min p = 0.0158). Indeed, when total distance travelled during the entire habituation time is compared, GluN2B $^{2A(CTR)}$ mutants travelled significantly further than wild-type controls (**appendix 2**). This suggests a baseline level of increased locomotion, which could be interpreted as this mutation mimicking the effects of sub-anaesthetic ketamine. However, there was no significant difference between GluN2B$^{2A(CTD)}$ and wild-type during the 5 minutes immediately preceding ketamine administration, suggesting that GluN2B$^{(2ACTR)}$ mutant animals are able to be habituated to an environment and no-longer exhibit unusual levels of locomotion when the open field arena is familiar to them. From **figure 17A** it is clear that the wild-type animals are responding to ketamine in a similar way to those in the pilot study, displaying a significantly greater amount of locomotion than the saline group at 0-5 (p = 0.0016), 5-10 (p < 0.0001) and 10-15 min (p = 0.0198) post-administration. Again, the peak distance travelled by wild type animals was reached during the 5-10 min post ketamine administration and this was a 136% increase from the final 5 min of baseline recording (BL = 8.74m, 5-10 min = 20.86m). However, no such ketamine-induced increase was seen in the GluN2B$^{2A(CTD)}$ group. There was no difference between saline- and ketamine- treated GluN2B$^{2A(CTD)}$ animals at any time point during the protocol. In fact, at the time point when wild-type animals are exhibiting their peak ketamine-induced hyper-locomotion, the distance travelled by the GluN2B$^{2A(CTD)}$ group shows a 33% reduction from baseline level (BL = 12.29m, 5-10 min = 8.23m). This lack of a response to ketamine in the GluN2B$^{2A(CTD)}$ group is clear when total distance travelled during the 15 min 'response window' is compared (**Figure 17C**). There is a significant increase in the wild-type ketamine group (mean distance 48.09m KET, 16.13 SAL, p = 0.0070) but no significant difference in distance travelled between the ketamine- and saline-treated GluN2B$^{2A(CTD)}$ animals (mean distance 26.16 KET, 24.62 SAL, p = 0.9981). This shows that in the absence of the GluN2B CTD animals do not respond to ketamine by exhibiting short-term hyper-locomotion.

In the second of these complementary mouse lines (GluN2A$^{2B(CTD)}$) the reverse swap has taken place, to replace the GluN2A CTD with that of the GluN2B subtype. In this case a saline control group was omitted due to limited numbers of mutant animals available. Following ketamine administration wild-type animals exhibited a peak 60% increase in distance travelled from baseline level (BL = 11.15m, 5-10 min post-administration = 17.84m) suggesting that ketamine is acting to increase locomotion, although to a lesser degree than

in the previous two control groups (previously 137% and 136%). The GluN2A$^{2B(CTD)}$ mutant group displayed a significantly greater level of locomotion in the 15 min following ketamine administration than wild-type (**figure 17D**, mean distance 46.32m WT, 70.59m GluN2A-2B, p = 0.0019). There is also a trend towards increased locomotion in these mutants during some of the habituation and baseline recording sessions, prior to ketamine administration, this does not reach significance in the sidak's multiple comparisons test for any individual 5 min time period. However, there is a significant increase in the sum distance travelled during all habituation periods in the GluN2A$^{2B(CTR)}$ group (**appendix 2**). Therefore, it will be essential to repeat this experiment with saline control groups to ensure that the increased ketamine-induced locomotion is indeed an exaggerated response to ketamine and not a reflection of increased background levels of locomotion in these mutants (see **section 3.6**). However, the percentage change in locomotion from baseline to the peak of ketamine effect in the mutant group is 128%, considerably larger than the 60% displayed by the wild type group. This suggests that in the absence of the GluN2A CTD, and in the presence of additional GluN2B CTDs, there is an exaggerated hyper-locomotive response to ketamine. This provides further evidence for the GluN2B CTD having an essential role in the ketamine response.

Figure 17 – Effect of GluN2 c-terminal domain swap mutations on ketamine-induced hyper-locomotion (following page).

A. *Distance travelled by GluN2B$^{2A(CTR)}$ mutant and wild-type animals per 5 min across all open field exploration sessions. Asterisks represent a significant difference between the saline- and ketamine- treated wild-type groups (* = p<0.05). There were no significant differences detected between the saline- and ketamine- treated GluN2B$^{2A(CTR)}$ groups. 2-way ANOVA with Sidak's multiple comparisons test.* ***B.*** *Distance travelled by GluN2A$^{2B(CTR)}$ mutant and wild-type animals per 5 min across all open-field exploration sessions. * = p<0.05 GluN2A$^{2B(CTR}$ KET vs WT KET, 2-way ANOVA with Sidak's multiple comparisons test.* ***C.*** *Effect of GluN2B$^{2A(CTR)}$ mutation on distance travelled during ketamine response window. ns = p>0.05, * = p<0.05, ** = p<0.01, one-way ANOVA with Tukey's multiple comparisons test.* ***D.*** *Effect of GluN2A$^{2B(CTR)}$ mutation on distance travelled during ketamine response window. ** = p<0.01, unpaired t-test.* ***A & B*** *data points = mean, error bars = SEM.* ***C & D*** *data points = individual animals, error bars = SEM.*

A. Distance travelled by GluN2B-2A swap mutant and wild-type animals: all sessions

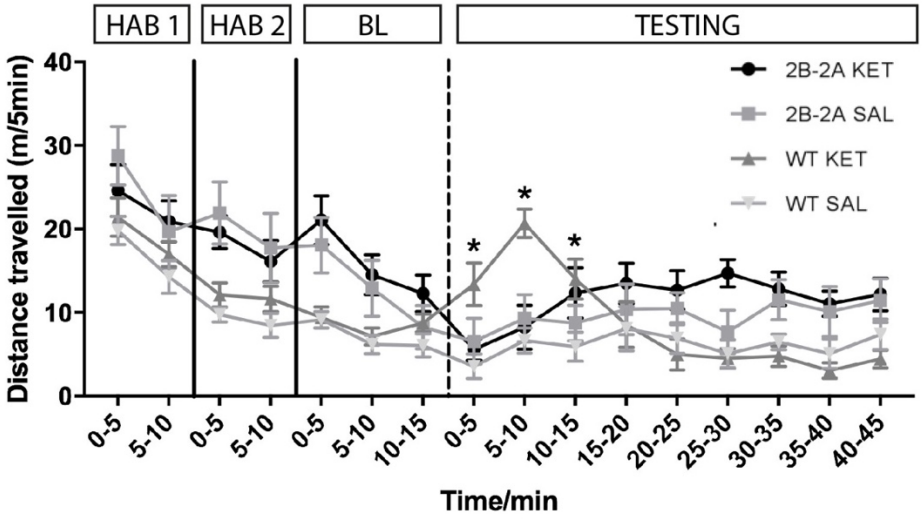

B. Distance travelled by GluN2A-2B swap mutant and wild-type animals: all sessions

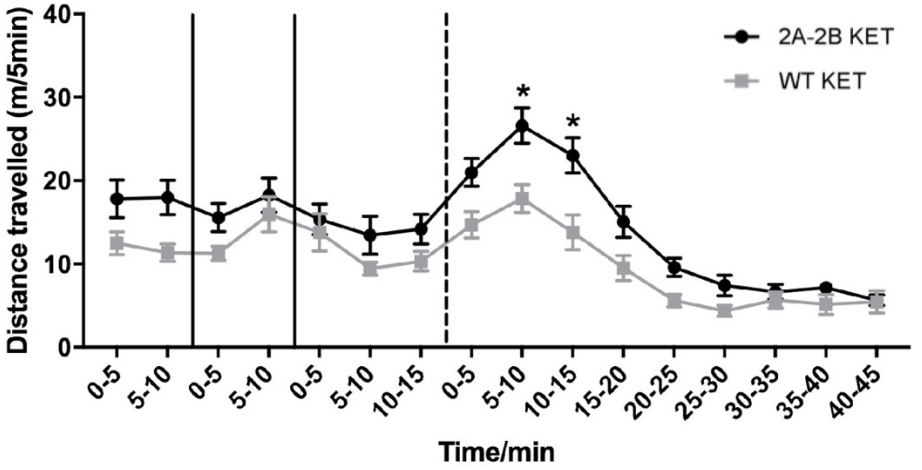

C. Distance travelled by GluN2B-2A swap mutant and wild-type animals: ketamine response window

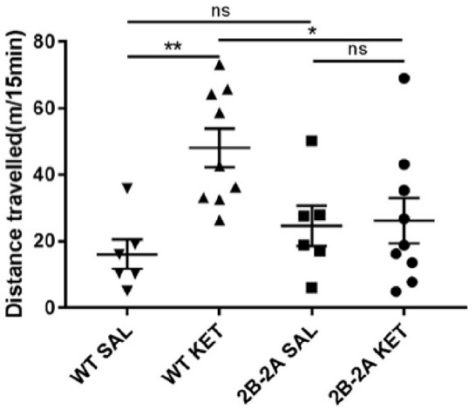

D. Distance travelled by GluN2A-2B swap mutant and wild-type animals: ketamine response window

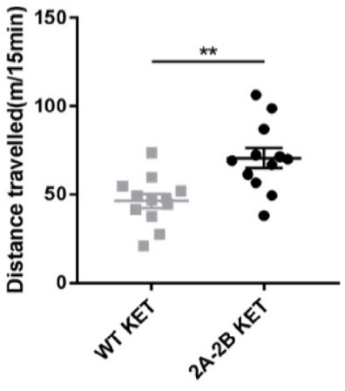

3.3.3 PSD-95 knockout mutants

PSD95$^{-/-}$ animals displayed reduced levels of locomotion as compared with wild type controls at two time points during the habituation sessions (**figure 18A** PSD95$^{-/-}$ vs WT: HAB1 0-5 min p = 0.0356, HAB2 5-10min p = 0.0320). However, during the baseline recording session no such differences were detected, there was also no significant difference in the sum distance travelled during all habituation periods (see **appendix 2**). Again, for this experiment a saline control group was omitted to enable a large enough n number for useful comparisons. However, in the wild-type group there was a 103% increase in locomotion at 5-10 mi post-administration, as compared with the 5 min preceding administration (BL = 7.45m, 5-10 min post-administration = 15.19m). This suggests that ketamine is having the expected effect. The PSD95$^{-/-}$ group had a significantly lower level of activity during this 5-10 min post-administration (**figure 18C** WT = 15.19m, PSD95$^{-/-}$ = 9.64m, p = 0.0307). This suggests that, similarly as with the GluN2B$^{2A(CTD)}$ mutants, the ketamine hyper-locomotive response is diminished in the absence of PSD95. However, when the total distance travelled during the 15 min 'ketamine response' window was compared, there was no significant difference between wild-type and PSD-95$^{-/-}$ or PSD-95$^{-/+}$ animals (WT = 36.61m, PSD95$^{-/-}$ = 24.58, p = 0.2349. WT = 36.61m, PSD95$^{-/+}$ = 43.57m, p = 0.6540). Therefore, although there is a similar trend, the effect of the PSD95$^{-/-}$ mutation is less pronounced than that of the GluN2B$^{2A(CTD)}$ swap, only reaching significance at one 5 min time point.

3.3.4 PSD-93 knockout mutants

PSD93$^{-/-}$ animals displayed reduced levels of locomotion as compared with the control group during the first 5 min of habituation to the open field (PSD93$^{-/-}$ vs WT: HAB1 0-5 min p = <0.0001). However, total distance travelled during all habituation sessions was not significantly altered (see **appendix 2**). Following ketamine administration both the wild-type and PSD93$^{-/-}$ groups show increased locomotion as compared with saline controls, this is significant at 0-5, 5-10 and 10-15 min post-administration (see **figure 18B**). This ketamine response is even more obvious when you compare the total distance travelled in the first 15 min following ketamine administration, as in **figure 18D**, where there is a highly significant difference between saline and ketamine groups (mean distance 12.82m WT SAL, 48.98 WT KET, p = <0.0001. mean distance 13.98m PSD93$^{-/-}$ SAL, 48.93m PSD93$^{-/-}$ KET, p = <0.0001), but no significant difference between wild-type and PSD93$^{-/-}$ (WT KET v PSD93$^{-/-}$ KET p = >0.9999, WT SAL v PSD93$^{-/-}$ SAL p = 0.9957). This shows that loss of PSD93$^{-/-}$ does not diminish the short-term hyper-locomotive response to ketamine. There does, however seem to be an

increase in the duration of that hyper-locomotion as the ketamine PSD93$^{-/-}$ group maintained a significant increase in distance travelled over the corresponding saline control group until the 20-25 min time point (PSD93$^{-/-}$ KET = 15.18, PSD93$^{-/-}$ SAL = 50.1, p = 0.0398), which is 10 minutes longer than the wild-type group.

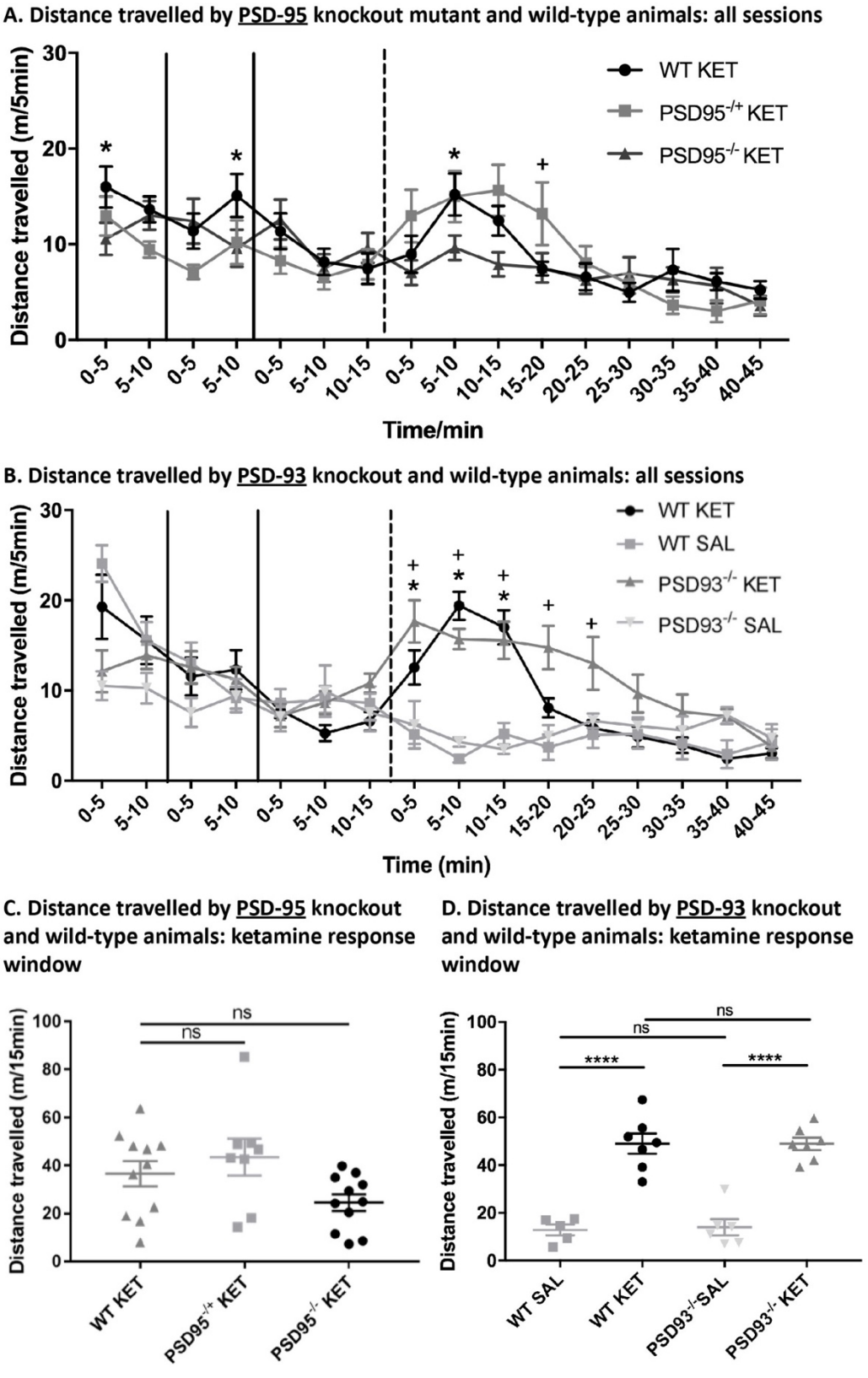

Figure 18 - Effect of PSD95 & PSD93 protein knockout on ketamine-induced hyper-locomotion (continued on following page).

A. *Distance travelled by homozygous PSD95 knockout, heterozygous PSD95 knockout and wild-type animals per 5 min across all open field exploration sessions. * = p<0.05 PSD95$^{-/-}$ KET vs WT KET, + = p<0.05 PSD95$^{-/+}$ KET vs WT KET, two-way ANOVA with Dunnett's multiple comparisons. n = 11(PSD95$^{-/-}$), 8(PSD95$^{-/+}$), 11(WT).* ***B.*** *Distance travelled by homozygous PSD93 knockout and wild-type animals per 5 min across all open field exploration sessions. * = p<0.05 WT KET vs WT SAL, + = p<0.05 PSD93$^{-/-}$KET vs PSD93$^{-/-}$ SAL, two-way ANOVA with Tukey's multiple comparisons. N = 5(WT SAL), 7(WT KET), 6(PSD93$^{-/-}$ SAL), 7(PSD93$^{-/-}$ KET).* ***C.*** *Effect of PSD95 knockout mutation on distance travelled during ketamine response window. ns = p>0.05, one-way ANOVA with Tukey's multiple comparisons.* ***D.*** *Effect of PSD93 knockout mutation on distance travelled during ketamine response window. ns = p>0.05, *** = p<0.001, one-way ANOVA with Tukey's multiple comparisons.* ***A & B*** *data points = mean, error bars = SEM.* ***C & D*** *data points = individual animals, error bars = SEM.*

3.4 Ketamine-induced 'antidepressant' effects

A reduction in immobility time in the forced-swim test (FST) has been reported 24hr after a 10mg/kg dose of ketamine (Zanos et al. 2016, Ma et al. 2013, Liu et al. 2012). The aim of these experiments was to replicate these published findings, with a view to then testing the 4 mutant lines for ketamine-induced 'antidepressant' effects. Two pilot studies were carried out, the first found no significant difference in mean immobility time between ketamine- and saline-treated groups (KET = 61.25% & SAL = 67.66%, p = 0.653). There was, however, an increase in the spread of data points in the ketamine group, as can be observed in **figure 19A**. In particular, there are two animals in the ketamine group with immobility times considerably lower than the saline group cluster, suggesting that a subset of animals may be responding in the expected way to ketamine treatment. A repeat pilot study was then carried out with modifications to the protocol aimed at increasing the efficiency of ketamine dose delivery and decreasing the stress of the animals on the testing day. This second pilot study also scored three different behaviours related to the animals' attempts to escape: swimming, paddling and immobility. With swimming being the strongest attempt at escape and immobility being the absence of an attempt. A significant increase in the percentage of time spent swimming was observed in the ketamine treated group (SAL=36.3%, KET=57.78%, p=0.018). There was also a trend towards decreased immobility in the ketamine treated group, visible in **figure 19B**, although this did not reach significance (SAL=22.22%, KET=2.13%, p=0.084). This indicates that ketamine treatment is increasing the drive of the animals to escape, and thus is inducing an 'antidepressant' phenotype. There was no significant difference in time spent paddling (SAL=41.48%, KET=40.09%, p=0.86). A third pilot study has since been carried out following small modifications of the protocol including increased handling of animals prior to the experimental day, increased familiarisation of animals with

testing room, and adaptation of FST apparatus to reduce the ability of animals to view other objects in the room during the test. This final pilot study found a significant reduction in immobility time in the ketamine treated group, confirming the findings from the second pilot study and demonstrating that it is possible to replicate the reported 'antidepressant' effects of 10mg/kg ketamine in mice. Results from this third pilot study will be reported in the undergraduate dissertation of Samuel Bates (BMedSci, University of Edinburgh).

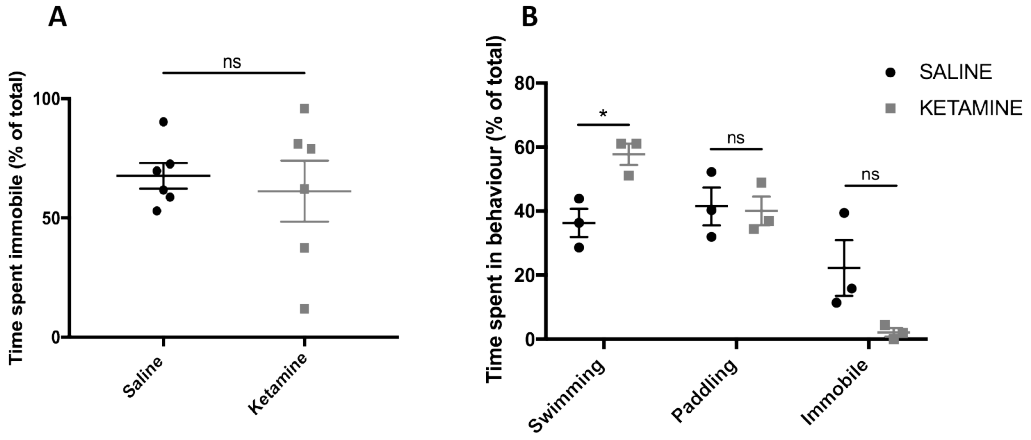

Figure 19 - Effect of ketamine on immobility time of wild-type animals in forced swim test.

A. Initial pilot study*. Percentage of 4 min scoring period spent immobile (s), per mouse, in both ketamine and saline treated groups. No significant difference between saline and ketamine treated groups (p=0.6533) Unpaired t-test. N = 6 per group.* ***B. Second pilot study****. Protocol modifications included increased handling prior to experimental day, delivery of ketamine solution in smaller volume (5ml/kg) and scoring of three different behavioural states. Significant increase in time spent swimming in ketamine group (p=0.0381). No difference in other behavioural measures (Paddling p=0.9969, Immobile p=0.0538). Two way ANOVA with Sidak's multiple comparisons. Second pilot study was carried out by Victoria Hohendorf, an undergraduate student, under the supervision of Dr Szu-Han Wang and Sarah Lemprière.*

3.5 Chapter discussion

3.5.1 Wild-type hyper-locomotive response to ketamine administration

In humans, sub-anaesthetic doses of ketamine produce two phases of response. These are a short-term dissociation, charactertised by perceptual distortions, and a long-term antidepressant effect. The short-term hyper-locomotive response of wild-type animals to administration of a sub-anaesthetic dose of ketamine described here is consistent with the existing literature (Irifune *et al.*, 1991; Imre *et al.*, 2006; Chatterjee *et al.*, 2011) and is considered to be translationally relevant to the short-term dissociative effects seen in humans. This translational relevance comes partly from the short duration of response. Although plasma concentration of ketamine was not analysed in the experiments presented

here, it has a short half-life in mice of ~13 min (Maxwell *et al.*, 2006; Li *et al.*, 2015; Zanos *et al.*, 2016). This suggests that the short term hyper-locomotion observed here is taking place only during the presence of relatively high concentrations of ketamine, which is in stark contrast to the antidepressant effects which are still detectable up to 7 days post-administration (Autry *et al.*, 2011). Similarly, psychotic-like effects of sub-anaesthetic doses of ketamine in humans have been reported during infusion and for a short time (<40min) following infusion (Krystal *et al.*, 1994). The hyper-locomotive response of wild type animals to ketamine administration was consistently observed throughout all the experiments presented here, which were carried out across a period of over 12 months. This highlights the utility and the reliability of this model as a measure of short-term ketamine response. There was also no difference in wild type hyper-locomotive ketamine response between male and female animals (see **appendix 1**), this was consistent with the literature (Zanos *et al.*, 2016).

3.5.2 The importance of the GluN2B c-terminal domain for ketamine-induced hyper-locomotion

The most striking observation from the set of experiments presented here is the absence of a ketamine-induced hyper-locomotive effect in the GluN2B$^{2A(CTD)}$ animals and an exaggerated response in the GluN2A$^{2B(CTD)}$ mutants. Taken together these observations suggest that the GluN2B c-terminal domain is important for this short-term behavioural response to ketamine. Although there is evidence that the truncation or removal of CTDs from the NMDAR can have an effect on channel conductance properties (Maki *et al.*, 2012), replacement of one CTD with that of another subtype is able to rescue that phenotype (Berberich *et al.*, 2005). This suggests that the presence of a GluN2 CTD is important for channel function, but the replacement of the GluN2B CTD with that of GluN2A would leave the GluN2B subtype specific channel properties unaltered. Indeed, NMDA-evoked unitary currents from GluN2B$^{2A(CTR)}$ cultured neurons are no different from those in wild type neurons, both being approximately 50pS which is typical for GluN2B-containing NMDARs (Martel *et al.*, 2012). Therefore, it is unlikely that the absence of ketamine effect seen here with the CTD swap mutation is caused by alteration in ion channel properties. There has been evidence to suggest that GluN2A-containing receptors are more likely to be synaptic, with GluN2B-containing receptors more likely to be found at extrasynaptic sites (Martel *et al.*, 2009). As the CTD is the receptor domain considered important for this trafficking, there is the possibility that the replacement of the GluN2A CTD with that of GluN2B could reduce the

number of NMDARs present at synaptic sites. However, NMDAR-mediated EPSCs in GluN2B$^{2A(CTR)}$ and GluN2A$^{2B(CTR)}$ mutants are no different from control (Ryan *et al.*, 2013). Furthermore, neuronal cultures from GluN2B$^{2A(CTR)}$ animals do not differ from wild type cultures in the proportion of NMDARs that are extrasynaptic, as determined by the quantal activation-mediated blockade of synaptic NMDARs using MK-801 followed by the recording of whole cell currents (Martel *et al.*, 2012). Finally, there is no difference in the amount of GluN2B in PSD-enriched or non-PSD enriched fractions of hippocampal preparations from wild type and GluN2B$^{2A(CTR)}$ animals (Martel *et al.*, 2012). This suggests that a reduction in trafficking of NMDARs to the synapse is unlikely to account for the ketamine response phenotype seen in GluN2B$^{2A(CTD)}$ animals. Even so, an electron microscopy experiment to confirm synaptic vs extra-synaptic NMDAR ratios in these mutants is planned, see **section 3.6.1.** The replacement mutation also does not alter the total amount of either subunit when probed with an antibody against the n-terminal domain in total forebrain extract (Martel *et al.*, 2012; Frank *et al.*, 2016). Ketamine is known to bind within the channel pore region therefore, as this is region unaltered by the CTD swap mutation, ketamine should be able to block GluN2B$^{2A(CTR)}$ and GluN2A$^{2B(CTR)}$ receptors to the same degree as wild-type receptors. This is a reasonable assumption to make based on the existing data showing no alteration of ion channel properties in the chimeric receptors (Martel *et al.*, 2012). However, an experiment to specifically test the blockade of NMDA currents by ketamine in these mutants is planned (see **section 3.6.1**).

The main role of GluN2 CTDs is to couple to intracellular signalling cascades by binding to a diverse range of signalling proteins (Sprengel *et al.*, 1998; Traynelis *et al.*, 2010). The different GluN2 subtypes have been found to bind to different sets of signalling proteins, thus enabling them to modulate intracellular signalling in a specific way (Krapivinsky *et al.*, 2003; Barria & Malinow, 2005; Martel *et al.*, 2012). Taken together, this suggests that a likely explanation for the disruption of the ketamine response observed in the GluN2B$^{2A(CTR)}$ mutants is that modulation of a GluN2B CTD-specific intracellular signalling event is required for the ketamine response. This implies that it is not simple blockade of ion flow, which should take place as normal in GluN2B$^{2A(CTR)}$ animals, which is responsible for its psychotomimetic effects, but that a specific action of the CTD is involved. This is not the first time GluN2B has been implicated in the ketamine response. *In vivo* deletion of GluN2B only from principal cortical neurons mimics and occludes ketamine's antidepressant effects (Miller *et al.*, 2014). However, the results presented here build on that evidence in two ways. Firstly they show a

similar GluN2B specificity of the short-term 'psychotomimetic' response of ketamine and secondly, they narrow down that specific requirement to the CTD of the subunit. As the intracellular signalling function of the CTD is the most likely to be involved here, we can therefore look to specific GluN2B CTD interactors for hypotheses as to the molecular mechanism underlying short-term ketamine action.

There are several proteins known to interact specifically with the GluN2B CTD, over that of the other GluN2 subtypes. These include the Ras GTPase-activating protein SynGAP (Wang *et al.*, 2013), the guanine nucleotide exchange factor Ras-GRF1 (Krapivinsky *et al.*, 2003), and Ca^{2+}/calmodulin-dependent protein kinase II (Leonard *et al.*, 1999; Strack *et al.*, 2000; Barria & Malinow, 2005; El Gaamouch *et al.*, 2012). These are connected functionally, as well as by their association with GluN2B. Upon NMDAR activation there is an influx of Ca^{2+} which triggers the phosphorylation of CaMKII, which in turn phosphorylates SynGAP. When phosphorylated, SynGAP exerts a greater inhibitory action on Ras and thus suppresses ERK activation (Komiyama *et al.*, 2002; Wang *et al.*, 2013). Ras-GRF1 on the other had responds to NMDAR activity by promoting activation of Ras, and thus ERK activation (Krapivinsky *et al.*, 2003). The interaction between Ras-GFR1 and GluN2B was found to be essential for NMDAR-dependent ERK activation in neuronal cultures (Krapivinsky *et al.*, 2003). Thus, the nature of Ras and ERK signalling resulting from NMDAR activation is controlled by the relative activities of SynGAP and Ras-GFR1. The convergence of these GluN2B interactors on the ERK pathway is interesting, as increased ERK activation has been observed following sub-anaesthetic ketamine administration. Increased levels of phosphorylated ERK were identified in PFC as early as 30 min post administration (the earliest time point tested) (Li *et al.*, 2010). Indeed, blockade of ERK signalling has been found to prevent the antidepressant action of ketamine in the forced swim test (Reus *et al.*, 2014). ERK activation is usually associated with transcriptional activation and new protein synthesis which, although it is taking place following sub-anaesthetic doses of ketamine (Li *et al.*, 2010), is likely to be too slow to be responsible for the hyper-locomotion observed here. However, the Ras-ERK pathway has been implicated in the control of synaptic delivery of GluR1 AMPA receptors (Zhu *et al.*, 2002; Patterson *et al.*, 2010). This raises the possibility that ketamine-induced alterations in the rate of delivery of pre-existing AMPARs to the postsynaptic membrane could play a role in the rapid behavioural response, and that this alteration is dependent upon the presence of one or more specific GluN2B CTD interactors at the NMDAR. Indeed, a link between GluN2B-containing NMDA receptor activity, SynGAP, Ras-ERK signalling, and synaptic weakening via

removal of AMPA receptors has been established (Kim *et al.*, 2005; Rockliffe & Gawler, 2006). However, as ketamine is a known NMDAR antagonist, blocking Ca^{2+} influx through the NMDAR the activation of this pathway in this context still appears counter-intuitive. Some relevant hypotheses as to how ketamine is able to increase neuronal activity were discussed in **sections 1.3.4.5 & 1.3.4.7** of the introductory chapter and are also covered in several reviews (Seamans, 2008; Miller *et al.*, 2016). Perhaps the hypothesis most relevant to the finding reported here, is that of tonic GluN2B-specific suppression of protein synthesis in response to activation by ambient glutamate. It is suggested that upon ketamine binding to GluN2B-containing NMDARs this tonic suppression is lifted, resulting in the increased levels of synaptic proteins observed following sub-anaesthetic ketamine administration. Evidence to support this hypothesis consists of the observation that protein synthesis is upregulated following both knockout of GluN2B and genetic replacement of GluN2B with GluN2A *in vitro*. Ketamine application was able to increase protein synthesis in wild-type but not GluN2B knockout cultures. Similar results were found *in vivo*, with ketamine unable to induce increases in BDNF, SAP-102, GluA1 or p-mTOR in animals where GluN2B has been selectively removed from principal cortical neurons (Miller *et al.*, 2014)

Although the NMDAR is considered to be an ionotropic glutamate receptor, there is recent evidence that glutamate binding is able to induce LTD in the absence of ion flux (Nabavi *et al.*, 2013; Stein *et al.*, 2015; Carter & Jahr, 2016). Further to this, an ion flow independent reduction in FRET between GluN1 subunits within individual NMDARs has been identified. This can be prevented with intracellular infusion of an antibody targeting the GluN1 CTD (Dore *et al.*, 2015). This suggests that the GluN1 subunit is able to alter conformation and induce signalling changes in response to agonist binding, in the absence of ion flux. It remains to be seen whether the same is true for the GluN2B CTD, however it is an interesting possibility. A conformational change to the GluN2B CTD in response to ketamine binding within the pore could, in theory, reveal or conceal binding sites for interacting proteins and control activation/inactivation of interacting molecules. For example, alterations in the ability of SynGAP or Ras-GRF1 to bind to the CTD could potentially lead to alterations in ERK signalling independent to changes in Ca^{2+} influx. Indeed, a Ca^{2+}-independent activation of SynGAP has been observed in response to the binding of APV in cortical neurons. This was hypothesised to be induced via a conformational change to the CTD, although no direct evidence of this was provided (Rockliffe & Gawler, 2006). APV binds to the glutamate binding site on the NMDAR and competes with glutamate to produce an antagonistic effect, which is

a different mechanism of action to the channel pore blocking effect of ketamine. It also appears to have an opposite effect on ERK activation to ketamine. However, the concept of Ca^{2+}-independent alterations to SynGAP activity is an interesting one. Further investigations planned to test the hypothesis of GluN2B CTD conformational change induced by ketamine binding are outlined in **section 3.6.4.**

CTD identity has also been found to influence excitotoxicity independently of the identity of the other receptor domains. The GluN2B CTD promotes neuronal death better in response to NMDA application than the GluN2A CTD. This was determined from experiments on neuronal cultures, and in vivo using the same GluN2B$^{2A(CTR)}$ mouse line used for the experiments presented here. NMDA application promoted more cell death in wild type than GluN2B$^{2A(CTR)}$ animals (Martel *et al.*, 2012). Evidence suggests that this enhanced vulnerability to excitotoxicity could be via the GluN2B CTD coupling more strongly to PSD95 and NMDAR activity-dependent nitric oxide (NO) production (Martel *et al.*, 2012). NO release is able to modulate neurotransmitter release and has been implicated in the regulation of neuronal excitability and firing (Prast & Philippu, 2001). There is some evidence to suggest that ketamine is acting to reduce NO production and that this is important for its antidepressant effects (Zhang *et al.*, 2013; Liebenberg *et al.*, 2015). Reduced NO production has the downstream effect of stimulating mTOR signalling (Harraz *et al.*, 2016). NO donor therapy has been reported to reduce short-term ketamine hyper-locomotion in mice (Kandratavicius *et al.*, 2015). Taken together, this raises the possibility that ketamine could be acting via reduced NO production, that this is predominantly via the GluN2B CTD, and is therefore not taking place in the GluN2B$^{2a(CTR)}$ mutant animals.

Overall, the finding that the GluN2B CTD is important for ketamine's short-term hyper-locomotive effect builds upon the existing literature to point us towards several possible mechanisms by which ketamine may be acting. However, there is much further work required to take us forward, some of which is outlined in **section 3.6** below.

3.5.3 Ketamine-induced hyper-locomotion in the absence of the NMDAR supercomplex

Further to the striking effects of the CTD replacement mutations on ketamine-induced hyper-locomotion, PSD95 knockout also reduced the response to ketamine administration. This effect was only significant at 5-10 min post-administration. The ketamine hyper-locomotive response was preserved in PSD93 knockout animals, and the duration of this response was greater than that of wild type animals. There is a tripartite requirement for PSD93, PSD95

and the GluN2B CTD for the formation of NMDAR 1.5MDa supercomplexes (Frank *et al.*, 2016). Therefore, the presence of the ketamine hyper-locomotive response in PSD93 KO animals suggests that it is not the formation of the supercomplex itself that is required for ketamine action, because that complex formation would also be disrupted in PSD93 KO. The increased duration of hyper-locomotion observed in PSD93 KO animals is also interesting, as an increase in PSD95 levels at the synapse has previously been observed in the same PSD93 KO line as used here (Dr Melissa Cizeron, PhD thesis). This raises the possibility that the exaggerated ketamine response observed in the PSD93KO animals could be a result of increased PSD95 levels, which would provide further evidence for a requirement of PSD95. This is consistent with the upregulation of PSD95 expression following sub-anaesthetic ketamine administration (Li *et al.*, 2010; Lisek *et al.*, 2017). Taken together with the findings discussed in **section 3.5.2**, this suggests a role of both PSD95 and the GluN2B CTD in ketamine action which is independent of NMDAR 1.5MDa supercomplex formation. Interestingly, SynGAP associates with NMDAR complexes via PSD95 and SAP102 (Kim *et al.*, 1998; Wang *et al.*, 2013), therefore the potential role for PSD95 in ketamine hyper-locomotion adds more weight to the idea that SynGAP could also be involved. Perhaps the less dramatic phenotype in PSD95 KO, as compared with the GluN2B$^{2A(CTR)}$ animals, could be due to the ability of SynGAP to continue to associate with NMDARs via SAP102 in the absence of PSD95 (Kim *et al.*, 1998). Further to that, there is evidence that SynGAP can bind to the GluN2B CTD independently of the MAGUKs altogether, via its interaction with CAMKIIa (Li *et al.*, 2001). Diminished hyper-locomotive response in the absence of PSD95 is also consistent with the suggestion that the NO-related mechanism, thought to be responsible for the role of GluN2B NMDARs in excitotoxicity, may also be involved in the ketamine response. There is evidence that PSD95 is coupling GluN2B to nNOS, and PSD95 knockdown or disruption of the PSD95-nNOS interface both have anti excitotoxic effects (Sattler *et al.*, 1999; Cao *et al.*, 2005; Zhou *et al.*, 2010). We now know that PSD95 knockout disrupts ketamine-induced hyper-locomotion, however it remains to be seen whether disrupting the PSD95-nNOS interface has an effect on ketamine response.

3.5.4 Ketamine's action in the forced-swim test

Although the short-term hyper-locomotive response to ketamine is a useful assay of its rapid effect, it is the long-lasting antidepressant effect which is currently of particular clinical interest. It is still unknown whether these two different responses are mediated by the same molecular mechanism. The aim will be to establish whether the GluN2B CTD and PSD95 are

also involved in ketamine's long-term antidepressant effects. Regardless of the findings this will be a critically important experiment. If the antidepressant effect of ketamine is not dependent upon GluN2B and PSD95, then it will provide an important distinction between the mechanism underlying the desirable, and the undesirable, effects of ketamine. If it is dependent on GluN2B and PSD95, it opens up the possibility of targeting their downstream signalling molecules during further investigation into treatments for depression. Although the scope of this PhD project was not sufficient to complete this work, two pilot studies were carried out to investigate the effect of ketamine administration on wild type mice in the forced-swim test. There are some reports of greater antidepressant potency of ketamine in female mice (Carrier & Kabbaj, 2013; Zanos *et al.*, 2016), although no such gender specific effect was seen in the first FST pilot study (see **appendix 1**). There were not sufficient animal numbers for a meaningful comparison of gender in the second FST pilot study. The results from these pilot studies highlight the importance of thorough preliminary work ahead of any behavioural study, and lay the ground work for the testing of mutant cohorts, which is ongoing.

3.6 Future directions

The evidence presented here raises some interesting suggestions as to how ketamine could be acting at the molecular level, however it is incomplete, and further avenues of investigation will need to be followed before further conclusions can be drawn.

3.6.1 Additional control experiments

An important next step for this work will be to confirm the observation of increased ketamine-induced hyper-locomotion in GluN2A$^{(2BCTR)}$ by repeating the experiment with the inclusion of saline control groups. This is essential to ensure that the increased locomotion observed in the GluN2A$^{(2BCTR)}$ is indeed an exaggerated response to ketamine administration, and not simply due to a generally higher level of locomotion in these animals. This is of additional importance as a trend towards increased locomotion was observed in GluN2A$^{(2BCTR)}$ animals in the habituation sessions. Although this additional experiment is important, the primary evidence for the involvement of GluN2B CTD in ketamine action comes from the absence of a hyper-locomotive effect of ketamine in GluN2B$^{(2ACTR)}$ mutant animals, and all appropriate saline controls were included in that experiment. For similar reasons, it will be important to repeat the PSD95 knockout hyper-locomotion experiment with saline controls. Homozygous PSD95 mutant animals displayed reduced levels of locomotion at two time points during the habituation sessions, although no significant

difference in total distance travelled during habituation was observed (**appendix 2**). However, it will be important to ensure that these animals are physically capable of levels of locomotion above those observed here. One option for this could be to include a cocaine-stimulated positive control group, cocaine induces hyper-locomotion in mice but acts at the dopamine transporter, not the NMDA receptor (Giros *et al.*, 1996).

Although basal synaptic NMDA current is normal in swap mutants, which suggests that receptors are localized to synapses in the usual way, there is some literature suggesting that CTD is important in receptor trafficking, and that GluN2B subunit-containing NMDARs are more likely to be found extra-synaptically (Stocca & Vicini, 1998; Tovar & Westbrook, 1999; Martel *et al.*, 2009). Therefore, it could be argued that the alteration of the CTD in GluN2B$^{2A(CTD)}$ and GluN2A$^{2B(CTD)}$ mutants could be affecting NMDAR targeting to the synapse, and thus altering the ketamine response in that way. In order to address this potential concern, electron microscopy could be used to establish the ratio of synaptic to extra synaptic NMDARs in GluN2B$^{2A(CTD)}$ and GluN2A$^{2B(CTD)}$ mutants, in comparison with control animals. Further to this, basic immunostaining for GluN1, GluN2A and GluN2B extracellular domains will confirm whether or not the brain wide distribution of NMDAR subtypes is perturbed in GluN2B$^{2A(CTD)}$ and GluN2A$^{2B(CTD)}$ mutants.

Ketamine is known to bind to the PCP site within the NMDAR channel pore (Macdonald *et al.*, 1987; Zeilhofer *et al.*, 1992), which is formed by the transmembrane domains of the receptor subunits. The genetic manipulations in the GluN2B$^{2A(CTD)}$ and GluN2A$^{2B(CTD)}$ mutants are specific to the CTD. However, it could be suggested that this modification of the CTD is having an allosteric effect on pore structure which could prevent ketamine binding in the GluN2B$^{2A(CTD)}$ mutants. Especially as binding at extracellular receptor domains has been found to induce conformational change in the NMDAR CTD (Dore *et al.*, 2015), it is not impossible that the inverse may be taking place. This theory can be tested by establishing with hippocampal slice electrophysiology whether ketamine can still block ion flow through NMDARs in GluN2B$^{2A(CTD)}$ and GluN2A$^{2B(CTD)}$ mutants. This work is ongoing.

3.6.2 Long-term 'antidepressant' action of ketamine

As discussed in **section 3.5.4** it will be essential to know whether the GluN2B CTD is also required for the long-term antidepressant effect of ketamine. The pilot studies described in **section 3.4** have begun this work. A reduction in immobility time is the key measurement of antidepressant effects in this assay. A power calculation based on the second pilot study

carried out suggests that, if the trend towards a reduction in immobility time in the second pilot study represents a true effect, 4 animals per group would be required for it to be statistically significant with an alpha error level of 0.05 and a beta error level of 0.2 (power 0.8). This suggests a small increase in sample size would be sufficient to detect the effect of ketamine. Using this information repeat FST experiments are being carried out to test for the presence or absence of a ketamine-induced antidepressant effect in GluN2B$^{2A(CTD)}$, GluN2A$^{2B(CTD)}$ and other mutant lines.

3.6.3 Biochemical analysis

Although it is possible to speculate on the potential signalling cascades involved in ketamine action from what we know about GluN2B and PSD95 interactors, it will be important to investigate this further experimentally. There are a host of signalling molecules and synaptic proteins previously identified as having a role in ketamine action. These include: BDNF, p-mTOR, p-4E-BP1, p-p70S6K, p-ERK, Synapsin, PSD95, Arc, GluR1, Rheb and others (Li *et al.*, 2010; Haile *et al.*, 2014; Harraz *et al.*, 2016). The simple next step will be to establish whether these changes can be detected in western blot of protein extracts from wild type ketamine- and saline-treated animals, and whether those changes are still detectable in the mutant lines in which ketamine-induced behaviour is diminished. Of particular interest will be the ratio of ERK to phosphor-ERK as discussed in **section 3.5.2.** This work has already begun, see **appendix 3** for characterisation of antibodies. Further to this, the question of whether the effect on the ketamine response in GluN2B$^{2A(CTR)}$ and PSD95KO animals is due to loss of SynGAP at the NMDAR can be addressed with some immunoprecipitation experiments. This would establish whether SynGAP is able to interact with the NMDAR in the absence of the GluN2B CTD or PSD95.

3.6.4 Metabotropic action of GluN2B

The most convincing data for a metabotropic effect of the NMDAR to date has come from measuring FRET between fluorescently tagged cytoplasmic domains of GluN1 subunits expressed in cultured neurons (Dore *et al.*, 2015). The potential metabotropic action of the GluN2B CTD in response to ketamine could be investigated in a similar way by fluorescently tagging the GluN2B CTD and measuring FRET in response to ketamine binding.

3.6.5 Action of other non-competitive NMDAR antagonists

Another interesting question to answer will be whether or not this GluN2B CTD-specific action is a unique characteristic of ketamine, or whether other non-competitive NMDAR antagonists can act in the same way. For example, MK-801 is able to induce hyper-

locomotion (Liljequist *et al.*, 1991) and only a short-term antidepressant response (Autry *et al.*, 2011). Therefore, measuring the behavioural responses to MK-801 in WT and GluN2B$^{2A(CTR)}$ mice would be an informative next step. Further to this, memantine does not produce antidepressant responses, despite also being a non-competitive NMDAR antagonist (Gideons *et al.*, 2014).

3.6.6 Role of SynGAP

To test the hypothesis that SynGAP action is underlying both the requirement of GluN2B and PSD95 for ketamine action, SynGAP1 mutant animals could be tested in the hyper-locomotion protocol. Several SynGAP1 mutant lines are available (Komiyama *et al.*, 2002), including a knockout line and a line with a loss of enzymatic function only (unpublished), which would be useful in determining the role of SynGAP action on Ras specifically.

3.6.7 PSD95-nNOS interface

The potential role of PSD95-nNOS interaction in the ketamine response could be probed using existing molecules generated to disrupt that interaction in vivo (Florio *et al.*, 2009; Carey *et al.*, 2017). Absence of ketamine-induced hyper-locomotion in the presence of these molecules would confirm a role for this interaction.

Chapter 4 Ketamine-induced alterations to the synaptome map

4.1 Introduction

Sub-anaesthetic doses of the NMDA receptor antagonist ketamine have been found to increase levels of the synaptic proteins Synapsin I, PSD95, GluR1 and Arc during the 72 hours following administration (Li *et al.*, 2010; Tang *et al.*, 2015). Protein synthesis is required for both the short-term psychotomimetic and long-term antidepressant effects of ketamine (Autry *et al.*, 2011). Generation of new dendritic spines has also been identified in the medial prefrontal cortex and hippocampus 24h after a sub-anaesthetic dose of ketamine (Li *et al.*, 2010; Ardalan *et al.*, 2017). This suggests that alteration of the protein composition of synapses, and/or generation of new synapses may play a role in the mechanism of ketamine action. However, it is still not known which brain regions are involved in this synaptic response to ketamine. The dose dependency of synaptic protein changes is also yet to be established. There is existing evidence that it is only sub-anaesthetic doses of ketamine that are able to induce an antidepressant response (Li *et al.*, 2010). The activation of mTOR and ERK signalling by ketamine administration also seems to be specific to doses below 80mg/kg (Li *et al.*, 2010). Therefore, it remains to be seen if changes in synaptic protein levels follow the same pattern. The results presented in this chapter focus on the investigation of two of the synaptic proteins previously identified as part of the ketamine response, Arc and PSD95 (Li *et al.*, 2010; Autry *et al.*, 2011; Tang *et al.*, 2015). In order to do this, two reporter mouse lines were used, in which the endogenous PSD95 or Arc protein is tagged with a fluorescent marker ($PSD95^{eGFP}$ and Arc^{VENUS}, respectively). In addition to both being upregulated by sub-anaesthetic ketamine administration (Li *et al.*, 2010), PSD95 and Arc are both incorporated into the 1.5MDa NMDA receptor supercomplex at the postsynaptic density (Frank *et al.*, 2016). They also interact with each other, PSD95 is Arc's most abundant interacting protein and this interaction appears to be essential for the targeting of Arc to the synapse (Fernandez *et al.*, 2017). Both proteins play important roles in brain function and cognition as demonstrated by the effect of knockout on animal behaviour. Knockout of Arc impairs long term memory (Plath *et al.*, 2006), and loss or reduction of PSD95 has been found to impair learning of a spatial memory task and increase anxiety-like behaviour (Migaud *et al.*, 1998; Nagura *et al.*, 2012). However, Arc differs from PSD95 in that its levels are highly dynamic and regulated by neuronal activity (Link *et al.*, 1995; Lyford *et al.*, 1995). Arc transcription can be induced by NMDAR activation (Steward *et al.*, 1998; Steward & Worley, 2001; Rao *et al.*, 2006), AMPAR inhibition (Rao *et al.*, 2006), BDNF (Ying *et al.*, 2002; Yasuda *et al.*, 2007; Benekareddy *et al.*, 2013) and forskolin application in culture (Waltereit *et al.*, 2001). In

addition to this, Arc translation can be induced by activation of mGluRs (Waung *et al.*, 2008) and NMDARs (Bloomer *et al.*, 2007). Although Arc and PSD95 are both upregulated following 10mg/kg ketamine administration, the change in Arc is transient and detected only at 1 & 2h post-administration, whereas the change in PSD95 is detected at 2, 6, 24 & 72h (Li *et al.*, 2010).

4.1.1 Activity-regulated cytoskeleton-associated protein (Arc/Arg3.1)

There is previous evidence that Arc protein is able to accumulate at synapses, at the nucleus, and more diffusely in the cytoplasm (Moga *et al.*, 2004; Korb *et al.*, 2013; Fernandez *et al.*, 2017). The circumstances under which Arc is directed to these different subcellular compartments, and the function of its presence there, is still under investigation (Bramham *et al.*, 2010; Nikolaienko *et al.*, 2017). However, Arc is known to be essential for several forms of experimentally-induced synaptic plasticity. It is thought that Arc is able to modify synaptic strength by increasing AMPA receptor endocytosis (Chowdhury *et al.*, 2006) and is also able to stabilize F-actin during structural plasticity (Messaoudi *et al.*, 2007). Constitutive levels of Arc expression are low, but increase in response to synaptic activity (Link *et al.*, 1995; Lyford *et al.*, 1995) and there is evidence that Arc is directed specifically to recently-activated synapses (Steward *et al.*, 1998; Steward & Worley, 2001; Farris & Steward, 2010). However, it has proven difficult to visualize this synaptic Arc accumulation in brain tissue at the level of the single synapse, although this has been successfully done in cultured neurons (Okuno *et al.*, 2012; Fernandez *et al.*, 2017). Previously published Arc reporter mouse models contain a fluorescent construct under the control of the Arc promoter and do not tag the endogenous protein itself (Guzowski *et al.*, 1999; Wang *et al.*, 2006). There is also an existing transgenic mouse model in which a construct, containing the 7kb promoter of Arc and an mEGFP-tagged form of Arc, has been inserted into the genome. This model has proved extremely useful and provided important insights into the synaptic targeting of Arc, and its interaction with CAMKIIβ (Okuno *et al.*, 2012). However, in the mEGFP-Arc Tg mice the tagged form of Arc which has been inserted is additional to endogenous Arc, and has been randomly inserted into the genome, both of which could have functional consequences. In contrast, the Arc^{VENUS} mouse line is a 'knock-in', containing the coding sequence for Venus (form of YFP) inserted at the c-terminal end of the Arc open reading frame (ORF), before the stop codon. This results in the production of Venus-tagged endogenous Arc protein, in homozygous $Arc^{VENUS/VENUS}$ mice 100% of Arc protein will contain the tag. Therefore, the Arc^{VENUS} mouse line has the potential to provide new information about the synaptic accumulation of Arc protein *in vivo*.

The Arc^{VENUS} mouse line is novel (Fernandez *et al.*, 2017). When combined with the synaptome mapping method, first described by Dr Melissa Cizeron in her PhD thesis and in (Zhu *et al.*, 2018), it is possible to quantify Arc accumulations at single synapse resolution across an entire coronal slice of mouse brain. This method consists of imaging the individual synaptic accumulations of the tagged protein using a high-throughput spinning disk confocal microscope, which is able to take a grid of many thousands of individual images to cover a coronal section of mouse brain. The synaptic accumulations of tagged protein, or 'puncta', are then detected and quantified from the images, creating a map of the synaptic distribution of that protein across the brain. This map was termed the 'synaptome' due to the potential to use this method to map all the post-synaptic densities in the brain, and the nature of their composition at the protein level. This is based on the existing use of the term 'connectome' to describe a map of the structural connectivity within the brain (Oh *et al.*, 2014). This chapter contains the characterisation of the Arc^{VENUS} signal and an Arc synaptome map at baseline levels of stimulation, before going on to describe the modifications to this map by ketamine.

4.1.2 Post-synaptic density protein 95 (PSD95)

PSD95 is present at glutamatergic synapses and is an essential component of the 1.5MDa NMDA receptor supercomplex (Frank *et al.*, 2016). Within these complexes PSD95 is much more abundant than Arc (20-fold), indicating that ~5% of PSD95 complexes contain Arc. ~58% of Arc was found to be within PSD95 complexes (Fernandez *et al.*, 2017). Although PSD95 expression can be upregulated by mGluR activation in neuronal culture (Todd *et al.*, 2003), and at the whole brain level by electroconvulsive seizure (ECS) (Dyrvig *et al.*, 2014), this activity-regulation is not as rapid or as dramatic as that of Arc and the other immediate early genes (IEGs). For example, mRNA levels of the IEG c-Fos are over 2000% of sham control at 1h post-ECS, whereas PSD95 mRNA levels peak at 120% of sham at 16h post-ECS (Dyrvig *et al.*, 2014). The PSD95 synaptome map has already been characterized by Dr Cizeron and was generated using the PSD95^{eGFP} mouse line described in the methods section of this thesis. The majority of PSD95^{eGFP} puncta were found to be at postsynaptic sites and the brain regions with the highest puncta density were the hippocampus and the neocortex. The hippocampus and the fiber tracts were the regions with the most diverse range of punctum characteristics, which included size, shape, density and intensity. Within hippocampal sub-regions gradients of change in puncta intensity, density and size were identified and quantified (Dr Melissa Cizeron PhD thesis;(Zhu *et al.*, 2018)). It was found that the PSD95 synaptome map was reorganized during development, and in the presence of null mutations of other MAGUK

proteins (Dr Melissa Cizeron PhD thesis; (Zhu *et al.*, 2018)). However, is not yet known whether this map is able to be modified on a shorter time scale, for example by pharmacological intervention or changes in neuronal activity.

4.1.3 Experimental aims

The aim of the first set of experiments, described in **sections 4.3 and 4.4**, was to utilize the Arc^{VENUS} mouse line and the synaptome mapping pipeline to generate the first Arc synaptome map. The aim of the second set of experiments, described in **sections 4.5-4.7**, was to utilise the Arc^{VENUS} and $PSD95^{eGFP}$ mouse lines combined with the synaptome mapping pipeline to investigate the effect of two different doses of ketamine on synaptic protein levels. This will build on the existing literature in two main ways. Firstly, the use of a low 'antidepressant' and a high dose of ketamine will investigate the dose dependency of the response of these two synaptic proteins. Secondly, the use of the synaptome mapping method will allow the screening of multiple brain regions for changes in levels of Arc and PSD95 at the synapse.

4.2 Summary of methods used in this chapter

4.2.1 Animals

In order to detect ketamine-induced changes in synaptic protein levels, two different knock-in mouse lines were used. The Arc^{VENUS} mouse line contains the coding sequence for Venus, a variant of yellow fluorescent protein, at the end of the Arc coding region. Similarly, the $PSD95^{EGFP}$ line contains the sequence for enhanced green fluorescent protein (eGFP) at the end of the PSD95 coding region. Both of these knock-ins result in the fluorescent tagging of the endogenous protein product. All animals used in the following experiments were homozygous for either the Arc^{VENUS} or the $PSD95^{eGFP}$ tag and therefore 100% of the relevant protein in these animals is tagged. Please see **appendix 4** for western blots showing addition of tag to endogenous Arc protein, similar characterisation of $PSD95^{EGFP}$ line can be found in Dr Fei Zhu's PhD thesis.

4.2.2 Immunohistochemistry

A primary antibody against VGlut1 (cat no. 75-066, Neuromab) was used at a concentration of 1:250. An anti-mouse IGg1 Alexa Fluor 555 secondary antibody (cat no. A21127, ThermoFisher Scientific) was then applied at a concentration of 1:500. 4',6-Diamidino-2-Phenylindole (DAPI) was used at a concentration of 1:1000 to visualise nuclei. Please see **section 2.3.3** for full IHC protocol.

4.2.3 Ketamine treatment & sample preparation

Ketamine (Vetalar, Boehringer Ingelheim) was administered at either 10mg/kg or 100mg/kg, at a volume of 10ml/kg, via subcutaneous injection. Sterile saline at a volume of 10ml/kg was administered via the same route to the control groups. Arc^{VENUS} animals were culled by perfusion fixation at 1h, 6h or 24h post-administration of ketamine. $PSD95^{eGFP}$ animals were culled by perfusion fixation at 24h post-administration. Each group contained 4-5 animals. For the baseline Arc synaptome map animals were taken from their home cages and immediately culled by perfusion fixation. Brains were processed as described in **sections 2.4.1 - 2.4.4** and coronal sections were taken on a cryostat at a thickness of 18µm. Two representative Bregma levels were selected for imaging, these were Bregma 2.10mm and -1.70mm. These regions were chosen to enable study of the prefrontal cortex and hippocampus, both previously implicated in the ketamine response (Li *et al.*, 2010; Fuchikami *et al.*, 2015), alongside the screening of multiple other regions that have not yet been studied in this context.

4.2.4 Imaging & analysis

Sections were imaged on a spinning disk (50 nm) confocal microscope (Revolution XDi, Andor), using a 100X, oil immersion lens with an NA of 1.4. The pixel size produced by this microscope is 84nm. Please see **table 4** in **section 2.3.6** for information on the imaging parameters used for each of the datasets presented here. Fluorescent puncta were detected from the resulting TIFF images and their density, size and intensity were quantified using the Ensemble method (Ricky Qiu). Sections were manually divided into previously defined anatomical regions and average values for each punctum parameter were calculated for each region. For comparison of left and right hemispheres in baseline Arc synaptome map a two-way ANOVA followed by Sidak's multiple comparisons was used. For comparison of saline groups, a two-way ANOVA followed by Tukey's multiple comparisons was used to compare the 1h groups with both the 6h and 24h groups independently. For the ketamine study individual t-tests, one per region, were carried out to compare control and ketamine-treated animals and screen for regions with statistically significant changes. No correction for multiple comparisons was applied, however, results are interpreted with consideration of the increased likelihood of false positives resulting from this method. The effect size of the two ketamine doses, as compared to the appropriate saline control group, was calculated using the Cohen's d equation and presented in the form of a blue to white to red colour scale on an anatomical brain map.

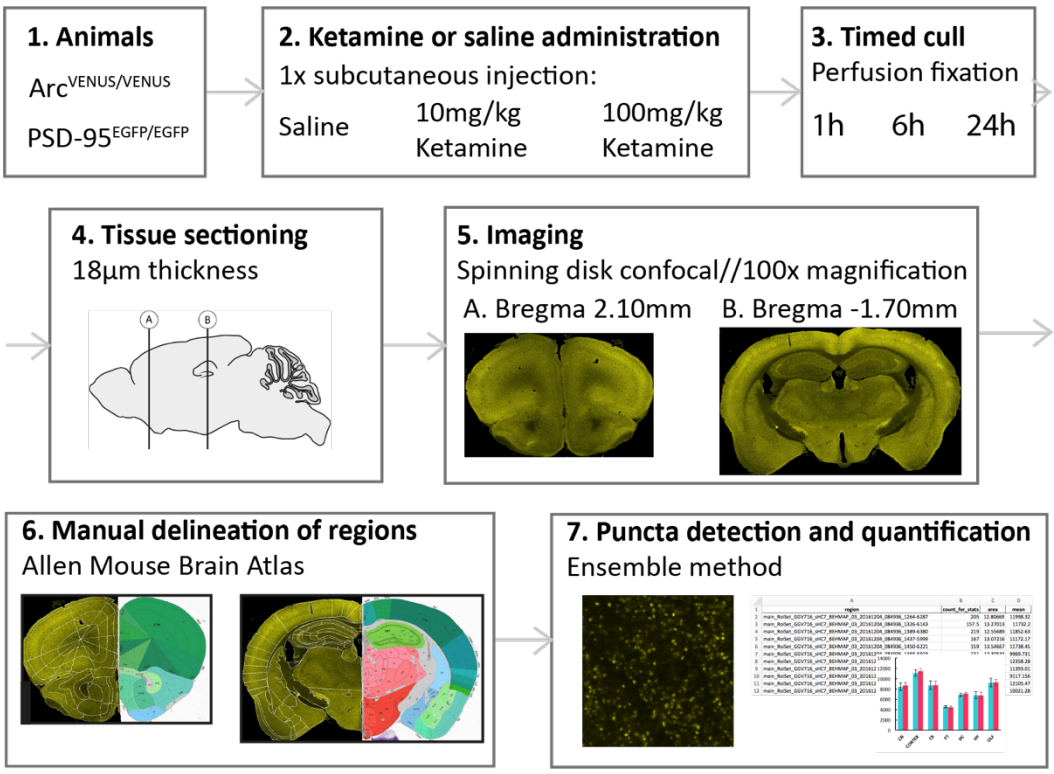

Figure 20 - Summary of the ketamine synaptome mapping protocol.

For generation of the basal Arc synaptome map step 2 was omitted and animals were culled by perfusion fixation immediately upon removal from home cage. Only section B (bregma -1.70) was analysed for basal map, whereas both A and B were analysed for ketamine synaptome.

4.3 Characterisation of subcellular distribution of Arc-Venus signal

4.3.1 Synaptic accumulations of Arc

When imaged at high resolution (SDM confocal, 100X, NA1.4, 50µm pinhole) the fluorescent signal in Arc^{VENUS} mice is visible both as small (~0.4µm diameter) punctate accumulations and larger (~7µm diameter) oval-shaped accumulations. In hippocampus these small puncta are primarily situated in dendritic layers such as the stratum radiatum and stratum moleculare, whereas the larger oval-shaped accumulations are located within cell body layers, such as the granule cell layer of the dentate gyrus. The left-hand panels in **figure 21** show representative images of the small punctate accumulations of Arc in several hippocampal sub-regions. For comparison the corpus callosum is also shown, this area of fiber tracts is known to have few synapses and therefore provides a useful negative control for imaging synaptic proteins. The vesicular glutamate transporter 1 (VGlut1), a marker of the presynaptic terminals of excitatory neurons (Liguz-Lecznar & Skangiel-Kramska, 2007), has been used in **figure 21** to show the location of these Arc puncta. There are clear differences in Arc puncta density, intensity and size between hippocampal sub regions. The dentate gyrus

molecular layer (DGmo) shows relatively few Arc puncta, sparsely distributed (**figure 21 A1)**. This is not due to a low number of synapses however, as there are considerably more VGlut1 puncta than Arc puncta in this area (**A2 & A3**). In the polymorphic layer of the dentate gyrus (DGpo) larger Arc-Venus puncta are visible, these have more varied shapes than the round puncta of the molecular layer (**B1**). These large puncta are tightly juxtaposed with the large VGlut1 puncta visible in this area (**B3**). It is in the DGpo that large ring-shaped PSDs can be observed at specialised dendritic spines known as thorny excrescences, these receive input from the large synaptic boutons of the mossy fibers which project from DG granule cells (Amaral *et al.*, 2007). In the CA1 stratum radiatum (CA1sr) a high density of both Arc and VGlut1 puncta can be observed, again Arc puncta are situated close to VGlut1, although the high density in this region does make it harder to be certain of this (**C1-3**). In the CA1 stratum lucidum (CA1slu) a similar pattern of puncta as the dentate gyrus polymorphic layer can be observed (**D1-3**). This area also contains large thorny excrescence synapses (Amaral *et al.*, 2007). As expected there were very few Arc or VGlut1 puncta in the corpus callosum (**E1-3**). The juxta-positioning of Arc puncta with VGlut1 puncta in these different areas of the hippocampus is consistent with Arc protein being situated at the postsynaptic side of the synapse. The ability to image synaptic accumulations of Arc here demonstrates the utility of this knock-in reporter mouse over some previously published Arc reporters which only allow the detection of Arc expressing cells, not individual synapses (Guzowski *et al.*, 1999; Vousden *et al.*, 2015).

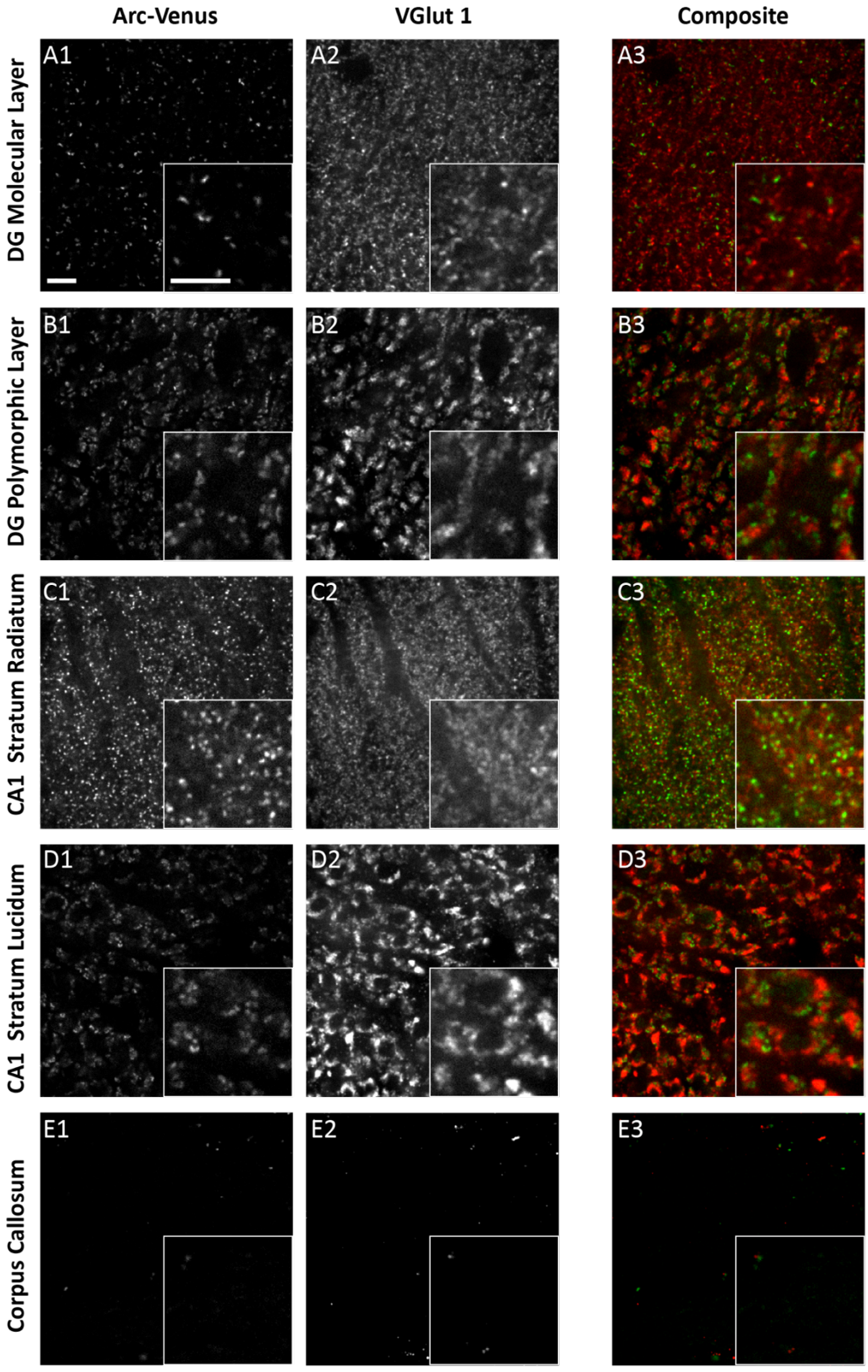

Figure 21 - Arc signal can be detected close to presynaptic terminals in the hippocampus.

Immunohistochemistry with antibody for VGlut1 (column 2 & red), Arc-Venus endogenous signal (column 1 & green). ***Scale bars = 5µm.*** *See* ***appendix 5*** *for antibody control images.*

4.3.2 Nuclear accumulations of Arc

Figure 22 contains representative images from two hippocampal cell body layers, and from the isocortex, which show the larger (~7µm) accumulations of Arc. 4',6-Diamidino-2-Phenylindole (DAPI) has been used to visualise cell nuclei. It is clear from the composite images on the right of **figure 22**, that the large accumulations of Arc (see filled arrow for example) are co-localised with the nuclear stain, suggesting that this Arc protein is present either in the nucleus, or clustered close to its surface. Arc protein has been observed in nuclei previously using immunohistochemistry with an Arc antibody (Korb *et al.*, 2013). In some cases, there is also visible Arc-Venus accumulation around the edge of the nucleus and in processes extending outwards, (see outline arrow in **figure 22** for example), which also indicates the occasional presence of detectable levels of Arc protein in the cytoplasm. Again this has been reported with antibody staining previously (Korb *et al.*, 2013).

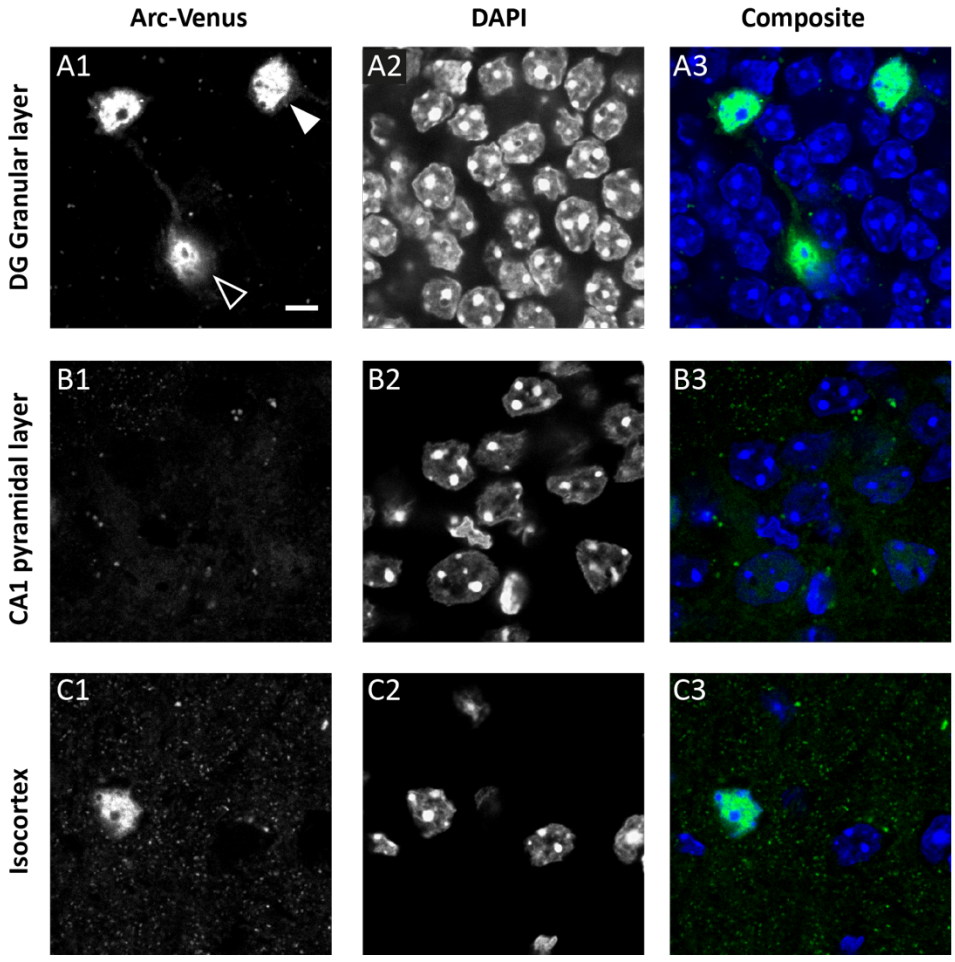

Figure 22 - Arc can be co-localised with nuclei in the hippocampus.

*Immunohistochemistry with DAPI (column 2 & blue), Arc^{VENUS} endogenous signal (column 1 & green)**.** Scale bars = 5µm. See **appendix 5** for antibody control images.*

It is clear from the DAPI staining in **figure 22** that, in the regions sampled here, Arc is not present at high levels in every single nucleus. This fits with the existing literature which showed a sparse distribution of Arc positive nuclei in hippocampus at baseline levels of stimulation (Korb *et al.*, 2013).

4.4 Characterisation of Arc synaptome map

4.4.1 Inter-regional diversity

In order to characterise the diversity in Arc synaptic puncta characteristics further, and to provide quantification, entire Arc^{VENUS} brain sections were imaged with a high throughput spinning disk confocal microscope. The images acquired were then quantified using the ensemble method, as described, to generate average punctum density, intensity and size values for different anatomically defined brain regions. This quantification excludes the large nuclear accumulations based on their size. The Allen brain atlas was used to delineate recognised anatomical regions in order to compare punctum characteristics across brain areas. Six main regions were initially analysed to determine the overall pattern of punctate Arc protein expression, and to compare the left and right hemispheres, these regions are illustrated in **figure 23B**. As the bar charts in **figure 23 C-E** show, there was no difference in punctum density, intensity or size between the left and right hemispheres of the brain in the main regions analysed. An ordinary two-way ANOVA found no significant effect of hemisphere overall (density $p = 0.1134$, size $p = 0.1723$, intensity $p = 0.7633$), and Sidak's multiple comparisons testing found no significant difference between hemispheres in any one of the main regions. There was, however an overall effect of brain region on all three punctum parameters (density $p < 0.0001$, size $p < 0.0001$, intensity $p < 0.0001$). This demonstrates the diversity in the nature of Arc accumulation at the synapse between anatomically-defined brain regions. By far the area with the densest distribution of Arc puncta was the isocortex, which contained around two times more puncta per $100\mu m^2$ than the second densest region which was the olfactory areas. At the other end of the scale, the fiber tract regions contained fewer than 3 puncta per $100\mu m^2$ (**figure 23C**). The cortex was also the area with the brightest puncta on average, and the fiber tracts the dimmest (**D**). The hypothalamus had the largest puncta, despite having relatively few of them (**E**). The colour maps in **figure 23** show this diversity of puncta density, size and intensity across different brain regions in more detail, and allow us to make several observations about the Arc synaptome map at baseline levels of stimulation. Firstly, looking at the hippocampus on these brain maps it is possible to see that the trends observed in the representative images

presented in **figure 21** hold true when the entire area is analysed quantitatively. There is a higher density of puncta in the CA1sr as compared with the DGmo (CA1sr = Left m:53.39 per 100μm^2 & sd:4.12, Right m:55.58 & sd:2.67; DGmo inf = Left m:17.03 & sd:2.50, Right m:17.92 & sd:2.37)(**figure 23C**). The same is true for puncta intensity (CA1sr = Left m:8824 & sd:580, Right m:8988 & sd:425; DGmo inf = Left m:6044 & sd:420, Right m:6136 & sd:527)(**D**). The DGpo and CA3slu contain larger puncta than other dendritic regions of the hippocampus (DGpo = Left m:0.110μm^2 & sd:0.003, Right m:0.109 & sd:0.002, CA3slu = Left m:0.009 & sd:0.002, Right m:0.088 & sd:0.001, for reference CA1sr = Left m:0.084 & sd:0.001, Right m:0.088 & sd:0.001)(**E**). Indeed, of the main anatomical regions highlighted in **figure 23B** the hippocampus appears to show most puncta diversity in terms of the density and size measurements. There is also considerable diversity within the isocortex, with a gradual decrease in puncta density visible from the most superficial to the deeper cortical layers (e.g. SSp lyr1 = Left m:53.55 & sd:6.16, Right m:56.93 & sd:2.47, lyr6b = Left m:18.40 sd:6.40, Right m:20.70 sd:3.36). A similar trend can be observed in the puncta intensity measurement, although layer 4 appears to have particularly bright puncta. The somatosensory cortex is the area of isocortex with the highest density and intensity of Arc puncta. There is a gradual decline in both parameters as distance from the somatosensory cortex increases, with the lowest density and intensity found in the most ventral region of the isocortex (ENTl) and the most medial region (RSPv). Raw density, intensity and size mean values and standard deviation for each brain region can be found in the tables in **appendix 11**. The thalamus was excluded from this analysis due to a technical artefact, which consisted of a dark area in the thalamus of some brain sections, visible in **figure 23A**. This was not present in the ketamine synaptome mapping cohorts presented in the rest of this results chapter and did not appear to affect any additional brain regions outside of the thalamus.

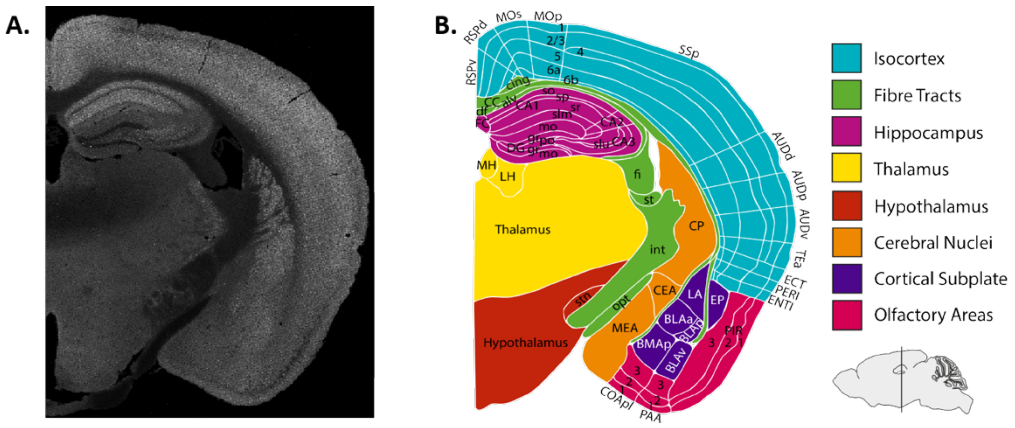
A.
B.
Isocortex
Fibre Tracts
Hippocampus
Thalamus
Hypothalamus
Cerebral Nuclei
Cortical Subplate
Olfactory Areas

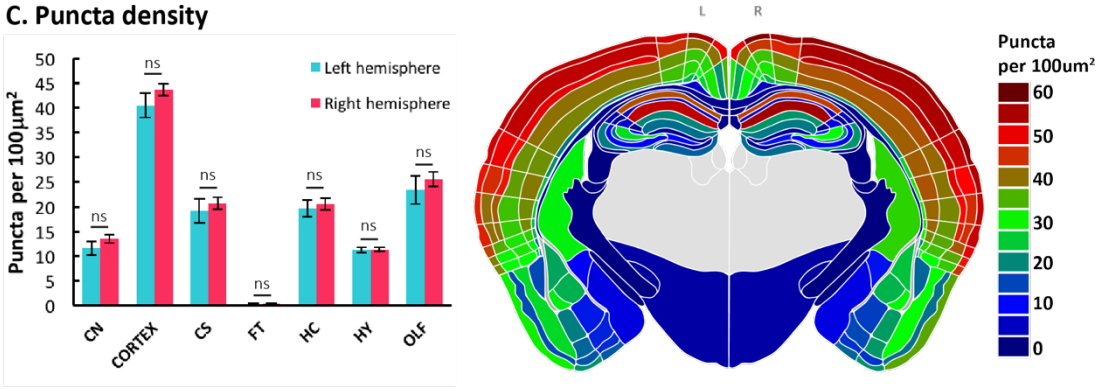
C. Puncta density
Puncta per 100µm²
Left hemisphere
Right hemisphere
CN
CORTEX
CS
FT
HC
HY
OLF
Puncta per 100um²

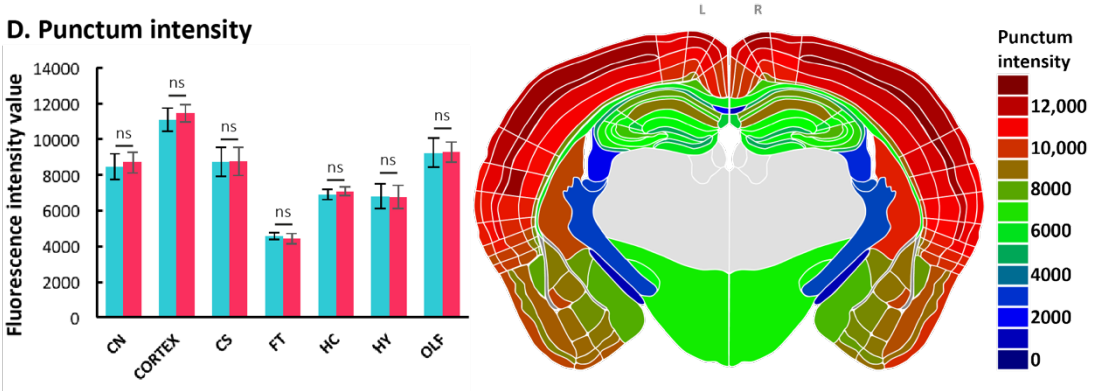
D. Punctum intensity
Fluorescence intensity value
Punctum intensity

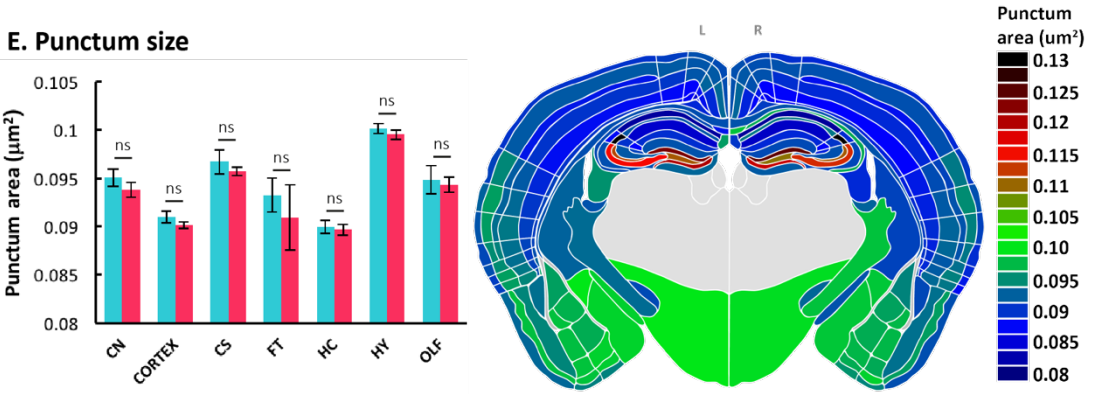
E. Punctum size
Punctum area (µm²)
Punctum area (um²)

Figure 23 - (previous page) Density, intensity and size of Arc puncta across multiple brain regions at baseline.

A. *Example montage image showing basal Arc-Venus signal in bregma -1.70mm coronal section. One hemisphere shown, montage of ~15,000 individual tile images.* ***B.*** *Diagram showing regions delineated for quantification, based on Allen Brain Atlas, please see* ***appendix 8*** *for list of brain region abbreviations. For initial analysis, presented in bar charts in C, D and E, main regions (denoted by colour code) were delineated. For secondary analysis, presented in colour maps, all outlined regions were delineated.* ***C, D & E*** *Arc-Venus punctum quantification. Puncta detected and quantified using Ensemble method, n = 4 mice, all* $Arc^{VENUS/VENUS}$*.* ***Bar charts*** *show the average values for the main regions as defined in B. Bars represent the mean value for the defined region, error bars = SEM, comparison is made between left and right hemispheres. ns = not significant, 2-way ANOVA with Sidak's multiple comparisons.* ***Brain maps*** *show the mean value for each smaller anatomical region as a colour scale from blue-green-red.*

4.4.2 Intra-regional diversity

Within hippocampal sub-regions it is possible to visually observe gradients of Arc puncta distribution in montage images. By delineating smaller areas within the CA1sr, CA1so and CA3sr it is possible to carry out a quantification of the nature of these gradients. Two kinds of gradient were identified using this method: tangential gradients which run parallel to pyramidal cell body layers and radial gradients which run perpendicular to pyramidal cell body layers, see **figure 24**. The tangential gradients follow the same axis as the CA subfield classification (CA1-CA2-CA3). The radial gradients follow the dendritic projections of principal neurons from proximal to the cell body, out to the most distal.

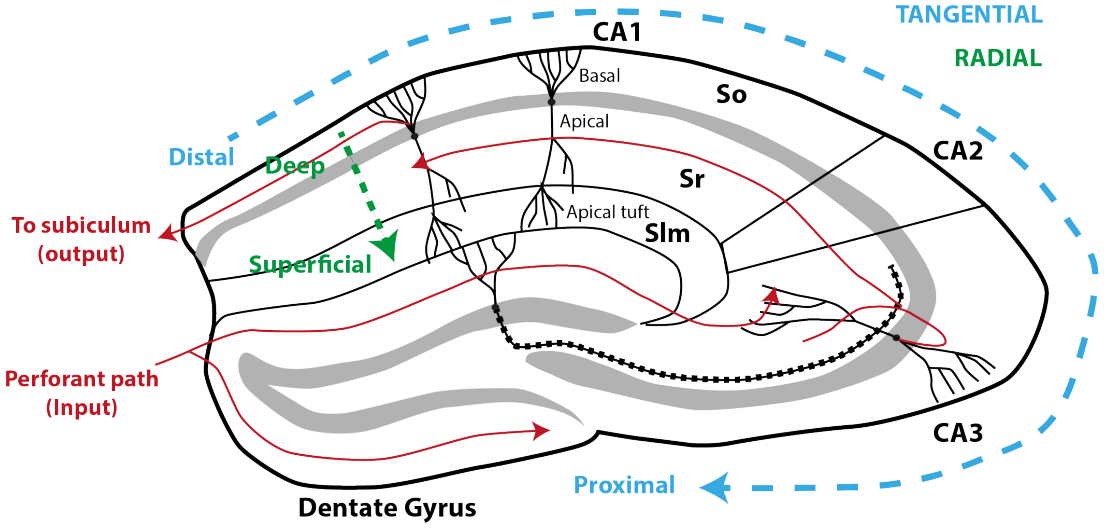

Figure 24 - Tangential and radial axes in hippocampus

The tangential axis was investigated in the CA1 field, where a gradient in Arc was most visible from the montage images. Puncta density was found to decrease along this axis in the CA1sr, with a dramatic drop in the last two segments before the start of the CA2 field (**figure 25A**). A similar gradient was seen in the CA1so but here there was also a lower density in the first segment, closest to the FC, giving the graph an 'inverted u' shape. Intensity of detected puncta also decreased along this axis in both CA1so and CA1sr and punctum size decreased slightly. Identification of gradients along the tangential axis suggests that there are differences between the dendritic trees of pyramidal cells situated at different points along the CA1 field. Changes along the radial axis were also identified in the CA1sr, with puncta density increasing as distance from the pyramidal cell body layer increased and then rapidly decreasing again in the last segment before the start of the CA1slm (**figure 25B**). Punctum intensity followed a similar pattern. Punctum size gradually increased along this axis and reached its highest level in the final segment before the CA1slm. In the CA3sr a gradual increase in puncta density can be seen as distance from the pyramidal cell body layer increases, although this flattens out in the last segment before the start of the CA3slm (**figure 25C**). There is also a small increase in punctum intensity along this axis, and a small u-shaped trend in punctum size. Alterations along the radial axis suggest differences between the proximal and distal branches of the dendritic tree of the same pyramidal cell. This is a basic quantification of some of the visible trends within the hippocampus, but they highlight the potential for the Arc-Venus reporter mouse line, combined with the synaptome mapping pipeline to identify subtle alterations in Arc distribution within anatomically defined brain regions.

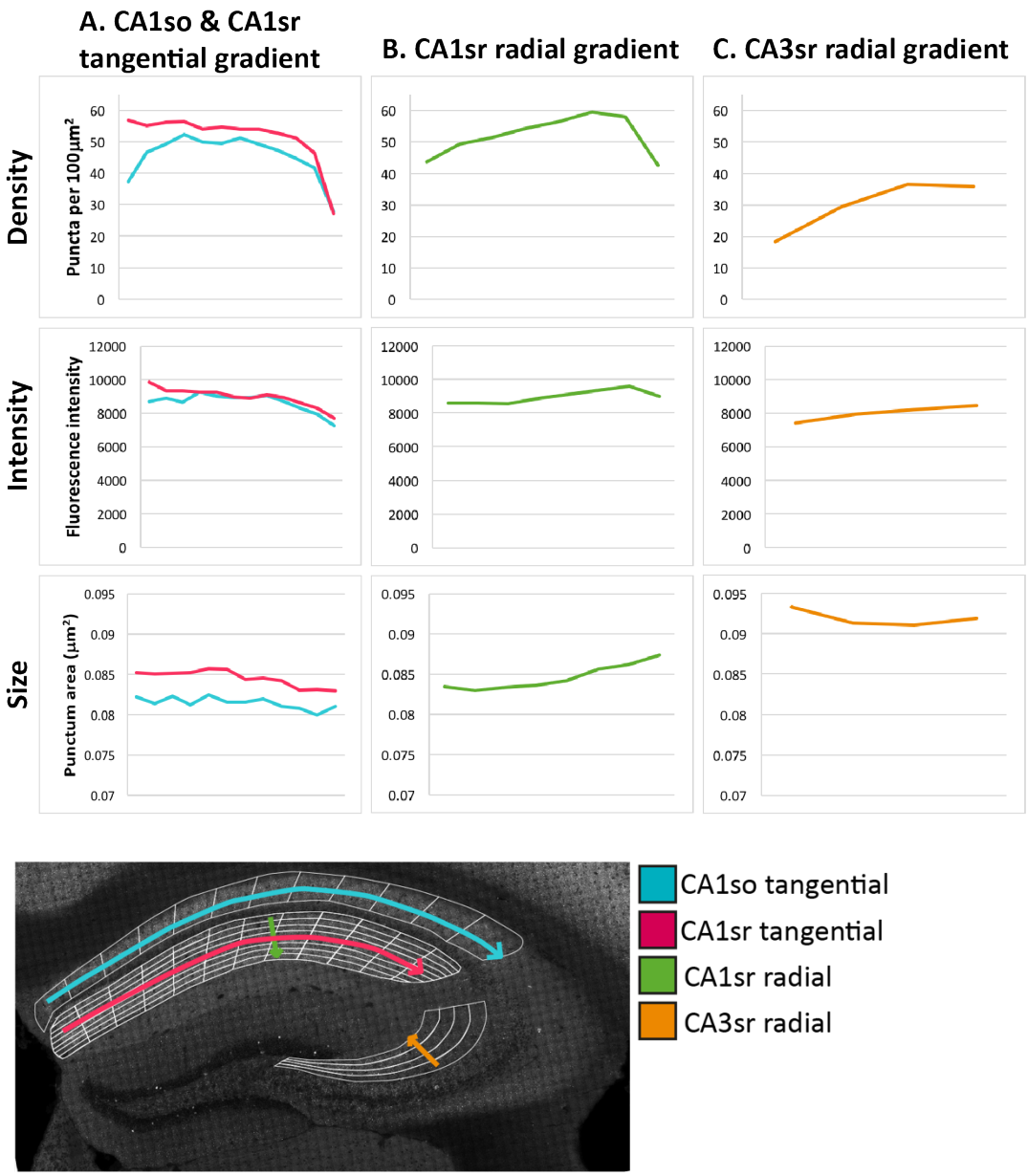

Figure 25 - Tangential and radial hippocampal gradients in Arc synaptome map.

n = 1, average of two hemispheres. Delineations used to generate this data are illustrated in bottom panel. Schematic diagram of tangential and radial gradients in relation to hippocampal anatomy can be found in ***figure 24****.*

4.5 Effect of saline injection on Arc synaptome map

Novel experiences and stressful experiences have both been reported to increase Arc expression levels (Ramirez-Amaya *et al.*, 2005; Grinevich *et al.*, 2009; Jakkamsetti *et al.*, 2013). The control group for the ketamine study described here received a single saline injection 1h, 6h or 24h pre-sacrifice. This itself was a novel, and mildly stressful experience, which therefore has the potential to induce changes in Arc expression. In order to investigate

this further, and to provide background information for the interpretation of the ketamine results presented in **section 4.6**, the Arc synaptome map was compared at 1h, 6h and 24h post saline administration. The results of this comparison are presented in **figure 26**. Although there is no home cage (baseline) control group included in this data, an overall effect of time point was identified for both the density and size parameters (density: $p<0.0001$, intensity: $p=0.0586$, size: $p=0.0003$. Ordinary 2-way ANOVA, type III sum of squares). This suggests that injection of saline is having an effect on these parameters during the 24h following administration. Tukey's multiple comparisons testing was used to compare the 1h time point with the 6h and 24h time points individually to identify which brain regions may be responsible for this effect. No significant changes were identified in any regions contained within the bregma 2.10mm section (**figure 26A**). In the bregma -1.70mm section several regions within the hippocampus displayed significantly greater puncta density at 6h or 24h than at 1h post-administration (**figure 26B**). This included the stratum lucidum in all CA fields, the molecular and polymorphic layers of the DG, and the CA2 stratum oriens and radiatum. The molecular layer of the DG showed an increase in both puncta density and puncta size (density: DGmolinf $p=0.0002$, DGmolsup $p<0.0001$; intensity: DGmolinf $p=0.0046$, DGmolsup $p=0.0146$). Several fiber tract regions also showed increased size of detected puncta at 6h and 24h as compared with 1h post-saline. Taken together, these observations show that it is possible to modify the Arc synaptome map with a brief novel, and mildly stressful, experience such as administration of a saline injection, and that in this case those modifications are limited to specific anatomical regions. This is interesting because it gives an indication of the sensitivity of this method and provides important information for the interpretation of the ketamine results presented in the following sections.

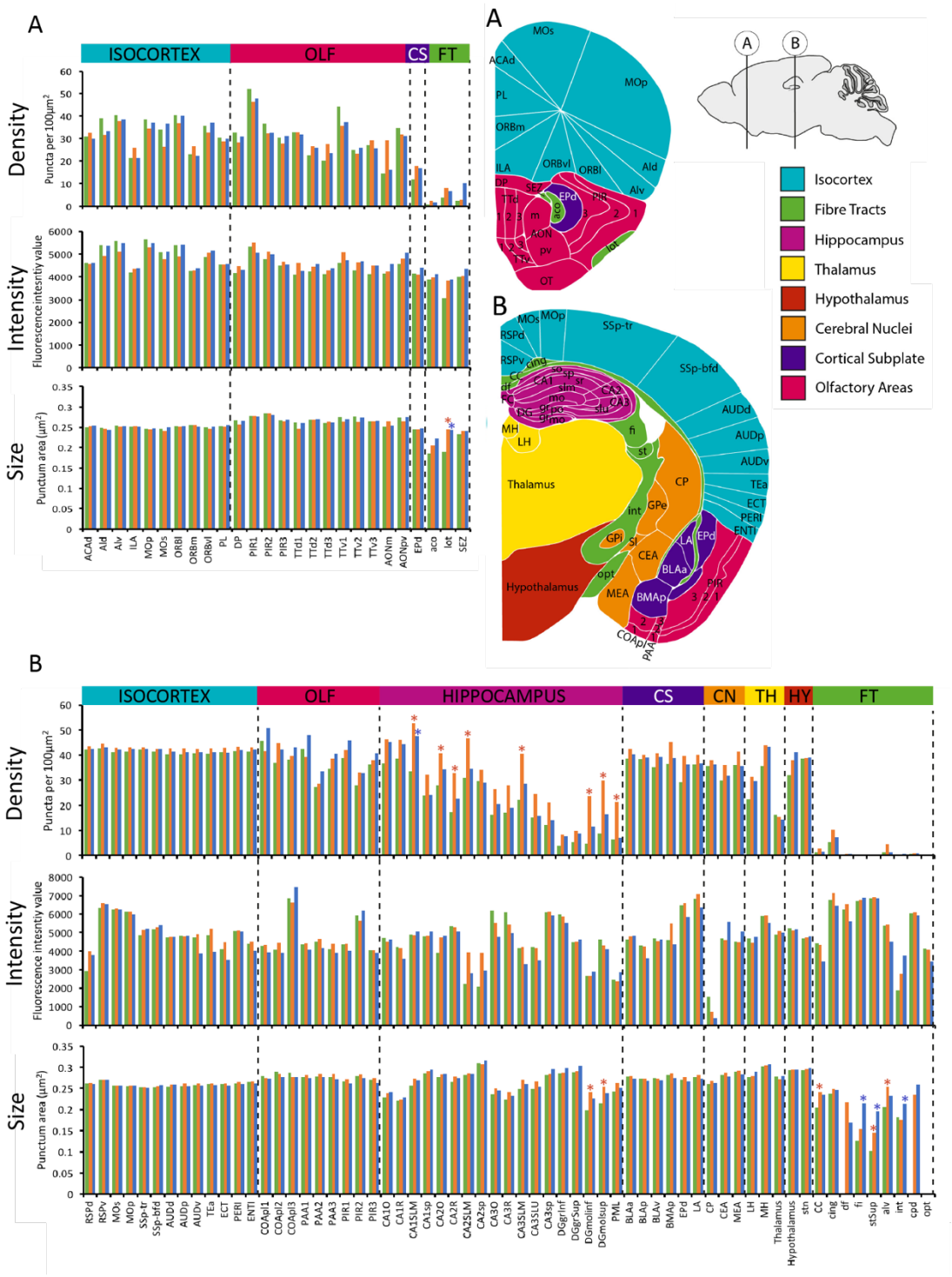

Figure 26 - Effect of saline injection on Arc synaptome map.

A. *Bregma 2.10mm.* ***B.*** *Bregma -1.70mm. Bars represent mean of 3-5 animals per group. Asterisks represent significant change from 1h group as determined by 2-way ANOVA followed by Tukey's multiple comparisons testing.*

4.6 Ketamine-induced modification of the Arc synaptome map

4.6.1 Changes in number of Arc puncta detected

Following on from the characterisation of the basal Arc synaptome map, and the modifications induced by novel experience, this section describes the results of an experiment investigating the effect of two different doses of ketamine on the Arc synaptome map across the 24h following administration. The density of Arc puncta (number of detected puncta per 100μm^2) was quantified in 89 individual brain regions per hemisphere, across two bregma levels, as illustrated in **figure 27**. For each region one value was generated per mouse by taking an average of the two hemispheres.

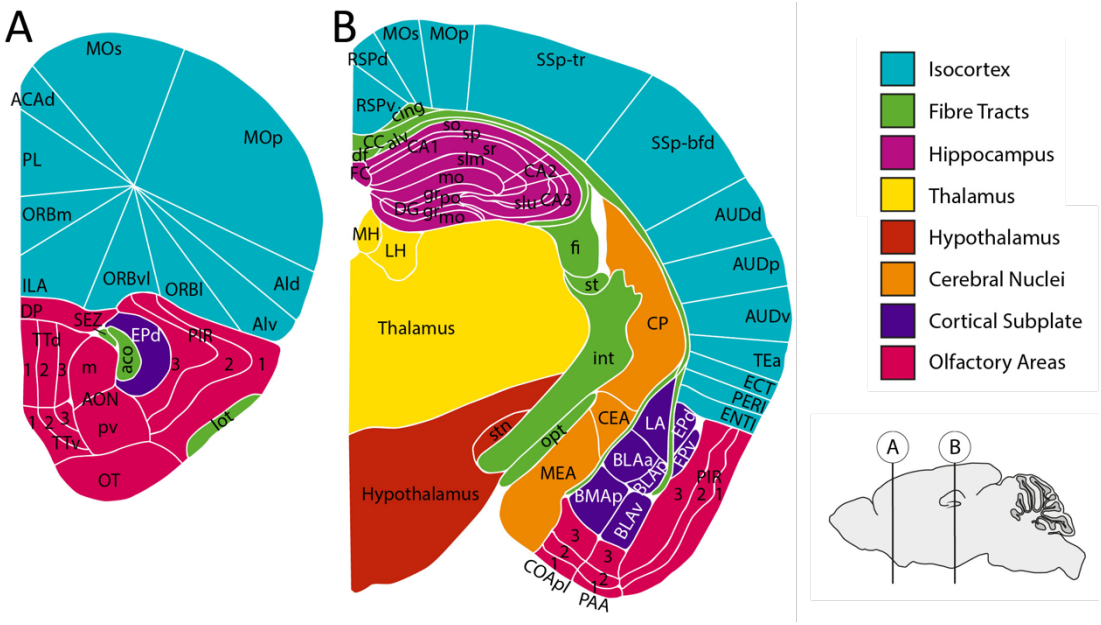

Figure 27 - Sub-regions delineated for analysis of ketamine-treated brain sections.

Main region classification based on Allen Brain Atlas. *A = bregma 2.10mm, B = bregma -1.70mm. See* ***appendix 8*** *for list of abbreviations of brain region names.*

In order visualise changes induced by ketamine administration, the effect size (Cohen's d) of the change from saline control group was calculated for both the low- and high-dose ketamine groups, for each of the 89 brain regions. These values are presented as a colour scale, in which blue is a decrease from saline control and red is an increase, applied to the corresponding regions in the brain maps in **figure 28**. The Cohen's d effect size gives a value based on the number of standard deviations which separate the means of the two groups. Please see **appendix 17** for examples of the spread of data underlying different Cohen's d values.

Multiple t-tests (one per region) were used to screen brain regions for significant changes, the asterisks in **figure 28** denote regions in which a significant change was found. It is clear from viewing **figure 28** that the majority of the ketamine-induced alterations are taking place in the bregma -1.70mm section (section B). Indeed, only one region within the bregma 2.10mm section reached a significant level of change (TTv2: saline = 115.8, low-dose = 49.31, p=0.0381). At the 1h time-point there is a general trend towards increases in puncta density following both low- and high-doses across many of the main regions contained within the bregma -1.70mm section. In the low-dose group there is a cluster of regions with significant increases in the olfactory areas, hippocampus and cortical subplate. In the high dose group there are fewer significantly-increased regions and these are almost all contained within the hippocampus. At 6h post-administration high- and low-doses of ketamine appear to be having opposing effects on Arc-Venus puncta density. There is still a general trend towards an increase in the low-dose group, with significantly-increased regions clustered within the isocortex, hippocampus, cortical subplate, cerebral nuclei, thalamus and hypothalamus. Only the olfactory areas and fiber tracts are left unaltered. Conversely, the high-dose group is now showing a general decrease in puncta density, as compared with the saline control group, with significant decreases seen predominantly in the hippocampus. At 24h post-administration, a similar trend as the 6h time point can be observed, with the high dose inducing a general decrease and the low dose producing a general increase, however fewer individual regions are significantly altered. The low-dose group shows a clustering of significant increases in regions within the hippocampus, thalamus and fiber tracts. These results show that both low- and high-doses of ketamine are able to induce changes in the density of Arc puncta. These changes follow the general pattern of a short-term increase induced by both doses, followed by a low-dose induced increase and a high-dose induced decrease at 6h and 24h. They also show highly brain-region specific effects, with the hippocampus affected throughout and the isocortex altered specifically at 6h post-administration.

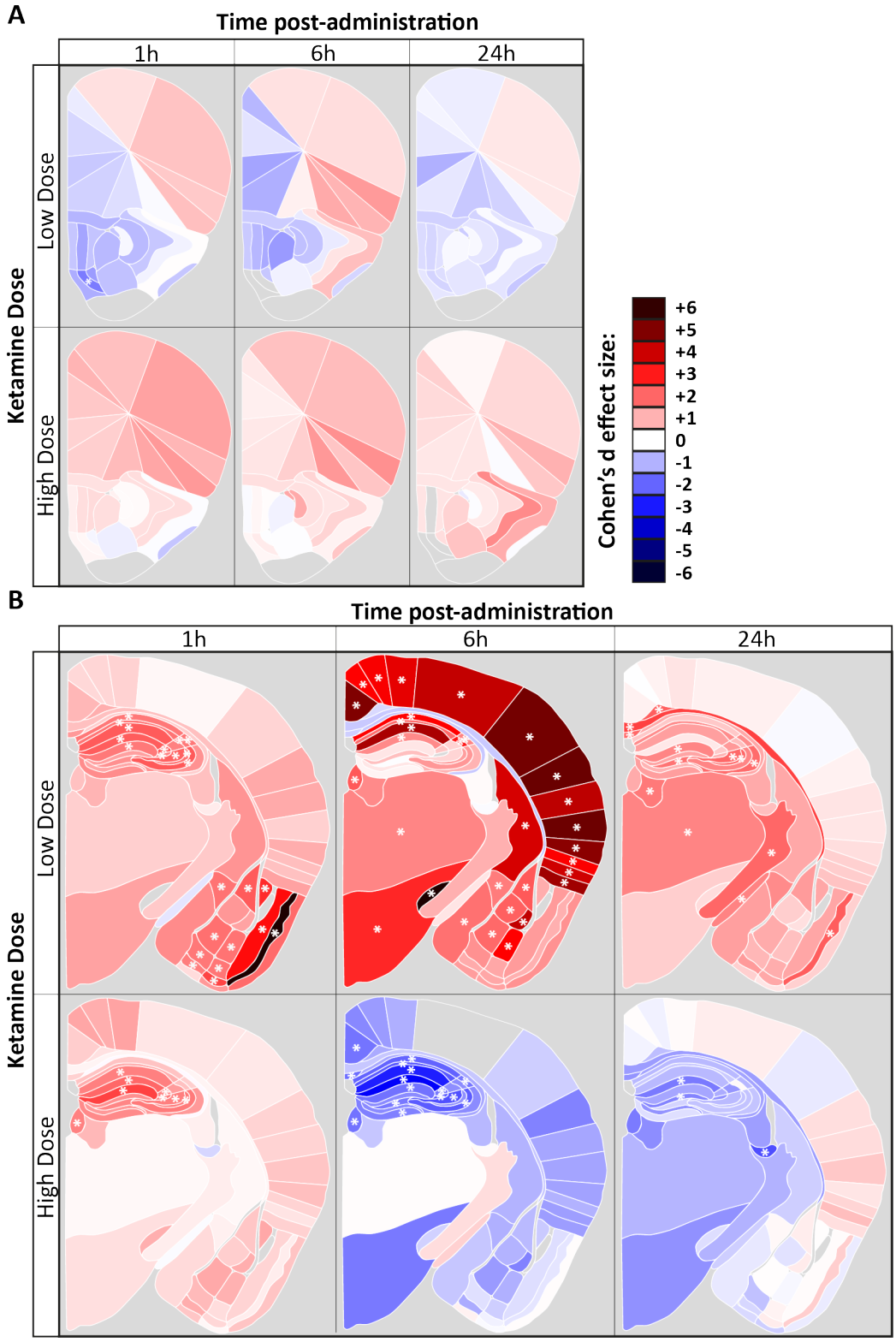

Figure 28 - Ketamine-induced changes in the density of Arc puncta.

(continued on next page) Colour scale represents effect size of change in puncta number from relevant saline control group (Cohen's d). Blue indicates decrease, red indicates increase. Asterisks represent regions with a statistically significant change from saline control p<0.05

(multiple t-tests). N=3-5 depending upon brain region. Grey = brain region not included due to damage in one or more sections resulting in n<2 for that region.

4.6.2 Changes in intensity of detected Arc puncta

The same analysis was carried out for the average puncta intensity measurements for each of the 89 brain regions. It is clear from a comparison of **figure 28** and **figure 29** that the effects of ketamine on the average intensity of detected Arc puncta are much less pronounced than its effects on puncta density. There are only a few individual regions showing significant change, despite the relatively low stringency of the multiple t-test approach. These regions are all contained within the bregma -1.70mm section and the low dose groups. There is a decrease in puncta number in the dentate gyrus granule cell layers at 1h (DGgrsup p=0.02, DGgrinf p=0.044), an increase in hypothalamus at 6h (p=0.02) and increases in SSp-tr (p=0.03), CA1R (p=0.048) and opt (p=0.003) at 24h. There was no pattern of change in anatomically-related regions and no individual regions reached the Bonferroni-corrected threshold for this experiment, which was p<0.00056. Therefore, it seems that ketamine is not having an effect on the mean fluorescence intensity of detected Arc^{VENUS} puncta at these doses or time-points.

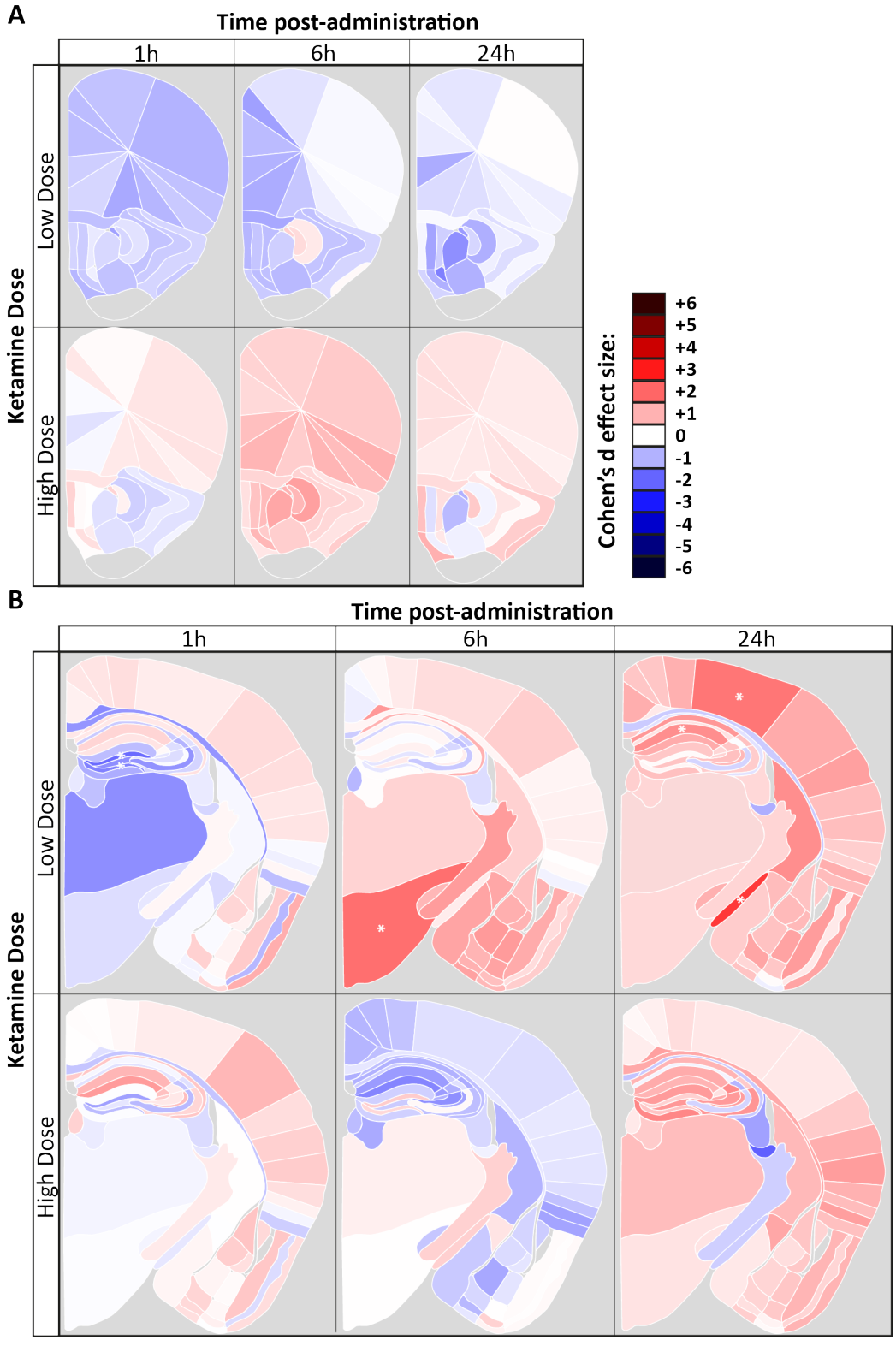

Figure 29 - Ketamine-induced changes in the average intensity of Arc puncta.

(continued on next page) Colour scale represents effect size of change in average puncta intensity from relevant saline control group (Cohen's d). Blue indicates decrease, red indicates increase. Asterisks represent regions with a statistically significant change from saline control

(multiple t-tests). N=3-5 depending upon brain region. Grey = brain region not included due to damage in one or more sections resulting in n<2 for that region.

4.6.3 Changes in size of detected Arc puncta

Again, from viewing **figure 30** the alterations in the size of detected puncta appear to be less dramatic than those in puncta density, visible in **figure 28**. There were very few changes taking place in the bregma 2.10mm section. At 1h post-administration the low dose induced decreases in TTv2 & 3 (p= 0.028 & 0.034), and the high dose induced an increase in motor cortex (p=0.047). However, these changes did not reach the Bonferroni corrected p value for this experiment (p<0.00056) and were not part of a pattern of changes in anatomically-related regions. Therefore, from this data it appears that ketamine is not having an effect on the mean size of detected Arc puncta at bregma 2.10mm. In the bregma -1.70mm section there is some clustering of significant changes in hippocampus. At 1h post-administration this takes the form of increase size of detected puncta in the low-dose group in DGmolsup (p=0.035) and CA2O (p=0.019), and both molecular layers of the DG are increased in the high-dose group (DGmolsup p=0.011, DGmolinf p=0.031). This is followed by decreases in multiple hippocampal sub-regions in the high-dose group only at 6h and 24h post-administration. This includes regions from CA1, CA3 and dentate gyrus. At 24h post-administration significant decreases in the high-dose group were also detected in several fiber tract regions (cing p=0.048, CC p=0.035, df p=0.030), thalamus (thal p=0.035, LH p=0.047), stn (p=0.008) and COApl2 (p=0.026). At 24h post-administration there were also significant changes detected in the low dose group in opt (p=0.019) and stn (p=0.021) however these were isolated changes, unlike the pattern of changes induced by the high dose.

Overall this indicates that a high dose of ketamine is able to alter the mean size of detected Arc puncta, predominantly in the hippocampus, and that this takes the form of an increase in the dentate gyrus at 1h post-administration, followed by a more widespread decrease which lasts until at least 24h post-administration.

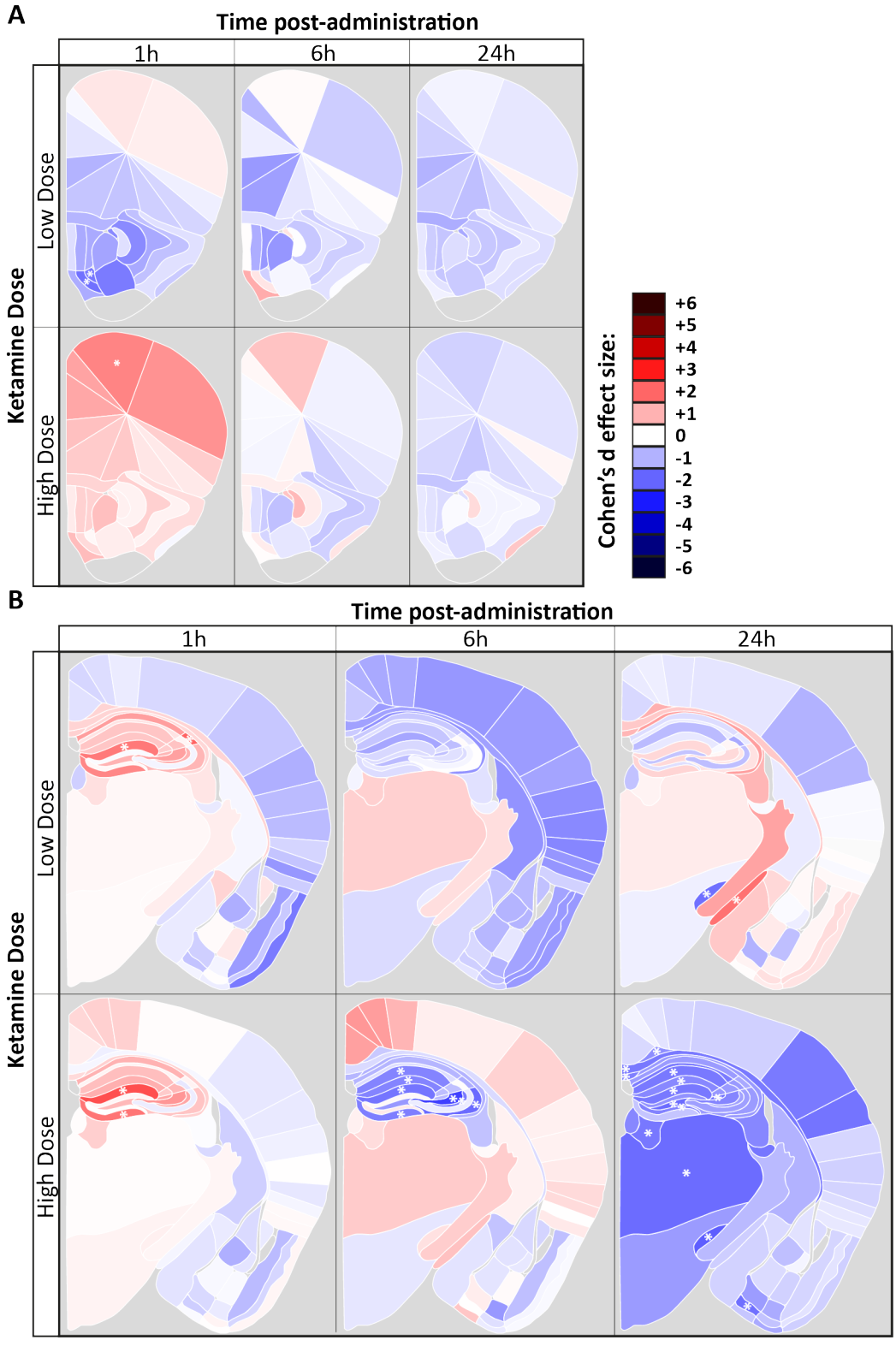

Figure 30 - Ketamine-induced changes in the average <u>size</u> of Arc puncta.

(continued on next page) Colour scale represents effect size of change in average puncta size from relevant saline control group (Cohen's d). Blue indicates decrease, red indicates increase. Asterisks represent regions with a statistically significant change from saline control (multiple

t-tests). N=3-5 depending upon brain region. Grey = brain region not included due to damage in one or more sections resulting in n<3 for that region.

4.6.1 Summary

In summary, both low- and high-doses of ketamine are able to rapidly modify the synaptome map of Arc. This modification is predominantly in the form of alterations to the density of Arc puncta present. The alterations in Arc puncta density show an interesting dose- and region-dependency. At 1h post-administration, both doses increase puncta density above saline control levels, whereas at 6h and 24h the low dose is able to induce an increase, but the high dose results in a general decrease. Most changes take place in the more rostral section (section B, -1.70mm), the hippocampus is affected at all time points but many other regions have time- and dose- specific effects. The most striking of these is the increased density in isocortex specifically in the low-dose 6h group. Such dramatic effects are not seen in the other puncta measurements, however there is a reduction in puncta size following high-dose ketamine in the hippocampus at 6h and in additional regions at 24h.

4.7 Ketamine-induced modification of the PSD95 synaptome map

The PSD95 synaptome was mapped at 24h post ketamine administration only, the results of which are presented in **figure 31**. In the bregma 2.10mm section in the low dose group there was a decrease in puncta density in alv (p=0.003) and ald (p=0.01) and a decrease in size in lot (p=0.032). In the high dose group there were significant decreases in density and intensity, and increases in size, seen in multiple regions within the olfactory areas including parts of the piriform cortex (PIR) and the anterior olfactory nucleus (AON). There are no significant changes in density or intensity in the bregma -1.70mm section, with the exception of an isolated increase in density in COApl2 (p=0.031). There were decreases in puncta size in several regions of isocortex (RSPd p=0.034, MOs p=0.014, MOp p=0.022, SSp-tr p=0.036) and the CP (p=0.033) in the low dose group.

Overall, there do seem to be some effects of ketamine on the PSD95 synaptome at 24h post-administration, predominantly in the high-dose group and the olfactory areas. These effects do not mimic those seen in the Arc synaptome in terms of the regions affected.

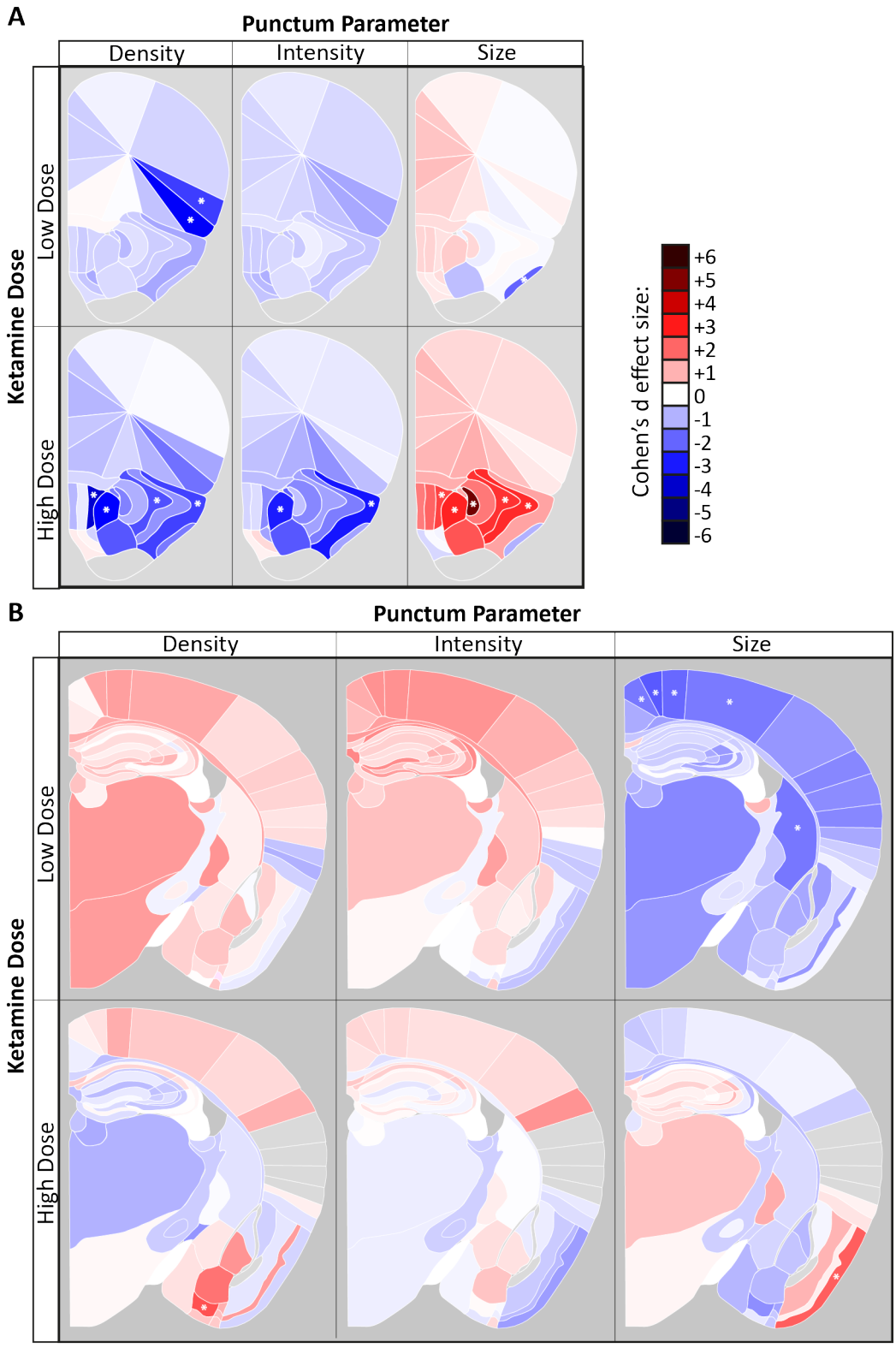

Figure 31 - Ketamine-induced changes in PSD95 synaptome map at 24h.

(continued on next page) Colour scale represents effect size of change in average puncta size from relevant saline control group (Cohen's d). Blue indicates decrease, red indicates increase. Asterisks represent regions with a statistically significant change from saline control (multiple

t-tests). N=3-5 depending upon brain region. Grey = brain region not included due to damage in one or more sections resulting in n<2 for that region.

4.8 Chapter discussion

4.8.1 Basal Arc synaptome map

Immunohistochemical staining has so far provided most information on the brain-wide and subcellular distribution of endogenous Arc protein (Nishimura *et al.*, 2003; Gao *et al.*, 2015). However, despite the availability of various antibodies raised against the Arc protein, individual accumulations of Arc at synaptic sites have been historically difficult to visualise with sufficient clarity in brain tissue. Several reporter mouse lines have been developed by placing fluorescent reporters under the control of the Arc promoter (Eguchi & Yamaguchi, 2009; Grinevich *et al.*, 2009; Susaki *et al.*, 2014), but they are not a direct measure of endogenous protein levels. Therefore, the Arc^{VENUS} reporter line is the first method, to our knowledge, which enables the clear and reproducible visualization of synaptic and nuclear accumulations of endogenous Arc protein in brain tissue. Further to this, the basal Arc synaptome map presented here is the first time that the distribution of endogenous Arc protein has been imaged and quantified at single synapse resolution across an entire brain slice. Whilst interesting in itself, this map also provides a dataset of 'baseline' Arc distribution for reference purposes. The baseline Arc synaptome map showed a great deal of inter-regional and intra-regional diversity in all three punctum characteristics. Puncta density values varied from 58 per μm^2 in layer 1 of the motor cortex down to 0.05 in some fiber tract regions. The highest levels of Arc puncta density and intensity were seen in the isocortex and the CA1 field of the hippocampus, where *Arc* mRNA levels are also known to be highest (Link *et al.*, 1995; Lyford *et al.*, 1995). The areas with the lowest puncta density were fiber tract regions and cell body layers of the hippocampus, which both contain few synapses. Particular diversity in Arc punctum characteristics was observed in the hippocampus and isocortex, therefore these regions are discussed in more detail below.

4.8.1.1 Synaptic accumulations of Arc

Prior to synaptome mapping, co-staining with both a pre-synaptic (VGlut1) and a nuclear marker (DAPI) were used to identify the nature and location of Arc^{VENUS} fluorescence at the subcellular level. The hippocampus was used as the focus of this investigation as it has a well-studied structure and connectivity. VGlut1 is a vesicular glutamate transporter situated at the pre-synaptic terminals of glutamatergic neurons (Liguz-Lecznar & Skangiel-Kramska, 2007). There are two other members of the VGlut family (VGlut2 & VGlut3), however in the adult mouse VGlut1 is the predominant form expressed in hippocampus (Fremeau *et al.*,

2001). Arc^{VENUS} puncta and VGlut1 immunofluorescence puncta were juxtaposed in hippocampal sub-regions, which suggests that the majority of the Arc puncta being imaged and quantified here are situated at the postsynaptic side of glutamatergic synapses. This fits with the proteomic evidence which places Arc at the PSD as part of the NMDA receptor supercomplex (Frank *et al.*, 2016), where it interacts with PSD95 (Fernandez *et al.*, 2017). The physical co-localisation of tagged PSD95 and Arc has also been observed in neuronal culture (Okuno *et al.*, 2012; Fernandez *et al.*, 2017), and EM experiments have detected Arc at postsynaptic sites (Moga *et al.*, 2004). This synaptic localization of Arc is known to be activity-regulated (Steward *et al.*, 1998). In response to experimentally-induced patterned neuronal activity, *Arc* mRNA is rapidly produced and transported out to dendrites, where it accumulates close to activated synaptic sites (Steward *et al.*, 1998; Farris & Steward, 2010). Arc protein follows a similar pattern of distribution (Moga *et al.*, 2004), and local translation has been found to take place in the dendrites. Indeed, application of glutamate is able to rapidly (within 15s) induce translation of pre-existing Arc mRNA at dendritic sites (Na *et al.*, 2016). However, the picture is complicated by evidence that suggests that, following induction by activity, Arc protein is then targeted to inactive synapses (Okuno *et al.*, 2012). It may be that Arc is indeed targeted to recently activated synapses, but does not enter the spine until cessation of that bout of activity. It is important to remember that all of the evidence available so far comes from experimental manipulations of neuronal activity levels using HFS and BDNF or TTX application, which may not reflect responses to physiological patterns of activity. Uncaging of glutamate at individual spines has enabled the real-time observation of rapid glutamate-induced Arc translation events in dendrites (Na *et al.*, 2016). A potential future direction would be to apply this method to Arc^{VENUS} neurons to visualise the accumulation of Arc protein following activation of a single spine. In the absence of this evidence however, it seems likely that Arc-positive synapses are more likely to have recently experienced activation than Arc-negative synapses. In the results presented in this thesis, VGlut1-labelled presynaptic terminals were often observed without a partner Arc punctum juxtaposed, although quantification of nearest neighbour distances would be beneficial to confirm this subjective visual observation. This suggests that Arc is not present at detectable levels in all synapses. This sparsity of Arc puncta distribution was particularly pronounced in the DG. This observation also fits with the previous finding that Arc is much less abundant than PSD95 at baseline levels of neuronal activity (Fernandez *et al.*, 2017). Indeed, in the PSD95 synaptome map, no such sparse punctum distribution is observed in the DGmo (Dr

Melissa Cizeron PhD thesis). Given the importance of the presence of PSD95 for the targeting of Arc to synapses (Fernandez *et al.*, 2017), this suggests that in this basal state of the animal there are likely to be glutamatergic synapses with a large capacity for increasing their Arc content in response to activity. There have been two roles identified for Arc at synaptic sites. Arc is able to induce an increase in endocytosis of AMPA receptor subunits through direct interactions with parts of the endocytic machinery at the synapse (Chowdhury *et al.*, 2006; Vazdarjanova *et al.*, 2006; Okuno *et al.*, 2012; DaSilva *et al.*, 2016), producing a reduction in synaptic strength. This function is involved in both translation-dependent LTD (Park *et al.*, 2008; Waung *et al.*, 2008) and homeostatic scaling (Rial Verde *et al.*, 2006; Shepherd *et al.*, 2006; Peebles *et al.*, 2010; Beique *et al.*, 2011). There is also evidence that Arc is involved in the structural modifications taking place during homeostatic plasticity (Peebles *et al.*, 2010). Local Arc expression is also necessary for stabilizing F-actin polymerization associated with LTP consolidation, which appears to be via the augmentation of phosphorylated cofilin at activated spines (Messaoudi *et al.*, 2007). However, Arc does not interact directly with either actin or cofilin (Nair *et al.*, 2017). Although it is not yet clear how Arc is able to facilitate two opposing forms of plasticity, there is evidence that post-translational modification of the protein could determine its function. For example, SUMOlyated Arc has been found to interact with the F-Actin-binding protein Debrin A (Nair *et al.*, 2017). It is impossible to know from the data presented in this thesis the function of the synaptic Arc accumulations observed in the Arc^{VENUS} mice. However, based on the existing literature, it seems likely that Arc presence at the synapse is a response to recent activity at that site and that Arc is acting there to alter synaptic strength in response to that activity. Please see **section 4.9** for suggested future experimental directions to confirm this.

4.8.1.2 Nuclear accumulations of Arc

Large, oval-shaped Arc accumulations were found to co-localise with DAPI staining, suggesting that they are within, or on the surface of, nuclei. Nuclear Arc localization has been observed using other methods of Arc visualization (Lyford *et al.*, 1995; Irie *et al.*, 2000; Bloomer *et al.*, 2007; Korb *et al.*, 2013), and there is evidence to suggest that Arc can act in the nucleus to increase the expression of PML nuclear bodies, resulting in decreased GluA1 transcription (Bloomer *et al.*, 2007; Korb *et al.*, 2013). The sparse distribution of Arc-positive nuclei in the DG granule cell layer is consistent with previous observations, and the number of Arc-positive nuclei can be increased by various kinds of stimulation (Ramirez-Amaya *et al.*, 2005; Vazdarjanova *et al.*, 2006). Indeed, both kainic acid induced seizure and novel

experience were found to increase the amount of nuclear Arc in the hippocampus in Arc^{VENUS} mice (Sarah Lemprière MSc dissertation and **appendix 12**, respectively). The causes and effects of Arc protein targeting to different subcellular compartments are still unclear. Therefore, the ability to visualise the subcellular distribution of endogenous Arc protein in brain tissue slices from Arc^{VENUS} mice clearly, and without the inherent variability of immunostaining protocols, is an important tool for future research efforts. Suggested future directions for this work can be found in **section 4.9**.

4.8.1.3 Diversity between hippocampal sub-regions

Different hippocampal sub-regions displayed different Arc punctum characteristics, which fit with the known size and shape of the postsynaptic terminals within those regions. In CA3slu and DGpo large Arc puncta assembled into rosettes were observed. Dendritic spines in these regions, known as thorny excrescences, are also particularly large. They synapse on to the giant presynaptic boutons of the mossy fibers projecting from the DG granule cell layer and contain ring-shaped PSDs (**see figure 32**). This correlation between known PSD characteristics and the nature of Arc puncta provides further evidence for the localization of Arc to the PSD. The area with the highest density and intensity of Arc puncta was the CA1sr, which fits with the previous evidence showing high levels of Arc mRNA in the CA1 field (Link *et al.*, 1995; Lyford *et al.*, 1995). The lowest Arc puncta density was seen in the granule cell and pyramidal layers, which naturally contain more cell bodies and fewer dendrites.

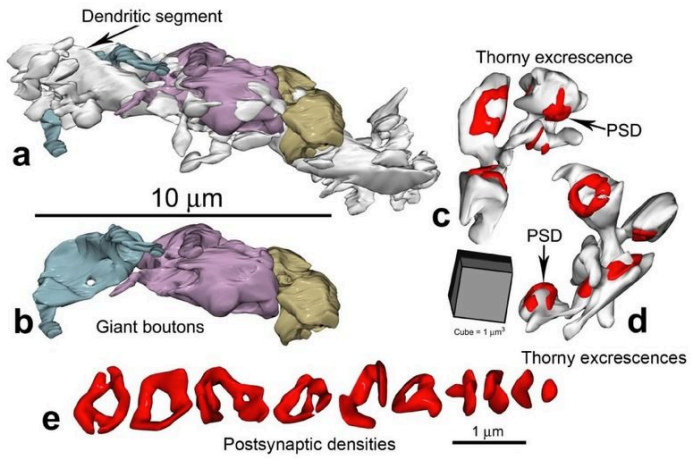

Figure 32 - Three-dimensional reconstructions of CA3 dendritic segments, thorny excresences and postsynaptic densities in wild-type mice.

Typical examples of dendritic segments (a), presynaptic giant boutons (b) and thorny excrescences with their postsynaptic densities shown in red (c-e). ***Figure taken from (Witton et al., 2015).***

4.8.1.4 Diversity within hippocampal sub-regions

As well as diversity between hippocampal sub-regions, there are also gradients of change in Arc punctum measurements within individual sub-regions. Gradients in Arc puncta density, intensity and size were observed along both the radial and the tangential axis of the hippocampal CA1 field. This suggests both differences in the nature of Arc protein accumulation between proximal and distal synapses on the dendritic tree of the same pyramidal cell (radial), and differences between the synapses of individual pyramidal neurons (tangential), see **figure 33**. In the Arc basal synaptome map there is a general reduction in Arc puncta density, intensity and size from distal to proximal along the tangential axis of CA1. Differences in Arc mRNA levels in the nucleus and cytoplasm along the tangential axis of CA1 have been described previously. Pyramidal cells in distal CA1 are more likely to induce overlapping Arc mRNA expression during exposure to two different environments than those in proximal CA1, which are more likely to respond to one environment only (Hartzell *et al.*, 2013). This fits with other data which identified a higher spatial specificity of place fields in proximal CA1 as compared with distal CA1 (Henriksen *et al.*, 2010). Therefore, the Arc synaptome gradient could reflect the increasing spatial specificity of cells in the proximal direction, thus gradually reducing the likelihood of synaptic activity in any one environment along that axis. However, from this initial Arc synaptome data it is difficult to know whether this change is indeed due to a reduction in synaptic activity or a more general reduction in

synapse number along this axis. Such a gradient was not observed in the PSD95 synaptome map (Dr Melissa Cizeron PhD thesis), suggesting that it is likely to be the former.

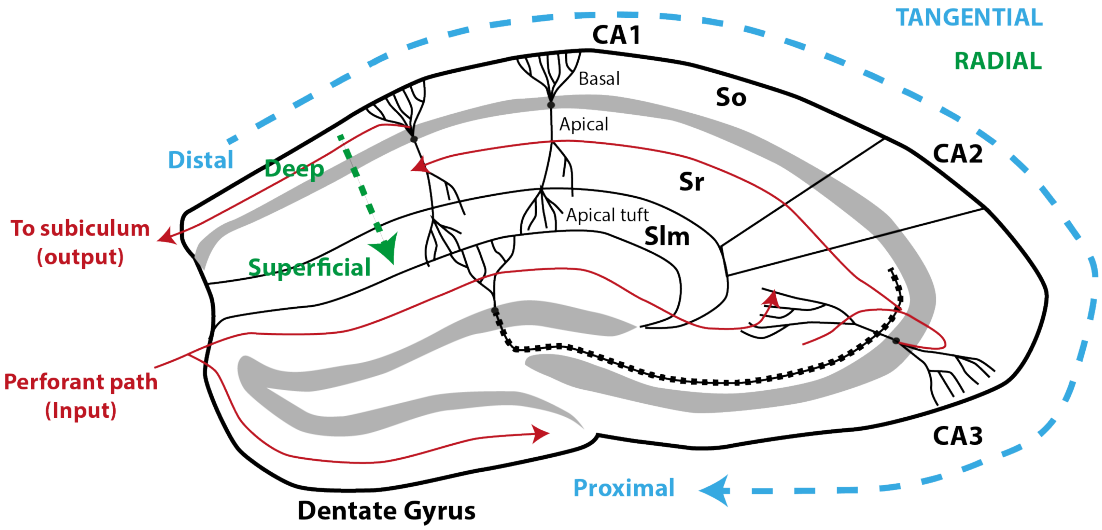

Figure 33 - Schematic diagram of hippocampal structure and basic circuitry.

*Arrows indicate the direction in which changes across gradients are plotted in **figure 25**. **Tangential** gradients suggest differences between neighbouring pyramidal neurons, **radial** gradients suggest differences between proximal and distal dendrites of the same pyramidal neuron.*

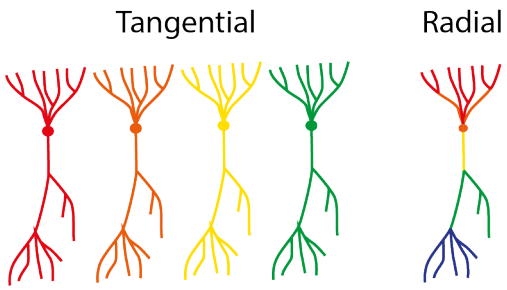

Figure 34 - Schematic diagram showing interpretation of tangential and radial hippocampal gradients on pyramidal cell characteristics.

A radial gradient in Arc puncta in the CA1sr was also observed. This took the form of increasing puncta density, intensity and size with increasing distance from the soma. There was however, a sharp drop in puncta density in the last segment before the beginning of the CA1slm. Similar radial gradients were observed in the PSD95 and SAP102 synaptome maps (Zhu *et al.*, 2018) although direct comparison of these datasets with the current one is difficult because of differences between analysis methods. The CA1sr contains the proximal regions of the apical dendrites of the CA1 pyramidal cells, which receive input primarily from the CA3 via the Schaffer collateral (Amaral & Laveneux, 2007), see **figure 33**. Within the CA1sr, both the number of perforated synapses and the AMPA content of synapses increases with increasing distance from the soma (Nicholson *et al.*, 2006). Perforated synapses contain more NMDA and AMPA receptors than non-perforated synapses, and are therefore expected

to generate larger synaptic currents when activated (Desmond & Weinberg, 1998; Ganeshina *et al.*, 2004a, b). In theory these synapses could therefore be more likely to induce Arc expression. Overall these observations of gradients within certain anatomical regions of the Arc synaptome map highlight the ability of this method to surpass existing anatomical classifications, and allow the study of synapse composition in more depth. Although gradients were observed in the PSD95 and SAP102 synaptome maps, this is the first time such synaptic gradients have been observed in a protein known to be targeted to recently-activated synapses. The mapping of Arc and PSD95, with accompanying co-localisation analysis, in the same animal would provide important information on the degree to which Arc gradients are defined by synapse number vs activity. Mapping Arc gradients in stimulated animals (e.g. kainate-induced seizure) would also provide information on their stability and underlying mechanisms.

4.8.1.5 Isocortex

The existing literature has identified the isocortex as the area containing the highest levels of Arc mRNA and protein (Link *et al.*, 1995; Lyford *et al.*, 1995), and a similar observation can be made from the Arc synaptome map. The isocortex is the brain region responsible for higher cognitive functions such as language, episodic memory and voluntary movement. It has a laminar structure which has historically been split into six layers, I being the most superficial and VI the deepest (Brodmann, 1909). Each layer contains different cell types and has a distinct set of inputs and outputs, see **figure 35A**. The more superficial (layers I-IV) are the main input layers of the cortex and contain mostly localised intracortical connections, whereas the deepest (layers V & VI) are the main output layers and form long distance projections to subcortical regions and the contralateral hemisphere (Noback *et al.*, 2005; Molyneaux *et al.*, 2007). In the Arc synaptome map there was a general decrease in puncta density from the superficial to deep layers of isocortex. A similar pattern of puncta density across cortical layers was observed in the PSD95 and SAP102 synaptome maps (Zhu *et al.*, 2018), suggesting that this is more likely to be a general change in the number of excitatory synapses rather than something that is specific to Arc. Indeed, an EM study in human adult temporal cortex also found greater densities of synapses (defined as pre- and post-synaptic membrane specializations separated by a synaptic cleft) in the more superficial cortical layers (DeFelipe *et al.*, 1999), see **figure 35B**. In addition to this there is a particularly high intensity of Arc puncta in layer 4, which is not observed in the PSD95 or SAP102 synaptome maps, or human EM data. This is interesting as layer 4 receives the majority of inputs from outside the

cortex and is thought to be the main recipient of incoming sensory information (Noback *et al.*, 2005). A high level of Arc protein in layer 4 has been observed at lower resolution with IHC. In that experiment auditory deprivation was able to reduce this increased staining in layer 4 of the auditory cortex and instead shift it to layer 4 in other areas, including the visual cortex (Pernia *et al.*, 2017). Taken together this suggests that, in addition to differences in general synapse number between cortical layers there are also Arc-specific differences, perhaps due to differences in patterns of synaptic input onto cells in those regions.

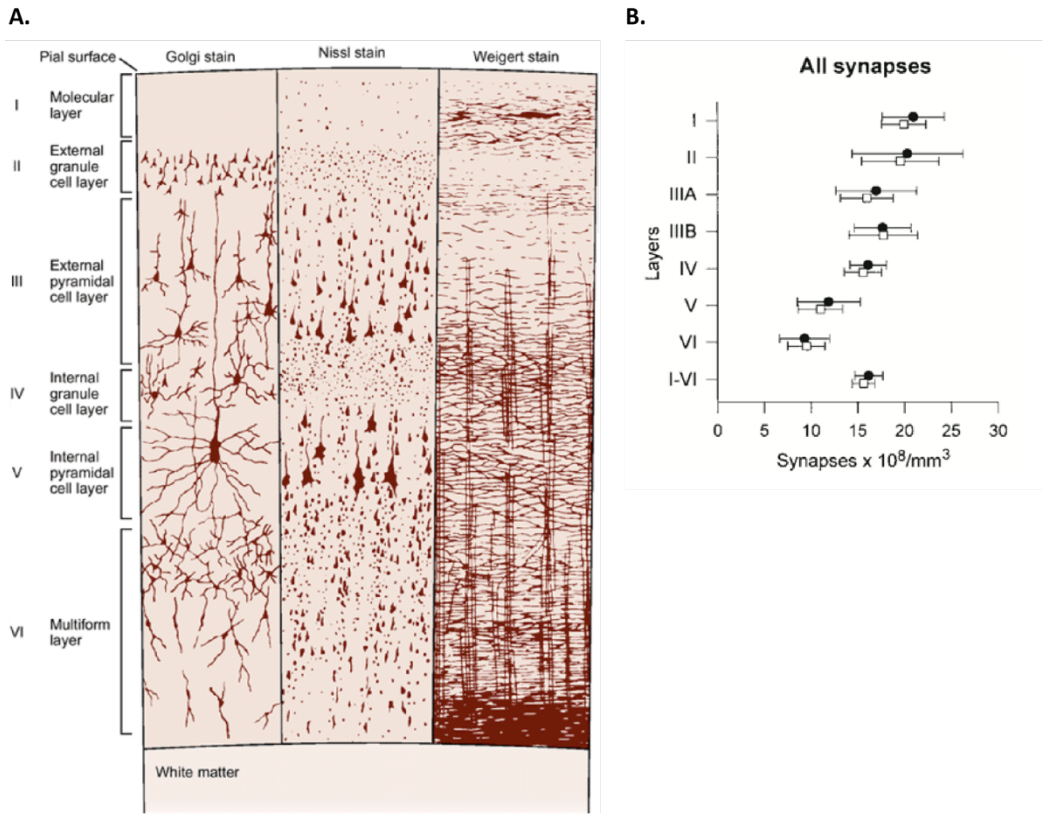

Figure 35 - Representative column of neocortex showing layers 1-6 & synapse density per layer of human temporal cortex.

A. Representative column of neocortex showing layers 1-6. *Golgi stain shows a subset of neurons including their processes, Nissl stain shows cell bodies and Weigert stain shows myelinated fiber paths.* ***Taken from (Kandel et al., 2000). B. Synapse density per layer of human temporal cortex.*** *Mean and 95% confidence intervals of the total number of synapses obtained using 10 photomicrographs per layer (solid circles) or 15 photomicrographs per layer (open squares).* ***Taken from (DeFelipe et al., 1999).***

4.8.1.6 Summary

Overall, looking at the hippocampus and isocortex as examples enables us to conclude that the Arc synaptome map can identify differences in the nature of Arc protein accumulation at synapses both between, and within, previously-defined anatomical regions. It is also clear that, whilst some of these observed differences are likely to be as a result of diversity in the density, size or shape of excitatory synapses in these regions, there are also some interesting observations which appear to be specific to Arc. Examples of these are the sparse distribution of Arc puncta in the DGmo and the high intensity of Arc puncta in layer 4 of isocortex. Given the evidence that Arc protein is targeted to synapses in response to patterned synaptic activity (Steward *et al.*, 1998), these observations could be the products of the particular patterns of input received at synapses within these anatomical regions in the 'home cage' environment. A more systematic comparison of the Arc and PSD95 synaptome maps, using mice containing knock-in fluorescent reporters for both proteins, would shed more light upon these Arc-specific synaptome features. In the future, the Arc synaptome could perhaps be used to measure alterations in neuronal activity patterns at the single synapse level on a whole-brain scale. See **section 4.9** for more detail on these potential future directions.

4.8.2 Effect of a stressful novel experience on Arc synaptome map

In order to test the ability of the Arc synaptome map to be modified by pharmacological agents, and to investigate the molecular mechanism(s) underlying the action of ketamine, a ketamine synaptome mapping study was designed. The design of this study included groups of animals injected only with sterile saline and sacrificed at three different time points. The data from these animals was presented separately here to investigate the effect of a novel, and mildly stressful, experience on the Arc synaptome map. Saline injection induced an increase in Arc puncta density at 6h post-administration, as compared with the 1h and 24h groups. This increase was specific to a number of hippocampal sub-regions and some areas of fiber tracts. Without the inclusion of a naïve control group it is not possible to tell whether there are already changes taking place at the 1h time point. However, there does seem to be a peak in the hippocampus at 6h. There is considerable literature on the effect of novel experiences on Arc mRNA and protein levels. Increased numbers of Arc positive cells have been observed in hippocampus and parietal cortex for 30min-2h following a 5 min exploration of a novel environment (Ramirez-Amaya *et al.*, 2005). Arc in the dendrites has also been observed in the CA1 field of hippocampus 4h following 5 min of novelty (Jakkamsetti *et al.*, 2013). The results presented here add to that knowledge by

demonstrating that Arc is also increased at the synaptic level, and that this can be detected as late as 6h following a novel experience. This experience of SC injection also has the potential to be stressful for the animal, however, there is no change in Arc punctum measurements in the usual stress-response brain regions. These include the amygdala (Ressler, 2010), where Arc mRNA has previously been found to be increased following acute restraint stress (Trneckova *et al.*, 2007) and the hypothalamus, which contains the hypothalamic paraventricular nucleus (PVN) (Herman *et al.*, 2008). However, increases in Arc mRNA have also been observed in some hippocampal regions following acute predator scent stress (Kozlovsky *et al.*, 2008). Overall these observations suggest that the Arc synaptome mapping method can be used to detect a response of Arc to relatively subtle stimuli, whether the response here can be classed as a 'stress' or a 'novelty' response is less simple and would require further experimentation. Given the activity-regulated nature of Arc transport to synapses, there is the possibility that this method could be used to map synapses activated during the encoding of a novel experience. A pilot experiment to do this was carried out as part of this PhD project, however no significant changes were observed in Arc punctum measurements between control and novel experience groups. A summary of the results from this experiment can be found in **appendix 12.**

4.8.3 Effect of ketamine administration on the Arc synaptome map

Following the characterisation of the baseline Arc synaptome map, and modifications induced by the administration of saline injection, the effect of ketamine administration was investigated. Understanding the molecular mechanism of ketamine action is of particular importance because of the clinical relevance of its rapid-onset, long-lasting antidepressant effects. Despite considerable work over the last decade the molecular mechanism underlying this response is still not fully understood, and it remains unclear why the antidepressant response would be specific only to sub-anaesthetic doses (Raffa *et al.*, 2017; Strasburger *et al.*, 2017). Our current understanding of the response of Arc to sub anaesthetic ketamine administration comes from western blots showing that Arc levels in synaptoneurosomes of the prefrontal cortex are increased 1h and 2h post-administration of 10mg/kg ketamine (Li *et al.*, 2010). ISH has also shown increased arc mRNA in isocortex, including somatosensory and motor areas, 90 min following 25 or 50 mg/kg ketamine administration (de Bartolomeis *et al.*, 2013). However, until now the response of Arc to sub-anaesthetic and anaesthetic doses of ketamine has not been compared, and it has not been possible to quantify the

accumulation of Arc protein at individual synapses in response to ketamine across entire brain sections.

4.8.3.1 Dose-dependent, two-phase response of Arc to ketamine

The results presented here in **section 4.6** add to our current understanding of the action of ketamine on Arc in several ways. Firstly, they have enabled the identification of two distinct responses of synaptic Arc to a sub-anaesthetic (low) and an anaesthetic (high) dose of ketamine. This can be summarised as a two-phase response. In the first phase, both low and high doses induced an increase in Arc puncta density in hippocampus at 1h post-administration, and the low dose also affected some olfactory and cortical subplate regions in the same way. In the second phase (6h + 24h) the two doses had opposing effects on puncta density. At 6h the low dose again produced an increase in hippocampus and cortical subplate but now also had the same effect on isocortex, cortical nuclei, thalamus and hypothalamus. Whereas the high dose produced decreases in puncta density in hippocampus, accompanied by reductions in puncta size in this region. At the 24h time point there is again a general increase in puncta density above saline control in the low dose group, particularly in regions within the hippocampus, thalamus and fiber tracts, but there is no longer an effect on isocortex. There is also still a general decrease in puncta density in the high-dose group, mostly within hippocampus and fiber tracts, and this is again accompanied by a decrease in puncta size in these regions.

When interpreting the results presented here it is important to take into consideration the timeline of ketamine presence in the brain tissue. Ketamine is metabolised rapidly and has been found to have a half-life in a laboratory mouse of approximately 13 min (Maxwell *et al.*, 2006). Ideally measurements of receptor occupancy would have been taken from animals within the synaptome mapping cohorts. However, in the absence of that data, published *ex vivo* radiography evidence from the same background strain of mouse (C57/BL6) can provide a guide. 30mg/kg ketamine delivered via a subcutaneous route reached a maximum level of MK801 binding site occupancy after 15 min and was rapidly cleared, resulting in no significant level of occupancy after 1h. The maximum level of occupancy reached by this dose was >50% (Lord *et al.*, 2013). This strongly suggests that for the low dose (10mg/kg) group in the Arc synaptome mapping study ketamine is likely to have been cleared from NMDAR binding sites by the first time point (1h). The same kind of receptor occupancy data does not appear to be available for a dose close to the 100mg/kg, used as the high dose for the Arc synaptome mapping experiment. However, at 60 min post administration of 100mg/kg ketamine it is

possible to detect ketamine in the blood, at a serum concentration of ~2ug/ml, see **figure 36** (Maxwell *et al.*, 2006). Therefore, it is possible that during the first phase at 1h post-administration there is still some blockade of NMDARs by ketamine in the high-dose group. However, during phase two (6h-24h) it is highly unlikely that any ketamine is remaining. Taken together this existing evidence suggests that most of the changes seen in the Arc synaptome map here are a downstream response to the transient blockade of NMDARs by ketamine and not an acute response to the current presence of ketamine at receptor sites.

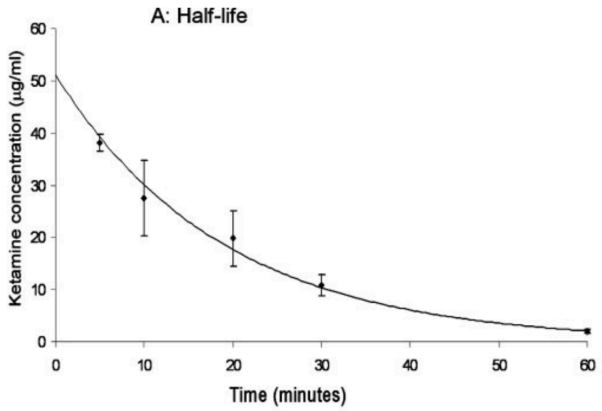

Figure 36 - Serum half-life of ketamine, average of 4 strains of laboratory mice.

($t_{1/2}$ = 13 min). *100mg/kg ketamine administered intraperitoneally. Strains tested = FVB, C3H, C57, DBA.* ***Figure taken from (Maxwell et al., 2006).***

The most dramatic effect of ketamine administration seen here was on the number of Arc puncta detected, rather than their size or fluorescence intensity. This raises the question of whether this represents specific changes in the delivery of Arc to synapses, or changes in the number of synapses in general. Synaptogenesis has been reported in the PFC 24h following administration of 10mg/kg ketamine (Li *et al.*, 2010; Ardalan *et al.*, 2017) and in hippocampus 24h following a 15mg/kg dose of S-ketamine (Ardalan *et al.*, 2017). The increase in Arc puncta number is observed here as early as 1h post-administration, which is a time point not assessed in the referenced synaptogenesis studies and could be considered too rapid for this kind of response. However, synaptogenesis has been observed in the nucleus accumbens 1h following a single administration of cocaine (Dos Santos *et al.*, 2017), showing that in general the generation of synapses in response to a pharmacological agent is possible on this timescale. Conversely, the reduction in Arc puncta density at 6h and 24h following the 100mg/kg dose could be the result of the removal of Arc from previously Arc-positive synapses, or a loss of synapse number in general. There does not appear to be any previous

evidence of anaesthetic doses of ketamine causing a loss of synapses or cell death in adult animals, although this has been observed in juveniles (Slikker *et al.*, 2007). Answering the question of synaptogenesis vs Arc transport was part of the motivation behind mapping the PSD95 synaptome in response to ketamine administration. No widespread changes were seen in the density, intensity or size of PSD95 puncta at 24h post-administration in the brain regions which were affected in the Arc synaptome map. This argues against changes in general excitatory synapse number as being the cause for the alterations in Arc puncta number. In the Arc synaptome map only a handful of individual regions had a significant alteration in average punctum intensity in response to ketamine. However, there were a cluster of regions, predominantly within the hippocampus that had a reduction in average punctum size at 6h and 24h post-administration of a high dose. Taken together, this suggests that in response to low-dose ketamine administration Arc protein is delivered to synapses which previously did not contain it at detectable levels (Arc-negative synapses). It also suggests that in response to high-dose ketamine administration Arc is first driven to previously Arc-negative synapses, producing an increase in puncta number at 1h. This is followed by the depletion of Arc from synapses at 6h and 24h, reducing the number of synapses containing detectable levels of Arc and also reducing the average size of those detectable puncta. However, it is important to remember that all of these values are the mean of a potentially diverse population of synapses and therefore it is possible that subtler changes in different subpopulations of synapses within these delineated regions could be taking place. A future aim is to analyse this data in more depth to identify these subpopulations. See **section 4.9** for more details.

4.8.3.2 Screening of brain regions

The Arc synaptome results provide a considerable amount of data on the brain regions affected by ketamine administration across these two phases of response. The hippocampus was affected at all three time points and was the area that displayed the most strikingly different response to the low and high doses. The hippocampus has previously been implicated in the pathophysiology of depression. Reduced hippocampal volume is observed in MDD patients and can be rescued with antidepressant treatment (Malykhin *et al.*, 2010). Further to this, microinfusion of R-ketamine specifically into DG and CA3 produces an antidepressant response (Shirayama & Hashimoto, 2017), suggesting that the hippocampus is functionally involved in ketamine's antidepressant action. An increase in Arc protein level has been detected in western blot of hippocampal tissue 30 min after administration of

3mg/kg ketamine (Autry *et al.*, 2011). The evidence from the Arc synaptome map builds upon this by showing that alterations of Arc protein levels in the hippocampus are at least partially due to alterations in the amount of protein at synaptic sites; that this can last up to 24h; and that the hippocampus responds differently to low and high doses of ketamine. The hippocampus is involved in information processing which is essential for memory formation and retrieval (Squire, 1992; Whitlock *et al.*, 2006). It receives input from widespread areas of neocortex via the entorhinal cortex (EC), processes this information and produces output which is delivered back to neocortical areas again via the EC (Teyler & Rudy, 2007). An effect of ketamine on synaptic Arc levels in the hippocampus suggests that modification of synaptic strength is taking place either via increased AMPA receptor endocytosis or remodelling of spines, which has the potential to alter the way information is processed as it passes through the hippocampus. Indeed, 30mg/kg ketamine has been found to induce AMPAR endocytosis-dependent synaptic depression at Schaffer collateral synapses in CA1, peaking at 20 min post-administration and lasting for over 4h (Duan *et al.*, 2013). This synaptic depression was linked to the memory impairments caused by ketamine (Moosavi *et al.*, 2012) but could have relevance to its antidepressant effects also.

The isocortex was affected by ketamine administration specifically at 6h post-administration. This effect was particularly striking in the low-dose group and involved every sub-region within isocortex. There is less existing information on the role of isocortical regions in the ketamine response than for the hippocampus. From the data presented here the effects in the isocortex seem to be temporally secondary to the onset of effects in hippocampus, and more transient in nature. There is some evidence that in MDD patients whose symptoms are improved by ketamine administration, stimulus-evoked somatosensory cortical responses are also increased at 6.5h post-infusion (Cornwell *et al.*, 2012).

The synaptome mapping results here also identified clusters of affected areas in the cortical subplate, cerebral nuclei, thalamus, hypothalamus, olfactory areas and fiber tracts. These were predominantly changes in puncta density induced by the low dose. Some of these regions do not have a previously identified role in the response to ketamine, for example microinfusion of R-ketamine into the basolateral amygdala does not induce an antidepressant response (Shirayama & Hashimoto, 2017). These synaptome map findings suggest a widespread alteration of synaptic composition following low-dose ketamine administration, involving a diverse network of brain regions. Different members of this

network appear to be altered at different time points following administration, with alterations in the hippocampus a common feature throughout. Although these results cannot tell us which of these altered regions is responsible for the behavioural changes caused by ketamine, they do provide a list of areas for further investigation along with a timeline of their response. Some potential follow-up experiments based on this list have been described in **section 4.9**.

The majority of the previous work on ketamine's antidepressant action has focussed upon the prefrontal cortex, and there is some compelling evidence that this region is functionally important for ketamine's antidepressant actions (Shirayama & Hashimoto, 2017). This includes the finding that both microinfusion of ketamine into the infralimbic (IL) PFC and optogenetic stimulation of the same area are able to induce long-lasting antidepressant responses similar to systemic ketamine administration (Fuchikami *et al.*, 2015). Further to this, the previous evidence for an increase in Arc protein levels following sub-anaesthetic ketamine administration came from synaptoneurosomes taken from the mPFC (Li *et al.*, 2010). The PFC has been identified as important for the cognitive control of flexible actions, with the IL area thought to be specifically involved in the development and expression of inflexible reward seeking (Barker *et al.*, 2014). However, in the results described here no significant alterations in Arc puncta density, intensity or size were detected in the infralimbic area of the PFC, which was unexpected. However, it should be noted that in general the bregma level containing these regions (2.10mm) showed greater levels of variation between mice, with an average 45% larger standard deviation in the density measurement at 1h post-administration than the bregma 1.70mm section. This suggests that a greater degree of biological variation in Arc levels in prefrontal regions could be masking subtle changes in Arc puncta measurements. Therefore, before drawing conclusions on this point, it would be beneficial to repeat this experiment with a larger number of animals per group. However, if there is indeed no change in the synaptome map of the prefrontal cortex, this would be contradictory to previous evidence.

4.8.3.3 Possible mechanisms underlying response of Arc to ketamine

As mentioned, these results allow us to identify distinct effects of low- and high-dose ketamine on Arc puncta number, which do not follow a conventional dose-response relationship. In the second phase of response the low dose induced an increase in Arc puncta density across multiple regions, whereas the high dose induced a general decrease sometimes in the very same regions. This could be described as an indicator of an 'inverted

u' dose-response relationship, in which response increases with dose only to a point, after which the trend reverses and there is a decrease in response with increasing dose. What is particularly interesting about this observation is that the low (10mg/kg) dose has been repeatedly reported in the literature as 'antidepressant' in mice from 1-24h post-administration (Li *et al.*, 2010; Beurel *et al.*, 2011; Wang *et al.*, 2015; Can *et al.*, 2016; Zanos *et al.*, 2016). Whereas this response has not been observed for doses over 80mg/kg (Li *et al.*, 2010; Chatterjee *et al.*, 2011), which would include the 100mg/kg high dose used here. This suggests a correlation between a sustained (>1h) increase in numbers of Arc-positive synapses and the presence of an 'antidepressant' response. This conclusion is tentative however, as behavioural testing was not carried out on the animals involved in this mapping study. It is also interesting to note that increased Arc mRNA and protein have been observed in cortical regions and parts of the hippocampus following repeated administration of conventional antidepressant treatments (SSRIs, SNRIs and tricyclic antidepressants), and that short-term treatments are not able to induce this increase (Pei *et al.*, 2003; De Foubert *et al.*, 2004; Ferres-Coy *et al.*, 2013). These drugs only show antidepressant effects after repeated administration, again linking an increase in Arc levels with antidepressant efficacy. A similar 'inverted u' dose response relationship has been described for the release of glutamate in the PFC following ketamine administration. Ketamine doses of between 10-30mg/kg induce an increase in glutamate over the first 100 min post-administration, whereas 50mg/kg does not and 200mg/kg decreases glutamate levels (Moghaddam *et al.*, 1997). An increase in general neuronal activity has also been observed in several regions in response to sub-anaesthetic doses only. For example a 35mg/kg dose of ketamine induces an increase in the uptake of ^{14}C-2-deoxyglucose (2-DG) in multiple brain regions including PFC and parts of hippocampus, but this was not observed with an anaesthetic (100mg/kg) dose (Duncan *et al.*, 1998). This correlation of the dose-response of ketamine-induced neuronal activity, glutamate release and Arc puncta density is interesting, as increased glutamate release can increase Arc levels via mGluR and NMDAR activation, which induces the translation of existing Arc mRNA (Bloomer *et al.*, 2008; Waung *et al.*, 2008; Na *et al.*, 2016) and transcription of new Arc mRNA (Steward *et al.*, 1998; Steward & Worley, 2001). Interestingly, the IEG c-fos staining showed a different pattern of induction to both glutamate and Arc, with increases seen in PFC and other areas of isocortex but not the hippocampus. In the case of c-fos, 100mg/kg induced a greater response than 35mg/kg, not showing the described 'inverted u' dose-response (Duncan *et al.*, 1998). This suggests that perhaps the patterns of

activity produced by this ketamine-induced glutamate 'surge' do not activate all IEGs in the same way, and that some of the synaptome map response described here may be Arc specific.

Several members of the MAPK and mTOR signalling cascades have also been found to be activated by low but not high doses of ketamine. At 1h post-administration 5 and 10 mg/kg doses are able to increase levels of p4E-BP1, pmTOR, pp70S6K, pERK and pAkt in synaptoneurosomes of PFC, but an 80mg/kg dose does not (Li *et al.*, 2010). The response of ERK is particularly interesting as ERK phosphorylation is downstream of NMDAR and mGluR activation (Mao *et al.*, 2004; Chen *et al.*, 2017) and Arc transcription and translation are ERK dependent (Panja *et al.*, 2009; Pintchovski *et al.*, 2009; Kumar *et al.*, 2012), as is the targeting of Arc mRNA to activated synaptic sites (Huang *et al.*, 2007). There is also recent evidence that Arc protein itself is directly phosphorylated by ERK, and that this may increase transport of Arc into the cytoplasm (Nikolaienko *et al.*, 2017). The ability of glutamate to upregulate Arc has been found to depend upon NMDAR-mediated ERK phosphorylation (Chen *et al.*, 2017). When viewed together with the glutamate response this suggests that increased Arc levels in the low dose group could be the result of a ketamine-induced increase in glutamate release, inducing NMDAR and/or mGluR activation and ERK phosphorylation. Similarly, the reduction of glutamate release in response to an anaesthetic dose provides a potential explanation for the reduction in Arc during the second phase in the high dose group. However, this hypothesis does not explain why there was first a short-term increase in Arc puncta density in the high-dose group. The literature on glutamate increase identified no such short term increase in glutamate in PFC following 100mg/kg ketamine (Moghaddam *et al.*, 1997).

Whether or not the glutamate 'surge' is responsible for the observed changes in Arc, it remains the case that ketamine is an NMDA receptor antagonist, and that at certain time points and dosages it is able to increase the levels of an activity-regulated protein. As discussed, Arc transcription and translation is induced by NMDA receptor activity (Steward *et al.*, 1998; Steward & Worley, 2001; Bloomer *et al.*, 2008). There is some evidence that at low doses ketamine is able to act preferentially at inhibitory interneurons in PFC, thus increasing excitability of the principal excitatory neurons in that region (Zhang *et al.*, 2008; Quirk *et al.*, 2009). If this is taking place in hippocampus and cortex, then it could explain the ability of ketamine to induce glutamate release and the expression of IEGs such as Arc and c-

fos. At high doses this preference for interneurons would be inconsequential, with ketamine also causing blockade of NMDARs on principal excitatory neurons, and would perhaps result in the decreased Arc levels seen with anaesthetic doses. However, again this hypothesis does not explain the short-term increase in Arc levels seen prior to the decreases induced by an anaesthetic dose.

4.8.4 Effect of ketamine administration on PSD95 synaptome map

PSD95, an important interactor of Arc (Fernandez *et al.*, 2017), has also previously been found to be increased in synaptoneurosomes of PFC following low dose ketamine administration (Li *et al.*, 2010). However, the increase in PSD95 began later than Arc, at 2h post-administration, and lasted much longer, until 72h. This different timeline of PSD95 response to ketamine informed the design of the PSD95 synaptome mapping experiment presented here and therefore only a 24h time point was investigated. The effect of ketamine on PSD95 was less dramatic and less widespread than its effect on Arc. The low dose induced a decrease in PSD95 puncta in two isocortical regions, and a decrease in size of PSD95 puncta in four other isocortical regions. This is in contrast to the Arc results which did not see a pattern of change in the isocortex at 24h. The high dose induced a decrease in density and intensity, and an increase in the size of PSD95 puncta. Most of the affected regions were clustered within the olfactory areas contained within the 'prefrontal' bregma 2.10mm brain section. Again, these regions were unchanged in the Arc synaptome. As discussed in **section 4.8.3.1** this lack of correlation between changes taking place in the Arc and PSD95 synaptome maps suggests that the observed alterations in Arc puncta number are not simply a reflection of a change in excitatory synapse number. One expectation when mapping the PSD95 synaptome at this time point was that it would be possible to identify increases in the number of PSD95 puncta in the medial prefrontal cortex (ILA, ORBm, PL, ACAd) as a result of the ketamine-induced synaptogenesis previously reported in the literature (Li *et al.*, 2010; Ardalan *et al.*, 2017). This was not the case as no increase in PSD95 puncta density was observed in these regions.

4.9 Future directions

4.9.1 Further analysis of existing data

The synaptome mapping datasets presented here contain an immense amount of information, which has been analysed and presented in a simple way for the purposes of this thesis. The statistical approaches used here are not optimal for understanding the complexities of this data and therefore an important future direction of this research will be

to apply more complex statistical analyses to this data. These could include Bayesian inference approaches. A model based on this kind of approach was designed for Dr Melissa Cizeron's synaptome mapping data by Dr Nathan Skene. Adapting this method to accommodate the design of the ketamine study described here could provide a superior method of analysis to the multiple t-test approach used for this thesis. Further to this, more detailed analysis of the existing data which goes beyond comparison of the mean values per region would provide more information about the presence of subpopulations of puncta within anatomical regions. Again, steps were made towards this goal by Dr Zhen Qiu in the analysis of the $PSD95^{EGFP}$ synaptome maps generated by Dr Melissa Cizeron (Zhu *et al.*, 2018). These could be adapted for the Arc ketamine dataset.

4.9.2 Arc^{VENUS} mice

As the results presented in this thesis show, the Arc^{VENUS} mouse line can be used in conjunction with the synaptome mapping pipeline to study large scale synaptic responses to stimuli. However, this mouse line also has a potential use for investigating in more detail the regulation of Arc subcellular distribution. Generating primary neuronal cultures from these animals could allow the visualization of the response of Arc in different subcellular compartments to specific cellular stimuli. For example, when combined with a technique which allows the uncaging of glutamate at single spines (Noguchi *et al.*, 2011), the response of Arc to activity could be visualised at the single synapse level. This could be combined with various other antagonists or specific blockers to establish which receptor types/subtypes are involved in the response of Arc to glutamate. This kind of information would also aid in the interpretation of the results of Arc synaptome mapping experiments.

4.9.3 Arc synaptome mapping

The Arc synaptome mapping method, used for the first time here, has multiple potential future applications. One important future direction of this work will be to build upon the baseline Arc synaptome map by including additional markers. This could start with the mapping of Arc and PSD95 in the same animal. Work towards this goal is already underway with the generation of an Arc^{VENUS}x$PSD95^{Mcherry}$ mouse line. The $PSD95^{mCherry}$ mouse line is designed in the same way as the $PSD95^{EGFP}$ line described in the methods section of this thesis, with the exception that the sequence for mCherry (a form of RFP) has been inserted at the end of the PSD95 coding region in the place of EGFP. The excitation and emission spectra of mCherry are sufficiently separated from those of Venus to allow simultaneous imaging of both fluorophores, whereas this is not the case with EGFP and Venus. Performing

synaptome mapping of both Arc and PSD95 in the same animals would enable the identification of patterns in the Arc synaptome that can be explained by patterns in excitatory synapse number, and type, as well as those which are specific to Arc and therefore more likely to be caused by region-specific patterns of synaptic activity. It could be argued that these Arc-specific features, for example the sparse distribution of Arc-positive synapses in the DGmo already identified, are the most likely to be altered by Arc-modulating stimuli such as behavioural stimulation. Further to this, the incorporation of a quantification of the nuclear localisation of Arc into the synaptome mapping pipeline would allow a more complete view of the brain wide distribution of Arc. The alteration of the Arc synaptome map by saline injection described here suggests that this method can be used to map the response of synaptic Arc to fairly subtle stimuli. A future aim would be to extend this work to map the Arc synaptome response to learning and memory paradigms. A pilot study towards this aim was carried out as part of this PhD project, the results of which can be found in **appendix 12.** It is hoped that this method could eventually be used to map the synaptic equivalent of the memory 'engram'.

4.9.4 Further investigations of ketamine action

Although the evidence here adds to our understanding of the molecular events following the administration of ketamine, there is still much which is not fully clear. The future direction of research into ketamine action is too broad to be covered in this thesis, however some suggestions are described below. Firstly, it will be essential to confirm the presence of the described bi-directional Arc synaptome changes along with the presence or absence of a ketamine-induced antidepressant response. This would strengthen the evidence for a correlation between sustained increases in Arc positive synapse number and the antidepressant response. It may also be possible to correlate the degree of antidepressant response with the magnitude of change in Arc, which would be particularly convincing. Following on from that correlation it will then be important to test for a causal link between presence of Arc at the synapse and antidepressant response. This could be done rather bluntly by the testing of Arc knockout, or conditional knock out mice, to allow normal development of the animal, followed by behavioural testing. Absence of an antidepressant response of ketamine in Arc knockout animals would indicate a functional role for the protein. However, it would be important to ensure that these animals did not display any other phenotypes which would bias the FST, TST or NSFT tests used. Arc knockout mice have been generated previously and displayed an inability to form long term memories and

alterations in LTP (Plath *et al.*, 2006). A more elegant way of investigating the functional requirement of Arc for ketamine's antidepressant effects would be to knock down Arc expression by infusion of Arc antisense oligodeoxynucleotides (ODNs) into target brain regions (for example hippocampus) at various time points following ketamine administration before behavioural testing. Thus, identifying if Arc upregulation is required for the behavioural response, and whether there is a critical time period during which Arc is acting in this way. This kind of technique has already been used to investigate the role of Arc in consolidation of LTP (Messaoudi *et al.*, 2007).

It would be interesting to characterize the functional alterations taking place alongside the changes in Arc level observed here. In a very simple way, the functional response to changes in Arc could begin to be investigated by performing immunohistochemistry for AMPA receptors on the existing brain slices from ketamine-treated Arc^{VENUS} mice. A correlation between increased Arc at synapses and decreased AMPA receptors would indicate that perhaps Arc is acting to reduce synaptic strength via its ability to increase AMPA receptor endocytosis. Further to this, slice electrophysiology could be used to identify changes in different properties of synaptic transmission and plasticity following ketamine in the regions identified here, the hippocampus being an obvious place to start with this. A particularly interesting question, which could be addressed here, would be how the functional response to ketamine differs between anaesthetic and sub-anaesthetic doses, which we now know produce such different changes at the level of synaptic Arc protein. Further to this, the question of whether the responses of Arc described here are specific to ketamine could be addressed by using another NMDAR antagonist working at the same site, for example memantine. Memantine does not cause the same rapid-acting, long-lasting antidepressant effect that ketamine does (Gideons *et al.*, 2014), and therefore comparison of the Arc synaptome map changes induced by these two compounds could shed more light on the elements of the response required for those antidepressant effects.

Chapter 5 Conclusions and future directions

5.1 Summary of findings

5.1.1 Use of synaptome mapping to study Arc

In the Arc^{VENUS} mouse line fluorescently-tagged Arc was detectable as both punctate accumulations situated at the post-synaptic side of glutamatergic synapses, and large oval accumulations situated within/around the nuclei of certain cells. The use of the synaptome mapping method to quantify these accumulations of fluorescently-tagged Arc protein at synapses across a whole coronal brain section is the first time that the subcellular distribution of Arc has been studied in this way. It has allowed several observations to be made, including the identification of gradients of change within defined anatomical regions. This provides a useful reference dataset for future research into the brain-wide functions of synaptic Arc. This follows on from the work carried out by Dr Melissa Cizeron, in which she generated the first synaptome maps of the MAGUK proteins PSD95 and SAP102. The Arc synaptome map presented here is the first time that a dynamic and activity-regulated protein has been studied using this technique. It is also the first time this technique has been used to detect alterations to a synaptome map on such a short (hours) timescale. In this case these changes were pharmacologically-induced, but this proof of principle opens the door to the possibility of mapping the effects of more subtle interventions, such as learning experiences.

5.1.1 Insights into ketamine's molecular mechanism of action

The findings presented in this thesis provide two new insights into the molecular mechanism of ketamine, which are of interest in the context of its antidepressant actions. Firstly, the absence of a low dose ketamine-induced hyper-locomotive response in $GluN2B^{2A(CTR)}$ mutant animals suggests a critical involvement of the c-terminal domain of the GluN2B subunit in this short-term effect of ketamine. Secondly, there is the observation that low- and high-doses of ketamine are able to induce opposite effects on Arc protein accumulation at synapses. In this case only the low dose of ketamine was able to induce a sustained increase in Arc accumulation at synapses, with the high dose depleting Arc from synapses from 6h onwards. This enables us to draws a correlation between synaptic Arc levels and ketamine-induced antidepressant responses, which have been observed following sub-anaesthetic but not anaesthetic doses. Other changes specific to sub-anaesthetic doses of ketamine include glutamate release and activation of mTOR and ERK signalling, all of which could be upstream from the observed changes in Arc. The PSD95 synaptome map did not change along with the Arc map at 24h post-ketamine administration, suggesting that the changes observed in Arc puncta number are unlikely to be the result of synaptogenesis. The potential implications of these two main findings have been discussed in detail within the respective results chapters,

however they do not stand in isolation but are linked by the interaction of Arc with the GluN2B CTD, and can therefore also be interpreted in relation to one another. Arc forms part of the 1.5MDa NMDA receptor supercomplex, the assembly of which is reliant upon the presence of the GluN2B c-terminal domain, PSD95 and PSD93 (Frank *et al.*, 2016). Further to this, PSD95 is essential for the transport of Arc to the synapse (Fernandez *et al.*, 2017). If the absence of the GluN2B c-terminal domain leads to an alteration in the amount of Arc present at the synapse, via its interaction with PSD95, this provides a route by which Arc could be involved in the GluN2B-specific actions of ketamine. Future directions to address this hypothesis are described in **section 5.3**.

5.2 Limitations of work presented here

The limitations of this work, and future directions designed to address these limitations, have been discussed within the individual results chapters. The main limitation of using the two approaches discussed here to investigate the action of ketamine is that synaptome mapping does not provide functional information, and the behavioural tests used only provide a very coarse level of functional information. Therefore, it is impossible for us to tell from the work presented here, whether the alterations observed in the Arc synaptome are functionally involved in either of the behavioural responses to ketamine action measured in the open-field or the forced swim test. Likewise, it is unclear what is happening at the molecular level at the synapse during the behavioural responses observed. Therefore, it will be important to carry out further experiments to attempt to link these two findings together, as described in **section 5.3**.

5.3 Future directions

Some specific ideas for future directions of the work presented in **chapter 3 and 4** have already been discussed within those chapters. However, presented here are some key future directions which are inspired by the work in both chapters taken together.

5.3.1 Effect of GluN2B$^{2A(CTR)}$ and GluN2A$^{2B(CTR)}$ mutations on interaction of Arc with PSD proteins

The question of whether the c-terminal domain replacement mutations are able to alter the amount of Arc present at the synapse can be addressed with a biochemical analysis of GluN2B$^{2A(CTR)}$ and GluN2A$^{2B(CTR)}$ brains. This could involve several experiments, the simplest of which would be to prepare a post-synaptic density fraction of brain homogenate and compare levels of Arc in wild-type and mutant animals. Further to this, immunoprecipitation could be carried out with antibodies for the n-terminal domains of GluN1, GluN2A and

GluN2B to establish whether the CTD replacement mutations alter the amount of Arc and PSD95 associating with the general population of NMDARs, or specific subtypes respectively. A reduction of synapse- or NMDAR-associated Arc in GluN2B$^{2A(CTR)}$ mutants would provide some evidence for the involvement of Arc in ketamine action.

5.3.2 Synaptome mapping of GluN2B$^{2A(CTR)}$ and GluN2A$^{2B(CTR)}$ mutants

As discussed in **section 5.1**, perhaps the most pressing question that links these findings is whether the increases seen in Arc protein accumulation at synapses in response to low doses of ketamine are in some way regulated by an action of the GluN2B c-terminal domain. This could be tested by administering ketamine to mice containing both the GluN2B$^{2A(CTR)}$ genetic modification, and the Arc^{VENUS} tag. Generation of this mouse line has already begun. The aim of this experiment would be to establish whether the dose-dependent effects of ketamine on the Arc synaptome are affected by the GluN2B$^{2A(CTR)}$ modification. If, for example, these changes to the synaptome were absent or perturbed in GluN2B$^{2A(CTR)}$ animals, this would implicate both the GluN2B CTD in the mechanism underlying the Arc response to ketamine, and Arc in the mechanism underlying the behavioural response to ketamine. This experiment could be followed up by a similar analysis of the Arc synaptome response in GluN2A$^{2B(CTR)}$ mutants to establish whether this is exaggerated in animals in which the behavioural response to ketamine is exaggerated.

5.3.3 Synaptome mapping and behavioural testing in the same animals

Similarly, it would be interesting to establish whether alterations in the synaptome map can be detected at the early time point at which the hyper-locomotive response to ketamine is present. This would be most informative if animals were first tested in the open-field to establish the amount of hyper-locomotion displayed by each individual, before being immediately culled and brains preserved for synaptome mapping. This would provide the opportunity to correlate any synaptome changes with the degree of hyper-locomotive response to ketamine observed. This could be combined with the experiment suggested in **section 5.3.1.** If the Arc synaptome map is altered during the time period that hyper-locomotion is observed, this would implicate Arc as having a role in the molecular mechanism of this effect, potentially via its interaction with the GluN2B c-terminal domain.

5.3.4 Testing the behavioural response to ketamine in Arc knockout animals

The most important experiment to carry out, in order to establish whether the alterations observed in the Arc synaptome are functionally relevant for ketamine's behavioural actions, will be to study the behavioural response to ketamine displayed by animals which lack, or

have reduced levels of, Arc protein. One option for this experiment would be the use of a complete Arc knockout mouse line such as that generated by the laboratory of Prof. Dietmar Kuhl and used previously to study the role of Arc in memory (Plath *et al.*, 2006; Ploski *et al.*, 2008). These animals fail to form lasting memories in several kinds of learning tasks, whereas short-term memory was intact. Therefore testing of ketamine's effect on behaviour in these mice would need to avoid tasks which could be affected by this memory impairment. For example, if hyper-locomotion in an open field arena is measured, this should not rely upon any habituation sessions taking place too far from the time of testing. Further to this, it is possible to reduce the amount of Arc protein in an acute way via the infusion of Arc antisense ODNs into specific brain regions of interest (Guzowski *et al.*, 2000). In this way, the changes in synaptic Arc levels in specific regions seen in the synaptome maps could be tested for a functional role in the behavioural action of ketamine. For example, does the infusion of Arc antisense ODNs into the hippocampus following a low dose of ketamine prevent the antidepressant effects detectable with the forced swim test? Is there a critical period of time during which Arc is acting to produce these effects?

5.3.5 Long-term goals of this area of research

As described in **chapter 1** of this thesis, the current antidepressant treatments available to patients have two main limitations. The first of which is that they are not effective for all patients, the second is that they take several weeks of repeat dosing before symptoms are reduced. Ketamine has been found to be effective in previously treatment-resistant MDD patients and is antidepressant in humans and mice after just one dose. In the long-term it is hoped that the work presented here, along with the future directions described, will contribute significantly to our understanding of the molecular events underlying the observed effects of ketamine. This kind of knowledge will be essential for the development of a ketamine-based antidepressant treatment which lacks ketamine's undesirable psychotomimetic effects. One important piece of information which will emerge from the future experiments described in **section 3.6.2** will be whether or not the antidepressant effects of ketamine are reliant on the GluN2B CTD, as the psychotomimetic effects appear to be. If they are not, and it becomes clear that the psychotomimetic and antidepressant effects of ketamine are mediated by different molecular mechanisms, this may provide an opportunity to identify therapeutic targets relevant specifically to its antidepressant effects.

References

aan het Rot M, Collins KA, Murrough JW, Perez AM, Reich DL, Charney DS & Mathew SJ. (2010). Safety and Efficacy of Repeated-Dose Intravenous Ketamine for Treatment-Resistant Depression. *Biological Psychiatry* **67,** 139-145.

Abbas AI, Yadav PN, Yao WD, Arbuckle MI, Grant SGN, Caron MG & Roth BL. (2009). PSD-95 Is Essential for Hallucinogen and Atypical Antipsychotic Drug Actions at Serotonin Receptors. *Journal of Neuroscience* **29,** 7124-7136.

Abel KM, Allin MPG, Hemsley DR & Geyer MA. (2003). Low dose ketamine increases prepulse inhibition in healthy men. *Neuropharmacology* **44,** 729-737.

Absalom A & Menon D. (2010). *Encyclopedia of Psychopharmacology*. Springer.

Amaral D & Laveneux P. (2007). *The Hippocampus book*. Oxford Univ. Press.

Amaral DG, Scharfman HE & Lavenex P. (2007). The dentate gyrus: fundamental neuroanatomical organization (dentate gyrus for dummies). *Dentate Gyrus: a Comphrehensive Guide to Structure, Function, and Clinical Implications* **163,** 3-+.

Anand A, Charney DS, Oren DA, Berman RM, Hu XS, Cappiello A & Krystal JH. (2000). Attenuation of the neuropsychiatric effects of ketamine with lamotrigine - Support for hyperglutamatergic effects of N-methyl-D-aspartate receptor antagonists. *Archives of General Psychiatry* **57,** 270-276.

Anis NA, Berry SC, Burton NR & Lodge D. (1983). THE DISSOCIATIVE ANESTHETICS, KETAMINE AND PHENCYCLIDINE, SELECTIVELY REDUCE EXCITATION OF CENTRAL MAMMALIAN NEURONS BY N-METHYL-ASPARTATE. *British Journal of Pharmacology* **79,** 565-575.

Anson LC, Chen PE, Wyllie DJA, Colquhoun D & Schoepfer R. (1998). Identification of amino acid residues of the NR2A subunit that control glutamate potency in recombinant NR1/NR2A NMDA receptors. *Journal of Neuroscience* **18,** 581-589.

Ardalan M, Wegener G, Rafati AH & Nyengaard JR. (2017). S-Ketamine Rapidly Reverses Synaptic and Vascular Deficits of Hippocampus in Genetic Animal Model of Depression. *International Journal of Neuropsychopharmacology* **20,** 247-256.

Autry AE, Adachi M, Nosyreva E, Na ES, Los MF, Cheng PF, Kavalali ET & Monteggia LM. (2011). NMDA receptor blockade at rest triggers rapid behavioural antidepressant responses. *Nature* **475,** 91-U109.

Azevedo FAC, Carvalho LRB, Grinberg LT, Farfel JM, Ferretti REL, Leite REP, Jacob W, Lent R & Herculano-Houzel S. (2009). Equal Numbers of Neuronal and Nonneuronal Cells Make the Human Brain an Isometrically Scaled-Up Primate Brain. *Journal of Comparative Neurology* **513,** 532-541.

Barker JM, Taylor JR & Chandler LJ. (2014). A unifying model of the role of the infralimbic cortex in extinction and habits. *Learning & Memory* **21,** 441-448.

Barria A & Malinow R. (2005). NMDA receptor subunit composition controls synaptic plasticity by regulating binding to CaMKII. *Neuron* **48,** 289-301.

Bayes A, van de Lagemaat LN, Collins MO, Croning MDR, Whittle IR, Choudhary JS & Grant SGN. (2011). Characterization of the proteome, diseases and evolution of the human postsynaptic density. *Nature Neuroscience* **14,** 19-21.

Bechtholt-Gompf AJ, Smith KL, John CS, Kang HH, Carlezon WA, Cohen BM & Ongur D. (2011). CD-1 and Balb/cJ mice do not show enduring antidepressant-like effects of ketamine in tests of acute antidepressant efficacy. *Psychopharmacology* **215,** 689-695.

Beique JC, Na Y, Kuhl D, Worley PF & Huganir RL. (2011). Arc-dependent synapse-specific homeostatic plasticity. *Proceedings of the National Academy of Sciences of the United States of America* **108,** 816-821.

Benekareddy M, Nair AR, Dias BG, Suri D, Autry AE, Monteggia LM & Vaidya VA. (2013). Induction of the plasticity-associated immediate early gene Arc by stress and hallucinogens: role of brain-derived neurotrophic factor. *International Journal of Neuropsychopharmacology* **16,** 405-415.

Berberich S, Punnakkal P, Jensen V, Pawlak V, Seeburg PH, Hvalby O & Kohr G. (2005). Lack of NMDA receptor subtype selectivity for hippocampal long-term potentiation. *Journal of Neuroscience* **25,** 6907-6910.

Berman FW & Murray TF. (1996). Characterization of 3H MK-801 binding to N-methyl-D-aspartate receptors in cultured rat cerebellar granule neurons and involvement in glutamate-mediated toxicity. *Journal of biochemical toxicology* **11,** 217-226.

Berman RM, Cappiello A, Anand A, Oren DA, Heninger GR, Charney DS & Krystal JH. (2000). Antidepressant effects of ketamine in depressed patients. *Biological Psychiatry* **47,** 351-354.

Beurel E, Song L & Jope RS. (2011). Inhibition of glycogen synthase kinase-3 is necessary for the rapid antidepressant effect of ketamine in mice. *Molecular Psychiatry* **16,** 1068-1070.

Bito H, Deisseroth K & Tsien RW. (1996). CREB phosphorylation and dephosphorylation: A Ca2(+)- and stimulus duration-dependent switch for hippocampal gene expression. *Cell* **87,** 1203-1214.

Bliss TVP & Lomo T. (1973). LONG-LASTING POTENTIATION OF SYNAPTIC TRANSMISSION IN DENTATE AREA OF ANESTHETIZED RABBIT FOLLOWING STIMULATION OF PERFORANT PATH. *Journal of Physiology-London* **232,** 331-356.

Bloomer WAC, VanDongen HMA & VanDongen AMJ. (2007). Activity-regulated cytoskeleton-associated protein Arc/Arg3.1 binds to spectrin and associates with nuclear promyelocytic leukemia (PML) bodies. *Brain Research* **1153,** 20-33.

Bloomer WAC, VanDongen HMA & VanDongen AMJ. (2008). Arc/Arg3.1 translation is controlled by convergent N-methyl-D-aspartate and G(s)-coupled receptor signaling pathways. *Journal of Biological Chemistry* **283,** 582-592.

Bluthgen N, van Bentum M, Merz B, Kuhl D & Hermey G. (2017). Profiling the MAPK/ERK dependent and independent activity regulated transcriptional programs in the murine hippocampus in vivo. *Scientific Reports* **7**.

Bodnoff SR, Suranyicadotte B, Aitken DH, Quirion R & Meaney MJ. (1988). THE EFFECTS OF CHRONIC ANTIDEPRESSANT TREATMENT IN AN ANIMAL-MODEL OF ANXIETY. *Psychopharmacology* **95,** 298-302.

Bogdanova OV, Kanekar S, D'Anci KE & Renshaw PF. (2013). Factors influencing behavior in the forced swim test. *Physiology & Behavior* **118,** 227-239.

Bolivar VJ, Caldarone BJ, Reilly AA & Flaherty L. (2000). Habituation of activity in an open field: A survey of inbred strains and F-1 hybrids. *Behavior Genetics* **30,** 285-293.

Brady S, Siegel G, Albers RW & Price D. (2005). *Basic Neurochemistry: Molecular, Cellular and Medical Aspects*. Academic Press.

Bramham CR, Alme MN, Bittins M, Kuipers SD, Nair RR, Pai B, Panja D, Schubert M, Soule J, Tiron A & Wibrand K. (2010). The Arc of synaptic memory. *Experimental Brain Research* **200,** 125-140.

Breier A, Malhotra AK, Pinals DA, Weisenfeld NI & Pickar D. (1997). Association of ketamine-induced psychosis with focal activation of the prefrontal cortex in healthy volunteers. *American Journal of Psychiatry* **154,** 805-811.

Broadhead MJ, Horrocks MH, Zhu F, Muresan L, Benavides-Piccione R, DeFelipe J, Fricker D, Kopanitsa MV, Duncan RR, Klenerman D, Komiyama NH, Lee SF & Grant SGN. (2016). PSD95 nanoclusters are postsynaptic building blocks in hippocampus circuits. *Scientific Reports* **6**.

Brodmann KJAB. (1909). Vergleichende Lokalisationslehre der Grosshirnrinde in ihren Prinzipien dargestellt auf Grund des Zellenbaues.

Burnashev N, Schoepfer R, Monyer H, Ruppersberg JP, Gunther W, Seeburg PH & Sakmann B. (1992). CONTROL BY ASPARAGINE RESIDUES OF CALCIUM PERMEABILITY AND MAGNESIUM BLOCKADE IN THE NMDA RECEPTOR. *Science* **257,** 1415-1419.

Can A, Zanos P, Moaddel R, Kang HJ, Dossou KSS, Wainer IW, Cheer JF, Frost DO, Huang X-P & Gould TD. (2016). Effects of Ketamine and Ketamine Metabolites on Evoked Striatal Dopamine Release, Dopamine Receptors, and Monoamine Transporters. *Journal of Pharmacology and Experimental Therapeutics* **359,** 159-170.

Cao J, Viholainen JI, Dart C, Warwick HK, Leyland ML & Courtney MJ. (2005). The PSD95-nNOS interface: a target for inhibition of excitotoxic p38 stress-activated protein kinase activation and cell death. *Journal of Cell Biology* **168,** 117-126.

Cao VY, Ye YZ, Mastwal S, Ren M, Coon M, Liu Q, Costa RM & Wang KH. (2015). Motor Learning Consolidates Arc-Expressing Neuronal Ensembles in Secondary Motor Cortex. *Neuron* **86,** 1385-1392.

Carey LM, Lee WH, Gutierrez T, Kulkarni PM, Thakur GA, Lai YY & Hohmann AG. (2017). SMALL MOLECULE INHIBITORS OF PSD95 nNOS PROTEIN PROTEIN INTERACTIONS SUPPRESS FORMALIN-EVOKED Fos PROTEIN EXPRESSION AND NOCICEPTIVE BEHAVIOR IN RATS. *Neuroscience* **349,** 303-317.

Carlisle HJ, Fink AE, Grant SGN & O'Dell TJ. (2008). Opposing effects of PSD-93 and PSD-95 on long-term potentiation and spike timing-dependent plasticity. *Journal of Physiology-London* **586,** 5885-5900.

Carrier N & Kabbaj M. (2013). Sex differences in the antidepressant-like effects of ketamine. *Neuropharmacology* **70,** 27-34.

Carter BC & Jahr CE. (2016). Postsynaptic, not presynaptic NMDA receptors are required for spike-timing-dependent LTD induction. *Nature Neuroscience* **19,** 1218-1224.

Chatterjee M, Ganguly S, Srivastava M & Palit G. (2011). Effect of 'chronic' versus 'acute' ketamine administration and its 'withdrawal' effect on behavioural alterations in mice: Implications for experimental psychosis. *Behavioural Brain Research* **216,** 247-254.

Chatterton JE, Awobuluyi M, Premkumar LS, Takahashi H, Talantova M, Shin Y, Cui JK, Tu SC, Kevin ASK, Nakanishi N, Tong G, Lipton SA & Zhang DX. (2002). Excitatory glycine receptors containing the NR3 family of NMDA receptor subunits. *Nature* **415,** 793-798.

Chawla MK, Guzowski JF, Ramirez-Amaya V, Lipa P, Hoffman KL, Marriott LK, Worley PF, McNaughton BL & Barnes CA. (2005). Sparse, environmentally selective expression of arc RNA in the upper blade of the rodent fascia dentata by brief spatial experience. *Hippocampus* **15,** 579-586.

Chen S & Diamond JS. (2002). Synaptically released glutamate activates extrasynaptic NMDA receptors on cells in the ganglion cell layer of rat retina. *Journal of Neuroscience* **22,** 2165-2173.

Chen T, Zhu J, Yang LK, Feng Y, Lin W & Wang YH. (2017). Glutamate-induced rapid induction of Arc/Arg3.1 requires NMDA receptor-mediated phosphorylation of ERK and CREB. *Neuroscience Letters* **661,** 23-28.

Chen XB, Winters C, Azzam R, Li X, Galbraith JA, Leapman RD & Reese TS. (2008). Organization of the core structure of the postsynaptic density. *Proceedings of the National Academy of Sciences of the United States of America* **105,** 4453-4458.

Cheng DM, Hoogenraad CC, Rush J, Ramm E, Schlager MA, Duong DM, Xu P, Wijayawardana SR, Hanfelt J, Nakagawa T, Sheng M & Peng JM. (2006). Relative and absolute quantification of postsynaptic density proteome isolated from rat forebrain and cerebellum. *Molecular & Cellular Proteomics* **5,** 1158-1170.

Cho JH, Huang B & Gray JM. (2016). RNA sequencing from neural ensembles activated during fear conditioning in the mouse temporal association cortex. *Scientific Reports* **6**.

Chowdhury GMI, Behar KL, Cho W, Thomas MA, Rothman DL & Sanacora G. (2012). H-1- C-13 -Nuclear Magnetic Resonance Spectroscopy Measures of Ketamine's Effect on Amino Acid Neurotransmitter Metabolism. *Biological Psychiatry* **71,** 1022-1025.

Chowdhury S, Shepherd JD, Okuno H, Lyford G, Petralia RS, Plath N, Kuhl D, Huganir RL & Worley PF. (2006). Arc/Arg3.1 interacts with the endocytic machinery to regulate AMPA receptor trafficking. *Neuron* **52,** 445-459.

Ciabarra AM, Sullivan JM, Gahn LG, Pecht G, Heinemann S & Sevarino KA. (1995). CLONING AND CHARACTERIZATION OF CHI-1 - A DEVELOPMENTALLY-REGULATED MEMBER OF A NOVEL CLASS OF THE IONOTROPIC GLUTAMATE-RECEPTOR FAMILY. *Journal of Neuroscience* **15,** 6498-6508.

Clark BA & Cull-Candy SG. (2002). Activity-dependent recruitment of extrasynaptic NMDA receptor activation at an AMPA receptor-only synapse. *Journal of Neuroscience* **22,** 4428-4436.

Clements JD & Westbrook GL. (1991). ACTIVATION KINETICS REVEAL THE NUMBER OF GLUTAMATE AND GLYCINE BINDING-SITES ON THE N-METHYL-D-ASPARTATE RECEPTOR. *Neuron* **7,** 605-613.

Coba MP, Pocklington AJ, Collins MO, Kopanitsa MV, Uren RT, Swamy S, Croning MDR, Choudhary JS & Grant SGN. (2009). Neurotransmitters Drive Combinatorial Multistate Postsynaptic Density Networks. *Science Signaling* **2**.

Collingridge GL, Lee Y, Bortolotto ZA, Kang H & Lodge D. (2017). Antidepressant Actions of Ketamine Versus Hydroxynorketamine. *Biological Psychiatry* **81,** E65-E67.

Collins MO, Husi H, Yu L, Brandon JM, Anderson CNG, Blackstock WP, Choudhary JS & Grant SGN. (2006). Molecular characterization and comparison of the components and multiprotein complexes in the postsynaptic proteome. *Journal of Neurochemistry* **97,** 16-23.

Cornwell BR, Salvadore G, Furey M, Marquardt CA, Brutsche NE, Grillon C & Zarate CA. (2012). Synaptic Potentiation Is Critical for Rapid Antidepressant Response to Ketamine in Treatment-Resistant Major Depression. *Biological Psychiatry* **72,** 555-561.

Cruz SL, Soberanes-Chavez P, Paez-Martinez N & Lopez-Rubalcava C. (2009). Toluene has antidepressant-like actions in two animal models used for the screening of antidepressant drugs. *Psychopharmacology* **204,** 279-286.

Cryan JF, Mombereau C & Vassout A. (2005). The tail suspension test as a model for assessing antidepressant activity: Review of pharmacological and genetic studies in mice. *Neuroscience and Biobehavioral Reviews* **29,** 571-625.

Daniell LC. (1990). THE NONCOMPETITIVE N-METHYL-D-ASPARTATE ANTAGONISTS, MK-801, PHENCYCLIDINE AND KETAMINE, INCREASE THE POTENCY OF GENERAL-ANESTHETICS. *Pharmacology Biochemistry and Behavior* **36,** 111-115.

Danysz W, Essmann U, Bresink I & Wilke R. (1994). GLUTAMATE ANTAGONISTS HAVE DIFFERENT EFFECTS ON SPONTANEOUS LOCOMOTOR-ACTIVITY IN RATS. *Pharmacology Biochemistry and Behavior* **48,** 111-118.

DaSilva LLP, Wall MJ, de Almeida LP, Wauters SC, Januario YC, Muller J & Correa SAL. (2016). Activity-Regulated Cytoskeleton- Associated Protein Controls AMPAR Endocytosis through a Direct Interaction with Clathrin-Adaptor Protein 2. *Eneuro* **3**.

de Bartolomeis A, Sarappa C, Buonaguro EF, Marmo F, Eramo A, Tomasetti C & Iasevoli F. (2013). Different effects of the NMDA receptor antagonists ketamine, MK-801, and memantine on postsynaptic density transcripts and their topography: Role of Homer signaling, and implications for novel antipsychotic and pro-cognitive targets in psychosis. *Progress in Neuro-Psychopharmacology & Biological Psychiatry* **46,** 1-12.

De Foubert G, Carney SL, Robinson CS, Destexhe EJ, Tomlinson R, Hicks CA, Murray TK, Gaillard JP, Deville C, Xhenseval V, Thomas CE, O'Neill MJ & Zetterstrom TSC. (2004). Fluoxetine-induced change in rat brain expression of brain-derived neurotrophic factor varies depending on length of treatment. *Neuroscience* **128,** 597-604.

DeFelipe J, Marco P, Busturia I & Merchan-Perez A. (1999). Estimation of the number of synapses in the cerebral cortex: Methodological considerations. *Cerebral Cortex* **9,** 722-732.

Desmond NL & Weinberg RJ. (1998). Enhanced expression of AMPA receptor protein at perforated axospinous synapses. *Neuroreport* **9,** 857-860.

Diazgranados N, Ibrahim L, Brutsche NE, Newberg A, Kronstein P, Khalife S, Kammerer WA, Quezado Z, Luckenbaugh DA, Salvadore G, Machado-Vieira R, Manji HK & Zarate CA. (2010). A Randomized Add-on Trial of an N-methyl-D-aspartate Antagonist in Treatment-Resistant Bipolar Depression. *Archives of General Psychiatry* **67,** 793-802.

DiazGranados N, Ibrahim LA, Brutsche NE, Ameli R, Henter ID, Luckenbaugh DA, Machado-Vieira R & Zarate CA. (2010). Rapid Resolution of Suicidal Ideation After a Single Infusion of an N-Methyl-D-Aspartate Antagonist in Patients With Treatment-Resistant Major Depressive Disorder. *Journal of Clinical Psychiatry* **71,** 1605-1611.

Domino EF. (1984). CITATION CLASSIC - PHARMACOLOGIC EFFECTS OF CI-581, A NEW DISSOCIATIVE ANESTHETIC, IN MAN. *Current Contents/Life Sciences***,** 16-16.

Dore K, Aow J & Malinow R. (2015). Agonist binding to the NMDA receptor drives movement of its cytoplasmic domain without ion flow. *Proceedings of the National Academy of Sciences of the United States of America* **112,** 14705-14710.

Dos Santos M, Salery M, Forget B, Perez MAG, Betuing S, Boudier T, Vanhoutte P, Caboche J & Heck N. (2017). Rapid Synaptogenesis in the Nucleus Accumbens Is Induced by a Single Cocaine Administration and Stabilized by Mitogen-Activated Protein Kinase Interacting Kinase-1 Activity. *Biological Psychiatry* **82,** 806-818.

Dotson JW, Ackerman DL & West LJ. (1995). KETAMINE ABUSE. *Journal of Drug Issues* **25,** 751-757.

Dravid SM, Erreger K, Yuan HJ, Nicholson K, Le P, Lyuboslavsky P, Almonte A, Murray E, Mosely C, Barber J, French A, Balster R, Murray TF & Traynelis SF. (2007). Subunit-specific mechanisms and proton sensitivity of NMDA receptor channel block. *Journal of Physiology-London* **581,** 107-128.

Duan TT, Tan JW, Yuan Q, Cao J, Zhou QX & Xu L. (2013). Acute ketamine induces hippocampal synaptic depression and spatial memory impairment through dopamine D1/D5 receptors. *Psychopharmacology* **228,** 451-461.

Duncan GE, Moy SS, Knapp DJ, Mueller RA & Breese GR. (1998). Metabolic mapping of the rat brain after subanesthetic doses of ketamine: potential relevance to schizophrenia. *Brain Research* **787,** 181-190.

Durieux ME. (1995). INHIBITION BY KETAMINE OF MUSCARINIC ACETYLCHOLINE-RECEPTOR FUNCTION. *Anesthesia and Analgesia* **81,** 57-62.

Dyrvig M, Christiansen SH, Woldbye DPD & Lichota J. (2014). Temporal gene expression profile after acute electroconvulsive stimulation in the rat. *Gene* **539,** 8-14.

Eguchi M & Yamaguchi S. (2009). In vivo and in vitro visualization of gene expression dynamics over extensive areas of the brain. *Neuroimage* **44,** 1274-1283.

El Gaamouch F, Buisson A, Moustie O, Lemieux M, Labrecque S, Bontempi B, De Koninck P & Nicole O. (2012). Interaction Between alpha CaMKII and GluN2B Controls ERK-Dependent Plasticity. *Journal of Neuroscience* **32,** 10767-10779.

Emptage N, Bliss TVP & Fine A. (1999). Single synaptic events evoke NMDA receptor-mediated release of calcium from internal stores in hippocampal dendritic spines. *Neuron* **22,** 115-124.

Esnault C, Gualdrini F, Horswell S, Kelly G, Stewart A, East P, Matthews N & Treisman R. (2017). ERK-Induced Activation of TCF Family of SRF Cofactors Initiates a Chromatin Modification Cascade Associated with Transcription. *Molecular Cell* **65,** 1081-+.

Farris SL & Steward O. (2010). Activity induces Arc mRNA degradation that is dependent upon translation and NMDA receptor activation. *Faseb Journal* **24**.

Fernandez E, Collins MO, Frank RAW, Zhu F, Kopanitsa MV, Nithianantharajah J, Lempriere SA, Fricker D, Elsegood KA, McLaughlin CL, Croning MDR, McLean C, Armstrong JD, Hill WD, Deary IJ, Cencelli G, Bagni C, Fromer M, Purcell SM, Pocklington AJ, Choudhary JS, Komiyama NH & Grant SGN. (2017). Arc Requires PSD95 for Assembly into Postsynaptic Complexes Involved with Neural Dysfunction and Intelligence. *Cell Reports* **21,** 679-691.

Fernandez E, Collins MO, Uren RT, Kopanitsa MV, Komiyama NH, Croning MDR, Zografos L, Armstrong JD, Choudhary JS & Grant SGN. (2009). Targeted tandem affinity purification of PSD-95 recovers core postsynaptic complexes and schizophrenia susceptibility proteins. *Molecular Systems Biology* **5,** 17.

Ferreira JS, Papouin T, Ladepeche L, Yao A, Langlais VC, Bouchet D, Dulong J, Mothet JP, Sacchi S, Pollegioni L, Paoletti P, Olit SHR & Groc L. (2017). Co-agonists differentially tune GluN2B-NMDA receptor trafficking at hippocampal synapses. *Elife* **6**.

Ferres-Coy A, Artigas F & Bortolozzi A. (2013). RNAi-mediated serotonin transporter suppression rapidly increases serotonergic neurotransmission and hippocampal neurogenesis. *European Neuropsychopharmacology* **23,** S6-S6.

Flavell SW & Greenberg ME. (2008). Signaling mechanisms linking neuronal activity to gene expression and plasticity of the nervous system. *Annual Review of Neuroscience* **31,** 563-590.

Florio SK, Loh C, Huang SM, Iwamaye AE, Kitto KF, Fowler KW, Treiberg JA, Hayflick JS, Walker JM, Fairbanks CA & Lai Y. (2009). Disruption of nNOS-PSD95 protein-protein interaction inhibits acute thermal hyperalgesia and chronic mechanical allodynia in rodents. *British Journal of Pharmacology* **158,** 494-506.

Frank RAW, Komiyama NH, Ryan TJ, Zhu F, O'Dell TJ & Grant SGN. (2016). NMDA receptors are selectively partitioned into complexes and supercomplexes during synapse maturation. *Nature Communications* **7,** 13.

Fremeau RT, Troyer MD, Pahner I, Nygaard GO, Tran CH, Reimer RJ, Bellocchio EE, Fortin D, Storm-Mathisen J & Edwards RH. (2001). The expression of vesicular glutamate transporters defines two classes of excitatory synapse. *Neuron* **31,** 247-260.

Frey U, Krug M, Reymann KG & Matthies H. (1988). ANISOMYCIN, AN INHIBITOR OF PROTEIN-SYNTHESIS, BLOCKS LATE PHASES OF LTP PHENOMENA IN THE HIPPOCAMPAL CA1 REGION INVITRO. *Brain Research* **452,** 57-65.

Frey U & Morris RGM. (1997). Synaptic tagging and long-term potentiation. *Nature* **385,** 533-536.

Frohlich J & Van Horn JD. (2014). Reviewing the ketamine model for schizophrenia. *Journal of Psychopharmacology* **28,** 287-302.

Fuchikami M, Thomas A, Liu RJ, Wohleb ES, Land BB, DiLeone RJ, Aghajanian GK & Duman RS. (2015). Optogenetic stimulation of infralimbic PFC reproduces ketamine's rapid and sustained antidepressant actions. *Proceedings of the National Academy of Sciences of the United States of America* **112,** 8106-8111.

Fukazawa Y, Saitoh Y, Ozawa F, Ohta Y, Mizuno K & Inokuchi K. (2003). Hippocampal LTP is accompanied by enhanced F-actin content within the dendritic spine that is essential for late LTP maintenance in vivo. *Neuron* **38,** 447-460.

Ganeshina O, Berry RW, Petralia RS, Nicholson DA & Geinisman Y. (2004a). Differences in the expression of AMPA and NMDA receptors between axospinous perforated and nonperforated synapses are related to the configuration and size of postsynaptic densities. *Journal of Comparative Neurology* **468,** 86-95.

Ganeshina O, Berry RW, Petralia RS, Nicholson DA & Geinisman Y. (2004b). Synapses with a segmented, completely partitioned postsynaptic density express more AMPA receptors than other axospinous synaptic junctions. *Neuroscience* **125,** 615-623.

Gao F, Song XY, Zhu DX, Wang XC, Hao AJ, Nadler JV & Zhan RZ. (2015). Dendritic morphology, synaptic transmission, and activity of mature granule cells born following pilocarpine-induced status epilepticus in the rat. *Frontiers in Cellular Neuroscience* **9**.

Gao XM, Elmer GI, Adams-Huet B & Tamminga CA. (2009). Social memory in mice: Disruption with an NMDA antagonist and attenuation with antipsychotic drugs. *Pharmacology Biochemistry and Behavior* **92,** 236-242.

Gao Y, Tatavarty V, Korza G, Levin MK & Carson JH. (2008). Multiplexed dendritic targeting of alpha calcium calmodulin-dependent protein kinase II, neurogranin, and activity-regulated cytoskeleton-associated protein RNAs by the A2 pathway. *Molecular Biology of the Cell* **19,** 2311-2327.

Garcia LSB, Comim CM, Valvassori SS, Reus GZ, Barbosa LM, Andreazza AC, Stertz L, Fries GR, Gavioli EC, Kapczinski F & Quevedo J. (2008). Acute administration of ketamine

induces antidepressant-like effects in the forced swimming test and increases BDNF levels in the rat hippocampus. *Progress in Neuro-Psychopharmacology & Biological Psychiatry* **32,** 140-144.

Ghasemi M, Raza M & Dehpour AR. (2010). NMDA receptor antagonists augment antidepressant-like effects of lithium in the mouse forced swimming test. *Journal of Psychopharmacology* **24,** 585-594.

Ghoneim MM, Hinrichs JV, Mewaldt SP & Petersen RC. (1985). KETAMINE - BEHAVIORAL-EFFECTS OF SUBANESTHETIC DOSES. *Journal of Clinical Psychopharmacology* **5,** 70-77.

Ghosh A & Greenberg ME. (1995). CALCIUM SIGNALING IN NEURONS - MOLECULAR MECHANISMS AND CELLULAR CONSEQUENCES. *Science* **268,** 239-247.

Gideons ES, Kavalali ET & Monteggia LM. (2014). Mechanisms underlying differential effectiveness of memantine and ketamine in rapid antidepressant responses. *Proceedings of the National Academy of Sciences of the United States of America* **111,** 8649-8654.

Giorgi C, Yeo GW, Stone ME, Katz DB, Burge C, Turrigiano G & Moore MJ. (2007). The EJC factor eIF4AIII modulates synaptic strength and neuronal protein expression. *Cell* **130,** 179-191.

Giros B, Jaber M, Jones SR, Wightman RM & Caron MG. (1996). Hyperlocomotion and indifference to cocaine and amphetamine in mice lacking the dopamine transporter. *Nature* **379,** 606-612.

Gray EG. (1959). AXO-SOMATIC AND AXO-DENDRITIC SYNAPSES OF THE CEREBRAL CORTEX - AN ELECTRON MICROSCOPE STUDY. *Journal of Anatomy* **93,** 420-&.

Gray JA, Shi Y, Usui H, During MJ, Sakimura K & Nicoll RA. (2011). Distinct Modes of AMPA Receptor Suppression at Developing Synapses by GluN2A and GluN2B: Single-Cell NMDA Receptor Subunit Deletion In Vivo. *Neuron* **71,** 1085-1101.

Grinevich V, Kolleker A, Eliava M, Takada N, Takuma H, Fukazawa Y, Shigemoto R, Kuhl D, Waters J, Seeburg PH & Osten P. (2009). Fluorescent Arc/Arg3.1 indicator mice: A versatile tool to study brain activity changes in vitro and in vivo. *Journal of Neuroscience Methods* **184,** 25-36.

Guo ML, Xue B, Jin DZ, Mao LM & Wang JQ. (2012). Interactions and phosphorylation of postsynaptic density 93 (PSD-93) by extracellular signal-regulated kinase (ERK). *Brain Research* **1465,** 18-25.

Guzowski JF, Lyford GL, Stevenson GD, Houston FP, McGaugh JL, Worley PF & Barnes CA. (2000). Inhibition of activity-dependent arc protein expression in the rat hippocampus impairs the maintenance of long-term potentiation and the consolidation of long-term memory. *Journal of Neuroscience* **20,** 3993-4001.

Guzowski JF, McNaughton BL, Barnes CA & Worley PF. (1999). Environment-specific expression of the immediate-early gene Arc in hippocampal neuronal ensembles. *Nature Neuroscience* **2,** 1120-1124.

Haas DA & Harper DG. (1992). Ketamine: A Review of Its Pharmacologic Properties and

Use in Ambulatory Anesthesia. *Anesth Prog*.

Haile CN, Murrough JW, Iosifescu DV, Chang LC, Al Jurdi RK, Foulkes A, Iqbal S, Mahoney JJ, De La Garza R, Charney DS, Newton TF & Mathew SJ. (2014). Plasma brain derived neurotrophic factor (BDNF) and response to ketamine in treatment-resistant depression. *International Journal of Neuropsychopharmacology* **17,** 331-336.

Halliwell RF, Peters JA & Lambert JJ. (1989). THE MECHANISM OF ACTION AND PHARMACOLOGICAL SPECIFICITY OF THE ANTICONVULSANT NMDA ANTAGONIST MK-801 - A VOLTAGE CLAMP STUDY ON NEURONAL CELLS IN CULTURE. *British Journal of Pharmacology* **96,** 480-494.

Hansen KB, Ogden KK, Yuan HJ & Traynelis SF. (2014). Distinct Functional and Pharmacological Properties of Triheteromeric GluN1/GluN2A/GluN2B NMDA Receptors. *Neuron* **81,** 1084-1096.

Harraz MM, Tyagi R, Cortes P & Snyder SH. (2016). Antidepressant action of ketamine via mTOR is mediated by inhibition of nitrergic Rheb degradation. *Molecular Psychiatry* **21,** 313-319.

Harris AZ & Pettit DL. (2007). Extrasynaptic and synaptic and uniform pools in rat hi NMDA receptors form stable ppocampal slices. *Journal of Physiology-London* **584,** 509-519.

Hartvig P, Valtysson J, Lindner KJ, Kristensen J, Karlsten R, Gustafsson LL, Persson J, Svensson JO, Oye I, Antoni G, Westerberg G & Langstrom B. (1995). CENTRAL-NERVOUS-SYSTEM EFFECTS OF SUBDISSOCIATIVE DOSES OF (S)-KETAMINE ARE RELATED TO PLASMA AND BRAIN CONCENTRATIONS MEASURED WITH POSITRON EMISSION TOMOGRAPHY IN HEALTHY-VOLUNTEERS. *Clinical Pharmacology & Therapeutics* **58,** 165-173.

Hartzell AL, Burke SN, Hoang LT, Lister JP, Rodriguez CN & Barnes CA. (2013). Transcription of the Immediate-Early Gene Arc in CA1 of the Hippocampus Reveals Activity

Differences along the Proximodistal Axis That Are Attenuated by Advanced Age. *Journal of Neuroscience* **33,** 3424-3433.

Hayase T, Yamamoto Y & Yamamoto K. (2006). Behavioral effects of ketamine and toxic interactions with psychostimulants. *Bmc Neuroscience* **7**.

Henriksen EJ, Colgin LL, Barnes CA, Witter MP, Moser MB & Moser EI. (2010). Spatial Representation along the Proximodistal Axis of CA1. *Neuron* **68,** 127-137.

Herman JP, Flak J & Jankord R. (2008). Chronic stress plasticity in the hypothalamic paraventricular nucleus. *Advances in Vasopressin and Oxytocin: from Genes to Behaviour to Disease* **170,** 353-364.

Herman MA & Jahr CE. (2007). Extracellular glutamate concentration in hippocampal slice. *Journal of Neuroscience* **27,** 9736-9741.

Herman MA, Nahir B & Jahr CE. (2011). Distribution of Extracellular Glutamate in the Neuropil of Hippocampus. *Plos One* **6**.

Hetem LAB, Danion JM, Diemunsch P & Brandt C. (2000). Effect of a subanesthetic dose of ketamine on memory and conscious awareness in healthy volunteers. *Psychopharmacology* **152,** 283-288.

Horak M & Wenthold RJ. (2009). Different Roles of C-terminal Cassettes in the Trafficking of Full-length NR1 Subunits to the Cell Surface. *Journal of Biological Chemistry* **284,** 9683-9691.

Huang F, Chotiner JK & Steward O. (2007). Actin polymerization and ERK phosphorylation are required for Arc/Arg3.1 mRNA targeting to activated synaptic sites on dendrites. *Journal of Neuroscience* **27,** 9054-9067.

Husi H & Grant SGN. (2001). Isolation of 2000-kDa complexes of N-methyl-D-aspartate receptor and postsynaptic density 95 from mouse brain. *Journal of Neurochemistry* **77,** 281-291.

Husi H, Ward MA, Choudhary JS, Blackstock WP & Grant SGN. (2000). Proteomic analysis of NMDA receptor-adhesion protein signaling complexes. *Nature Neuroscience* **3,** 661-669.

Ibrahim L, Diazgranados N, Luckenbaugh DA, Machado-Vieira R, Baumann J, Mallinger AG & Zarate CA. (2011). Rapid decrease in depressive symptoms with an N-methyl-D-aspartate antagonist in ECT-resistant major depression. *Progress in Neuro-Psychopharmacology & Biological Psychiatry* **35,** 1155-1159.

Imre G, Fokkema DS, Den Boer JA & Ter Horst GJ. (2006). Dose-response characteristics of ketamine effect on locomotion, cognitive function and central neuronal activity. *Brain Research Bulletin* **69,** 338-345.

Irie Y, Yamagata K, Gan YH, Miyamoto K, Do E, Kuo CH, Taira E & Miki N. (2000). Molecular cloning and characterization of amida, a novel protein which interacts with a neuron-specific immediate early gene product arc, contains novel nuclear localization signals, and causes cell death in cultured cells. *Journal of Biological Chemistry* **275,** 2647-2653.

Irifune M, Sato T, Kamata Y, Nishikawa T, Nomoto M, Fukuda T & Kawahara M. (1998). Inhibition by diazepam of ketamine-induced hyperlocomotion and dopamine turnover in mice. *Canadian Journal of Anaesthesia-Journal Canadien D Anesthesie* **45,** 471-478.

Irifune M, Shimizu T & Nomoto M. (1991). KETAMINE-INDUCED HYPERLOCOMOTION ASSOCIATED WITH ALTERATION OF PRESYNAPTIC COMPONENTS OF DOPAMINE NEURONS IN THE NUCLEUS-ACCUMBENS OF MICE. *Pharmacology Biochemistry and Behavior* **40,** 399-407.

Ishii T, Moriyoshi K, Sugihara H, Sakurada K, Kadotani H, Yokoi M, Akazawa C, Shigemoto R, Mizuno N, Masu M & Nakanishi S. (1993). MOLECULAR CHARACTERIZATION OF THE FAMILY OF THE N-METHYL-D-ASPARTATE RECEPTOR SUBUNITS. *Journal of Biological Chemistry* **268,** 2836-2843.

Jakkamsetti V, Tsai NP, Gross C, Molinaro G, Collins KA, Nicoletti F, Wang KH, Osten P, Bassell GJ, Gibson JR & Huber KM. (2013). Experience-Induced Arc/Arg3.1 Primes CA1 Pyramidal Neurons for Metabotropic Glutamate Receptor-Dependent Long-Term Synaptic Depression. *Neuron* **80,** 72-79.

Johnson JW & Ascher P. (1987). GLYCINE POTENTIATES THE NMDA RESPONSE IN CULTURED MOUSE-BRAIN NEURONS. *Nature* **325,** 529-531.

Kandel ER, Schwatz JH & Jessel TM. (2000). *Principles of Neural Science*. McGraw Hill.

Kandratavicius L, Balista PA, Wolf DC, Abrao J, Evora PR, Rodrigues AJ, Chaves C, Maia-De-Oliveira JP, Leite JP, Dursun SM, Baker GB, Guimaraes FS & Hallak JEC. (2015). Effects of nitric oxide-related compounds in the acute ketamine animal model of schizophrenia. *Bmc Neuroscience* **16**.

Kapur S & Seeman P. (2002). NMDA receptor antagonists ketamine and PCP have direct effects on the dopamine D-2 and serotonin 5-HT2 receptors - implications for models of schizophrenia. *Molecular Psychiatry* **7,** 837-844.

Kauderer BS & Kandel ER. (2000). Capture of a protein synthesis-dependent component of long-team depression. *Proceedings of the National Academy of Sciences of the United States of America* **97,** 13342-13347.

Kawashima T, Okuno H, Nonaka M, Adachi-Morishima A, Kyo N, Okamura M, Takemoto-Kimura S, Worley PF & Bito H. (2009). Synaptic activity-responsive element in the Arc/Arg3.1 promoter essential for synapse-to-nucleus signaling in activated neurons. *Proceedings of the National Academy of Sciences of the United States of America* **106,** 316-321.

Khlestova E, Johnson JW, Krystal JH & Lisman J. (2016). The Role of GluN2C-Containing NMDA Receptors in Ketamine's Psychotogenic Action and in Schizophrenia Models. *Journal of Neuroscience* **36,** 11151-11157.

Kim JH, Liao DZ, Lau LF & Huganir RL. (1998). SynGAP: a synaptic RasGAP that associates with the PSD-95/SAP90 protein family. *Neuron* **20,** 683-691.

Kim MJ, Dunah AW, Wang YT & Sheng M. (2005). Differential roles of NR2A- and NR2B-containing NMDA receptors in and AMPA receptor Ras-ERK signaling trafficking. *Neuron* **46,** 745-760.

Kinney JW, Davis CN, Tabarean I, Conti B, Bartfai T & Behrens MM. (2006). A specific role for NR2A-containing NMDA receptors in the maintenance of parvalbumin and GAD67 immunoreactivity in cultured interneurons. *Journal of Neuroscience* **26,** 1604-1615.

Kiselycznyk C, Jury NJ, Halladay LR, Nakazawa K, Mishina M, Sprengel R, Grant SGN, Svenningsson P & Holmes A. (2015). NMDA receptor subunits and associated signaling molecules mediating antidepressant-related effects of NMDA-GluN2B antagonism. *Behavioural Brain Research* **287,** 89-95.

Kiyama Y, Manabe T, Sakimura K, Kawakami F, Mori H & Mishina M. (1998). Increased thresholds for long-term potentiation and contextual learning in mice lacking the NMDA-type glutamate receptor epsilon 1 subunit. *Journal of Neuroscience* **18,** 6704-6712.

Kobayashi H, Yamamoto S, Maruo T & Murakami F. (2005). Identification of a cis-acting element required for dendritic targeting of activity-regulated cytoskeleton-associated protein mRNA. *European Journal of Neuroscience* **22,** 2977-2984.

Kohr G, Jensen V, Koester HJ, Mihaljevic ALA, Utvik JK, Kvello A, Ottersen OP, Seeburg PH, Sprengel R & Hvalby O. (2003). Intracellular domains of NMDA receptor subtypes

are determinants for long-term potentiation induction. *Journal of Neuroscience* **23,** 10791-10799.

Koike H, Fukumoto K, Iijima M & Chaki S. (2013). Role of BDNF/TrkB signaling in antidepressant-like effects of a group II metabotropic glutamate receptor antagonist in animal models of depression. *Behavioural Brain Research* **238,** 48-52.

Koike H, Iijima M & Chaki S. (2011). Involvement of AMPA receptor in both the rapid and sustained antidepressant-like effects of ketamine in animal models of depression. *Behavioural Brain Research* **224,** 107-111.

Komiyama NH, Watabe AM, Carlisle HJ, Porter K, Charlesworth P, Monti J, Strathdee DJC, O'Carroll CM, Martin SJ, Morris RGM, O'Dell TJ & Grant SGN. (2002). SynGAP regulates ERK/MAPK signaling, synaptic plasticity, and learning in the complex with postsynaptic density 95 and NMDA receptor. *Journal of Neuroscience* **22,** 9721-9732.

Korb E, Wilkinson CL, Delgado RN, Lovero KL & Finkbeiner S. (2013). Arc in the nucleus regulates PML-dependent GluA1 transcription and homeostatic plasticity. *Nature neuroscience* **16,** 874-883.

Kotermanski SE & Johnson JW. (2009). Mg2+ Imparts NMDA Receptor Subtype Selectivity to the Alzheimer's Drug Memantine. *Journal of Neuroscience* **29,** 2774-2779.

Kotermanski SE, Wood JT & Johnson JW. (2009). Memantine binding to a superficial site on NMDA receptors contributes to partial trapping. *Journal of Physiology-London* **587,** 4589-4603.

Kozlovsky N, Matar MA, Kaplan Z, Kotler M, Zohar J & Cohen H. (2008). The immediate early gene Arc is associated with behavioral resilience to stress exposure in an animal model of posttraumatic stress disorder. *European Neuropsychopharmacology* **18,** 107-116.

Krapivinsky G, Krapivinsky L, Manasian Y, Ivanov A, Tyzio R, Pellegrino C, Ben-Ari Y, Clapham DE & Medina I. (2003). The NMDA receptor is coupled to the ERK pathway by a direct interaction between NR2B and RasGRF1. *Neuron* **40,** 775-784.

Kristensen AS, Jenkins MA, Banke TG, Schousboe A, Makino Y, Johnson RC, Huganir R & Traynelis SF. (2011). Mechanism of Ca2+/calmodulin-dependent kinase II regulation of AMPA receptor gating. *Nature Neuroscience* **14,** 727-U327.

Krystal JH, Abi-Saab W, Perry E, D'Souza D, Liu NJ, Gueorguieva R, McDougall L, Hunsberger T, Belger A, Levine L & Breier A. (2005). Preliminary evidence of attenuation of the disruptive effects of the NMDA glutamate receptor antagonist, ketamine, on

working memory by pretreatment with the group II metabotropic glutamate receptor agonist, LY354740, in healthy human subjects. *Psychopharmacology* **179,** 303-309.

Krystal JH, D'Souza DC, Karper LP, Bennett A, Abi-Dargham A, Abi-Saab D, Cassello K, Bowers MB, Vegso S, Heninger GR & Charney DS. (1999). Interactive effects of subanesthetic ketamine and haloperidol in healthy humans. *Psychopharmacology* **145,** 193-204.

Krystal JH, Karper LP, Seibyl JP, Freeman GK, Delaney R, Bremner JD, Heninger GR, Bowers MB & Charney DS. (1994). SUBANESTHETIC EFFECTS OF THE NONCOMPETITIVE NMDA ANTAGONIST, KETAMINE, IN HUMANS - PSYCHOTOMIMETIC, PERCEPTUAL, COGNITIVE, AND NEUROENDOCRINE RESPONSES. *Archives of General Psychiatry* **51,** 199-214.

Kumar V, Fahey PG, Jong YJI, Ramanan N & O'Malley KL. (2012). Activation of Intracellular Metabotropic Glutamate Receptor 5 in Striatal Neurons Leads to Up-regulation of Genes Associated with Sustained Synaptic Transmission Including Arc/Arg3.1 Protein. *Journal of Biological Chemistry* **287,** 5412-5425.

Kuner T & Schoepfer R. (1996). Multiple structural elements determine subunit specificity of Mg2+ block in NMDA receptor channels. *Journal of Neuroscience* **16,** 3549-3558.

Lahti AC, Koffel B, Laporte D & Tamminga CA. (1995). SUBANESTHETIC DOSES OF KETAMINE STIMULATE PSYCHOSIS IN SCHIZOPHRENIA. *Neuropsychopharmacology* **13,** 9-19.

Lahti AC, Weiler MA, Michaelidis T, Parwani A & Tamminga CA. (2001). Effects of ketamine in normal and schizophrenic volunteers. *Neuropsychopharmacology* **25,** 455-467.

Laplante M & Sabatini DM. (2009). mTOR signaling at a glance. *Journal of Cell Science* **122,** 3589-3594.

Larsen MH, Olesen M, Woldbye DPD, Hay-Schmidt A, Hansen HH, Ron LCB & Mikkelsen JD. (2005). Regulation of activity-regulated cytoskeleton protein (Arc) mRNA after acute and chronic electroconvulsive stimulation in the rat. *Brain Research* **1064,** 161-165.

Laube B, Hirai H, Sturgess M, Betz H & Kuhse J. (1997). Molecular determinants of agonist discrimination by NMDA receptor subunits: Analysis of the glutamate binding site on the NR2B subunit. *Neuron* **18,** 493-503.

Laurie DJ & Seeburg PH. (1994). REGIONAL AND DEVELOPMENTAL HETEROGENEITY IN SPLICING OF THE RAT-BRAIN NMDAR1 MESSENGER-RNA. *Journal of Neuroscience* **14,** 3180-3194.

Leonard AS, Lim IA, Hemsworth DE, Horne MC & Hell JW. (1999). Calcium/calmodulin-dependent protein kinase II is associated with the N-methyl-D-aspartate receptor. *Proceedings of the National Academy of Sciences of the United States of America* **96,** 3239-3244.

Leung LY & Baillie TA. (1986). COMPARATIVE PHARMACOLOGY IN THE RAT OF KETAMINE AND ITS 2 PRINCIPAL METABOLITES, NORKETAMINE AND (Z)-6-HYDROXYNORKETAMINE. *Journal of Medicinal Chemistry* **29,** 2396-2399.

Li NX, Lee B, Liu RJ, Banasr M, Dwyer JM, Iwata M, Li XY, Aghajanian G & Duman RS. (2010). mTOR-Dependent Synapse Formation Underlies the Rapid Antidepressant Effects of NMDA Antagonists. *Science* **329,** 959-964.

Li WD, Okano A, Tian QB, Nakayama K, Furihata T, Nawa H & Suzuki T. (2001). Characterization of a novel synGAP isoform, synGAP-beta. *Journal of Biological Chemistry* **276,** 21417-21424.

Li X, Sinues PML, Dallmann R, Bregy L, Hollmen M, Proulx S, Brown SA, Detmar M, Kohler M & Zenobi R. (2015). Drug Pharmacokinetics Determined by Real-Time Analysis of Mouse Breath. *Angewandte Chemie-International Edition* **54,** 7815-7818.

Liebenberg N, Joca S & Wegener G. (2015). Nitric oxide involvement in the antidepressant-like effect of ketamine in the Flinders sensitive line rat model of depression. *Acta Neuropsychiatrica* **27,** 90-96.

Liguz-Lecznar M & Skangiel-Kramska J. (2007). Vesicular glutamate transporters (VGLUTs): The three musketeers of glutamatergic system. *Acta Neurobiologiae Experimentalis* **67,** 207-218.

Liljequist S, Ossowska K, Grabowskaanden M & Anden NE. (1991). EFFECT OF THE NMDA RECEPTOR ANTAGONIST, MK-801, ON LOCOMOTOR-ACTIVITY AND ON THE METABOLISM OF DOPAMINE IN VARIOUS BRAIN-AREAS OF MICE. *European Journal of Pharmacology* **195,** 55-61.

Lima-Ojeda JM, Vogt MA, Pfeiffer N, Dormann C, Kohr G, Sprengel R, Gass P & Inta D. (2013). Pharmacological blockade of GluN2B-containing NMDA receptors induces antidepressant-like effects lacking psychotomimetic action and neurotoxicity in the perinatal and adult rodent brain. *Progress in Neuro-Psychopharmacology & Biological Psychiatry* **45,** 28-33.

Link W, Konietzko U, Kauselmann G, Krug M, Schwanke B, Frey U & Kuhl D. (1995). SOMATODENDRITIC EXPRESSION OF AN IMMEDIATE-EARLY GENE IS REGULATED BY

SYNAPTIC ACTIVITY. *Proceedings of the National Academy of Sciences of the United States of America* **92,** 5734-5738.

Lisek M, Ferenc B, Studzian M, Pulaski L, Guo F, Zylinska L & Boczek T. (2017). Glutamate Deregulation in Ketamine-Induced Psychosis-A Potential Role of PSD95, NMDA Receptor and PMCA Interaction. *Frontiers in Cellular Neuroscience* **11**.

Liu LD, Wong TP, Pozza MF, Lingenhoehl K, Wang YS, Sheng M, Auberson YP & Wang YT. (2004). Role of NMDA receptor subtypes in governing the direction of hippocampal synaptic plasticity. *Science* **304,** 1021-1024.

Lord B, Wintmolders C, Langlois X, Nguyen L, Lovenberg T & Bonaventure P. (2013). Comparison of the ex vivo receptor occupancy profile of ketamine to several NMDA receptor antagonists in mouse hippocampus. *European Journal of Pharmacology* **715,** 21-25.

Lu W, Isozaki K, Roche KW & Nicoll RA. (2010). Synaptic targeting of AMPA receptors is regulated by a CaMKII site in the first intracellular loop of GluA1. *Proceedings of the National Academy of Sciences of the United States of America* **107,** 22266-22271.

Lyford GL, Yamagata K, Kaufmann WE, Barnes CA, Sanders LK, Copeland NG, Gilbert DJ, Jenkins NA, Lanahan AA & Worley PF. (1995). ARC, A GROWTH-FACTOR AND ACTIVITY-REGULATED GENE, ENCODES A NOVEL CYTOSKELETON-ASSOCIATED PROTEIN THAT IS ENRICHED IN NEURONAL DENDRITES. *Neuron* **14,** 433-445.

Macdonald JF, Miljkovic Z & Pennefather P. (1987). USE-DEPENDENT BLOCK OF EXCITATORY AMINO-ACID CURRENTS IN CULTURED NEURONS BY KETAMINE. *Journal of Neurophysiology* **58,** 251-266.

Maeng S, Zarate CA, Du J, Schloesser RJ, McCammon J, Chen G & Manji HK. (2008). Cellular mechanisms underlying the antidepressant effects of ketamine: Role of alpha-amino-3-hydroxy-5-methylisoxazole-4-propionic acid receptors. *Biological Psychiatry* **63,** 349-352.

Maki BA, Aman TK, Amico-Ruvio SA, Kussius CL & Popescu GK. (2012). C-terminal Domains of N-Methyl-D-aspartic Acid Receptor Modulate Unitary Channel Conductance and Gating. *Journal of Biological Chemistry* **287,** 36071-36080.

Malhotra AK, Adler CM, Kennison SD, Elman I, Pickar D & Breier A. (1997). Clozapine blunts N-methyl-D-aspartate antagonist-induced psychosis: A study with ketamine. *Biological Psychiatry* **42,** 664-668.

Malykhin NV, Carter R, Seres P & Coupland NJ. (2010). Structural changes in the hippocampus in major depressive disorder: contributions of disease and treatment. *Journal of Psychiatry & Neuroscience* **35,** 337-343.

Mantovani M, Pertile R, Calixto JB, Santos ARS & Rodrigues ALS. (2003). Melatonin exerts an antidepressant-like effect in the tail suspension test in mice: evidence for involvement of N-methyl-D-aspartate receptors and the L-arginine-nitric oxide pathway. *Neuroscience Letters* **343,** 1-4.

Mao LM, Tang QS, Samdani S, Liu ZG & Wang JQ. (2004). Regulation of MAPK/ERK phosphorylation via ionotropic glutamate receptors in cultured rat striatal neurons. *European Journal of Neuroscience* **19,** 1207-1216.

Martel MA, Ryan TJ, Bell KFS, Fowler JH, McMahon A, Al-Mubarak B, Komiyama NH, Horsburgh K, Kind PC, Grant SGN, Wyllie DJA & Hardingham GE. (2012). The Subtype of GluN2 C-terminal Domain Determines the Response to Excitotoxic Insults. *Neuron* **74,** 543-556.

Martel MA, Wyllie DJA & Hardingham GE. (2009). IN DEVELOPING HIPPOCAMPAL NEURONS, NR2B-CONTAINING N-METHYL-D-ASPARTATE RECEPTORS (NMDARs) CAN MEDIATE SIGNALING TO NEURONAL SURVIVAL AND SYNAPTIC POTENTIATION, AS WELL AS NEURONAL DEATH. *Neuroscience* **158,** 334-343.

Massey PV, Johnson BE, Moult PR, Auberson YP, Brown MW, Molnar E, Collingridge GL & Bashir ZI. (2004). Differential roles of NR2A and NR2B-containing NMDA receptors in cortical long-term potentiation and long-term depression. *Journal of Neuroscience* **24,** 7821-7828.

Matsuzaki M, Honkura N, Ellis-Davies GCR & Kasai H. (2004). Structural basis of long-term potentiation in single dendritic spines. *Nature* **429,** 761-766.

Maxwell CR, Ehrlichman RS, Liang YL, Trief D, Kanes SJ, Karp J & Siegel SJ. (2006). Ketamine produces lasting disruptions in encoding of sensory stimuli. *Journal of Pharmacology and Experimental Therapeutics* **316,** 315-324.

Mayer ML & Westbrook GL. (1987). PERMEATION AND BLOCK OF N-METHYL-D-ASPARTIC ACID RECEPTOR CHANNELS BY DIVALENT-CATIONS IN MOUSE CULTURED CENTRAL NEURONS. *Journal of Physiology-London* **394,** 501-527.

Mayer ML, Westbrook GL & Guthrie PB. (1984). VOLTAGE-DEPENDENT BLOCK BY MG-2+ OF NMDA RESPONSES IN SPINAL-CORD NEURONS. *Nature* **309,** 261-263.

McGee AW, Topinka JR, Hashimoto K, Petralia RS, Kakizawa S, Kauer F, Aguilera-Moreno A, Wenthold RJ, Kano M & Bredt DS. (2001). PSD-93 knock-out mice reveal that

neuronal MAGUKs are not required for development or function of parallel fiber synapses in cerebellum. *Journal of Neuroscience* **21,** 3085-3091.

Messaoudi E, Kanhema T, Soule J, Tiron A, Dagyte G, da Silva B & Bramham CR. (2007). Sustained Arc/Arg3.1 synthesis controls long-term potentiation consolidation through regulation of local actin polymerization in the dentate gyrus In vivo. *Journal of Neuroscience* **27,** 10445-10455.

Migaud M, Charlesworth P, Dempster M, Webster LC, Watabe AM, Makhinson M, He Y, Ramsay MF, Morris RGM, Morrison JH, O'Dell TJ & Grant SGN. (1998). Enhanced long-term potentiation and impaired learning in mice with mutant postsynaptic density-95 protein. *Nature* **396,** 433-439.

Miller OH, Moran JT & Hall BJ. (2016). Two cellular hypotheses explaining the initiation of ketamine's antidepressant actions: Direct inhibition and disinhibition. *Neuropharmacology* **100,** 17-26.

Miller OH, Yang L, Wang CC, Hargroder E, Zhang Y, Delpire E & Hall BJ. (2014). GluN2B-Containing NMDA Receptors Regulate Depression-Like Behavior and are Critical for the Rapid Antidepressant Actions of Ketamine. *Elife* **3**.

Moga DE, Calhoun ME, Chowdhury A, Worley P, Morrison JH & Shapiro ML. (2004). Activity-regulated cytoskeletal-associated protein is localized to recently activated excitatory synapses. *Neuroscience* **125,** 7-11.

Moghaddam B, Adams B, Verma A & Daly D. (1997). Activation of glutamatergic neurotransmission by ketamine: A novel step in the pathway from NMDA receptor blockade to dopaminergic and cognitive disruptions associated with the prefrontal cortex. *Journal of Neuroscience* **17,** 2921-2927.

Molyneaux BJ, Arlotta P, Menezes JRL & Macklis JD. (2007). Neuronal subtype specification in the cerebral cortex. *Nature Reviews Neuroscience* **8,** 427-437.

Monyer H, Burnashev N, Laurie DJ, Sakmann B & Seeburg PH. (1994). DEVELOPMENTAL AND REGIONAL EXPRESSION IN THE RAT-BRAIN AND FUNCTIONAL-PROPERTIES OF 4 NMDA RECEPTORS. *Neuron* **12,** 529-540.

Monyer H, Sprengel R, Schoepfer R, Herb A, Higuchi M, Lomeli H, Burnashev N, Sakmann B & Seeburg PH. (1992). HETEROMERIC NMDA RECEPTORS - MOLECULAR AND FUNCTIONAL DISTINCTION OF SUBTYPES. *Science* **256,** 1217-1221.

Moore JW, Turner DC, Corlett PR, Arana FS, Morgan HL, Absalom AR, Adapa R, de Wit S, Everitt JC, Gardner JM, Pigott JS, Haggard P & Fletcher PC. (2011). Ketamine

administration in healthy volunteers reproduces aberrant agency experiences associated with schizophrenia. *Cognitive Neuropsychiatry* **16,** 364-381.

Moosavi M, Khales GY, Rastegar K & Zarifkar A. (2012). The effect of sub-anesthetic and anesthetic ketamine on water maze memory acquisition, consolidation and retrieval. *European Journal of Pharmacology* **677,** 107-110.

Morgan CJA & Curran HV. (2006). Acute and chronic effects of ketamine upon human memory: a review. *Psychopharmacology* **188,** 408-424.

Morgan CJA, Muetzelfeldt L & Curran HV. (2010). Consequences of chronic ketamine self-administration upon neurocognitive function and psychological wellbeing: a 1-year longitudinal study (vol 105, pg 121, 2010). *Addiction* **105,** 766-766.

Moser EI, Krobert KA, Moser MB & Morris RGM. (1998). Impaired spatial learning after saturation of long-term potentiation. *Science* **281,** 2038-2042.

Murrough JW, Losifescu DV, Chang LC, Al Jurdi RK, Green CE, Perez AM, Lqbal S, Pillemer S, Foulkes A, Shah A, Charney DS & Mathew SJ. (2013). Antidepressant Efficacy of Ketamine in Treatment-Resistant Major Depression: A Two-Site Randomized Controlled Trial. *American Journal of Psychiatry* **170,** 1134-1142.

Na Y, Park S, Lee C, Kim DK, Park JM, Sockanathan S, Huganir RL & Worley PF. (2016). Real-Time Imaging Reveals Properties of Glutamate-Induced Arc/Arg 3.1 Translation in Neuronal Dendrites. *Neuron* **91,** 561-573.

Nabavi S, Kessels HW, Alfonso S, Aow J, Fox R & Malinow R. (2013). Metabotropic NMDA receptor function is required for NMDA receptor-dependent long-term depression. *Proceedings of the National Academy of Sciences of the United States of America* **110,** 4027-4032.

Nagura H, Ishikawa Y, Kobayashi K, Takao K, Tanaka T, Nishikawa K, Tamura H, Shiosaka S, Suzuki H, Miyakawa T, Fujiyoshi Y & Doi T. (2012). Impaired synaptic clustering of postsynaptic density proteins and altered signal transmission in hippocampal neurons, and disrupted learning behavior in PDZ1 and PDZ2 ligand binding-deficient PSD-95 knockin mice. *Molecular Brain* **5**.

Nair RR, Patil S, Tiron A, Kanhema T, Panja D, Schiro L, Parobczak K, Wilczynski G & Bramham CR. (2017). Dynamic Arc SUMOylation and Selective Interaction with F-Actin-Binding Protein Drebrin A in LTP Consolidation In Vivo. *Frontiers in synaptic neuroscience* **9,** 8-8.

Newcomer JW, Farber NB, Jevtovic-Todorovic V, Selke G, Melson AK, Hershey T, Craft S & Olney JW. (1999). Ketamine-induced NMDA receptor hypofunction as a model of memory impairment and psychosis. *Neuropsychopharmacology* **20,** 106-118.

Neyton J & Paoletti P. (2006). Relating NMDA receptor function to receptor subunit composition: Limitations of the pharmacological approach. *Journal of Neuroscience* **26,** 1331-1333.

Nicholson DA, Trana R, Katz Y, Kath WL, Spruston N & Geinisman Y. (2006). Distance-dependent differences in synapse number and AMPA receptor expression in hippocampal CA1 pyramidal neurons. *Neuron* **50,** 431-442.

Nikolaienko O, Eriksen MS, Patil S, Bito H & Bramham CR. (2017). STIMULUS-EVOKED ERK-DEPENDENT PHOSPHORYLATION OF ACTIVITY-REGULATED CYTOSKELETON-ASSOCIATED PROTEIN (ARC) REGULATES ITS NEURONAL SUBCELLULAR LOCALIZATION. *Neuroscience* **360,** 68-80.

Nishimura M, Yamagata K, Sugiura H & Okamura H. (2003). The activity-regulated cytoskeleton-associated (Arc) gene is a new light-inducible early gene in the mouse suprachiasmatic nucleus. *Neuroscience* **116,** 1141-1147.

Nithianantharajah J, Komiyama NH, McKechanie A, Johnstone M, Blackwood DH, St Clair D, Emes RD, van de Lagemaat LN, Saksida LM, Bussey TJ & Grant SGN. (2013). Synaptic scaffold evolution generated components of vertebrate cognitive complexity. *Nature Neuroscience* **16,** 16-U37.

Noback C, Strominger N, Demarest R & Ruggiero D. (2005). Cerebral Cortex. In *The Human Nervous System*. Humana Press.

Noguchi J, Nagaoka A, Watanabe S, Ellis-Davies GCR, Kitamura K, Kano M, Matsuzaki M & Kasai H. (2011). In vivo two-photon uncaging of glutamate revealing the structure-function relationships of dendritic spines in the neocortex of adult mice. *Journal of Physiology-London* **589,** 2447-2457.

Nowak L, Bregestovski P, Ascher P, Herbet A & Prochiantz A. (1984). MAGNESIUM GATES GLUTAMATE-ACTIVATED CHANNELS IN MOUSE CENTRAL NEURONS. *Nature* **307,** 462-465.

Numakawa T, Suzuki S, Kumamaru E, Adachi N, Richards M & Kunugi H. (2010). BDNF function and intracellular signaling in neurons. *Histology and Histopathology* **25,** 237-258.

O'Brien RJ, Kamboj S, Ehlers MD, Rosen KR, Fischbach GD & Huganir RL. (1998). Activity-dependent modulation of synaptic AMPA receptor accumulation. *Neuron* **21,** 1067-1078.

Oh SW, Harris JA, Ng L, Winslow B, Cain N, Mihalas S, Wang QX, Lau C, Kuan L, Henry AM, Mortrud MT, Ouellette B, Nguyen TN, Sorensen SA, Slaughterbeck CR, Wakeman W, Li Y, Feng D, Ho A, Nicholas E, Hirokawa KE, Bohn P, Joines KM, Peng HC, Hawrylycz MJ, Phillips JW, Hohmann JG, Wohnoutka P, Koch C, Bernard A, Dang C, Jones AR, Zeng HK & Gerfen CR. (2014). A mesoscale connectome of the mouse brain. *Nature* **508,** 207-+.

Okuno H, Akashi K, Ishii Y, Yagishita-Kyo N, Suzuki K, Nonaka M, Kawashima T, Fujii H, Takemoto-Kimura S, Abe M, Natsume R, Chowdhury S, Sakimura K, Worley PF & Bito H. (2012). Inverse Synaptic Tagging of Inactive Synapses via Dynamic Interaction of Arc/Arg3.1 with CaMKII beta. *Cell* **149,** 886-898.

Panja D, Dagyte G, Bidinosti M, Wibrand K, Kristiansen AM, Sonenberg N & Bramham CR. (2009). Novel Translational Control in Arc-dependent Long Term Potentiation Consolidation in Vivo. *Journal of Biological Chemistry* **284,** 31498-31511.

Paoletti P, Ascher P & Neyton J. (1997). High-affinity zinc inhibition of NMDA NR1-NR2A receptors. *Journal of Neuroscience* **17,** 5711-5725.

Paoletti P, Perin-Dureau F, Fayyazuddin A, Le Goff A, Callebaut I & Neyton J. (2000). Molecular organization of a zinc binding N-terminal modulatory domain in a NMDA receptor subunit. *Neuron* **28,** 911-925.

Park S, Park JM, Kim S, Kim J-A, Shepherd JD, Smith-Hicks CL, Chowdhury S, Kaufmann W, Kuhl D, Ryazanov AG, Huganir RL, Linden DJ & Worley PF. (2008). Elongation factor 2 and fragile X mental retardation protein control the dynamic translation of Arc/Arg3.1 essential for mGluR-LTD. *Neuron* **59,** 70-83.

Pastuzyn ED, Day CE, Kearns RB, Kyrke-Smith M, Taibi AV, McCormick J, Yoder N, Belnap DM, Erlendsson S, Morado DR, Briggs JAG, Feschotte C & Shepherd JD. (2018). The Neuronal Gene Arc Encodes a Repurposed Retrotransposon Gag Protein that Mediates Intercellular RNA Transfer. *Cell* **172,** 275-+.

Patneau DK & Mayer ML. (1990). STRUCTURE-ACTIVITY-RELATIONSHIPS FOR AMINO-ACID TRANSMITTER CANDIDATES ACTING AT N-METHYL-D-ASPARTATE AND QUISQUALATE RECEPTORS. *Journal of Neuroscience* **10,** 2385-2399.

Patterson MA, Szatmari EM & Yasuda R. (2010). AMPA receptors are exocytosed in stimulated spines and adjacent dendrites in a Ras-ERK-dependent manner during

long-term potentiation. *Proceedings of the National Academy of Sciences of the United States of America* **107,** 15951-15956.

Peebles CL, Yoo J, Thwin MT, Palop JJ, Noebels JL & Finkbeiner S. (2010). Arc regulates spine morphology and maintains network stability in vivo. *Proceedings of the National Academy of Sciences of the United States of America* **107,** 18173-18178.

Pei Q, Zetterstrom TSC, Sprakes M, Tordera R & Sharp T. (2003). Antidepressant drug treatment induces Arc gene expression in the rat brain. *Neuroscience* **121,** 975-982.

Peng JM, Kim MJ, Cheng DM, Duong DM, Gygi SP & Sheng M. (2004). Semiquantitative proteomic analysis of rat Forebrain postsynaptic density fractions by mass spectrometry. *Journal of Biological Chemistry* **279,** 21003-21011.

Perez-Otano I, Larsen RS & Wesseling JF. (2016). Emerging roles of GluN3-containing NMDA receptors in the CNS. *Nature Reviews Neuroscience* **17,** 623-635.

Pernia M, Estevez S, Poveda C, Plaza I, Carro J, Juiz JM & Merchan MA. (2017). c-Fos and Arc/Arg3.1 expression in auditory and visual cortices after hearing loss: Evidence of sensory crossmodal reorganization in adult rats. *Journal of Comparative Neurology* **525,** 2677-2689.

Pintchovski SA, Peebles CL, Kim HJ, Verdin E & Finkbeiner S. (2009). The Serum Response Factor and a Putative Novel Transcription Factor Regulate Expression of the Immediate-Early Gene Arc/Arg3.1 in Neurons. *Journal of Neuroscience* **29,** 1525-1537.

Pitsikas N & Boultadakis A. (2009). Pre-training administration of anesthetic ketamine differentially affects rats' spatial and non-spatial recognition memory. *Neuropharmacology* **57,** 1-7.

Plath N, Ohana O, Dammermann B, Errington ML, Schmitz D, Gross C, Mao X, Engelsberg A, Mahlke C, Welzl H, Kobaz U, Stawrakakis A, Fernandez E, Waltereit R, Bick-Sander A, Therstappen E, Cooke SF, Blanquet V, Wurst W, Salmen B, Boesl MR, Lipp H-P, Grant SGN, Bliss TVP, Wolfer DP & Kuhl D. (2006). Arc/Arg3.1 is essential for the consolidation of synaptic plasticity and memories. *Neuron* **52,** 437-444.

Ploski JE, Pierre VJ, Smucny J, Park K, Monsey MS, Overeem KA & Schafe GE. (2008). The Activity-Regulated Cytoskeletal-Associated Protein (Arc/Arg3.1) Is Required for Memory Consolidation of Pavlovian Fear Conditioning in the Lateral Amygdala. *Journal of Neuroscience* **28,** 12383-12395.

Pollak DD, Rey CE & Monje FJ. (2010). Rodent models in depression research: Classical strategies and new directions. *Annals of Medicine* **42,** 252-264.

Pomarol-Clotet E, Honey GD, Murray GK, Corlett PR, Absalom AR, Lee M, McKenna PJ, Bullmore ET & Fletcher PC. (2006). Psychological effects of ketamine in healthy volunteers - Phenomenological study. *British Journal of Psychiatry* **189,** 173-179.

Popik P, Kos T, Sowa-Kucma M & Nowak G. (2008). Lack of persistent effects of ketamine in rodent models of depression. *Psychopharmacology* **198,** 421-430.

Powell T, Fernandes C & Schalkwyk L. (2012). Depression-Related Behavioral Tests. *Curr Protoc Mouse Biol* **Jun 1,** 119-127.

Pozzi L, Dorocic IP, Wang XM, Carlen M & Meletis K. (2014). Mice Lacking NMDA Receptors in Parvalbumin Neurons Display Normal Depression-Related Behavior and Response to Antidepressant Action of NMDAR Antagonists. *Plos One* **9**.

Prast H & Philippu A. (2001). Nitric oxide as modulator of neuronal function. *Progress in Neurobiology* **64,** 51-68.

Preskorn SH, Baker B, Kolluri S, Menniti FS, Krams M & Landen JW. (2008). An Innovative Design to Establish Proof of Concept of the Antidepressant Effects of the NR2B Subunit Selective N-Methyl-D-Aspartate Antagonist, CP-101,606, in Patients With Treatment-Refractory Major Depressive Disorder. *Journal of Clinical Psychopharmacology* **28,** 631-637.

Price RB, Nock MK, Charney DS & Mathew SJ. (2009). Effects of Intravenous Ketamine on Explicit and Implicit Measures of Suicidality in Treatment-Resistant Depression. *Biological Psychiatry* **66,** 522-526.

Quirk M, Sosulski D, Feierstein C, Uchida N & Mainen Z. (2009). A defined network of fast-spiking interneurons in orbitofrontal cortex: responses to behavioral contingencies and ketamine administration. *Frontiers in Systems Neuroscience* **3**.

Raffa RB, Pergolizzi JV, Jr., Taylor R, Jr. & Group NR. (2017). The rapid-onset antidepressant effect of ketamine: More surprises? *Journal of clinical pharmacy and therapeutics*.

Ramirez-Amaya V, Vazdarjanova A, Mikhael D, Rosi S, Worley PF & Barnes CA. (2005). Spatial exploration-induced Arc mRNA and protein expression: Evidence for selective, network-specific reactivation. *Journal of Neuroscience* **25,** 1761-1768.

Rao VR, Pintchovski SA, Chin J, Peebles CL, Mitra S & Finkbeiner S. (2006). AMPA receptors regulate transcription of the plasticity-related immediate-early gene Arc. *Nature Neuroscience* **9,** 887-895.

Rauner C & Kohr G. (2011). Triheteromeric NR1/NR2A/NR2B Receptors Constitute the Major N-Methyl-D-aspartate Receptor Population in Adult Hippocampal Synapses. *Journal of Biological Chemistry* **286,** 7558-7566.

Ressler KJ. (2010). Amygdala Activity, Fear, and Anxiety: Modulation by Stress. *Biological Psychiatry* **67,** 1117-1119.

Reus GZ, Vieira FG, Abelaira HM, Michels M, Tomaz DB, dos Santos MAB, Carlessi AS, Neotti MV, Matias BI, Luz JR, Dal-Pizzol F & Quevedo J. (2014). MAPK signaling correlates with the antidepressant effects of ketamine. *Journal of Psychiatric Research* **55,** 15-21.

Rial Verde EM, Lee-Osbourne J, Worley PF, Malinow R & Cline HT. (2006). Increased expression of the immediate-early gene arc/arg3.1 reduces AMPA receptor-mediated synaptic transmission. *Neuron* **52,** 461-474.

Robertson LM, Kerppola TK, Vendrell M, Luk D, Smeyne RJ, Bocchiaro C, Morgan JI & Curran T. (1995). REGULATION OF C-FOS EXPRESSION IN TRANSGENIC MICE REQUIRES MULTIPLE INTERDEPENDENT TRANSCRIPTION CONTROL ELEMENTS. *Neuron* **14,** 241-252.

Rockliffe N & Gawler D. (2006). Differential mechanisms of glutamate receptor regulation of SynGAP in cortical neurones. *Febs Letters* **580,** 831-838.

Rodriguez JJ, Davies HA, Errington ML, Verkhratsky A, Bliss TVP & Stewart MG. (2008). ARG3.1/ARC expression in hippocampal dentate gyrus astrocytes: ultrastructural evidence and co-localization with glial fibrillary acidic protein. *Journal of Cellular and Molecular Medicine* **12,** 671-678.

Rodriguez JJ, Davies HA, Silva AT, De Souza IEJ, Peddie CJ, Colyer FM, Lancashire CL, Fine A, Errington ML, Bliss TVP & Stewart MG. (2005). Long-term potentiation in the rat dentate gyrus is associated with enhanced Arc/Arg3.1 protein expression in spines, dendrites and glia. *European Journal of Neuroscience* **21,** 2384-2396.

Rosa AO, Lin J, Calixto JB, Santos ARS & Rodrigues ALS. (2003). Involvement of NMDA receptors and L-arginine-nitric oxide pathway in the antidepressant-like effects of zinc in mice. *Behavioural Brain Research* **144,** 87-93.

Ryan TJ, Emes RD, Grant SGN & Komiyama NH. (2008). Evolution of NMDA receptor cytoplasmic interaction domains: implications for organisation of synaptic signalling complexes. *Bmc Neuroscience* **9**.

Ryan TJ, Kopanitsa MV, Indersmitten T, Nithianantharajah J, Afinowi NO, Pettit C, Stanford LE, Sprengel R, Saksida LM, Bussey TJ, O'Dell TJ, Grant SGN & Komiyama NH. (2013).

Evolution of GluN2A/B cytoplasmic domains diversified vertebrate synaptic plasticity and behavior. *Nature Neuroscience* **16,** 25-U21.

Sanhueza M, Fernandez-Villalobos G, Stein IS, Kasumova G, Zhang P, Bayer KU, Otmakhov N, Hell JW & Lisman J. (2011). Role of the CaMKII/NMDA Receptor Complex in the Maintenance of Synaptic Strength. *Journal of Neuroscience* **31,** 9170-9178.

Sato Y, Kobayashi E, Hakamata Y, Kobahashi M, Wainai T, Murayama T, Mishina M & Seo N. (2004). Chronopharmacological studies of ketamine in normal and NMDA epsilon 1 receptor knockout mice. *British Journal of Anaesthesia* **92,** 859-864.

Sattler R, Xiang ZG, Lu WY, Hafner M, MacDonald JF & Tymianski M. (1999). Specific coupling of NMDA receptor activation to nitric oxide neurotoxicity by PSD-95 protein. *Science* **284,** 1845-1848.

Schneggenburger R. (1996). Simultaneous measurement of Ca2+ influx and reversal potentials in recombinant N-methyl-D-aspartate receptor channels. *Biophysical Journal* **70,** 2165-2174.

Scott DB, Blanpied TA, Swanson GT, Zhang C & Ehlers MD. (2001). An NMDA receptor ER retention signal regulated by phosphorylation and alternative splicing. *Journal of Neuroscience* **21,** 3063-3072.

Seamans J. (2008). Losing inhibition with ketamine. *Nature Chemical Biology* **4,** 91-93.

Seeman P, Ko F & Tallerico T. (2005). Dopamine receptor contribution to the action of PCP, LSD and ketamine psychotomimetics. *Molecular Psychiatry* **10,** 877-883.

Shannon F, Gail L, Conor DC & Oswald S. (2014). Selective localization of arc mRNA in dendrites involves activity- and translation-dependent mRNA degradation. *The Journal of neuroscience : the official journal of the Society for Neuroscience* **34,** 4481-4493.

Sheng M & Greenberg ME. (1990). THE REGULATION AND FUNCTION OF C-FOS AND OTHER IMMEDIATE EARLY GENES IN THE NERVOUS-SYSTEM. *Neuron* **4,** 477-485.

Shepherd JD, Rumbaugh G, Wu J, Chowdhury S, Plath N, Kuhl D, Huganir RL & Worley PF. (2006). Arc/Arg3.1 mediates homeostatic synaptic scaling of AMPA receptors. *Neuron* **52,** 475-484.

Shirayama Y & Hashimoto K. (2017). Effects of a single bilateral infusion of R-ketamine in the rat brain regions of a learned helplessness model of depression. *European Archives of Psychiatry and Clinical Neuroscience* **267,** 177-182.

Slikker W, Zou XJ, Hotchkiss CE, Divine RL, Sadovova N, Twaddle NC, Doerge DR, Scallet AC, Patterson TA, Hanig JP, Paule MG & Wang C. (2007). Ketamine-induced neuronal cell death in the perinatal rhesus monkey. *Toxicological Sciences* **98,** 145-158.

Smith DJ, Bouchal RL, Desanctis CA, Monroe PJ, Amedro JB, Perrotti JM & Crisp T. (1987). PROPERTIES OF THE INTERACTION BETWEEN KETAMINE AND OPIATE BINDING-SITES INVIVO AND INVITRO. *Neuropharmacology* **26,** 1253-1260.

Smith JW, Gastambide F, Gilmour G, Dix S, Foss J, Lloyd K, Malik N & Tricklebank M. (2011). A comparison of the effects of ketamine and phencyclidine with other antagonists of the NMDA receptor in rodent assays of attention and working memory. *Psychopharmacology* **217,** 255-269.

Smith-Hicks C, Xiao B, Deng RK, Ji YF, Zhao X, Shepherd JD, Posern G, Kuhl D, Huganir RL, Ginty DD, Worley PF & Linden DJ. (2010). SRF binding to SRE 6.9 in the Arc promoter is essential for LTD in cultured Purkinje cells. *Nature Neuroscience* **13,** 1082-U1073.

Sprengel R, Suchanek B, Amico C, Brusa R, Burnashev N, Rozov A, Hvalby O, Jensen V, Paulsen O, Andersen P, Kim JJ, Thompson RF, Sun W, Webster LC, Grant SGN, Eilers J, Konnerth A, Li JY, McNamara JO & Seeburg PH. (1998). Importance of the intracellular domain of NR2 subunits for NMDA receptor function in vivo. *Cell* **92,** 279-289.

Squire LR. (1992). MEMORY AND THE HIPPOCAMPUS - A SYNTHESIS FROM FINDINGS WITH RATS, MONKEYS, AND HUMANS. *Psychological Review* **99,** 195-231.

Stanton PK & Sarvey JM. (1984). BLOCKADE OF LONG-TERM POTENTIATION IN RAT HIPPOCAMPAL-CA1 REGION BY INHIBITORS OF PROTEIN-SYNTHESIS. *Journal of Neuroscience* **4,** 3080-3088.

Stein IS, Gray JA & Zito K. (2015). Non-Ionotropic NMDA Receptor Signaling Drives Activity-Induced Dendritic Spine Shrinkage. *Journal of Neuroscience* **35,** 12303-12308.

Steward O, Wallace CS, Lyford GL & Worley PF. (1998). Synaptic activation causes the mRNA for the IEG Arc to localise selectively near activated postsynaptic sites on dendrites. *Neuron* **21,** 741-751.

Steward O & Worley PF. (2001). Selective targeting of newly synthesized Arc mRNA to active synapses requires NMDA receptor activation. *Neuron* **30,** 227-240.

Stocca G & Vicini S. (1998). Increased contribution of NR2A subunit to synaptic NMDA receptors in developing rat cortical neurons. *Journal of Physiology-London* **507,** 13-24.

Stone JM, Dietrich C, Edden R, Mehta MA, De Simoni S, Reed LJ, Krystal JH, Nutt D & Barker GJ. (2012). Ketamine effects on brain GABA and glutamate levels with 1H-MRS: relationship to ketamine- induced psychopathology. *Molecular Psychiatry* **17,** 664-665.

Strack S, McNeill RB & Colbran RJ. (2000). Mechanism and regulation of calcium/calmodulin-dependent protein kinase II targeting to the NR2B subunit of the N-methyl-D-aspartate receptor. *Journal of Biological Chemistry* **275,** 23798-23806.

Strasburger SE, Bhimani PM, Kaabe JH, Krysiak JT, Nanchanatt DL, Nguyen TN, Pough KA, Prince TA, Ramsey NS, Savsani KH, Scandlen L, Cavaretta MJ & Raffa RB. (2017). What is the mechanism of Ketamine's rapid-onset antidepressant effect? A concise overview of the surprisingly large number of possibilities. *Journal of Clinical Pharmacy and Therapeutics* **42,** 147-154.

Sugihara H, Moriyoshi K, Ishii T, Masu M & Nakanishi S. (1992). STRUCTURES AND PROPERTIES OF 7 ISOFORMS OF THE NMDA RECEPTOR GENERATED BY ALTERNATIVE SPLICING. *Biochemical and Biophysical Research Communications* **185,** 826-832.

Susaki EA, Tainaka K, Perrin D, Kishino F, Tawara T, Watanabe TM, Yokoyama C, Onoe H, Eguchi M, Yamaguchi S, Abe T, Kiyonari H, Shimizu Y, Miyawaki A, Yokota H & Ueda HR. (2014). Whole-Brain Imaging with Single-Cell Resolution Using Chemical Cocktails and Computational Analysis. *Cell* **157,** 726-739.

Sutton MA, Taylor AM, Ito HT, Pham A & Schuman EM. (2007). Postsynaptic decoding of neural activity: eEF2 as a biochemical sensor coupling miniature synaptic transmission to local protein synthesis. *Neuron* **55,** 648-661.

Sweatt JD. (2001). The neuronal MAP kinase cascade: a biochemical signal integration system subserving synaptic plasticity and memory. *Journal of Neurochemistry* **76,** 1-10.

Tang AH, Chen HW, Li TP, Metzbower SR, MacGillavry HD & Blanpied TA. (2016). A trans-synaptic nanocolumn aligns neurotransmitter release to receptors. *Nature* **536,** 210-+.

Tang JJ, Xue WD, Xia BM, Ren L, Tao WW, Chen C, Zhang HL, Wu RY, Wang QS, Wu HX, Duan JN & Chen G. (2015). Involvement of normalized NMDA receptor and mTOR-related

signaling in rapid antidepressant effects of Yueju and ketamine on chronically stressed mice. *Scientific Reports* **5**.

Tang YP, Shimizu E, Dube GR, Rampon C, Kerchner GA, Zhuo M, Liu GS & Tsien JZ. (1999). Genetic enhancement of learning and memory in mice. *Nature* **401,** 63-69.

Teyler TJ & Rudy JW. (2007). The hippocampal indexing theory and episodic memory: Updating the index. *Hippocampus* **17,** 1158-1169.

Thiels E, Xie XP, Yeckel MF, Barrionuevo G & Berger TW. (1996). NMDA receptor-dependent LTD in different subfields of hippocampus in vivo and in vitro. *Hippocampus* **6,** 43-51.

Thomas CG, Miller AJ & Westbrook GL. (2006). Synaptic and extrasynaptic NMDA receptor NR2 subunits in cultured hippocampal neurons. *Journal of Neurophysiology* **95,** 1727-1734.

Tizabi Y, Bhatti BH, Manaye KF, Das JR & Akinfiresoye L. (2012). ANTIDEPRESSANT-LIKE EFFECTS OF LOW KETAMINE DOSE IS ASSOCIATED WITH INCREASED HIPPOCAMPAL AMPA/NMDA RECEPTOR DENSITY RATIO IN FEMALE WISTAR-KYOTO RATS. *Neuroscience* **213,** 72-80.

Todd PK, Mack KJ & Malter JS. (2003). The fragile X mental retardation protein is required for type-I metabotropic glutamate receptor-dependent translation of PSD-95. *Proceedings of the National Academy of Sciences of the United States of America* **100,** 14374-14378.

Tovar KR, McGinley MJ & Westbrook GL. (2013). Triheteromeric NMDA Receptors at Hippocampal Synapses. *Journal of Neuroscience* **33,** 9150-9160.

Tovar KR & Westbrook GL. (1999). The incorporation of NMDA receptors with a distinct subunit composition at nascent hippocampal synapses in vitro. *Journal of Neuroscience* **19,** 4180-4188.

Traynelis SF, Wollmuth LP, McBain CJ, Menniti FS, Vance KM, Ogden KK, Hansen KB, Yuan HJ, Myers SJ & Dingledine R. (2010). Glutamate Receptor Ion Channels: Structure, Regulation, and Function. *Pharmacological Reviews* **62,** 405-496.

Trinidad JC, Thalhammer A, Specht CG, Lynn AJ, Baker PR, Schoepfer R & Burlingame AL. (2008). Quantitative analysis of synaptic phosphorylation and protein expression. *Molecular & Cellular Proteomics* **7,** 684-696.

Trneckova L, Rotllant D, Klenerova V, Hynie S & Armario A. (2007). Dynamics of immediate early gene and neuropeptide gene response to prolonged immobilization stress: evidence against a critical role of the termination of exposure to the stressor. *Journal of Neurochemistry* **100,** 905-914.

Turrigiano GG, Leslie KR, Desai NS, Rutherford LC & Nelson SB. (1998). Activity-dependent scaling of quantal amplitude in neocortical neurons. *Nature* **391,** 892-896.

van Berckel BNM, Oranje B, van Ree JM, Verbaten MN & Kahn RS. (1998). The effects of low dose ketamine on sensory gating, neuroendocrine secretion and behavior in healthy human subjects. *Psychopharmacology* **137,** 271-281.

Vazdarjanova A, Ramirez-Amaya V, Insel N, Plummer TK, Rosi S, Chowdhury S, Mikhael D, Worley PF, Guzowski JF & Barnes CA. (2006). Spatial exploration induces ARC, a plasticity-related immediate-early gene, only in calcium/calmodulin-dependent protein kinase II-positive principal excitatory and inhibitory neurons of the rat forebrain. *Journal of Comparative Neurology* **498,** 317-329.

Vicini S, Wang JF, Li JH, Zhu WJ, Wang YH, Luo JAH, Wolfe BB & Grayson DR. (1998). Functional and pharmacological differences between recombinant N-methyl-D-aspartate receptors. *Journal of Neurophysiology* **79,** 555-566.

Vousden DA, Epp J, Okuno H, Nieman BJ, van Eede M, Dazai J, Ragan T, Bito H, Frankland PW, Lerch JP & Henkelman RM. (2015). Whole-brain mapping of behaviourally induced neural activation in mice. *Brain Structure & Function* **220,** 2043-2057.

Wagner LE, Gingrich KJ, Kulli JC & Yang J. (2001). Ketamine blockade of voltage-gated sodium channels - Evidence for a shared receptor site with local anesthetics. *Anesthesiology* **95,** 1406-1413.

Walker AK, Budac DP, Bisulco S, Lee AW, Smith RA, Beenders B, Kelley KW & Dantzer R. (2013). NMDA Receptor Blockade by Ketamine Abrogates Lipopolysaccharide-Induced Depressive-Like Behavior in C57BL/6J Mice. *Neuropsychopharmacology* **38,** 1609-1616.

Wallace CS, Lyford GL, Worley PF & Steward O. (1998). Differential intracellular sorting of immediate early gene mRNAs depends on signals in the mRNA sequence. *Journal of Neuroscience* **18,** 26-35.

Walsh T, McClellan JM, McCarthy SE, Addington AM, Pierce SB, Cooper GM, Nord AS, Kusenda M, Malhotra D, Bhandari A, Stray SM, Rippey CF, Roccanova P, Makarov V, Lakshmi B, Findling RL, Sikich L, Stromberg T, Merriman B, Gogtay N, Butler P, Eckstrand K, Noory L, Gochman P, Long R, Chen ZG, Davis S, Baker C, Eichler EE, Meltzer PS, Nelson SF, Singleton AB, Lee MK, Rapoport JL, King MC & Sebat J.

(2008). Rare structural variants disrupt multiple genes in neurodevelopmental pathways in schizophrenia. *Science* **320,** 539-543.

Waltereit R, Dammermann B, Wulff P, Scafidi J, Staubli U, Kauselmann G, Bundman M & Kuhl D. (2001). Arg3.1/Arc mRNA induction by Ca2+ and cAMP requires protein kinase A and mitogen-activated protein kinase/extracellular regulated kinase activation. *Journal of Neuroscience* **21,** 5484-5493.

Wang CC, Held RG, Chang SC, Yang LL, Delpire E, Ghosh A & Hall BJ. (2011). A Critical Role for GluN2B-Containing NMDA Receptors in Cortical Development and Function. *Neuron* **72,** 789-805.

Wang CC, Held RG & Hall BJ. (2013). SynGAP Regulates Protein Synthesis and Homeostatic Synaptic Plasticity in Developing Cortical Networks. *Plos One* **8**.

Wang KH, Majewska A, Schummers J, Farley B, Hu CC, Sur M & Tonegawa S. (2006). In vivo two-photon imaging reveals a role of arc in enhancing orientation specificity in visual cortex. *Cell* **126,** 389-402.

Wang N, Yu HY, Shen XF, Gao ZQ, Yang C, Yang JJ & Zhang GF. (2015). The rapid antidepressant effect of ketamine in rats is associated with down-regulation of pro-inflammatory cytokines in the hippocampus. *Upsala Journal of Medical Sciences* **120,** 241-248.

Watanabe M, Inoue Y, Sakimura K & Mishina M. (1992). DEVELOPMENTAL-CHANGES IN DISTRIBUTION OF NMDA RECEPTOR CHANNEL SUBUNIT MESSENGER-RNAS. *Neuroreport* **3,** 1138-1140.

Waung MW, Pfeiffer BE, Nosyreva ED, Ronesi JA & Huber KM. (2008). Rapid translation of Arc/Arg3.1 selectively mediates mGluR-dependent LTD through persistent increases in AMPAR endocytosis rate. *Neuron* **59,** 84-97.

Weitlauf C, Honse Y, Auberson YP, Mishina M, Lovinger DM & Winder DG. (2005). Activation of NR2A-containing NMDA receptors is not obligatory for NMDA receptor-dependent long-term potentiation. *Journal of Neuroscience* **25,** 8386-8390.

Whitlock JR, Heynen AJ, Shuler MG & Bear MF. (2006). Learning induces long-term potentiation in the hippocampus. *Science* **313,** 1093-1097.

Wieber J, Gugler R, Hengstmann JH & Dengler HJ. (1975). PHARMACOKINETICS OF KETAMINE IN MAN. *Anaesthesist* **24,** 260-263.

Williams K. (1993). IFENPRODIL DISCRIMINATES SUBTYPES OF THE N-METHYL-D-ASPARTATE RECEPTOR - SELECTIVITY AND MECHANISMS AT RECOMBINANT HETEROMERIC RECEPTORS. *Molecular Pharmacology* **44,** 851-859.

Witton J, Padmashri R, Zinyuk LE, Popov VI, Kraev I, Line SJ, Jensen TP, Tedoldi A, Cummings DM, Tybulewicz VLJ, Fisher EMC, Bannerman DM, Randall AD, Brown JT, Edwards FA, Rusakov DA, Stewart MG & Jones MW. (2015). Hippocampal circuit dysfunction in the Tc1 mouse model of Down syndrome. *Nature Neuroscience* **18,** 1291-+.

Wohleb ES, Gerhard D, Thomas A & Duman RS. (2017). Molecular and Cellular Mechanisms of Rapid-Acting Antidepressants Ketamine and Scopolamine. *Current Neuropharmacology* **15,** 11-20.

Wong EHF, Kemp JA, Priestley T, Knight AR, Woodruff GN & Iversen LL. (1986). THE ANTICONVULSANT MK-801 IS A POTENT N-METHYL-D-ASPARTATE ANTAGONIST. *Proceedings of the National Academy of Sciences of the United States of America* **83,** 7104-7108.

Wyllie DJA, Behe P & Colquhoun D. (1998). Single-channel activations and concentration jumps: comparison of recombinant NR1a/NR2A and NR1a/NR2D NMDA receptors. *Journal of Physiology-London* **510,** 1-18.

Xing JR, Kimura H, Wang CY, Ishizuka K, Kushima I, Arioka Y, Yoshimi A, Nakamura Y, Shiino T, Oya-Ito T, Takasaki Y, Uno Y, Okada T, Iidaka T, Aleksic B, Mori D & Ozaki N. (2016). Resequencing and Association Analysis of Six PSD-95-Related Genes as Possible Susceptibility Genes for Schizophrenia and Autism Spectrum Disorders. *Scientific Reports* **6**.

Yamakura T, Chavez-Noriega LE & Harris RA. (2000). Subunit-dependent inhibition of human neuronal nicotinic acetylcholine receptors and other ligand-gated ion channels by dissociative anesthetics ketamine and dizocilpine. *Anesthesiology* **92,** 1144-1153.

Yamakura T, Mori H, Masaki H, Shimoji K & Mishina M. (1993). DIFFERENT SENSITIVITIES OF NMDA RECEPTOR-CHANNEL SUBTYPES TO NONCOMPETITIVE ANTAGONISTS. *Neuroreport* **4,** 687-690.

Yao WD, Gainetdinov RR, Arbuckle MI, Sotnikova TD, Cyr M, Beaulieu JM, Torres GE, Grant SGN & Caron MG. (2004). Identification of PSD-95 as a regulator of dopamine-mediated synaptic and behavioral plasticity. *Neuron* **41,** 625-638.

Yasuda M, Fukuchi M, Tabuchi A, Kawahara M, Tsuneki H, Azuma Y, Chiba Y & Tsuda M. (2007). Robust stimulation of TrkB induces delayed increases in BDNF and Arc

mRNA expressions in cultured rat cortical neurons via distinct mechanisms. *Journal of Neurochemistry* **103,** 626-636.

Ying SW, Futter M, Rosenblum K, Webber MJ, Hunt SP, Bliss TVP & Bramham CR. (2002). Brain-derived neurotrophic factor induces long-term potentiation in intact adult hippocampus: Requirement for ERK activation coupled to CREB and upregulation of Arc synthesis. *Journal of Neuroscience* **22,** 1532-1540.

Yoshimura Y, Yamauchi Y, Shinkawa T, Taoka M, Donai H, Takahashi N, Isobe T & Yamauchi T. (2004). Molecular constituents of the postsynaptic density fraction revealed by proteomic analysis using multidimensional liquid chromatography-tandem mass spectrometry. *Journal of Neurochemistry* **88,** 759-768.

Zanos P, Moaddel R, Morris PJ, Georgiou P, Fischell J, Elmer GI, Alkondon M, Yuan PX, Pribut HJ, Singh NS, Dossou KSS, Fang YH, Huang XP, Mayo CL, Wainer IW, Albuquerque EX, Thompson SM, Thomas CJ, Zarate CA & Gould TD. (2016). NMDAR inhibition-independent antidepressant actions of ketamine metabolites. *Nature* **533,** 481-+.

Zanos P, Moaddel R, Morris PJ, Wainer IW, Albuquerque EX, Thompson SM, Thomas CJ, Zarate CA & Gould TD. (2017). Reply to: Antidepressant Actions of Ketamine Versus Hydroxynorketamine. *Biological Psychiatry* **81,** E69-E71.

Zarate CA, Singh JB, Carlson PJ, Brutsche NE, Ameli R, Luckenbaugh DA, Charney DS & Manji HK. (2006). A randomized trial of an N-methyl-D-aspartate antagonist in treatment-resistant major depression. *Archives of General Psychiatry* **63,** 856-864.

Zeilhofer HU, Swandulla D, Geisslinger G & Brune K. (1992). DIFFERENTIAL-EFFECTS OF KETAMINE ENANTIOMERS ON NMDA RECEPTOR CURRENTS IN CULTURED NEURONS. *European Journal of Pharmacology* **213,** 155-158.

Zhang GF, Wang N, Shi JY, Xu SX, Li XM, Ji MH, Zuo ZY, Zhou ZQ & Yang JJ. (2013). Inhibition of the L-arginine-nitric oxide pathway mediates the antidepressant effects of ketamine in rats in the forced swimming test. *Pharmacology Biochemistry and Behavior* **110,** 8-12.

Zhang YC, Behrens MM & Lisman JE. (2008). Prolonged exposure to NMDAR antagonist suppresses inhibitory synaptic transmission in prefrontal cortex. *Journal of Neurophysiology* **100,** 959-965.

Zhou L, Li F, Xu HB, Luo CX, Wu HY, Zhu MM, Lu W, Ji X, Zhou QG & Zhu DY. (2010). Treatment of cerebral ischemia by disrupting ischemia-induced interaction of nNOS with PSD-95. *Nature Medicine* **16,** 1439-U1123.

Zhou W, Wang N, Yang C, Li XM, Zhou ZQ & Yang JJ. (2014). Ketamine-induced antidepressant effects are associated with AMPA receptors-mediated upregulation of mTOR and BDNF in rat hippocampus and prefrontal cortex. *European Psychiatry* **29,** 419-423.

Zhu F, Cizeron M, Qiu Z, Benavides-Piccione R, Kopanitsa MV, Skene NG, Koniaris B, DeFelipe J, Fransen E, Komiyama NH & Grant SGN. (2018). Architecture of the Mouse Brain Synaptome. *Neuron* **99,** 781-+.

Zhu JJ, Qin Y, Zhao MM, Van Aelst L & Malinow R. (2002). Ras and Rap control AMPA receptor trafficking during synaptic plasticity. *Cell* **110,** 443-455.

Zorumski CF, Izumi Y & Mennerick S. (2016). Ketamine: NMDA Receptors and Beyond. *Journal of Neuroscience* **36,** 11158-11164.

Zukin RS & Bennett MVL. (1995). ALTERNATIVELY SPLICED ISOFORMS OF THE NMDARI RECEPTOR SUBUNIT. *Trends in Neurosciences* **18,** 306-313.

Appendices

<u>Appendix 1:</u> Comparison of male and female groups in open-field and FST behaviours, with and without ketamine administration

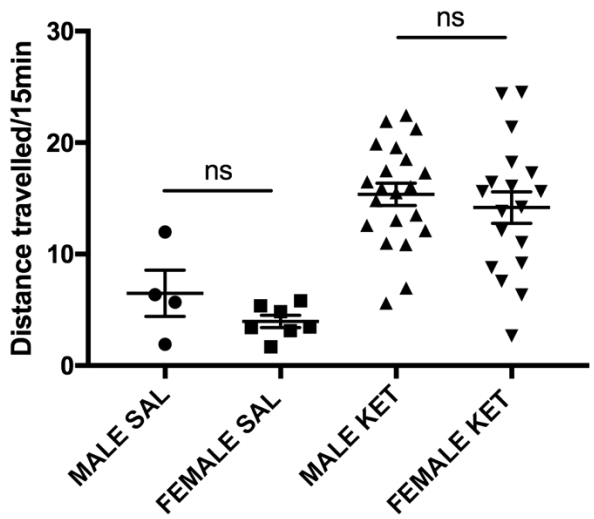

Appendix.figure 1 – No effect of gender on wild-type ketamine hyper-locomotive response. *Distance travelled by wild-type animals during ketamine response window. Pooled data from all experiments, with the exception of the pilot study which was all-male and is not included here. Data points = individual animals, error bars = SEM. One-way ANOVA, Sidak's multiple comparisons.*

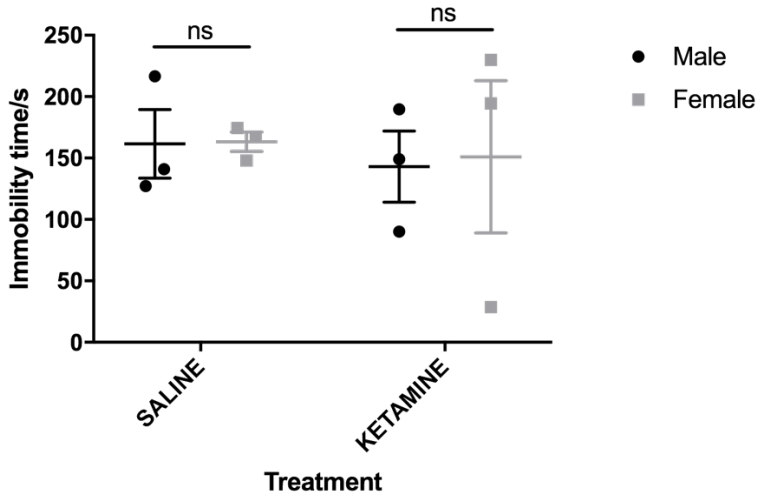

Appendix.figure 2 – No effect of gender on wild-type immobility time in FST*. Time spent immobile (s), total over whole 4 min scoring period, per mouse in both ketamine and saline treated groups. Data points = individual animals, error bars = SEM. One-way ANOVA, Sidak's multiple comparisons.*

Appendix 2: Total distance travelled during open-field habituation sessions

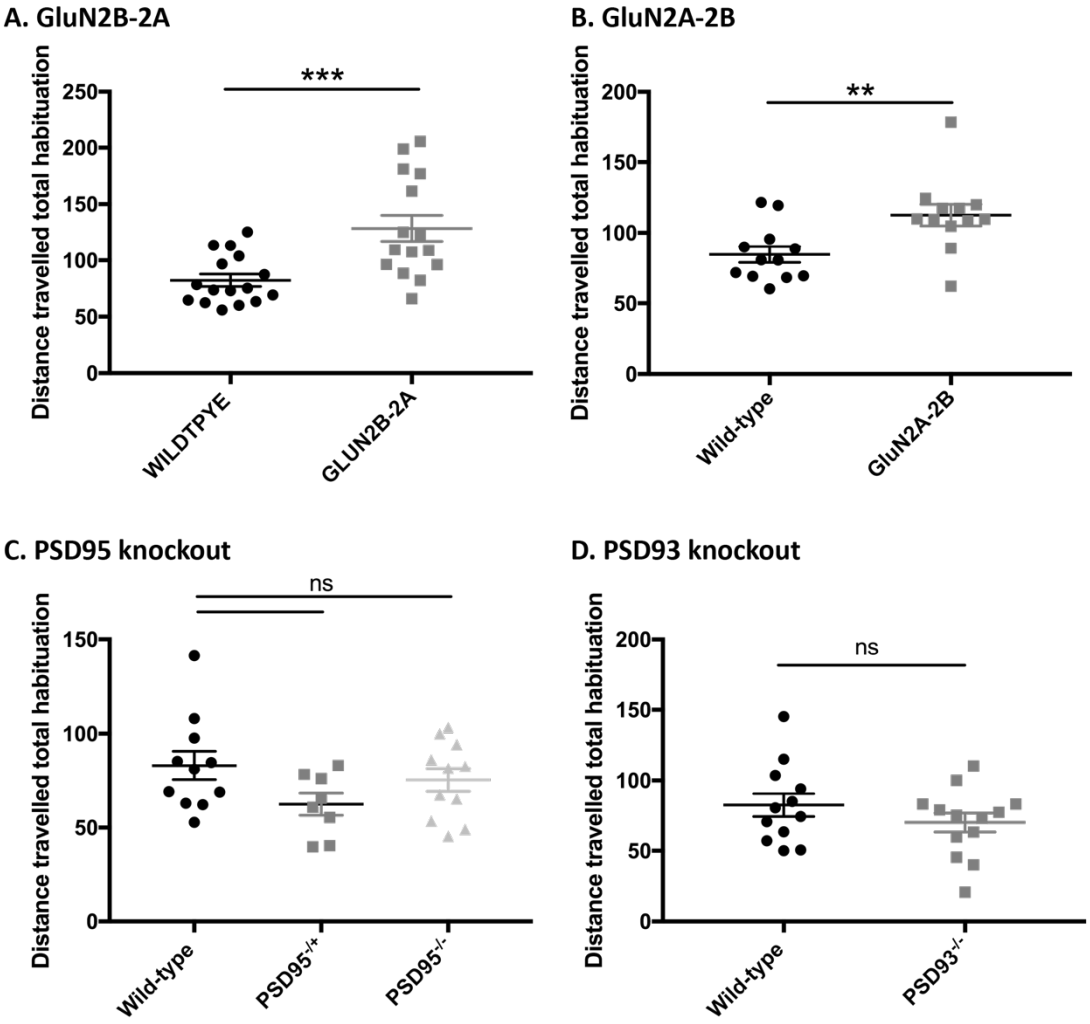

Appendix.figure 3 – Effect of genotype on baseline distance travelled during all habituation sessions. *Sum of distance travelled during all periods spent in open field prior to ketamine administration. This includes 2x 10 min habituation sessions on day 1 and 1x 15min habituation session on day 2. Each data point represents one mouse, line = mean, error bars = SEM. **= p<0.01, ***=p<0.001.*

<u>Appendix 3:</u> Test western blot images using antibodies for proteins previously altered as part of ketamine response.

BDNF	Akt	Erk
15 kDa	60 kDa	44, 42 kDa
Abcam: ab108319	CST: 9272	CST: 9102

p-Akt	p-Erk
60 kDa	44, 42 kDa
CST: 4060	CST: 4370

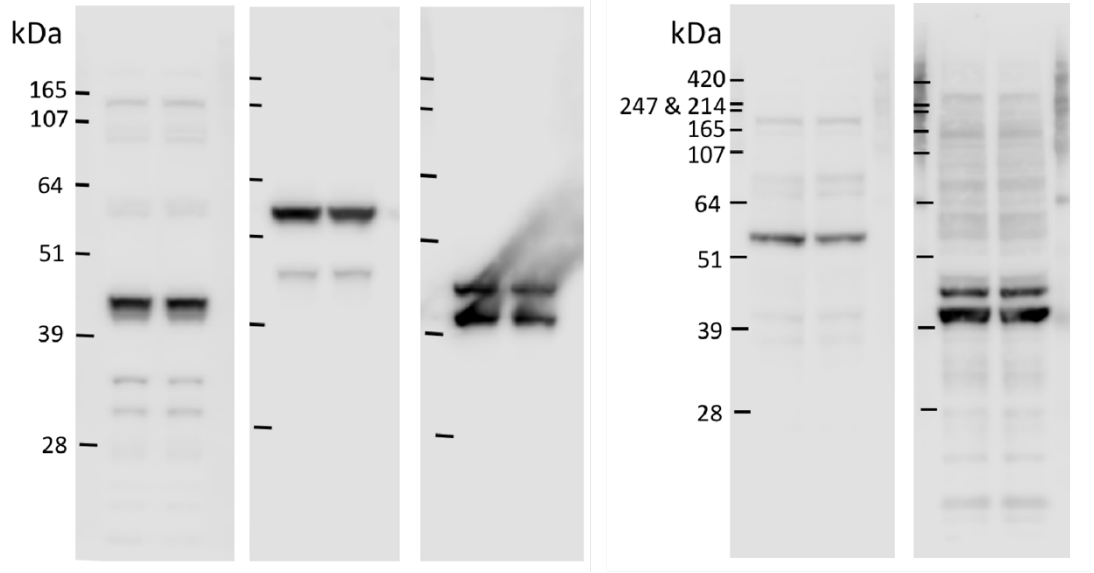

SynGAP	p-eEF2	eEF2
135 kDa	95 kDa	95 kDa
Millipore: 06-900	CST: 2332	CST: 2331

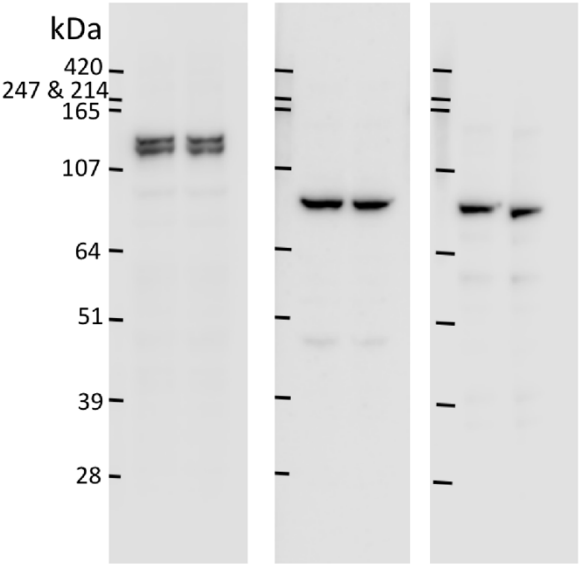

***Appendix.figure 4* - Extract from two wild-type mice used to test specificity of antibodies.** *Molecular weight ladder positions shown on left, table contains target protein, molecular weight of target protein, and manufacturer and catalogue number of antibody used.*

Appendix 4: Western blot images showing tagged and untagged forms of Arc in extract from wild-type controls, Arc^{VENUS}.

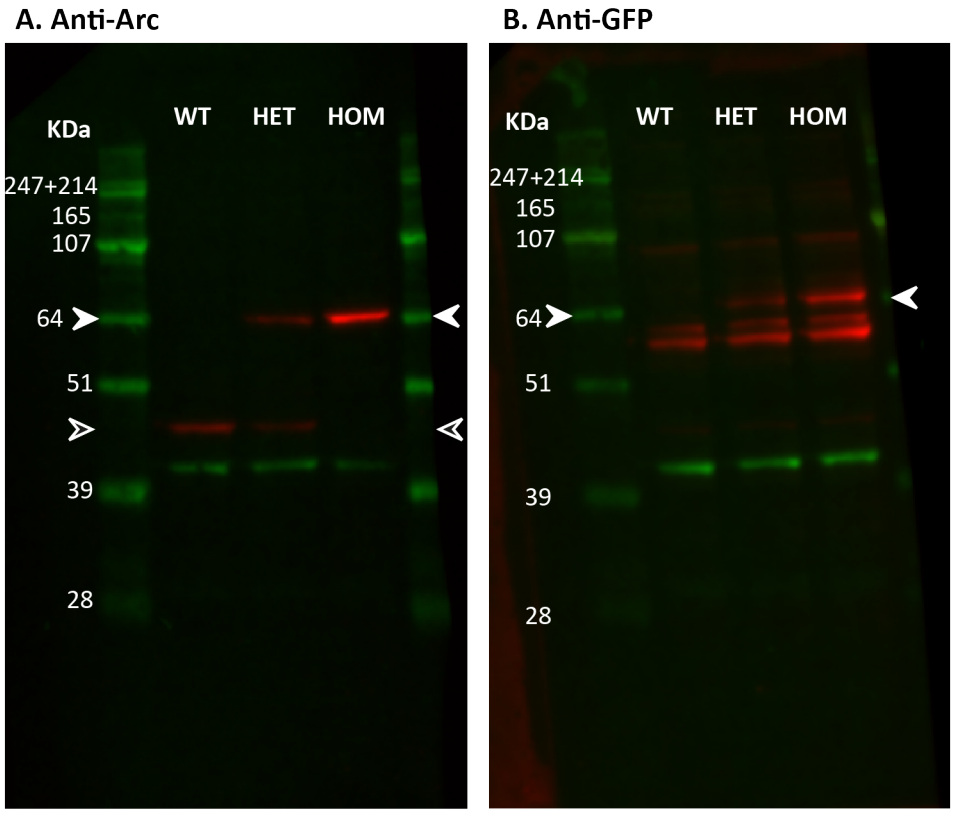

Appendix.figure 5 – Western blot showing tagged and un-tagged forms of Arc present in protein extract from animals wild-type (WT), heterozygous (HET) and homozygous for Arc^{VENUS} tag (HOM), probed with an anti-Arc antibody (A, Santa Cruz, SC-17869) and an anti-GFP antibody (B, Invitrogen, A-11122). A. *Red channel = anti-Arc, Green channel = β-Actin loading control and molecular weight ladder. Molecular weight of Arc is 45kDa, WT Arc band shown by open arrows in A, this band is strongest in the WT lane and not detectable in the Arc^{VENUS} HOM lane. Molecular weight of Venus (YFP) tag is approx. 27kDa, bringing the total tagged form of arc to a molecular weight of the tagged form of Arc to approx. 72kDa. A strong band in the Arc^{VNUES} HOM lane can been seen just above the 64kDa marker, this is likely to be the tagged form of Arc and has been highlighted with filled arrows in A.* ***B.*** *Red channel = Anti-GFP antibody, Green channel = β-Actin loading control and molecular weight ladder. Sequence of GFP and Venus considered sufficiently similar for anti-GFP primary to recognise Venus. Some non-specific bands can be observed. However, in Arc^{VENUS} HOM lane a bright band can be observed just above 64kDa marker, highlighted with filled arrows, which is where tagged form of Arc would be expected to be. A fainter band at the same molecular weight can be seen in the Arc^{VENUS}HET lane, and no band in the WT lane.*

Appendix 5: Control images from VGlut1 and DAPI IHC.

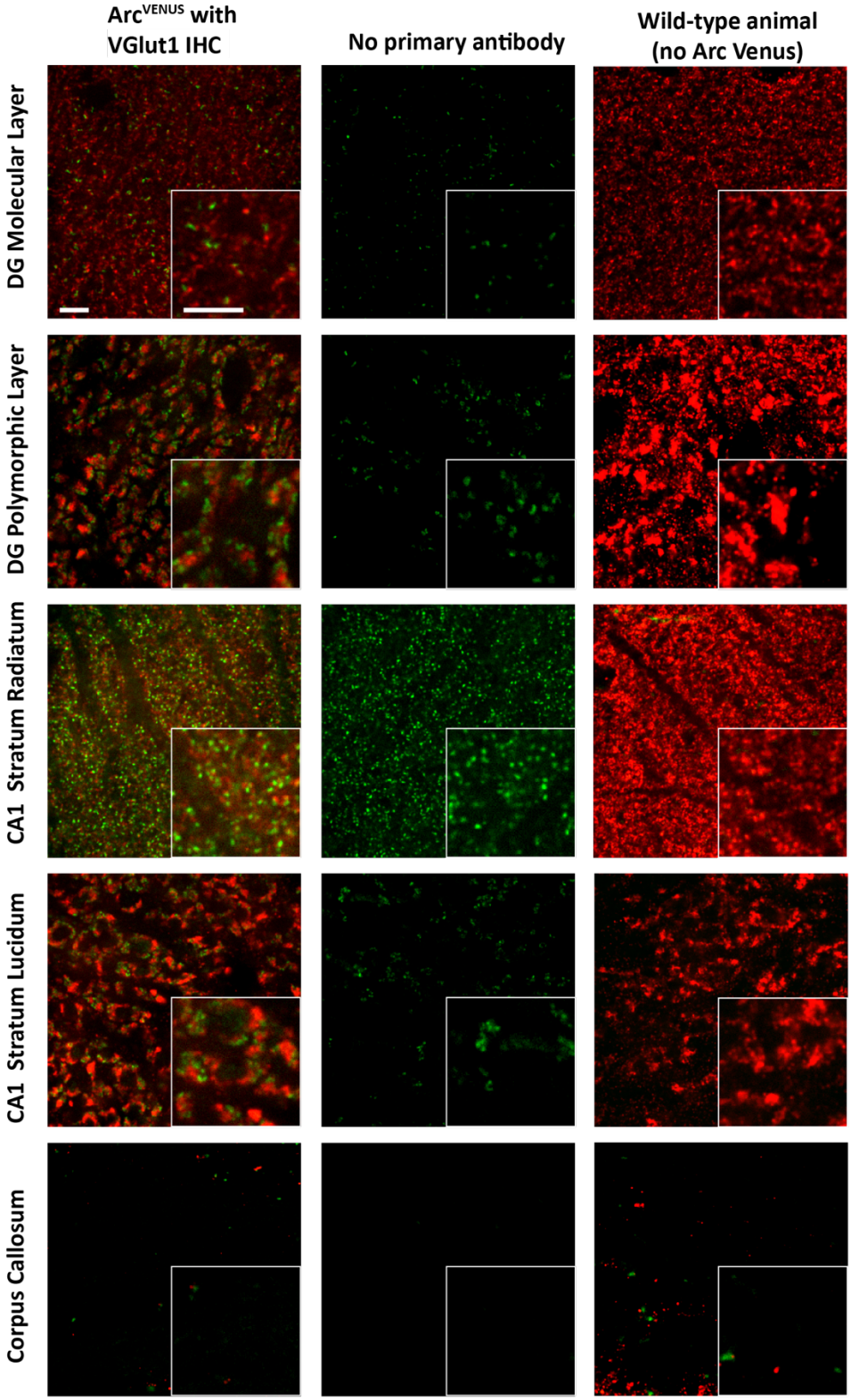

Appendix.Figure 6 – Control images from VGlut1 IHC and Arc^{VENUS} co-imaging. *Middle column shows control in which VGlut1 primary antibody was not applied but all other conditions remained the same. Right column shows the result of VGlut1 IHC staining on a mouse brain not containing the Arc^{VENUS} tag.*

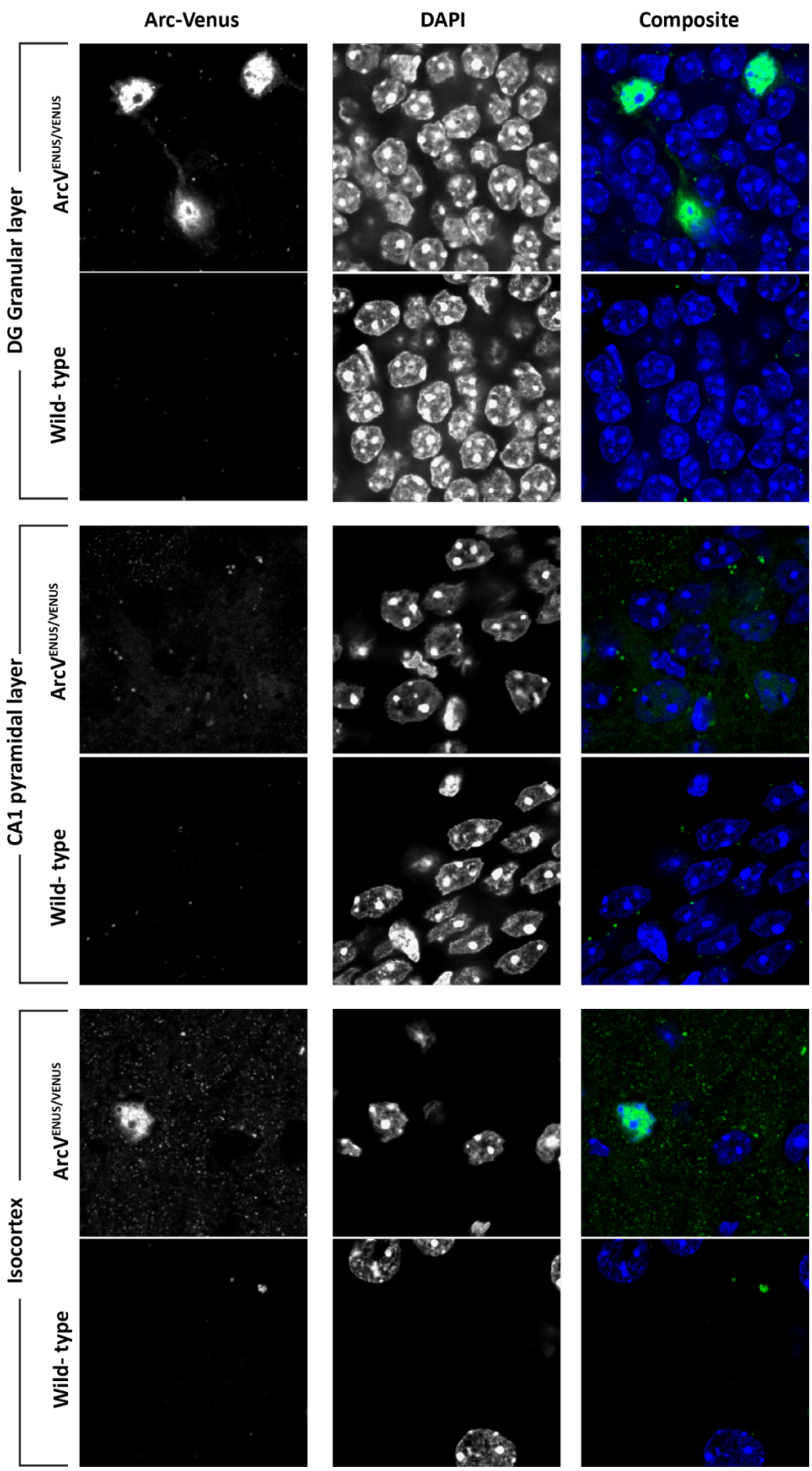
Arc-Venus
DAPI
Composite
DG Granular layer
CA1 pyramidal layer
Isocortex
Wild- type
ArcV^VENUS/VENUS

Appendix.figure 7 (previous page) – Control images from DAPI and Arc^{VENUS} co-imaging. *For each brain region imaged: top row = mouse homozygous for Arc^{VENUS} tag, bottom row = wild-type mouse in which no Arc^{VENUS} tag is present.*

Appendix 6: Example metadata from VGlut1 and Arc^{VENUS} co-imaging

Name : 2017_11_10_GGV430_CA1_SR_1 10/11/2017 15:24:30

Type : 16 bit grey/pseudo
Intensity : 1.000000 lux
x : 512 * 0.084034 : um
y : 512 * 0.084000 : um
Wavelength : 2

[Environment]
User=CJQW102
Configuration=Sarah new
Version=Andor iQ 3.5
[Environment End]
[Created]
Date=10/11/2017
Time=13:45:14
[Created End]
[Protocol Description]
Protocol - Sarah venus
6D View Compatible - No
Image - 2017_11_10_GGV430_CA1_SR_1
Camera Binning - Use Current
Wait Allocation - Off
Camera Selection - Use Current
Events
Keyboard Events - On
Default name - Spacebar
Triggered Events - Off
Repeat T - 1 time (0 ms - fastest)
Repeat - Channel (515,561)
Channel Description
Channel - 515
Camera EM Gain - 250
Camera Binning X - CURRENT
Camera Binning Y - CURRENT
Camera Exposure Time (s) - 0.12
Camera Exposure Units - 1
DSD Imaging Mode - 3
LUT - Green
Map Min - 621
Map Max - 7195
Trigger - Pre : X,X,X,X,X,X,X,X, :: Post : X,X,X,X,X,X,X,X,
AMH Filter Wheel - Current
AMH Intensity - Current
AMH Shutter - Current
IXBX AFMirror - Current
IXBX Analyzer - Current
IXBX Condenser - 0
IXBX DIC - Current
IXBX Fluo Filter 1 - 6
IXBX Fluo Filter 2 - Current
IXBX Fluo Filter 3 - Current
IXBX Fluo Shutter 1 - Current
IXBX Polarizer - Current
IXBX Port - 1
IXBX Trans Filter 1 - Current
IXBX Trans Shutter 1 - Current
LVPZT - DELTA_Z 0
ROTR Shutter 1 - Current
ROTR Shutter 2 - Current
ROTR Wheel 1 - 4
ROTR Wheel 2 - Current
ROTR Wheel 3 - Current

CSU Aperture - Current
CSU Camera Port - Current
CSU Lens 1 - Current
CSU Lens 2 - Current
CSU NIR Shutter - Current
CSU PB Mirror - Current
CSU PB Shutter - Current
CSU Port - Current
CSU Shutter - Open
Dichroic - 1
Emmision - 1
Excitation - 1
NDFilter - Current
AOTF Channel 1 Intensity - -1
AOTF Channel 2 Intensity - -1
AOTF Channel 3 Intensity - 40
AOTF Channel 4 Intensity - -1
AOTF Channel 5 Intensity - -1
AOTF Channel 6 Intensity - Current
AOTF Laser 1 Enabled - 0
AOTF Laser 1 External Control - Current
AOTF Laser 2 Enabled - 0
AOTF Laser 2 External Control - Current
AOTF Laser 3 Enabled - 1
AOTF Laser 3 External Control - Current
AOTF Laser 4 Enabled - 1
AOTF Laser 4 External Control - Current
AOTF Laser 5 Enabled - 0
AOTF Laser 5 External Control - Current
AOTF Laser 6 Enabled - 0
AOTF Laser 6 External Control - Current
AOTF MPD - 0
AOTF Position - 515
AOTF Shutter - Open
Channel - 561
Camera EM Gain - 250
Camera Binning X - CURRENT
Camera Binning Y - CURRENT
Camera Exposure Time (s) - 0.055
Camera Exposure Units - 1
DSD Imaging Mode - 3
LUT - Red
Map Min - 1178
Map Max - 4858
Trigger - Pre : X,X,X,X,X,X,X,X, :: Post : X,X,X,X,X,X,X,X,
AMH Filter Wheel - Current
AMH Intensity - Current
AMH Shutter - Current
IXBX AFMirror - Current
IXBX Analyzer - Current
IXBX Condenser - 0
IXBX DIC - Current
IXBX Fluo Filter 1 - 6
IXBX Fluo Filter 2 - Current
IXBX Fluo Filter 3 - Current
IXBX Fluo Shutter 1 - Current
IXBX Polarizer - Current
IXBX Port - 1
IXBX Trans Filter 1 - Current
IXBX Trans Shutter 1 - Current
LVPZT - DELTA_Z 0
ROTR Shutter 1 - Current
ROTR Shutter 2 - Current
ROTR Wheel 1 - 73
ROTR Wheel 2 - Current
ROTR Wheel 3 - Current
CSU Aperture - Current
CSU Camera Port - Current
CSU Lens 1 - Current
CSU Lens 2 - Current
CSU NIR Shutter - Current
CSU PB Mirror - Current
CSU PB Shutter - Current

CSU Port - Current
CSU Shutter - Open
Dichroic - 1
Emmision - 1
Excitation - 1
NDFilter - Current
AOTF Channel 1 Intensity - -1
AOTF Channel 2 Intensity - -1
AOTF Channel 3 Intensity - -1
AOTF Channel 4 Intensity - 40
AOTF Channel 5 Intensity - -1
AOTF Channel 6 Intensity - Current
AOTF Laser 1 Enabled - 0
AOTF Laser 1 External Control - Current
AOTF Laser 2 Enabled - 0
AOTF Laser 2 External Control - Current
AOTF Laser 3 Enabled - 1
AOTF Laser 3 External Control - Current
AOTF Laser 4 Enabled - 1
AOTF Laser 4 External Control - Current
AOTF Laser 5 Enabled - 0
AOTF Laser 5 External Control - Current
AOTF Laser 6 Enabled - 0
AOTF Laser 6 External Control - Current
AOTF MPD - 0
AOTF Position - 561
AOTF Shutter - Open

Snap - Frame

End - Channel

End - T

[Protocol Description End]
[Grab Parameters]
Camera=iXon Ultra
Window Left=0
Window Top=0
Window Right=511
Window Bottom=511
Window Width=512
Window Height=512
BinningX=1
BinningY=1
Image Width=512
Image Height=512
Exposure=120.0 ms
Rotation=0
FlipV=0
FlipH=0
TimeStamps=Hardware
[Grab Parameters End]
[Tab Device Info]
Camera=DU897_BV 8655
ControllerCard=USB
DriverVersion=2.100.33050.0
CofVersion=0
VxDVersion=0.0
SoftwareTrigger=Supported
BitDepth=16
FPGA_Version=205.205
Ocx_Version=5.4.15.10
Ocx_Time=20:32:52 Jun 14 2016
Ocx_File=C:\PROGRA~2\ANDORB~1\COMMON~1\KIDAND~1.OCX

[Tab Device Info End]
[Tab Exposure]
Window=512 : 512
Shutter=Open
Binning=1 x 1
Temperature - Actual =-70
Display Control - Fastest=Checked
Display Control - Display Rate=1
Gains - Pre-Amp-Gain=Gain 3
EM Gain - Enabled=Checked

Gains - EMGain=250
Exposure Time - Frame Transfer=Unchecked
Exposure Time - unit=ms
Exposure Time - exposure value=120.0
Exposure Time - Readout in ms=19.371
Experiment Control - FLZ=Unchecked
Experiment Control - Trig Mode=Free Run
Use Frame averaging=Checked
Frames to be averaged=2
Fastest Grab=Unchecked
Available memory=4095
[Tab Exposure End]
[Tab Temperature/Shutter]
Temperature Setting=-70
Actual Temperature=-70
Cooling=Steady
Fan=Full
TTL High Open=Checked
Shutter Open Transfer Time=60
Shutter Close Transfer Time=80
[Tab Temperature/Shutter End]
[Tab Speed/Amplifer]
Horizontal Readout=17.000
Vertical Readout time=[1.700]
ADC Channel=0
Vertical Clock Voltage=Normal
Output Amplifier=EM Port
Baseline Clamp=Checked
[Tab Speed/Amplifer End]
[Tab Image Orientation]
Flip=None
Rotation in Degrees=None
[Tab Image Orientation End]
[Image Info]
Window Left=0
Window Top=0
Window Right=511
Window Bottom=511
Window Width=512
Window Height=512
Window BinningX=1
Window BinningY=1
[Image Info End]
[First Frame]
SavedTime=10/11/2017 13:45:22.921
[First Frame End]

<u>Appendix 7:</u> Example metadata from DAPI and Arc^{VENUS} co-imaging

Name : 2017_11_10_GGV440_CA3_SLU_11 10/11/2017 12:44:56

Type : 16 bit grey/pseudo
Intensity : 1.000000 lux
x : 512 * 0.084034 : um
y : 512 * 0.084000 : um
Wavelength : 2

[Environment]
User=CJQW102
Configuration=Sarah new
Version=Andor iQ 3.5
[Environment End]
[Created]
Date=10/11/2017
Time=11:19:13
[Created End]
[Protocol Description]
Protocol - Sarah venus
6D View Compatible - No
Image - 2017_11_10_GGV440_CA3_SLU_1
Camera Binning - Use Current

Wait Allocation - Off
Camera Selection - Use Current
Events
Keyboard Events - On
Default name - Spacebar
Triggered Events - Off
Repeat T - 1 time (0 ms - fastest)
Repeat - Channel (515,561)
Channel Description
Channel - 515
Camera EM Gain - 250
Camera Binning X - CURRENT
Camera Binning Y - CURRENT
Camera Exposure Time (s) - 0.12
Camera Exposure Units - 1
DSD Imaging Mode - 3
LUT - Green
Map Min - 621
Map Max - 7195
Trigger - Pre : X,X,X,X,X,X,X,X, :: Post : X,X,X,X,X,X,X,X,
AMH Filter Wheel - Current
AMH Intensity - Current
AMH Shutter - Current
IXBX AFMirror - Current
IXBX Analyzer - Current
IXBX Condenser - 0
IXBX DIC - Current
IXBX Fluo Filter 1 - 6
IXBX Fluo Filter 2 - Current
IXBX Fluo Filter 3 - Current
IXBX Fluo Shutter 1 - Current
IXBX Polarizer - Current
IXBX Port - 1
IXBX Trans Filter 1 - Current
IXBX Trans Shutter 1 - Current
LVPZT - DELTA_Z 0
ROTR Shutter 1 - Current
ROTR Shutter 2 - Current
ROTR Wheel 1 - 4
ROTR Wheel 2 - Current
ROTR Wheel 3 - Current
CSU Aperture - Current
CSU Camera Port - Current
CSU Lens 1 - Current
CSU Lens 2 - Current
CSU NIR Shutter - Current
CSU PB Mirror - Current
CSU PB Shutter - Current
CSU Port - Current
CSU Shutter - Open
Dichroic - 1
Emmision - 1
Excitation - 1
NDFilter - Current
AOTF Channel 1 Intensity - -1
AOTF Channel 2 Intensity - -1
AOTF Channel 3 Intensity - 40
AOTF Channel 4 Intensity - -1
AOTF Channel 5 Intensity - -1
AOTF Channel 6 Intensity - Current
AOTF Laser 1 Enabled - 0
AOTF Laser 1 External Control - Current
AOTF Laser 2 Enabled - 0
AOTF Laser 2 External Control - Current
AOTF Laser 3 Enabled - 1
AOTF Laser 3 External Control - Current
AOTF Laser 4 Enabled - 1
AOTF Laser 4 External Control - Current
AOTF Laser 5 Enabled - 0
AOTF Laser 5 External Control - Current
AOTF Laser 6 Enabled - 0
AOTF Laser 6 External Control - Current
AOTF MPD - 0

AOTF Position - 515
AOTF Shutter - Open
Channel - 561
Camera EM Gain - 250
Camera Binning X - CURRENT
Camera Binning Y - CURRENT
Camera Exposure Time (s) - 0.055
Camera Exposure Units - 1
DSD Imaging Mode - 3
LUT - Red
Map Min - 1178
Map Max - 4858
Trigger - Pre : X,X,X,X,X,X,X,X, :: Post : X,X,X,X,X,X,X,X,
AMH Filter Wheel - Current
AMH Intensity - Current
AMH Shutter - Current
IXBX AFMirror - Current
IXBX Analyzer - Current
IXBX Condenser - 0
IXBX DIC - Current
IXBX Fluo Filter 1 - 6
IXBX Fluo Filter 2 - Current
IXBX Fluo Filter 3 - Current
IXBX Fluo Shutter 1 - Current
IXBX Polarizer - Current
IXBX Port - 1
IXBX Trans Filter 1 - Current
IXBX Trans Shutter 1 - Current
LVPZT - DELTA_Z 0
ROTR Shutter 1 - Current
ROTR Shutter 2 - Current
ROTR Wheel 1 - 73
ROTR Wheel 2 - Current
ROTR Wheel 3 - Current
CSU Aperture - Current
CSU Camera Port - Current
CSU Lens 1 - Current
CSU Lens 2 - Current
CSU NIR Shutter - Current
CSU PB Mirror - Current
CSU PB Shutter - Current
CSU Port - Current
CSU Shutter - Open
Dichroic - 1
Emmision - 1
Excitation - 1
NDFilter - Current
AOTF Channel 1 Intensity - -1
AOTF Channel 2 Intensity - -1
AOTF Channel 3 Intensity - -1
AOTF Channel 4 Intensity - 40
AOTF Channel 5 Intensity - -1
AOTF Channel 6 Intensity - Current
AOTF Laser 1 Enabled - 0
AOTF Laser 1 External Control - Current
AOTF Laser 2 Enabled - 0
AOTF Laser 2 External Control - Current
AOTF Laser 3 Enabled - 1
AOTF Laser 3 External Control - Current
AOTF Laser 4 Enabled - 1
AOTF Laser 4 External Control - Current
AOTF Laser 5 Enabled - 0
AOTF Laser 5 External Control - Current
AOTF Laser 6 Enabled - 0
AOTF Laser 6 External Control - Current
AOTF MPD - 0
AOTF Position - 561
AOTF Shutter - Open
Snap - Frame
End - Channel
End - T

[Protocol Description End]

[Grab Parameters]
Camera=iXon Ultra
Window Left=0
Window Top=0
Window Right=511
Window Bottom=511
Window Width=512
Window Height=512
BinningX=1
BinningY=1
Image Width=512
Image Height=512
Exposure=120.0 ms
Rotation=0
FlipV=0
FlipH=0
TimeStamps=Hardware
[Grab Parameters End]
[Tab Device Info]
Camera=DU897_BV 8655
ControllerCard=USB
DriverVersion=2.100.33050.0
CofVersion=0
VxDVersion=0.0
SoftwareTrigger=Supported
BitDepth=16
FPGA_Version=205.205
Ocx_Version=5.4.15.10
Ocx_Time=20:32:52 Jun 14 2016
Ocx_File=C:\PROGRA~2\ANDORB~1\COMMON~1\KIDAND~1.OCX

[Tab Device Info End]
[Tab Exposure]
Window=512 : 512
Shutter=Open
Binning=1 x 1
Temperature - Actual =-70
Display Control - Fastest=Checked
Display Control - Display Rate=1
Gains - Pre-Amp-Gain=Gain 3
EM Gain - Enabled=Checked
Gains - EMGain=250
Exposure Time - Frame Transfer=Unchecked
Exposure Time - unit=ms
Exposure Time - exposure value=120.0
Exposure Time - Readout in ms=19.371
Experiment Control - FLZ=Unchecked
Experiment Control - Trig Mode=Free Run
Use Frame averaging=Checked
Frames to be averaged=2
Fastest Grab=Unchecked
Available memory=4095
[Tab Exposure End]
[Tab Temperature/Shutter]
Temperature Setting=-70
Actual Temperature=-70
Cooling=Steady
Fan=Full
TTL High Open=Checked
Shutter Open Transfer Time=60
Shutter Close Transfer Time=80
[Tab Temperature/Shutter End]
[Tab Speed/Amplifer]
Horizontal Readout=17.000
Vertical Readout time=[1.700]
ADC Channel=0
Vertical Clock Voltage=Normal
Output Amplifier=EM Port
Baseline Clamp=Checked
[Tab Speed/Amplifer End]
[Tab Image Orientation]
Flip=None
Rotation in Degrees=None

[Tab Image Orientation End]
[Image Info]
Window Left=0
Window Top=0
Window Right=511
Window Bottom=511
Window Width=512
Window Height=512
Window BinningX=1
Window BinningY=1
[Image Info End]
[First Frame]
SavedTime=10/11/2017 11:19:36.609
[First Frame End]

Appendix 8: Abbreviations of brain regions included in synaptome mapping analyses.

ACAd	Anterior cingulate area
aco	Anterior commissure, olfactory limb
Ald	Agranular insular area, dorsal part
alv	*Alveus*
Alv	Agranular insular area, ventral part
AONm	Anterior olfactory nucleus, medial part
AONpv	Anterior olfactory nucleus, posteroventral part
AUDd	*Dorsal auditory area*
AUDp	*Primary auditory area*
AUDv	*Ventral auditory area*
BLAa	*Basolateral amygdala nucleus, anterior part*
BLAp	*Basolateral amygdala nucleus, posterior part*
BLAv	*Basolateral amygdala nucleus, ventral part*
BMAp	*Basomedial amygdalar nucleus, posterior part*
CA1_slm	*CA1 field, stratum lacunosum moleculare*
CA1_so	*CA1 field, stratum oriens*
CA1_sp	*CA1 field, pyramidal layer*
CA1_sr	*CA1 field, stratum radiatum*
CA2_slm	*CA2 field, stratum lacunosum moleculare*
CA2_so	*CA2 field, stratum oriens*
CA2_sp	*CA2 field, pyramidal layer*
CA2_sr	*CA2 field, stratum radiatum*
CA3_s	*CA3 field, stratum radiatum*
CA3_slm	*CA3 field, stratum lacunosum moleculare*
CA3_slu	*CA3 field, stratum lucidum*
CA3_so	*CA3 field, stratum oriens*
CA3_sp	*CA3 field, pyramidal layer*
cc	*Corpus callosum*
CEA	*Central amydalar nucleus*
cing	*Cingulum bundle*
COApl1	*Cortical amygdalar area, posterior part, lateral zone, layer 1*
COApl2	*Cortical amygdalar area, posterior part, lateral zone, layer 2*
COApl3	*Cortical amygdalar area, posterior part, lateral zone, layer 3*
CP	*Caudoputamen*
cpd	*Cerebral peduncle*
df	*Dorsal fornix*
DG_mo_inf	*Dentate gyrus, molecular layer, inferior part*
DG_mo_sup	*Dentate gyrus, molecular layer, superior part*
DG_po	*Dentate gyrus, polymorphic layer*
DG_sg_inf	*Dentate gyrus, granule cell layer, inferior part*
DG_sg_sup	*Dentate gyrus, granule cell layer, superior part*
DP	Dorsal peduncular area
ECT	*Ectorhinal area*
ENTl	*Entorhinal area, lateral part*
EP	*Endopiriform nucleus*
EPd	Endopiriform nucleus, dorsal part
FC	*Fasciola cinerea*
fi	*Fimbria*
Gpe	*Globus pallidus, external segment*
Hypothalamus	*Hypothalamus*
ILA	Infralimbic area
int	*Internal capsule*
LA	*Lateral amygdalar nucleus*
LH	*Lateral habenula*

lot	Lateral olfactory tract, body
MEA	*Medial amygdalar nucleus*
MH	*Medial habenula*
Mop	*Primary motor area*
MOp	Primary motor area
Mos	*Secondary motor area*
MOs	Secondary motor area
opt	*Optic tract*
ORBl	Orbital area, lateral part
ORBm	Orbital area, medial part
ORBvl	Orbital area, ventrolateral part
PAA1	*Piriform-amygdalar area, molecular layer*
PAA2	*Piriform-amygdalar area, pyramidal layer*
PAA3	*Piriform-amygdalar area, polymorph layer*
PERI	*Perirhinal area*
PIR1	*Piriform area, molecular layer*
PIR2	*Piriform area, pyramidal area*
PIR3	*Piriform area, polymorph layer*
PL	Prelimbic area
RSPd	*Retrosplenial area, dorsal part*
RSPv	*Retrosplenial area, ventral part*
SEZ	Subependymal zone
SSp	*Primary somatosensory area*
SSp-bfd	*Primary somatosensory area, barrel field*
SSp-tr	*Primary somatosensory area, trunk*
st	*Stria terminalis*
STN	*Subthalamic nucleus*
Tea	*Temporal association areas*
Thalamus	*Thalamus*
TTd1	Taemia tecta, dorsal part, layer 1
TTd2	Taemia tecta, dorsal part, layer 2
TTd3	Taemia tecta, dorsal part, layer 3
TTv1	Taemia tecta, ventral part, layer 1
TTv2	Taemia tecta, ventral part, layer 2
TTv3	Taemia tecta, ventral part, layer 3

Appendix 9: Example metadata from Arc baseline synaptome mapping.

Name : GGV430_sHC_BASALMAP_28.08.17 29/08/2017 13:04:42

Type : 16 bit grey/pseudo
Intensity : 1.000000 lux
x : 512 * 0.084034 : um
y : 512 * 0.084000 : um
Montage : 33673

[Environment]
User=CJQW102
Configuration=Sarah new
Version=Andor iQ 3.5
[Environment End]
[Created]
Date=28/08/2017
Time=16:45:13
[Created End]
[Protocol Description]
Protocol - Sarah venus
6D View Compatible - No
Image - GGV430_sHC_BASALMAP_28.08.17
Camera Binning - Use Current
Wait Allocation - Off
Camera Selection - Use Current
Scan - Sarah montage
Montage Acquisition
Events
Keyboard Events - On
Default name - Spacebar
Triggered Events - Off
Repeat T - 1 time (0 ms - fastest)
Repeat - Montage

Montage Positions - (33673 (223 by 151))
Repeat - Channel (515)
Channel Description
Channel - 515
Camera EM Gain - 250
Camera Binning X - CURRENT
Camera Binning Y - CURRENT
Camera Exposure Time (s) - 0.12
Camera Exposure Units - 1
DSD Imaging Mode - 3
LUT - Green
Map Min - 621
Map Max - 7195
Trigger - Pre : X,X,X,X,X,X,X,X, :: Post :
X,X,X,X,X,X,X,X,
AMH Filter Wheel - Current
AMH Intensity - Current
AMH Shutter - Current
IXBX AFMirror - Current
IXBX Analyzer - Current
IXBX Condenser - 0
IXBX DIC - Current
IXBX Fluo Filter 1 - 6
IXBX Fluo Filter 2 - Current
IXBX Fluo Filter 3 - Current
IXBX Fluo Shutter 1 - Current
IXBX Polarizer - Current
IXBX Port - 1
IXBX Trans Filter 1 - Current
IXBX Trans Shutter 1 - Current
LVPZT - DELTA_Z 0
ROTR Shutter 1 - Current
ROTR Shutter 2 - Current
ROTR Wheel 1 - 4
ROTR Wheel 2 - Current
ROTR Wheel 3 - Current
CSU Aperture - Current
CSU Camera Port - Current
CSU Lens 1 - Current
CSU Lens 2 - Current
CSU NIR Shutter - Current
CSU PB Mirror - Current
CSU PB Shutter - Current
CSU Port - Current
CSU Shutter - Open
Dichroic - 1
Emmision - 1
Excitation - 1
NDFilter - Current
AOTF Channel 1 Intensity - -1
AOTF Channel 2 Intensity - -1
AOTF Channel 3 Intensity - 40
AOTF Channel 4 Intensity - -1
AOTF Channel 5 Intensity - -1
AOTF Channel 6 Intensity - Current
AOTF Laser 1 Enabled - 0
AOTF Laser 1 External Control - Current
AOTF Laser 2 Enabled - 0
AOTF Laser 2 External Control - Current
AOTF Laser 3 Enabled - 1
AOTF Laser 3 External Control - Current
AOTF Laser 4 Enabled - 1
AOTF Laser 4 External Control - Current
AOTF Laser 5 Enabled - 0
AOTF Laser 5 External Control - Current
AOTF Laser 6 Enabled - 0
AOTF Laser 6 External Control - Current
AOTF MPD - 0
AOTF Position - 515
AOTF Shutter - Open
Snap - Frame
End - Channel
End - Montage

End - T

[Protocol Description End]
[XYZScan]
ScanName=Sarah montage
FileVersion=2
Centre=False
Channel=
WellPattern=
Density=0
Calibration=
XYFields=1 62435,45144,6822.8775408587
ZScan=
Montage=Edge Overlap 0
Plates=
MontageOffsets=33673 -4417.79831932773,-6393.1
…
[Region Info (Fields) End]
[Grab Parameters]
Camera=iXon Ultra
Window Left=0
Window Top=0
Window Right=511
Window Bottom=511
Window Width=512
Window Height=512
BinningX=1
BinningY=1
Image Width=512
Image Height=512
Exposure=120.0 ms
Rotation=0
FlipV=1
FlipH=0
TimeStamps=Hardware
[Grab Parameters End]
[Tab Device Info]
Camera=DU897_BV 8655
ControllerCard=USB
DriverVersion=2.100.33050.0
CofVersion=0
VxDVersion=0.0
SoftwareTrigger=Supported
BitDepth=16
FPGA_Version=205.205
Ocx_Version=5.4.15.10
Ocx_Time=20:32:52 Jun 14 2016
Ocx_File=C:\PROGRA~2\ANDORB~1\COMMON~1\KIDAND~1.OCX

[Tab Device Info End]
[Tab Exposure]
Window=512 : 512
Shutter=Open
Binning=1 x 1
Temperature - Actual =-70
Display Control - Fastest=Checked
Display Control - Display Rate=10
Gains - Pre-Amp-Gain=Gain 3
EM Gain - Enabled=Checked
Gains - EMGain=250
Exposure Time - Frame Transfer=Unchecked
Exposure Time - unit=ms
Exposure Time - exposure value=120.0
Exposure Time - Readout in ms=19.371
Experiment Control - FLZ=Unchecked
Experiment Control - Trig Mode=Free Run
Use Frame averaging=Checked
Frames to be averaged=2
Fastest Grab=Unchecked
Available memory=4095
[Tab Exposure End]
[Tab Temperature/Shutter]
Temperature Setting=-70

```
Actual Temperature=-70
Cooling=Steady
Fan=Full
TTL High Open=Checked
Shutter Open Transfer Time=60
Shutter Close Transfer Time=80
[Tab Temperature/Shutter End]
[Tab Speed/Amplifer]
Horizontal Readout=17.000
Vertical Readout time=[1.700]
ADC Channel=0
Vertical Clock Voltage=Normal
Output Amplifier=EM Port
Baseline Clamp=Checked
[Tab Speed/Amplifer End]
[Tab Image Orientation]
Flip=Vertical
Rotation in Degrees=None
[Tab Image Orientation End]
[Image Info]
Window Left=0
Window Top=0
Window Right=511
Window Bottom=511
Window Width=512
Window Height=512
Window BinningX=1
Window BinningY=1
[Image Info End]
[First Frame]
SavedTime=28/08/2017 16:45:17.711
[First Frame End]
```

Appendix 10: Stitching code used to generate montages for delineation as part of synaptome mapping pipeline.

```
function stitching_Melissa
root_dir = 'Z:\microscopy\2016-11_GGV_Behaviour_Mapping\';
out_dir = 'Z:\users\Sarah\PhD\Arc behaviour mapping\Stitched\';
Mouse_id = {'GGV430'};
Section_id = {'sHC9'};
d = dir(root_dir);
isub = [d(:).isdir]; %# returns logical vector
name_Folds = {d(isub).name}';
name_Folds(ismember(name_Folds,{'.','..'})) = [];
down_sampling_factor = 16;
split_char ='\';% for windows
%% divide the folder name
Mouse_list = cell(length(name_Folds)-2,1);
Section_list = cell(length(name_Folds)-2,1);
parfor i = 1:length(name_Folds)
   temp_folder_name_split = strsplit(name_Folds{i},'_');
   Mouse_list(i) = temp_folder_name_split(1);
   Section_list(i) = temp_folder_name_split(2);
end
%% select the mouse in the Mouse_id and Section_id.

n = 1;
for i = 1:length(Mouse_id)
   for j = 1:length(Section_id)
      temp_mouse_index = intersect(strmatch(Mouse_id{i},Mouse_list),strmatch(Section_id{j},Section_list));
      if ~isempty(temp_mouse_index)
         select_mouse_path{n} = [root_dir,name_Folds{temp_mouse_index(end)}];
         n = n +1;
      end
   end
end
if size(select_mouse_path,1) == 1
   select_mouse_path = select_mouse_path';
end
```

```
%% Then reorder the imported data based on the digitsfor i = 1:length(dir1)
row_num = zeros(length(select_mouse_path),1);
col_num = zeros(length(select_mouse_path),1);
for i = 1:length(select_mouse_path)
   disp(select_mouse_path{i});
   %% first get the number of rows and columns from the meta_data
   dir_meta = dir([select_mouse_path{i},split_char,'*.txt']);
   if ~isempty(dir_meta)
      fid = fopen([select_mouse_path{i},split_char,dir_meta(1).name]);
      montage_meta = textscan(fid,'%s',10 ,'headerlines', 33);%% according to the format of metadata --- CHANGE IF MONTAGE ROW
COLUMNS ARE AT DIFFERENT LINE
      col_num(i) = str2num(montage_meta{1}{6});
      row_num(i) = str2num(montage_meta{1}{8});
      fclose(fid);
      %% then get the image name and re-order the name
      dir_image{i} = dir([select_mouse_path{i},split_char,'*.tif']);
      temp_digits = zeros(length(dir_image{i}),1);
      parfor j = 1:length(dir_image{i})
         temp_file_name = strsplit(dir_image{i}(j).name(1:end-4),'_');
         temp_digits(j) = str2num(temp_file_name{end}(2:end));
      end
      digits{i} = temp_digits;
      [~,ind] = sort(temp_digits);

      %% then load the data and save the downsample image in the memory

      pctRunOnAll warning off;
      % montage = cell(row_num,1);
      iminfo = imfinfo([select_mouse_path{i},split_char,dir_image{i}(ind(1)).name]);
%       pctRunOnAll warning off
%       im = uint16(rand(iminfo.Height/4,iminfo.Width/4,length(dir1))*100);
      im = zeros(iminfo(1).Height/down_sampling_factor,iminfo(1).Width/down_sampling_factor,length(temp_digits));
      tic
      parfor j = 1:length(temp_digits)
%             tic
         %    for j = 1:col_num;
%           j
         %    montage{i} = [montage{i},imread(dir1(ind).name)];
         im(:,:,j) = imresize(imread([select_mouse_path{i},split_char,dir_image{i}(ind(j)).name]),1/down_sampling_factor,'nearest');
         %       disp(dir1(ind(i).name));
         %    ind = ind +1;
         %    end
         %    montage{i} = imresize(montage{i} ,1/down_sampling_factor);
%             t = toc
      end
      t = toc
      montage = cell(row_num(i),1);
      ind = 1;
      for m = 1:row_num(i)
         for n = 1:col_num(i)
            %       i,j
            %       im(:,:,index) = normaliz(im(:,:,index));
            %       ind = (i-1)*col_num+j;
            montage{m} = [montage{m},(im(:,:,ind))];
            ind = ind +1;
         end
      end
      montage_output = cell2mat(montage);
      temp_name = strsplit(select_mouse_path{i},split_char);

      imwrite(uint16(montage_output),[out_dir,'Montage_',temp_name{end},'.tif']);
%       temp_montage = reshape(im,[row_num*512/down_sampling_factor,col_num*512/down_sampling_factor]);

      %    filename{end} = sprintf('m%.5d',digits);
      %       filename = [strjoin(filename,'_'),'.tif'];
      %    end
      %    movefile(dir1(i).name,[temp_path,filename]);
      %    end
   end
end
```

Appendix 11: Tables of raw numbers from basal Arc synaptome map

A. Main regions

	DENSITY		INTENSITY		SIZE	
	MEAN	**SD**	**MEAN**	**SD**	**MEAN**	**SD**
CN_L	**11.68**	2.74	**8443**	1449	**0.095**	0.002
CN_R	**13.52**	1.81	**8709**	1175	**0.094**	0.002
CORTEX_L	**40.50**	4.94	**11101**	1293	**0.091**	0.001
CORTEX_R	**43.69**	2.49	**11450**	996	**0.090**	0.001
CS_L	**19.14**	4.86	**8734**	1657	**0.097**	0.002
CS_R	**20.69**	2.41	**8757**	1570	**0.096**	0.001
FT_L	**0.36**	0.25	**4564**	345	**0.093**	0.003
FT_R	**0.43**	0.18	**4433**	554	**0.091**	0.007
HC_L	**19.68**	3.51	**6896**	602	**0.090**	0.001
HC_R	**20.54**	2.55	**7094**	491	**0.090**	0.001
HY_L	**11.35**	1.02	**6809**	1367	**0.100**	0.001
HY_R	**11.35**	0.94	**6761**	1269	**0.100**	0.001
OLF_L	**23.41**	5.66	**9244**	1661	**0.095**	0.003
OLF_R	**25.59**	2.79	**9290**	1130	**0.094**	0.002

B. Detailed regions

	DENSITY		INTENSITY		SIZE	
	MEAN	**SD**	**MEAN**	**SD**	**MEAN**	**SD**
alv_L	**0.32**	0.12	**4729**	595	**0.091**	0.012
alv_R	**0.43**	0.18	**5033**	639	**0.097**	0.007
AUDd_L	**41.74**	4.63	**11488**	1356	**0.092**	0.002
AUDd_Layer1_L	**52.17**	7.91	**11742**	1320	**0.091**	0.002
AUDd_Layer1_R	**56.90**	2.86	**11479**	885	**0.090**	0.002
AUDd_Layer2-3_L	**50.04**	5.98	**12063**	1203	**0.095**	0.002
AUDd_Layer2-3_R	**52.69**	2.56	**11901**	867	**0.094**	0.001
AUDd_Layer4_L	**47.60**	5.25	**12557**	1258	**0.092**	0.002
AUDd_Layer4_R	**52.85**	1.32	**12944**	1028	**0.091**	0.000
AUDd_Layer5_L	**37.41**	4.19	**11163**	1563	**0.092**	0.001
AUDd_Layer5_R	**40.52**	1.00	**11575**	1021	**0.091**	0.001
AUDd_Layer6a_L	**37.55**	4.50	**10669**	1673	**0.089**	0.001
AUDd_Layer6a_R	**41.39**	1.88	**11415**	1087	**0.089**	0.001
AUDd_Layer6b_L	**20.60**	8.26	**8463**	1508	**0.091**	0.002
AUDd_Layer6b_R	**25.74**	5.57	**9157**	1070	**0.089**	0.001
AUDd_R	**45.79**	1.80	**11744**	968	**0.091**	0.001
AUDp_L	**41.41**	6.09	**11022**	1349	**0.093**	0.002
AUDp_Layer1_L	**47.04**	6.74	**10609**	779	**0.093**	0.001
AUDp_Layer1_R	**54.34**	4.06	**10956**	912	**0.092**	0.001
AUDp_Layer2-3_L	**45.31**	6.85	**11280**	1096	**0.096**	0.002
AUDp_Layer2-3_R	**48.50**	2.94	**11356**	675	**0.095**	0.002
AUDp_Layer4_L	**46.96**	6.97	**12292**	1193	**0.093**	0.002
AUDp_Layer4_R	**50.79**	2.84	**12529**	861	**0.092**	0.001
AUDp_Layer5_L	**36.55**	5.46	**10927**	1555	**0.093**	0.002
AUDp_Layer5_R	**39.63**	2.57	**11303**	955	**0.092**	0.001
AUDp_Layer6a_L	**39.25**	4.35	**10697**	1618	**0.090**	0.001
AUDp_Layer6a_R	**42.17**	1.52	**11343**	944	**0.089**	0.000
AUDp_Layer6b_L	**23.63**	9.97	**8573**	1642	**0.091**	0.002
AUDp_Layer6b_R	**30.63**	8.87	**9548**	1191	**0.090**	0.001
AUDp_R	**45.01**	2.28	**11425**	859	**0.092**	0.001
AUDv_L	**38.93**	6.10	**10587**	1433	**0.093**	0.002
AUDv_Layer1_L	**46.04**	6.84	**10402**	1168	**0.092**	0.001
AUDv_Layer1_R	**52.98**	4.77	**11048**	1275	**0.091**	0.001
AUDv_Layer2-3_L	**40.01**	6.20	**10501**	1247	**0.096**	0.002
AUDv_Layer2-3_R	**45.23**	2.62	**11005**	821	**0.094**	0.001
AUDv_Layer4_L	**41.60**	7.05	**11280**	1412	**0.093**	0.002
AUDv_Layer4_R	**48.06**	2.79	**11947**	994	**0.092**	0.001
AUDv_Layer5_L	**33.87**	5.60	**10448**	1570	**0.094**	0.002
AUDv_Layer5_R	**38.17**	2.29	**10987**	1239	**0.093**	0.001
AUDv_Layer6a_L	**37.79**	5.10	**10386**	1725	**0.091**	0.002
AUDv_Layer6a_R	**40.66**	1.97	**11025**	1001	**0.090**	0.001

AUDv_Layer6b_L	**24.92**	7.28	**8740**	1635	**0.091**	0.002
AUDv_Layer6b_R	**32.95**	10.54	**9825**	1193	**0.090**	0.004
AUDv_R	**43.41**	2.57	**11163**	1057	**0.092**	0.001
BLAa_L	**23.03**	7.02	**8891**	1847	**0.097**	0.003
BLAa_R	**17.46**	12.19	**8888**	1882	**0.072**	0.048
BLAp_L	**27.57**	6.29	**9715**	1931	**0.098**	0.004
BLAp_R	**21.25**	14.27	**9761**	1656	**0.073**	0.049
BLAv_L	**19.19**	4.26	**9043**	1490	**0.098**	0.003
BLAv_R	**16.11**	10.97	**9027**	1406	**0.073**	0.049
BMAp_L	**11.52**	3.54	**8390**	1464	**0.098**	0.001
BMAp_R	**10.73**	7.45	**8519**	1614	**0.073**	0.048
CA1_slm_L	**19.79**	4.65	**6554**	462	**0.090**	0.002
CA1_slm_R	**20.98**	3.06	**6654**	406	**0.089**	0.001
CA1_so_L	**42.55**	5.27	**8127**	725	**0.082**	0.001
CA1_so_R	**43.85**	3.17	**8362**	656	**0.082**	0.001
CA1_sp_L	**5.60**	0.94	**7262**	498	**0.092**	0.002
CA1_sp_R	**5.70**	1.84	**7314**	401	**0.094**	0.005
CA1_sr_L	**53.39**	4.12	**8825**	580	**0.084**	0.001
CA1_sr_R	**55.58**	2.67	**8988**	425	**0.084**	0.001
CA2_slm_L	**1.49**	0.80	**5539**	714	**0.087**	0.002
CA2_slm_R	**1.70**	0.28	**5765**	480	**0.087**	0.002
CA2_so_L	**3.57**	1.09	**5938**	580	**0.088**	0.001
CA2_so_R	**4.49**	0.84	**6269**	647	**0.090**	0.004
CA2_sp_L	**1.35**	0.60	**6923**	849	**0.158**	0.014
CA2_sp_R	**1.51**	0.49	**6988**	576	**0.153**	0.018
CA2_sr_L	**6.03**	1.15	**6336**	539	**0.090**	0.001
CA2_sr_R	**7.57**	0.53	**6396**	407	**0.090**	0.002
CA3_slm_L	**11.27**	3.30	**6089**	752	**0.091**	0.003
CA3_slm_R	**12.38**	1.56	**6246**	551	**0.089**	0.001
CA3_slu_L	**17.63**	2.58	**6701**	524	**0.112**	0.002
CA3_slu_R	**20.00**	1.58	**6919**	331	**0.111**	0.001
CA3_so_L	**18.98**	2.60	**6851**	567	**0.092**	0.002
CA3_so_R	**21.03**	0.67	**7216**	459	**0.091**	0.001
CA3_sp_L	**8.81**	3.15	**6558**	519	**0.115**	0.002
CA3_sp_R	**10.14**	2.99	**6757**	401	**0.113**	0.002
CA3_sr_L	**26.47**	1.47	**7515**	610	**0.092**	0.002
CA3_sr_R	**28.84**	2.60	**7817**	331	**0.092**	0.002
cc_L	**1.30**	0.73	**6114**	994	**0.092**	0.003
cc_R	**1.46**	0.60	**6323**	525	**0.092**	0.003
CEA_L	**9.33**	2.79	**8215**	1626	**0.100**	0.003
CEA_R	**11.03**	2.06	**8596**	1357	**0.098**	0.001
cing_L	**6.11**	0.57	**7670**	863	**0.089**	0.001
cing_R	**4.97**	1.76	**7456**	753	**0.090**	0.002
COApl1_L	**16.49**	2.76	**9419**	1716	**0.094**	0.004
COApl1_R	**13.00**	8.84	**8840**	1281	**0.071**	0.048
COApl2_L	**13.00**	3.00	**8998**	1393	**0.099**	0.002
COApl2_R	**10.08**	6.98	**8173**	1100	**0.073**	0.048
COApl3_L	**12.27**	0.57	**8847**	1179	**0.099**	0.002
COApl3_R	**11.38**	8.22	**8534**	1349	**0.073**	0.049
CP_L	**27.98**	5.12	**9674**	1672	**0.093**	0.002
CP_R	**32.39**	2.91	**10309**	1209	**0.091**	0.001
df_L	**0.11**	0.12	**2013**	2328	**0.044**	0.053
df_R	**0.05**	0.11	**966**	1931	**0.025**	0.049
DG_mo_inf_L	**17.03**	2.51	**6044**	420	**0.093**	0.003
DG_mo_inf_R	**17.92**	2.38	**6136**	527	**0.092**	0.003
DG_mo_sup_L	**18.17**	2.94	**6369**	625	**0.092**	0.003
DG_mo_sup_R	**19.00**	2.64	**6516**	543	**0.091**	0.002
DG_po_L	**10.16**	1.80	**6078**	426	**0.111**	0.003
DG_po_R	**11.11**	1.66	**6276**	510	**0.109**	0.002
DG_sg_inf_L	**1.46**	0.65	**4895**	333	**0.120**	0.008
DG_sg_inf_R	**1.43**	0.58	**5033**	445	**0.119**	0.009
DG_sg_sup_L	**1.46**	0.57	**5037**	367	**0.123**	0.003
DG_sg_sup_R	**1.51**	0.64	**5088**	475	**0.125**	0.002
ECT_L	**34.98**	6.81	**10118**	1599	**0.093**	0.002
ECT_Layer1_L	**43.23**	8.21	**10025**	1581	**0.091**	0.002
ECT_Layer1_R	**50.39**	6.22	**11001**	1472	**0.089**	0.001
ECT_Layer2-3_L	**35.36**	7.00	**10464**	1615	**0.095**	0.002
ECT_Layer2-3_R	**41.85**	4.46	**11125**	1135	**0.093**	0.001
ECT_Layer5_L	**31.14**	5.87	**9937**	1600	**0.093**	0.001

ECT_Layer5_R	**35.87**	1.48	**10453**	1184	**0.092**	0.001
ECT_Layer6a_L	**33.01**	5.73	**9585**	1562	**0.090**	0.002
ECT_Layer6a_R	**38.01**	2.06	**10182**	859	**0.090**	0.001
ECT_Layer6b_L	**23.36**	6.45	**8463**	1363	**0.091**	0.002
ECT_Layer6b_R	**30.30**	4.72	**9691**	605	**0.090**	0.002
ECT_R	**40.58**	2.56	**10791**	1158	**0.092**	0.001
ENTI_L	**29.87**	6.28	**9727**	1814	**0.094**	0.003
ENTI_Layer1_L	**38.25**	7.36	**9937**	2042	**0.091**	0.004
ENTI_Layer1_R	**44.93**	5.50	**10424**	1508	**0.088**	0.002
ENTI_Layer2-3_L	**28.84**	5.76	**9815**	1685	**0.096**	0.003
ENTI_Layer2-3_R	**33.12**	2.36	**10100**	1325	**0.094**	0.001
ENTI_Layer5_L	**28.98**	5.46	**9569**	1641	**0.095**	0.002
ENTI_Layer5_R	**33.85**	1.96	**9963**	1128	**0.093**	0.001
ENTI_Layer6a_L	**24.46**	9.26	**8492**	1785	**0.092**	0.002
ENTI_Layer6a_R	**28.33**	0.53	**9105**	908	**0.089**	0.002
ENTI_Layer6b_L	**16.63**	5.00	**8050**	1325	**0.096**	0.006
ENTI_Layer6b_R	**18.06**	6.16	**8408**	1068	**0.092**	0.003
ENTI_R	**33.85**	2.19	**10043**	1328	**0.093**	0.001
EP_L	**15.19**	4.81	**8029**	1590	**0.093**	0.002
EP_R	**17.36**	1.84	**8230**	1185	**0.091**	0.001
FC_L	**0.97**	0.44	**5595**	539	**0.096**	0.006
FC_R	**0.76**	0.28	**5677**	413	**0.090**	0.007
fi_L	**0.11**	0.12	**1873**	2174	**0.048**	0.055
fi_R	**0.16**	0.11	**2812**	1904	**0.067**	0.045
GPe_L	**0.54**	0.37	**4929**	3331	**0.078**	0.052
GPe_R	**0.87**	0.47	**6593**	1351	**0.099**	0.006
Hypothalamus_L	**2.76**	1.02	**6809**	1367	**0.100**	0.001
Hypothalamus_R	**2.87**	0.94	**6761**	1269	**0.100**	0.001
int_L	**0.27**	0.27	**3209**	2185	**0.070**	0.047
int_R	**0.22**	0.18	**3316**	2231	**0.074**	0.049
LA_L	**22.17**	6.11	**8761**	1781	**0.096**	0.002
LA_R	**24.44**	3.73	**8957**	1303	**0.095**	0.001
MEA_L	**7.08**	2.29	**7887**	1350	**0.099**	0.002
MEA_R	**7.52**	2.04	**7732**	1324	**0.098**	0.003
MOp_L	**39.85**	3.95	**10753**	1085	**0.090**	0.000
MOp_Layer1_L	**51.79**	6.28	**11322**	1200	**0.091**	0.001
MOp_Layer1_R	**55.20**	4.81	**11831**	1152	**0.090**	0.001
MOp_Layer2-3_L	**44.14**	5.23	**11250**	1010	**0.092**	0.001
MOp_Layer2-3_R	**45.77**	2.62	**11600**	898	**0.092**	0.001
MOp_Layer5_L	**36.82**	3.31	**10516**	1124	**0.090**	0.000
MOp_Layer5_R	**38.55**	1.75	**10924**	978	**0.090**	0.001
MOp_Layer6a_L	**34.03**	2.42	**10130**	1164	**0.088**	0.001
MOp_Layer6a_R	**34.49**	2.15	**10442**	1004	**0.087**	0.001
MOp_Layer6b_L	**22.82**	2.28	**8695**	962	**0.087**	0.000
MOp_Layer6b_R	**23.63**	2.66	**8937**	921	**0.087**	0.002
MOp_R	**40.82**	1.99	**11099**	1017	**0.090**	0.001
MOs_L	**39.09**	2.71	**11433**	1270	**0.091**	0.001
MOs_Layer1_L	**55.39**	7.46	**12249**	1785	**0.092**	0.002
MOs_Layer1_R	**58.26**	6.57	**12838**	1611	**0.091**	0.001
MOs_Layer2-3_L	**44.25**	4.01	**11944**	1273	**0.092**	0.001
MOs_Layer2-3_R	**44.63**	2.71	**12204**	1088	**0.092**	0.000
MOs_Layer5_L	**33.47**	2.36	**11031**	1220	**0.092**	0.001
MOs_Layer5_R	**33.66**	1.53	**11399**	970	**0.092**	0.001
MOs_Layer6a_L	**31.98**	2.52	**10137**	1228	**0.087**	0.000
MOs_Layer6a_R	**31.06**	1.31	**10379**	993	**0.087**	0.001
MOs_Layer6b_L	**23.49**	1.17	**8752**	918	**0.087**	0.001
MOs_Layer6b_R	**23.11**	2.14	**8813**	760	**0.086**	0.001
MOs_R	**38.93**	1.45	**11727**	1069	**0.091**	0.000
opt_L	**0.05**	0.11	**875**	1750	**0.025**	0.049
opt_R	**0.05**	0.11	**884**	1768	**0.023**	0.046
PAA1_L	**20.71**	6.89	**9530**	1546	**0.094**	0.003
PAA1_R	**15.57**	10.61	**8998**	1172	**0.071**	0.047
PAA2_L	**16.17**	5.61	**9067**	1486	**0.098**	0.002
PAA2_R	**10.16**	7.62	**8463**	846	**0.074**	0.050
PAA3_L	**17.38**	5.28	**9100**	1495	**0.098**	0.002
PAA3_R	**15.95**	11.05	**8842**	1066	**0.072**	0.048
PERI_L	**31.09**	7.48	**9618**	1727	**0.094**	0.002
PERI_Layer1_L	**38.95**	7.40	**9571**	1734	**0.091**	0.003
PERI_Layer1_R	**47.04**	4.93	**10294**	1651	**0.088**	0.001

PERI_Layer2-3_L	**29.79**	7.29	**9802**	1674	**0.096**	0.002
PERI_Layer2-3_R	**35.74**	2.47	**10310**	1324	**0.094**	0.001
PERI_Layer5_L	**31.14**	6.09	**9759**	1772	**0.094**	0.002
PERI_Layer5_R	**35.63**	2.36	**10153**	1155	**0.092**	0.001
PERI_Layer6a_L	**27.95**	7.98	**8722**	1608	**0.091**	0.002
PERI_Layer6a_R	**32.44**	1.74	**9289**	726	**0.089**	0.000
PERI_Layer6b_L	**17.92**	9.33	**8226**	1313	**0.093**	0.005
PERI_Layer6b_R	**19.44**	4.87	**8675**	601	**0.089**	0.000
PERI_R	**36.28**	1.72	**10065**	1252	**0.092**	0.001
PIR1_L	**30.38**	7.18	**9691**	1932	**0.093**	0.003
PIR1_R	**35.90**	2.84	**10134**	930	**0.092**	0.002
PIR2_L	**15.46**	4.42	**8645**	1638	**0.098**	0.002
PIR2_R	**18.30**	1.98	**9019**	710	**0.096**	0.001
PIR3_L	**26.19**	6.41	**9277**	1655	**0.095**	0.003
PIR3_R	**29.30**	2.91	**9517**	1019	**0.093**	0.001
RSPd_L	**35.36**	2.50	**11194**	1215	**0.091**	0.001
RSPd_Layer1_L	**50.01**	6.52	**11686**	1614	**0.091**	0.001
RSPd_Layer1_R	**50.25**	4.67	**11633**	1591	**0.092**	0.002
RSPd_Layer2-3_L	**39.74**	4.21	**11534**	1230	**0.092**	0.001
RSPd_Layer2-3_R	**39.63**	2.74	**11402**	1001	**0.092**	0.001
RSPd_Layer5_L	**32.12**	2.59	**11144**	1165	**0.093**	0.002
RSPd_Layer5_R	**32.20**	1.68	**11101**	799	**0.092**	0.001
RSPd_Layer6a_L	**29.14**	2.20	**10352**	1150	**0.088**	0.002
RSPd_Layer6a_R	**29.60**	1.78	**10496**	924	**0.088**	0.002
RSpd_Layer6b_L	**21.79**	3.93	**9061**	1114	**0.085**	0.002
RSPd_Layer6b_R	**26.76**	4.73	**9698**	146	**0.087**	0.003
RSPd_R	**33.95**	5.64	**10810**	1594	**0.091**	0.001
RSPv_L	**29.84**	1.45	**10039**	1017	**0.091**	0.001
RSPv_Layer1_L	**35.20**	2.78	**10161**	924	**0.091**	0.001
RSPv_Layer1_R	**30.82**	8.52	**9858**	1150	**0.092**	0.002
RSPv_Layer2-3_L	**20.44**	2.98	**9888**	950	**0.093**	0.001
RSPv_Layer2-3_R	**22.57**	3.70	**9725**	522	**0.093**	0.001
RSPv_Layer5_L	**31.01**	2.40	**10390**	798	**0.089**	0.000
RSPv_Layer5_R	**28.76**	4.14	**9967**	1243	**0.089**	0.001
RSPv_Layer6a_L	**26.03**	0.59	**9935**	936	**0.088**	0.001
RSPv_Layer6a_R	**24.36**	4.21	**9677**	1448	**0.087**	0.001
RSPv_Layer6b_L	**23.06**	4.86	**8968**	943	**0.086**	0.002
RSPv_Layer6b_R	**24.74**	2.37	**9092**	920	**0.085**	0.002
RSPv_R	**28.17**	1.15	**10015**	764	**0.090**	0.001
SSp_L	**44.60**	4.05	**11756**	1203	**0.090**	0.001
SSp_Layer1_L	**53.55**	6.16	**11929**	864	**0.090**	0.001
SSp_Layer1_R	**56.93**	2.47	**11902**	559	**0.089**	0.001
SSp_Layer2-3_L	**53.42**	5.52	**12480**	976	**0.092**	0.001
SSp_Layer2-3_R	**54.88**	1.45	**12333**	604	**0.092**	0.001
SSp_Layer4_L	**50.55**	4.25	**12707**	1200	**0.088**	0.001
SSp_Layer4_R	**53.88**	2.84	**12916**	768	**0.088**	0.001
SSp_Layer5_L	**39.95**	3.51	**11373**	1328	**0.090**	0.001
SSp_Layer5_R	**42.23**	2.14	**11764**	898	**0.089**	0.001
SSp_Layer6a_L	**38.39**	4.30	**10960**	1510	**0.088**	0.001
SSp_Layer6a_R	**41.25**	1.44	**11373**	920	**0.087**	0.001
SSp_Layer6b_L	**18.41**	6.40	**8433**	1300	**0.090**	0.001
SSp_Layer6b_R	**20.71**	3.38	**8921**	851	**0.089**	0.001
SSp_R	**47.44**	1.71	**11973**	744	**0.089**	0.001
st_L	**0.16**	0.11	**3110**	2101	**0.069**	0.046
st_R	**0.22**	0.18	**3361**	2277	**0.070**	0.046
STN_L	**1.62**	1.42	**6354**	1385	**0.068**	0.046
STN_R	**2.32**	1.06	**6704**	1369	**0.093**	0.004
TEa_L	**38.44**	6.03	**10586**	1606	**0.093**	0.002
TEa_Layer1_L	**45.96**	8.20	**10440**	1621	**0.091**	0.002
TEa_Layer1_R	**52.52**	7.05	**11171**	1772	**0.090**	0.000
TEa_Layer2-3_L	**40.12**	7.13	**10669**	1517	**0.095**	0.002
TEa_Layer2-3_R	**45.04**	3.97	**11210**	1391	**0.094**	0.001
TEa_Layer4_L	**39.90**	5.16	**11400**	1555	**0.094**	0.002
TEa_Layer4_R	**46.25**	3.61	**11923**	1390	**0.092**	0.000
TEa_Layer5_L	**33.12**	5.54	**10197**	1533	**0.093**	0.002
TEa_Layer5_R	**36.82**	2.32	**10738**	1286	**0.093**	0.001
TEa_Layer6a_L	**38.12**	5.45	**10370**	1671	**0.091**	0.002
TEa_Layer6a_R	**40.79**	1.60	**10835**	1091	**0.089**	0.001
TEa_Layer6b_L	**23.65**	6.58	**9055**	1862	**0.091**	0.002

TEa_Layer6b_R	**31.63**	7.29	**9874**	1251	**0.090**	0.002
TEa_R	**42.87**	2.69	**11132**	1382	**0.091**	0.000

Appendix 12: Preliminary results on nature of nuclear accumulation of Arc 4h following open field exploration and rotarod training.

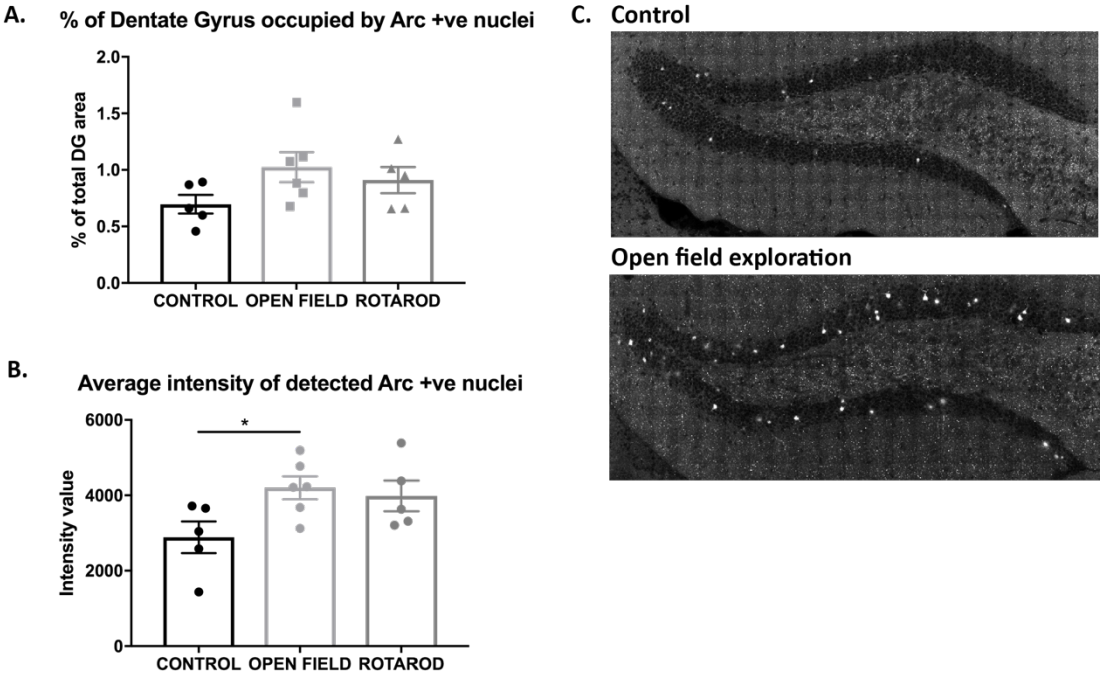

Appendix.figure 8 – A. *Percentage of dentate gyrus area occupied by Arc-positive nuclei.* ***B.*** *Average fluorescence intensity of detected Arc positive-nuclei. N=5-6. Data points = individual mice, bars = mean, error bars = SEM.* ***C.*** *Representative images of Arc signal in dentate gyrus in control and open field exploration exposed animals.*

Appendix 13: Example metadata file from Arc ketamine synaptome mapping.

Name : KET_GGV282_HC_24-09-1428/11/2014 11:19:55

Type : 16 bit grey/pseudo
Intensity : 1.000000 lux
x : 512 * 0.084034 : um
y : 512 * 0.084000 : um
Montage : 16440

[Environment]
User=CJQW102
Configuration=Sarah
[Environment End]
[Created]
Date=24/09/2014
Time=16:23:58
[Created End]
[Protocol Description]
Protocol - Montage 1channel no Z
Image - KET_GGV282_HC_24-09-14
Camera Binning - Use Current
Wait Allocation - Off
Camera Selection - Use Current
Scan - Montage
Montage Acquisition
Events
Keyboard Events - On
Default name - Spacebar
Move Channel - 488

Camera EM Gain - 250
Camera Binning X - CURRENT
Camera Binning Y - CURRENT
Camera Exposure Time (s) - 0.05
Camera Exposure Units - 1
LUT - Green
Map Min - 143
Map Max - 527
CoolLED Intensity 1 - Current
CoolLED Intensity 2 - Current
CoolLED Intensity 3 - Current
CoolLED Intensity 4 - Current
CoolLED Pulsed Mode - Current
CoolLED Shutter - Closed
CoolLED Wavelength - Current
IX81_BX61 EPI Filter - 6
IX81_BX61 BF Shutter - Current
IX81_BX61 EPI Shutter - Current
IX81_BX61 ND Filter - 5
IX81_BX61 Filter 1 - 0
IX81_BX61 Filter 2 - 0
IX81_BX61 Filter 3 - 0
IX81_BX61 Port - 1
LVPZT - DELTA_Z 0
CSU Aperture - Current
CSU Camera Port - Current
CSU Lens 1 - Current
CSU Lens 2 - Current
CSU NIR Shutter - Current
CSU PB Mirror - Current
CSU PB Shutter - Current
CSU Port - Current
CSU Shutter - Open
Dichroic - 1
Emmision - 525
Excitation - 1
NDFilter - Current
AOTF Channel 1 Intensity - 0
AOTF Channel 2 Intensity - 70
AOTF Channel 3 Intensity - 0
AOTF Channel 4 Intensity - 0
AOTF Channel 5 Intensity - Current
AOTF Channel 6 Intensity - Current
AOTF Laser 1 Enabled - 1
AOTF Laser 1 External Control - Current
AOTF Laser 2 Enabled - 1
AOTF Laser 2 External Control - Current
AOTF Laser 3 Enabled - 1
AOTF Laser 3 External Control - Current
AOTF Laser 4 Enabled - 1
AOTF Laser 4 External Control - Current
AOTF Laser 5 Enabled - 0
AOTF Laser 5 External Control - Current
AOTF Laser 6 Enabled - 0
AOTF Laser 6 External Control - Current
AOTF MPD - 1
AOTF Position - 488
AOTF Shutter - Open
Repeat T - 1 time (0 ms - fastest)
Repeat - Montage
Montage Positions - (16440 (120 by 137))
Snap - Frame
End - Montage
End - T

[Protocol Description End]
[XYZScan]
ScanName=Montage
FileVersion=2
Centre=False
Channel=
WellPattern=
Density=0

Calibration=
XYFields=1 39623,-38777,49.99
ZScan=
Montage=Edge Overlap 0
Plates=
MontageOffsets=16440 -1498.5,-3827.544,0 -1455.47478991596,-3827.544,0 -1412.44957983193,-3827.544,0 -1369.4243697479,-3827.544,
…
[Region Info (Fields) End]
[Grab Parameters]
Camera=Andor
Window Left=0
Window Top=0
Window Right=511
Window Bottom=511
Window Width=512
Window Height=512
BinningX=1
BinningY=1
Image Width=512
Image Height=512
Exposure=50.0 ms
Rotation=0
FlipV=0
FlipH=0
TimeStamps=Hardware
[Grab Parameters End]
[Tab Device Info]
Camera=DU897_BV 8655
ControllerCard=USB
DriverVersion=2.95.33002.0
CofVersion=0
VxDVersion=0.0
SoftwareTrigger=Supported
BitDepth=16
FPGA_Version=205.205
Ocx_Version=5.4.8.64
Ocx_Time=13:17:04 Jul 26 2013
Ocx_File=C:\PROGRA~2\ANDORB~1\COMMON~1\KIDAND~2.OCX

[Tab Device Info End]
[Tab Exposure]
Window=512 : 512
Shutter=Open
Binning=1 x 1
Temperature - Actual =-70
Display Control - Fastest=Checked
Display Control - Display Rate=3
Gains - Pre-Amp-Gain=Gain 3
EM Gain - Enabled=Checked
Gains - EMGain=250
Exposure Time - Frame Transfer=Unchecked
Exposure Time - unit=ms
Exposure Time - exposure value=50.0
Exposure Time - Readout in ms=19.379
Experiment Control - FLZ=Unchecked
Experiment Control - Trig Mode=Free Run
Use Frame averaging=Checked
Frames to be averaged=4
Fastest Grab=Unchecked
Available memory=4095
[Tab Exposure End]
[Tab Temperature/Shutter]
Temperature Setting=-70
Actual Temperature=-70
Cooling=Steady
Fan=Full
TTL High Open=Checked
Shutter Open Transfer Time=60
Shutter Close Transfer Time=80
[Tab Temperature/Shutter End]
[Tab Speed/Amplifer]
Horizontal Readout=17.000

Vertical Readout time=[1.700]
ADC Channel=0
Vertical Clock Voltage=Normal
Output Amplifier=EM Port
Baseline Clamp=Checked
[Tab Speed/Amplifer End]
[Tab Image Orientation]
Flip=None
Rotation in Degrees=None
[Tab Image Orientation End]
[Image Info]
Window Left=0
Window Top=0
Window Right=511
Window Bottom=511
Window Width=512
Window Height=512
Window BinningX=1
Window BinningY=1
[Image Info End]
[First Frame]
SavedTime=24/09/2014 16:24:00.683
[First Frame End]

Appendix 14: Example metadata file from PSD95 ketamine synaptome mapping.

Name : 2014-12-11_GKD182_KET_HC 12/12/2014 09:59:03

Type : 16 bit grey/pseudo
Intensity : 1.000000 lux
x : 512 * 0.084034 : um
y : 512 * 0.084000 : um
Montage : 31439

[Environment]
User=CJQW102
Configuration=Sarah
[Environment End]
[Created]
Date=11/12/2014
Time=11:23:44
[Created End]
[Protocol Description]
Protocol - Montage 1channel no Z
Image - 2014-12-11_GKD182_KET_HC
Camera Binning - Use Current
Wait Allocation - Off
Camera Selection - Use Current
Scan - Montage
Montage Acquisition
Events
Keyboard Events - On
Default name - Spacebar
Move Channel - 488
Camera EM Gain - 250
Camera Binning X - CURRENT
Camera Binning Y - CURRENT
Camera Exposure Time (s) - 0.05
Camera Exposure Units - 1
LUT - Green
Map Min - 143
Map Max - 527
CoolLED Intensity 1 - Current
CoolLED Intensity 2 - Current
CoolLED Intensity 3 - Current
CoolLED Intensity 4 - Current
CoolLED Pulsed Mode - Current
CoolLED Shutter - Closed
CoolLED Wavelength - Current
IX81_BX61 EPI Filter - 6
IX81_BX61 BF Shutter - Current
IX81_BX61 EPI Shutter - Current

IX81_BX61 ND Filter - 5
IX81_BX61 Filter 1 - 0
IX81_BX61 Filter 2 - 0
IX81_BX61 Filter 3 - 0
IX81_BX61 Port - 1
LVPZT - DELTA_Z 0
CSU Aperture - Current
CSU Camera Port - Current
CSU Lens 1 - Current
CSU Lens 2 - Current
CSU NIR Shutter - Current
CSU PB Mirror - Current
CSU PB Shutter - Current
CSU Port - Current
CSU Shutter - Open
Dichroic - 1
Emmision - 525
Excitation - 1
NDFilter - Current
AOTF Channel 1 Intensity - 0
AOTF Channel 2 Intensity - 60
AOTF Channel 3 Intensity - 0
AOTF Channel 4 Intensity - 0
AOTF Channel 5 Intensity - Current
AOTF Channel 6 Intensity - Current
AOTF Laser 1 Enabled - 1
AOTF Laser 1 External Control - Current
AOTF Laser 2 Enabled - 1
AOTF Laser 2 External Control - Current
AOTF Laser 3 Enabled - 1
AOTF Laser 3 External Control - Current
AOTF Laser 4 Enabled - 1
AOTF Laser 4 External Control - Current
AOTF Laser 5 Enabled - 0
AOTF Laser 5 External Control - Current
AOTF Laser 6 Enabled - 0
AOTF Laser 6 External Control - Current
AOTF MPD - 1
AOTF Position - 488
AOTF Shutter - Open
Repeat T - 1 time (0 ms - fastest)
Repeat - Montage
Montage Positions - (31439 (211 by 149))
Snap - Frame
End - Montage
End - T

[Protocol Description End]
[XYZScan]
ScanName=Montage
FileVersion=2
Centre=False
Channel=
WellPattern=
Density=0
Calibration=
XYFields=1 63407,-41484,6243.23260141059
ZScan=
Montage=Edge Overlap 0
Plates=
MontageOffsets=31439 -4969.64705882353,-3088.092,17.268857642086 -4926.62184873949,-3088.092,
…

[Region Info (Fields) End]
[Grab Parameters]
Camera=Andor
Window Left=0
Window Top=0
Window Right=511
Window Bottom=511
Window Width=512
Window Height=512
BinningX=1

BinningY=1
Image Width=512
Image Height=512
Exposure=50.0 ms
Rotation=0
FlipV=0
FlipH=0
TimeStamps=Hardware
[Grab Parameters End]
[Tab Device Info]
Camera=DU897_BV 8655
ControllerCard=USB
DriverVersion=2.95.33002.0
CofVersion=0
VxDVersion=0.0
SoftwareTrigger=Supported
BitDepth=16
FPGA_Version=205.205
Ocx_Version=5.4.8.64
Ocx_Time=13:17:04 Jul 26 2013
Ocx_File=C:\PROGRA~2\ANDORB~1\COMMON~1\KIDAND~2.OCX

[Tab Device Info End]
[Tab Exposure]
Window=512 : 512
Shutter=Open
Binning=1 x 1
Temperature - Actual =-70
Display Control - Fastest=Checked
Display Control - Display Rate=3
Gains - Pre-Amp-Gain=Gain 3
EM Gain - Enabled=Checked
Gains - EMGain=250
Exposure Time - Frame Transfer=Unchecked
Exposure Time - unit=ms
Exposure Time - exposure value=50.0
Exposure Time - Readout in ms=19.371
Experiment Control - FLZ=Unchecked
Experiment Control - Trig Mode=Free Run
Use Frame averaging=Checked
Frames to be averaged=2
Fastest Grab=Unchecked
Available memory=4095
[Tab Exposure End]
[Tab Temperature/Shutter]
Temperature Setting=-70
Actual Temperature=-70
Cooling=Steady
Fan=Full
TTL High Open=Checked
Shutter Open Transfer Time=60
Shutter Close Transfer Time=80
[Tab Temperature/Shutter End]
[Tab Speed/Amplifer]
Horizontal Readout=17.000
Vertical Readout time=[1.700]
ADC Channel=0
Vertical Clock Voltage=Normal
Output Amplifier=EM Port
Baseline Clamp=Checked
[Tab Speed/Amplifer End]
[Tab Image Orientation]
Flip=None
Rotation in Degrees=None
[Tab Image Orientation End]
[Image Info]
Window Left=0
Window Top=0
Window Right=511
Window Bottom=511
Window Width=512
Window Height=512
Window BinningX=1

Window BinningY=1
[Image Info End]
[First Frame]
SavedTime=11/12/2014 11:23:48.398
[First Frame End]

Appendix 15: Tables of raw numbers from ketamine Arc synaptome maps

	1H POST-ADMINISTRATION																	
	SALINE CONTROL						LOW DOSE KETAMINE (10mg/kg)						HIGH DOSE KETAMINE (100mg/kg)					
BREGMA	DENSITY		INTENSITY		SIZE		DENSITY		INTENSITY		SIZE		DENSITY		INTENSITY		SIZE	
2.10	MEAN	SD	MEAN	SD	MEAN	SD	MEAN	SD	MEAN	SD	MEAN	SD	MEAN	SD	MEAN	SD	MEAN	SD
ACAd	30.90	14.03	4632	692	0.251	0.014	27.79	9.65	4172	129	0.249	0.013	41.41	2.62	4803	280	0.263	0.004
AId	39.10	4.84	5412	685	0.250	0.009	41.68	0.50	4933	465	0.248	0.006	42.62	0.72	5652	614	0.254	0.003
AIv	40.55	2.41	5594	791	0.254	0.010	42.12	0.71	5110	548	0.249	0.007	43.17	1.14	5728	520	0.256	0.003
ILA	21.41	13.80	4208	205	0.251	0.023	14.62	7.71	4117	115	0.238	0.006	29.87	13.30	4191	130	0.263	0.010
MOp	38.67	3.70	5670	943	0.246	0.007	40.93	1.15	4908	461	0.248	0.009	42.14	1.07	5951	728	0.254	0.004
MOs	34.06	11.47	5075	760	0.247	0.009	37.92	4.99	4550	418	0.250	0.011	41.23	1.23	5113	403	0.258	0.003
ORBl	40.46	2.23	5408	670	0.253	0.009	40.33	2.49	4875	377	0.248	0.008	42.44	0.45	5593	417	0.256	0.003
ORBm	23.28	13.80	4270	386	0.255	0.018	15.06	7.69	4084	90	0.240	0.007	30.95	11.92	4156	139	0.268	0.012
ORBvl	35.85	6.68	4872	483	0.250	0.011	32.74	8.22	4430	235	0.243	0.005	40.44	1.75	4990	311	0.257	0.008
PL	30.43	14.32	4558	654	0.252	0.015	24.14	8.60	4133	128	0.248	0.011	38.68	6.04	4533	351	0.266	0.007
DP	32.71	13.12	4189	151	0.268	0.021	20.61	11.84	4070	144	0.252	0.010	37.49	11.79	4249	204	0.277	0.003
PIR1	52.08	2.16	5335	774	0.278	0.010	52.12	1.31	4929	731	0.275	0.005	52.04	1.03	5083	502	0.282	0.007
PIR2	36.70	5.53	4778	484	0.284	0.010	35.44	10.26	4443	533	0.278	0.003	39.02	4.93	4656	457	0.285	0.005
PIR3	30.38	13.21	4514	532	0.268	0.016	19.87	16.10	4184	298	0.252	0.012	34.60	6.13	4284	288	0.275	0.002
TTd1	33.04	14.99	4119	115	0.262	0.028	22.84	12.42	4046	152	0.252	0.018	36.97	20.77	4240	293	0.268	0.021
TTd2	22.71	9.40	4262	172	0.270	0.019	12.29	8.38	4169	94	0.253	0.009	27.24	11.85	4271	86	0.278	0.007
TTd3	20.11	8.37	4140	102	0.260	0.018	13.17	10.02	4117	132	0.244	0.011	25.21	13.52	4141	112	0.269	0.009
TTv1	44.49	9.80	4612	436	0.276	0.015	33.20	11.78	4235	348	0.263	0.004	45.55	7.21	4633	758	0.287	0.008
TTv2	25.03	9.15	4307	234	0.277	0.014	10.66	7.30	4172	137	0.255	0.009	26.19	14.20	4412	271	0.283	0.009
TTv3	27.15	11.34	4139	179	0.265	0.013	13.53	9.49	4088	199	0.244	0.012	25.59	17.02	4204	390	0.266	0.014
AONm	14.48	8.27	4150	128	0.252	0.017	7.69	6.25	4096	77	0.236	0.005	18.49	10.83	4101	124	0.263	0.005
AONpv	34.79	6.88	4581	492	0.275	0.012	25.44	14.93	4254	320	0.258	0.006	33.03	10.00	4398	440	0.277	0.006
EPd	12.02	6.30	4163	149	0.245	0.014	6.46	6.17	4100	196	0.228	0.008	12.38	7.23	4091	44	0.247	0.007
aco	0.78	0.81	3111	1752	0.148	0.097	0.70	0.97	2038	2355	0.106	0.123	0.81	0.69	3365	995	0.164	0.069
lot	3.78	5.38	3077	1061	0.189	0.080	0.78	1.03	1928	2227	0.117	0.135	0.73	0.63	2868	1913	0.180	0.120
SEZ	2.36	1.56	4006	95	0.233	0.014	1.23	1.43	2731	1602	0.137	0.094	2.68	2.08	4081	168	0.240	0.028

	6H POST-ADMINISTRATION																	
	SALINE CONTROL						LOW DOSE KETAMINE (10mg/kg)						HIGH DOSE KETAMINE (100mg/kg)					
BREGMA	DENSITY		INTENSITY		SIZE		DENSITY		INTENSITY		SIZE		DENSITY		INTENSITY		SIZE	
2.10	MEAN	SD	MEAN	SD	MEAN	SD	MEAN	SD	MEAN	SD	MEAN	SD	MEAN	SD	MEAN	SD	MEAN	SD
ACAd	32.62	14.90	4584	335	0.253	0.012	21.97	9.25	4262	216	0.240	0.014	35.79	7.09	5213	1410	0.254	0.008
AId	31.57	10.60	4928	1409	0.246	0.006	39.91	2.02	4905	658	0.246	0.009	41.33	0.76	6374	1409	0.244	0.008
AIv	37.85	6.37	5115	1593	0.251	0.006	41.70	1.81	5064	514	0.250	0.010	40.98	1.23	6528	1635	0.248	0.010
ILA	26.06	20.28	4357	322	0.252	0.023	10.03	3.76	4091	59	0.230	0.009	32.01	13.46	5053	1040	0.250	0.007
MOp	34.58	9.50	5286	1270	0.246	0.003	37.53	3.77	5205	815	0.241	0.009	40.44	0.97	6307	1662	0.245	0.009
MOs	26.44	19.45	4774	860	0.241	0.013	32.20	10.09	4554	270	0.242	0.012	37.74	3.31	5597	1820	0.251	0.013
ORBl	37.02	4.63	4900	1235	0.252	0.004	40.78	2.19	4735	199	0.251	0.010	41.29	1.58	6400	1741	0.246	0.010
ORBm	26.65	19.91	4293	309	0.256	0.024	9.95	2.92	4073	57	0.232	0.007	31.90	14.07	4878	1018	0.254	0.005
ORBvl	32.69	14.40	5058	860	0.247	0.011	34.90	5.20	4551	376	0.244	0.009	39.58	2.57	5893	1702	0.248	0.008
PL	28.68	19.05	4548	609	0.252	0.019	23.40	6.61	4141	89	0.248	0.012	31.82	9.52	5046	1373	0.251	0.007
DP	28.42	21.68	4474	530	0.257	0.024	17.45	5.21	4019	63	0.248	0.014	35.71	10.22	4976	1253	0.261	0.012
PIR1	46.42	9.98	5517	1678	0.278	0.007	52.95	1.18	4809	191	0.276	0.004	47.83	7.57	6169	1909	0.269	0.020
PIR2	32.39	15.57	5099	1180	0.284	0.008	36.64	4.42	4363	213	0.280	0.005	38.85	5.21	5783	1544	0.272	0.022
PIR3	27.95	21.18	4663	846	0.265	0.019	23.46	7.42	4165	88	0.259	0.013	33.33	10.70	5342	1446	0.260	0.013
TTd1	32.94	27.80	4611	859	0.247	0.047	19.05	8.08	4036	62	0.248	0.021	31.79	17.67	5080	1347	0.253	0.018
TTd2	26.60	22.54	4460	580	0.269	0.017	11.23	5.85	4152	78	0.249	0.021	28.71	15.29	5039	839	0.263	0.014
TTd3	27.61	22.81	4301	331	0.264	0.022	9.62	3.85	4096	92	0.239	0.015	28.11	16.14	4972	936	0.253	0.011
TTv1	35.68	28.11	5086	1160	0.264	0.023	N/A	N/A	N/A	N/A	N/A	N/A	37.97	14.54	5653	2125	0.265	0.019
TTv2	N/A	N/A	N/A	N/A	N/A	N/A	N/A	N/A	N/A	N/A	N/A	N/A	28.98	17.95	5697	1187	0.268	0.021
TTv3	29.23	22.39	4511	782	0.265	0.025	16.42	11.61	4061	63	0.252	0.018	28.93	18.34	5397	1584	0.254	0.016
AONm	29.23	24.68	4250	341	0.266	0.026	5.98	4.02	4100	43	0.232	0.023	25.87	20.23	5058	866	0.251	0.010
AONpv	31.79	23.04	4796	803	0.265	0.021	28.62	11.79	4274	153	0.263	0.015	31.49	17.34	5636	1561	0.260	0.014
EPd	17.92	17.68	4118	218	0.245	0.028	7.28	3.06	4168	96	0.228	0.017	25.11	18.06	4941	913	0.250	0.007
aco	2.42	3.07	3174	1784	0.165	0.104	0.50	0.17	3809	68	0.164	0.009	19.67	21.72	4492	856	0.235	0.034
lot	8.11	14.93	3078	1723	0.196	0.111	1.50	1.56	3193	1201	0.194	0.088	22.49	24.20	4198	1737	0.228	0.075
SEZ	3.03	3.04	3038	2032	0.181	0.121	1.33	0.92	3986	116	0.216	0.023	22.22	23.54	4522	536	0.247	0.025

	24H POST-ADMINISTRATION																	
	SALINE CONTROL						**LOW DOSE KETAMINE (10mg/kg)**						**HIGH DOSE KETAMINE (100mg/kg)**					
	DENSITY		INTENSITY		SIZE		DENSITY		INTENSITY		SIZE		DENSITY		INTENSITY		SIZE	
Bregma 2.10	**MEAN**	SD	**MEAN**	SD	**MEAN**	SD	**MEAN**	SD	**MEAN**	SD	**MEAN**	SD	**MEAN**	SD	**MEAN**	SD	**MEAN**	SD
ACAd	**29.91**	12.96	**4632**	622	**0.254**	0.021	**28.27**	12.20	**4553**	599	**0.246**	0.014	**36.20**	7.45	**4908**	659	**0.247**	0.013
Ald	**33.44**	10.92	**5374**	1396	**0.244**	0.014	**36.59**	10.96	**5117**	998	**0.246**	0.010	**40.79**	1.21	**5560**	576	**0.246**	0.012
Alv	**38.52**	5.21	**5493**	1345	**0.252**	0.017	**37.56**	9.89	**5339**	1153	**0.249**	0.010	**41.07**	1.20	**5889**	673	**0.248**	0.012
ILA	**21.41**	15.73	**4392**	238	**0.251**	0.029	**16.67**	15.43	**4258**	326	**0.236**	0.018	**25.42**	10.05	**4481**	418	**0.240**	0.016
MOp	**37.17**	7.26	**5501**	1289	**0.248**	0.017	**38.99**	4.52	**5529**	1202	**0.244**	0.010	**39.64**	1.44	**5782**	841	**0.242**	0.012
MOs	**36.72**	6.61	**5107**	869	**0.250**	0.019	**35.07**	8.52	**4804**	1037	**0.248**	0.010	**37.26**	4.62	**5442**	936	**0.241**	0.010
ORBl	**40.29**	3.23	**5426**	973	**0.253**	0.019	**35.14**	11.55	**5180**	1010	**0.244**	0.013	**40.18**	1.72	**5657**	443	**0.246**	0.012
ORBm	**22.41**	16.55	**4385**	333	**0.252**	0.029	**10.00**	4.59	**4100**	170	**0.231**	0.009	**28.32**	10.41	**4616**	713	**0.244**	0.016
ORBvl	**37.10**	4.31	**5156**	816	**0.252**	0.020	**30.11**	12.60	**4808**	837	**0.239**	0.013	**38.19**	2.61	**5394**	897	**0.241**	0.009
PL	**30.06**	12.74	**4587**	568	**0.255**	0.023	**26.25**	13.15	**4459**	547	**0.244**	0.011	**35.38**	9.56	**4827**	671	**0.248**	0.015
DP	**30.79**	14.10	**4322**	323	**0.267**	0.017	**22.18**	14.81	**4293**	561	**0.251**	0.013	**34.60**	8.93	**4546**	574	**0.255**	0.014
PIR1	**47.81**	4.29	**5069**	1149	**0.277**	0.012	**42.67**	19.45	**4961**	920	**0.272**	0.013	**51.06**	1.51	**5730**	925	**0.273**	0.009
PIR2	**32.51**	7.57	**4997**	1127	**0.281**	0.016	**31.80**	16.74	**4612**	660	**0.277**	0.014	**40.87**	3.12	**5065**	682	**0.280**	0.010
PIR3	**31.14**	10.52	**4560**	598	**0.269**	0.013	**23.10**	16.43	**4435**	647	**0.258**	0.016	**35.53**	8.79	**4757**	564	**0.267**	0.013
TTd1	**31.71**	18.30	**4281**	295	**0.261**	0.022	**23.71**	16.70	**4232**	467	**0.255**	0.019	**37.09**	12.83	**4674**	610	**0.256**	0.016
TTd2	**26.07**	13.76	**4585**	258	**0.270**	0.022	**18.25**	15.60	**4258**	291	**0.259**	0.013	**N/A**	N/A	**N/A**	N/A	**N/A**	N/A
TTd3	**23.59**	15.46	**4390**	272	**0.262**	0.023	**17.21**	16.60	**4209**	311	**0.247**	0.016	**28.87**	15.46	**4531**	397	**0.252**	0.021
TTv1	**37.52**	20.70	**4732**	786	**0.270**	0.016	**30.53**	24.14	**4325**	697	**0.267**	0.028	**N/A**	N/A	**N/A**	N/A	**N/A**	N/A
TTv2	**25.97**	15.10	**4695**	747	**0.274**	0.022	**16.51**	19.09	**4128**	235	**0.267**	0.012	**N/A**	N/A	**N/A**	N/A	**N/A**	N/A
TTv3	**25.74**	19.40	**4510**	206	**0.267**	0.022	**17.08**	21.77	**4066**	320	**0.247**	0.033	**32.93**	13.86	**4658**	591	**0.260**	0.014
AONm	**16.30**	17.79	**4565**	352	**0.254**	0.032	**14.79**	18.33	**4141**	236	**0.242**	0.020	**26.25**	17.15	**4312**	219	**0.252**	0.026
AONpv	**31.07**	11.93	**5053**	1068	**0.275**	0.020	**25.93**	17.07	**4352**	396	**0.264**	0.015	**38.34**	7.67	**4910**	620	**0.267**	0.015
EPd	**16.94**	15.14	**4415**	243	**0.248**	0.026	**12.07**	14.92	**4154**	258	**0.232**	0.019	**20.69**	12.52	**4377**	270	**0.245**	0.020
aco	**1.84**	2.32	**3100**	2073	**0.167**	0.114	**1.61**	3.04	**2018**	2053	**0.107**	0.110	**1.78**	1.56	**4038**	269	**0.203**	0.037
lot	**6.58**	12.30	**2920**	1948	**0.183**	0.126	**0.76**	0.75	**2290**	1635	**0.137**	0.100	**6.19**	11.14	**3886**	143	**0.244**	0.023
SEZ	**10.03**	16.83	**4366**	211	**0.241**	0.041	**2.45**	4.22	**3329**	1046	**0.156**	0.095	**6.40**	9.52	**4177**	164	**0.227**	0.026

	1H POST-ADMINISTRATION																	
	SALINE CONTROL						**LOW DOSE KETAMINE (10mg/kg)**						**HIGH DOSE KETAMINE (100mg/kg)**					
	DENSITY		INTENSITY		SIZE		DENSITY		INTENSITY		SIZE		DENSITY		INTENSITY		SIZE	
BREGMA -1.70	**MEAN**	SD	**MEAN**	SD	**MEAN**	SD	**MEAN**	SD	**MEAN**	SD	**MEAN**	SD	**MEAN**	SD	**MEAN**	SD	**MEAN**	SD
alv	**1.43**	1.76	**2912**	1908	**0.164**	0.112	**3.22**	3.73	**3492**	403	**0.214**	0.072	**1.54**	0.57	**3989**	211	**0.219**	0.045
AUDd	**40.26**	1.14	**6348**	609	**0.254**	0.007	**41.33**	0.67	**6615**	655	**0.248**	0.003	**40.95**	1.32	**6570**	96	**0.252**	0.013
AUDp	**40.22**	0.87	**6247**	548	**0.255**	0.007	**41.09**	0.57	**6430**	686	**0.250**	0.004	**40.73**	0.90	**6528**	182	**0.254**	0.011
AUDv	**40.74**	0.95	**6120**	348	**0.258**	0.006	**41.23**	0.33	**6263**	529	**0.253**	0.005	**41.47**	0.99	**6376**	433	**0.258**	0.009
BLAa	**38.78**	4.17	**4871**	561	**0.278**	0.006	**43.27**	2.14	**5292**	959	**0.272**	0.006	**41.01**	2.79	**5260**	650	**0.273**	0.004
BLAp	**38.42**	2.38	**5102**	736	**0.273**	0.007	**41.53**	2.86	**5207**	22	**0.269**	0.006	**40.77**	1.84	**5464**	447	**0.270**	0.005
BLAv	**35.24**	6.59	**4560**	707	**0.274**	0.004	**44.89**	2.69	**4833**	83	**0.276**	0.009	**41.34**	4.54	**4770**	347	**0.274**	0.005
BMAp	**36.65**	7.10	**4831**	845	**0.282**	0.010	**46.97**	1.98	**4789**	742	**0.282**	0.008	**42.87**	2.38	**4934**	596	**0.281**	0.004
CA1O	**36.79**	8.60	**4729**	670	**0.229**	0.010	**48.31**	1.09	**4961**	953	**0.239**	0.002	**42.73**	5.04	**4668**	341	**0.240**	0.013
CA1R	**38.78**	4.54	**4859**	704	**0.221**	0.006	**46.57**	1.86	**5360**	1149	**0.224**	0.002	**46.09**	4.24	**5371**	149	**0.227**	0.010
CA1SLM	**33.47**	14.77	**4124**	321	**0.256**	0.022	**57.13**	1.12	**4367**	1004	**0.269**	0.005	**56.40**	5.14	**4506**	253	**0.275**	0.012
CA1sp	**23.97**	10.42	**5104**	555	**0.286**	0.019	**38.47**	2.13	**4658**	775	**0.292**	0.003	**33.74**	5.81	**4925**	319	**0.289**	0.015
CA2O	**27.82**	13.98	**4399**	387	**0.277**	0.005	**47.66**	5.46	**4156**	790	**0.285**	0.001	**36.42**	12.28	**4268**	219	**0.278**	0.011
CA2R	**17.21**	13.80	**4267**	342	**0.265**	0.023	**39.27**	13.01	**4040**	695	**0.279**	0.011	**35.05**	13.96	**4332**	179	**0.281**	0.011
CA2SLM	**30.82**	13.65	**4090**	323	**0.282**	0.009	**54.19**	3.32	**4133**	814	**0.286**	0.001	**50.89**	10.18	**4327**	238	**0.287**	0.008
CA2sp	**29.64**	7.17	**6851**	1715	**0.310**	0.008	**39.26**	1.50	**5473**	785	**0.311**	0.004	**34.48**	2.51	**5747**	670	**0.307**	0.008
CA3O	**16.20**	9.06	**4368**	307	**0.236**	0.018	**30.57**	11.43	**4108**	620	**0.253**	0.017	**30.44**	12.54	**4534**	329	**0.250**	0.018
CA3R	**17.15**	6.74	**4511**	339	**0.224**	0.010	**32.34**	8.15	**4303**	630	**0.241**	0.017	**29.94**	8.78	**4588**	63	**0.245**	0.020
CA3SLM	**22.25**	11.56	**4106**	253	**0.249**	0.019	**43.34**	14.47	**3966**	582	**0.265**	0.014	**42.66**	11.25	**4267**	229	**0.268**	0.014
CA3SLU	**15.30**	7.77	**4359**	309	**0.249**	0.015	**29.64**	7.65	**4323**	841	**0.264**	0.017	**28.91**	7.89	**4573**	145	**0.269**	0.022
CA3sp	**12.27**	3.46	**5945**	1234	**0.282**	0.018	**24.14**	7.34	**4545**	545	**0.280**	0.008	**21.82**	8.23	**5038**	111	**0.278**	0.022
CC	**1.38**	0.97	**4069**	382	**0.204**	0.053	**2.60**	1.98	**3570**	340	**0.228**	0.020	**1.54**	1.33	**3529**	1012	**0.199**	0.060
CEA	**30.00**	8.11	**4700**	521	**0.281**	0.007	**42.22**	4.04	**4396**	787	**0.285**	0.007	**31.90**	12.54	**4697**	344	**0.278**	0.016
cing	**5.28**	4.07	**4220**	302	**0.237**	0.017	**15.78**	14.54	**3749**	317	**0.247**	0.018	**7.23**	6.26	**4124**	143	**0.234**	0.019
COApl1	**45.70**	9.30	**4885**	802	**0.281**	0.008	**48.96**	2.97	**4778**	1061	**0.280**	0.007	**50.89**	1.14	**5150**	336	**0.280**	0.005
COApl2	**37.12**	6.09	**4817**	654	**0.289**	0.007	**45.46**	2.68	**4707**	914	**0.284**	0.007	**42.12**	1.20	**5109**	507	**0.285**	0.006
COApl3	**38.20**	7.36	**4834**	2190	**0.287**	0.009	**48.72**	3.24	**5012**	273	**0.281**	0.009	**43.69**	1.89	**4878**	471	**0.283**	0.007
CP	**35.55**	2.16	**5341**	449	**0.261**	0.005	**38.31**	1.74	**5280**	926	**0.260**	0.005	**35.76**	2.09	**5343**	323	**0.257**	0.007
cpd	**0.58**	0.74	**2220**	2366	**0.132**	0.132	**N/A**	N/A	**N/A**	N/A	**N/A**	N/A	**1.08**	1.41	**3840**	314	**0.206**	0.064
df	**0.24**	0.31	**2070**	2401	**0.107**	0.124	**1.12**	0.89	**2724**	1830	**0.179**	0.120	**0.57**	0.71	**3336**	1034	**0.156**	0.074

DGgrInf	**3.91**	2.03	**6175**	1383	**0.285**	0.015	**10.53**	8.37	**4430**	310	**0.287**	0.005	**10.71**	7.47	**5204**	534	**0.286**	0.019
DGgrSup	**5.28**	3.13	**6084**	1084	**0.288**	0.017	**13.78**	9.91	**4459**	313	**0.287**	0.005	**14.49**	9.06	**5033**	355	**0.290**	0.020
DGmolinf	**4.54**	2.37	**4194**	294	**0.199**	0.006	**23.49**	19.17	**3799**	461	**0.235**	0.034	**22.36**	17.58	**4189**	120	**0.239**	0.033
DGmolsup	**8.80**	4.13	**4195**	275	**0.216**	0.011	**30.41**	18.33	**3882**	467	**0.247**	0.024	**32.95**	14.18	**4194**	114	**0.257**	0.024
ECT	**41.27**	1.71	**6104**	504	**0.260**	0.008	**42.93**	2.23	**5989**	759	**0.255**	0.003	**42.20**	1.57	**6183**	409	**0.259**	0.008
ENTI	**41.47**	2.26	**6009**	694	**0.265**	0.006	**44.71**	3.03	**5675**	938	**0.262**	0.004	**42.71**	1.98	**5610**	598	**0.266**	0.009
EPd	**29.32**	8.20	**4503**	460	**0.270**	0.008	**45.67**	1.56	**4578**	829	**0.272**	0.005	**38.41**	7.90	**4706**	362	**0.267**	0.013
fi	**0.17**	0.12	**2671**	1775	**0.101**	0.097	**0.41**	0.41	**2201**	1740	**0.134**	0.104	**0.22**	0.29	**1891**	1596	**0.098**	0.098
Hypothalamus	**32.16**	16.41	**4623**	708	**0.294**	0.013	**47.35**	2.61	**4317**	705	**0.294**	0.007	**37.85**	8.91	**4609**	628	**0.295**	0.007
int	**0.45**	0.44	**2439**	1801	**0.146**	0.104	**1.00**	1.07	**2642**	1790	**0.172**	0.115	**0.59**	0.76	**2856**	1111	**0.158**	0.072
LA	**36.21**	4.34	**4614**	500	**0.278**	0.006	**43.26**	1.70	**4954**	876	**0.275**	0.003	**39.35**	4.06	**4949**	360	**0.275**	0.006
LH	**22.45**	17.16	**4302**	376	**0.278**	0.026	**39.32**	17.43	**3890**	636	**0.286**	0.010	**35.55**	9.10	**4217**	305	**0.290**	0.009
MEA	**36.09**	11.14	**4682**	687	**0.289**	0.006	**49.07**	2.37	**4634**	812	**0.287**	0.007	**40.68**	7.21	**4762**	501	**0.287**	0.006
MH	**35.51**	7.94	**4584**	523	**0.302**	0.011	**43.73**	12.50	**4385**	860	**0.296**	0.009	**45.93**	3.08	**4859**	397	**0.302**	0.008
MOp	**41.54**	1.68	**6470**	1325	**0.255**	0.011	**42.41**	1.25	**7005**	1126	**0.252**	0.006	**43.23**	0.60	**6585**	400	**0.261**	0.011
MOs	**41.33**	1.55	**6828**	1518	**0.257**	0.010	**42.06**	1.10	**7338**	1373	**0.253**	0.007	**42.78**	0.97	**6845**	753	**0.263**	0.011
opt	**0.09**	0.12	**1550**	2132	**0.066**	0.092	**0.05**	0.06	**763**	881	**0.034**	0.041	**0.08**	0.16	**934**	1868	**0.054**	0.108
PAA1	**42.46**	8.06	**4671**	527	**0.278**	0.007	**50.64**	1.27	**4938**	500	**0.276**	0.006	**43.21**	7.98	**4668**	511	**0.278**	0.005
PAA2	**27.29**	8.91	**4515**	489	**0.279**	0.010	**43.91**	1.66	**4488**	668	**0.280**	0.004	**32.41**	11.08	**4605**	470	**0.280**	0.004
PAA3	**34.59**	7.40	**4674**	596	**0.278**	0.003	**44.61**	0.38	**4719**	725	**0.277**	0.007	**37.93**	8.02	**4725**	343	**0.277**	0.005
PERI	**41.70**	2.66	**5912**	490	**0.263**	0.006	**44.05**	3.15	**5968**	528	**0.257**	0.001	**42.50**	2.00	**5865**	378	**0.263**	0.010
PIR1	**38.86**	5.82	**4895**	444	**0.267**	0.001	**47.64**	3.45	**5466**	599	**0.262**	0.004	**43.55**	6.28	**5139**	619	**0.268**	0.006
PIR2	**27.88**	2.81	**5262**	546	**0.281**	0.006	**41.03**	1.43	**4806**	452	**0.278**	0.002	**29.97**	11.50	**5044**	452	**0.276**	0.010
PIR3	**36.22**	2.20	**4687**	361	**0.270**	0.004	**43.42**	2.31	**5097**	784	**0.265**	0.004	**38.77**	6.07	**4984**	454	**0.266**	0.006
PML	**6.55**	1.75	**4437**	312	**0.242**	0.017	**20.46**	14.50	**3888**	447	**0.261**	0.021	**20.61**	13.52	**4363**	54	**0.263**	0.029
RSPd	**42.14**	1.22	**6788**	1318	**0.263**	0.011	**42.66**	0.73	**7234**	1363	**0.258**	0.006	**43.32**	0.41	**6796**	894	**0.269**	0.011
RSPv	**42.58**	1.10	**6239**	1061	**0.270**	0.011	**43.70**	1.29	**6458**	1276	**0.267**	0.004	**43.69**	2.24	**6272**	609	**0.273**	0.010
SSp-bfd	**41.50**	1.37	**6725**	962	**0.252**	0.010	**42.23**	1.20	**7135**	787	**0.247**	0.004	**41.96**	1.68	**7927**	1620	**0.249**	0.010
SSp-tr	**42.13**	1.48	**6841**	1101	**0.252**	0.011	**42.28**	1.53	**7110**	1138	**0.248**	0.003	**42.77**	2.49	**7052**	447	**0.253**	0.010
stn	**38.64**	3.76	**5293**	1194	**0.294**	0.017	**N/A**	N/A	**N/A**	N/A	**N/A**	N/A	**41.85**	1.63	**5205**	1360	**0.296**	0.004
stSup	**0.14**	0.10	**1897**	1467	**0.076**	0.055	**0.22**	0.43	**970**	1940	**0.053**	0.105	**0.08**	0.10	**1362**	1737	**0.048**	0.059
TEa	**40.52**	1.47	**6068**	633	**0.260**	0.008	**41.74**	0.22	**6027**	613	**0.257**	0.005	**41.68**	1.33	**6297**	440	**0.258**	0.008
Thalamus	**16.22**	13.72	**4135**	362	**0.278**	0.020	**25.80**	17.23	**3615**	343	**0.280**	0.008	**17.52**	17.42	**4093**	290	**0.279**	0.016

Appendix 15 (cont.): Tables of raw numbers from ketamine Arc synaptome maps

	6H POST-ADMINISTRATION																	
	SALINE CONTROL						**LOW DOSE KETAMINE (10mg/kg)**						**HIGH DOSE KETAMINE (100mg/kg)**					
	DENSITY		INTENSITY		SIZE		DENSITY		INTENSITY		SIZE		DENSITY		INTENSITY		SIZE	
BREGMA -1.70	**MEAN**	SD	**MEAN**	SD	**MEAN**	SD	**MEAN**	SD	**MEAN**	SD	**MEAN**	SD	**MEAN**	SD	**MEAN**	SD	**MEAN**	SD
alv	**4.46**	3.79	**4001**	42	**0.254**	0.012	**2.50**	0.76	**4038**	28	**0.242**	0.006	**1.11**	1.14	**3447**	1006	**0.215**	0.060
AUDd	**42.71**	1.34	**6590**	845	**0.259**	0.008	**49.00**	0.96	**6709**	838	**0.249**	0.010	**40.98**	0.50	**6346**	847	**0.261**	0.012
AUDp	**42.58**	1.41	**6326**	867	**0.262**	0.008	**49.00**	1.67	**6469**	769	**0.251**	0.008	**41.23**	0.76	**6070**	615	**0.264**	0.013
AUDv	**42.41**	1.14	**6136**	743	**0.263**	0.007	**48.86**	1.31	**6296**	750	**0.252**	0.007	**41.16**	0.98	**5913**	577	**0.266**	0.012
BLAa	**42.53**	3.64	**5148**	440	**0.281**	0.013	**49.77**	3.26	**5845**	890	**0.270**	0.008	**38.66**	4.31	**4923**	557	**0.277**	0.009
BLAp	**39.98**	0.75	**5297**	555	**0.274**	0.008	**48.02**	2.92	**5822**	504	**0.267**	0.005	**37.01**	2.48	**5088**	699	**0.271**	0.010
BLAv	**40.79**	3.96	**4776**	319	**0.273**	0.008	**51.85**	3.12	**5556**	783	**0.270**	0.010	**33.29**	9.65	**4628**	511	**0.273**	0.008
BMAp	**45.26**	5.54	**4799**	199	**0.285**	0.012	**53.79**	1.78	**5410**	668	**0.276**	0.008	**36.16**	9.21	**4480**	404	**0.282**	0.005
CA1O	**46.51**	3.56	**4934**	741	**0.239**	0.003	**55.61**	2.00	**5029**	518	**0.234**	0.009	**34.06**	8.42	**4305**	427	**0.234**	0.008
CA1R	**46.26**	1.38	**5212**	676	**0.224**	0.002	**53.87**	2.00	**5294**	652	**0.220**	0.007	**33.95**	6.20	**4404**	538	**0.217**	0.006
CA1SLM	**52.84**	6.18	**4480**	478	**0.274**	0.004	**61.94**	5.77	**4469**	373	**0.267**	0.007	**18.00**	13.92	**3892**	136	**0.234**	0.037
CA1sp	**32.34**	4.92	**5134**	409	**0.291**	0.006	**40.04**	2.71	**4952**	242	**0.288**	0.011	**20.36**	6.28	**4844**	522	**0.286**	0.019
CA2O	**40.75**	7.49	**4521**	380	**0.283**	0.007	**52.02**	6.43	**4333**	205	**0.280**	0.010	**25.28**	10.04	**4157**	265	**0.276**	0.007
CA2R	**32.85**	10.10	**4334**	285	**0.278**	0.006	**39.19**	11.85	**4222**	151	**0.271**	0.012	**17.87**	10.41	**4084**	181	**0.267**	0.021
CA2SLM	**46.62**	7.67	**4451**	495	**0.286**	0.005	**54.53**	12.82	**4254**	305	**0.283**	0.008	**25.40**	16.38	**3956**	155	**0.272**	0.025
CA2sp	**34.20**	4.00	**6623**	1292	**0.307**	0.008	**44.71**	2.75	**5820**	551	**0.308**	0.007	**28.38**	3.73	**6098**	1432	**0.308**	0.007
CA3O	**26.52**	10.69	**4439**	356	**0.250**	0.011	**35.75**	7.75	**4467**	221	**0.250**	0.006	**12.81**	6.51	**4179**	240	**0.232**	0.005
CA3R	**27.76**	9.45	**4661**	438	**0.242**	0.011	**32.51**	7.90	**4675**	403	**0.239**	0.007	**10.94**	2.88	**4171**	89	**0.221**	0.003
CA3SLM	**40.55**	10.17	**4399**	518	**0.270**	0.006	**45.83**	15.76	**4241**	342	**0.263**	0.010	**18.31**	10.50	**3985**	158	**0.255**	0.024
CA3SLU	**24.62**	8.48	**4399**	237	**0.266**	0.009	**33.91**	6.11	**4445**	192	**0.262**	0.006	**13.45**	6.44	**4158**	134	**0.254**	0.003
CA3sp	**21.02**	5.23	**5665**	1139	**0.284**	0.017	**27.87**	4.89	**5087**	155	**0.282**	0.012	**11.77**	2.69	**5772**	1308	**0.279**	0.028
CC	**2.67**	2.24	**4047**	84	**0.241**	0.006	**1.48**	0.95	**4059**	106	**0.223**	0.021	**1.33**	1.16	**3998**	221	**0.232**	0.030
CEA	**36.03**	4.00	**4529**	166	**0.287**	0.008	**46.91**	8.08	**4885**	409	**0.282**	0.005	**28.30**	10.63	**4597**	223	**0.281**	0.008
cing	**10.19**	8.99	**4184**	55	**0.249**	0.010	**6.99**	2.92	**4287**	94	**0.235**	0.012	**2.70**	1.73	**4096**	148	**0.241**	0.012
COApl1	**41.79**	22.97	**4860**	707	**0.275**	0.012	**62.68**	2.34	**6009**	1139	**0.271**	0.006	**44.89**	10.79	**4649**	613	**0.282**	0.008
COApl2	**44.75**	7.72	**4848**	358	**0.284**	0.012	**52.72**	6.74	**5563**	932	**0.278**	0.007	**32.60**	13.84	**4526**	347	**0.284**	0.006
COApl3	**39.68**	13.99	**4751**	488	**0.277**	0.007	**55.35**	1.82	**5425**	908	**0.272**	0.011	**34.64**	11.97	**4507**	472	**0.278**	0.007
CP	**37.91**	2.01	**5299**	406	**0.267**	0.005	**45.69**	2.02	**5612**	624	**0.259**	0.006	**35.17**	3.61	**4944**	312	**0.268**	0.009

cpd	**0.78**	0.49	**3925**	222	**0.234**	0.034	**7.06**	7.85	**3951**	152	**0.220**	0.024	**0.81**	0.76	**3405**	1068	**0.209**	0.070
df	**0.67**	0.22	**3900**	148	**0.217**	0.031	**0.47**	0.40	**3097**	1736	**0.167**	0.100	**0.25**	0.23	**2565**	2223	**0.144**	0.126
DGgrInf	**8.39**	3.41	**5536**	1132	**0.287**	0.017	**9.57**	4.06	**5284**	371	**0.283**	0.007	**3.95**	2.10	**6099**	1118	**0.292**	0.021
DGgrSup	**9.71**	3.37	**5419**	857	**0.291**	0.015	**13.42**	5.33	**5209**	294	**0.286**	0.009	**4.85**	2.99	**6014**	969	**0.293**	0.020
DGmolinf	**23.63**	15.46	**4199**	263	**0.241**	0.026	**25.81**	16.10	**4204**	127	**0.230**	0.024	**4.19**	2.08	**4042**	255	**0.206**	0.012
DGmolsup	**29.93**	16.62	**4185**	237	**0.253**	0.019	**34.88**	14.16	**4225**	193	**0.244**	0.019	**6.60**	3.42	**4041**	243	**0.219**	0.019
ECT	**42.87**	1.89	**6124**	649	**0.262**	0.005	**50.27**	2.46	**6132**	654	**0.256**	0.004	**41.16**	1.44	**5682**	353	**0.265**	0.008
ENTl	**43.10**	2.41	**5860**	743	**0.266**	0.005	**51.30**	0.77	**5751**	689	**0.263**	0.003	**40.59**	1.07	**5177**	137	**0.267**	0.008
EPd	**39.58**	9.87	**4529**	154	**0.277**	0.014	**48.66**	6.87	**4860**	439	**0.269**	0.007	**31.60**	13.87	**4415**	199	**0.271**	0.008
fi	**0.37**	0.24	**2663**	1033	**0.153**	0.056	**0.39**	0.47	**1980**	1986	**0.118**	0.119	**0.16**	0.21	**1850**	2139	**0.088**	0.109
Hypothalamus	**37.89**	8.18	**4311**	112	**0.295**	0.010	**54.76**	1.95	**4663**	241	**0.291**	0.008	**17.59**	16.62	**4312**	53	**0.292**	0.005
int	**0.45**	0.33	**2345**	1643	**0.140**	0.097	**1.37**	1.21	**3856**	226	**0.179**	0.089	**0.65**	0.60	**3239**	1186	**0.200**	0.079
LA	**40.14**	5.13	**4793**	312	**0.281**	0.010	**49.59**	3.41	**5163**	563	**0.273**	0.006	**34.91**	6.68	**4603**	393	**0.276**	0.006
LH	**31.46**	18.18	**4257**	161	**0.280**	0.030	**54.31**	3.51	**4262**	221	**0.295**	0.007	**20.17**	6.19	**4111**	44	**0.292**	0.023
MEA	**41.40**	10.21	**4564**	173	**0.292**	0.010	**55.77**	1.05	**4976**	491	**0.287**	0.008	**32.66**	14.02	**4428**	224	**0.289**	0.007
MH	**44.09**	5.83	**5495**	943	**0.305**	0.008	**56.02**	4.84	**4743**	462	**0.304**	0.007	**33.43**	5.96	**4772**	563	**0.307**	0.022
MOp	**43.04**	1.67	**6597**	776	**0.257**	0.008	**49.92**	2.08	**6801**	766	**0.248**	0.007	**41.58**	0.62	**5945**	980	**0.267**	0.013
MOs	**42.93**	1.55	**7102**	910	**0.257**	0.008	**49.44**	2.22	**7191**	951	**0.249**	0.008	**41.16**	0.88	**6277**	972	**0.270**	0.013
opt	**0.04**	0.10	**711**	1589	**0.027**	0.060	**0.08**	0.12	**1104**	1655	**0.051**	0.079	**0.11**	0.12	**1838**	2122	**0.097**	0.112
PAA1	**39.36**	17.03	**4597**	630	**0.281**	0.015	**55.95**	7.19	**5456**	1228	**0.273**	0.006	**38.39**	16.70	**4696**	700	**0.278**	0.008
PAA2	**28.61**	12.16	**4508**	408	**0.284**	0.007	**41.67**	10.32	**5137**	1067	**0.278**	0.007	**26.37**	15.08	**4717**	274	**0.280**	0.009
PAA3	**38.63**	15.06	**4460**	361	**0.284**	0.013	**51.12**	3.00	**5267**	876	**0.273**	0.008	**29.67**	13.51	**4463**	462	**0.271**	0.004
PERI	**43.41**	1.99	**5937**	547	**0.266**	0.005	**50.96**	1.82	**5982**	631	**0.259**	0.005	**41.31**	1.08	**5382**	278	**0.266**	0.010
PIR1	**42.00**	11.84	**5097**	865	**0.271**	0.010	**54.80**	2.07	**5757**	1193	**0.261**	0.003	**42.36**	7.47	**5153**	817	**0.271**	0.012
PIR2	**33.01**	10.65	**5116**	373	**0.283**	0.009	**42.07**	5.55	**5375**	756	**0.273**	0.006	**29.40**	11.99	**5122**	58	**0.282**	0.009
PIR3	**37.98**	10.97	**4755**	545	**0.275**	0.014	**48.91**	2.34	**5480**	801	**0.261**	0.004	**33.68**	9.03	**4778**	616	**0.265**	0.005
PML	**21.39**	10.32	**4323**	143	**0.264**	0.015	**21.17**	12.55	**4372**	210	**0.252**	0.013	**7.27**	3.20	**4207**	207	**0.242**	0.019
RSPd	**43.51**	1.55	**7164**	1049	**0.263**	0.008	**50.07**	2.49	**7067**	986	**0.255**	0.007	**41.45**	0.72	**6229**	802	**0.275**	0.011
RSPv	**44.44**	1.80	**6530**	833	**0.270**	0.008	**51.66**	0.98	**6357**	815	**0.264**	0.008	**41.52**	1.19	**5763**	726	**0.281**	0.008
SSp-bfd	**42.47**	1.28	**6786**	585	**0.255**	0.006	**49.60**	1.51	**7273**	966	**0.245**	0.011	**41.77**	0.65	**6461**	984	**0.260**	0.010
SSp-tr	**43.19**	1.53	**6916**	903	**0.253**	0.008	**50.20**	1.86	**7291**	787	**0.241**	0.009	**N/A**	N/A	**N/A**	N/A	**N/A**	N/A
stn	**38.82**	1.41	**5427**	597	**0.297**	0.009	**54.70**	2.94	**5952**	524	**0.295**	0.008	**37.32**	3.34	**5044**	437	**0.301**	0.013
stSup	**0.27**	0.27	**2778**	1858	**0.109**	0.103	**0.26**	0.26	**2489**	2159	**0.088**	0.107	**0.29**	0.31	**2492**	1180	**0.117**	0.092
TEa	**42.68**	1.43	**6102**	640	**0.262**	0.006	**49.11**	1.21	**6243**	790	**0.253**	0.006	**40.84**	1.68	**5817**	668	**0.266**	0.009
Thalamus	**15.55**	12.73	**4077**	181	**0.272**	0.029	**39.63**	17.16	**4192**	217	**0.284**	0.008	**15.93**	5.52	**4107**	44	**0.289**	0.018

Appendix 15 (cont.): Tables of raw numbers from ketamine Arc synaptome maps

	24H POST-ADMINISTRATION																	
	SALINE CONTROL						**LOW DOSE KETAMINE (10mg/kg)**						**HIGH DOSE KETAMINE (100mg/kg)**					
BREGMA	DENSITY		INTENSITY		SIZE		DENSITY		INTENSITY		SIZE		DENSITY		INTENSITY		SIZE	
-1.70	**MEAN**	SD	**MEAN**	SD	**MEAN**	SD	**MEAN**	SD	**MEAN**	SD	**MEAN**	SD	**MEAN**	SD	**MEAN**	SD	**MEAN**	SD
alv	**1.30**	0.77	**3790**	331	**0.231**	0.031	**9.25**	9.18	**3680**	264	**0.261**	0.014	**0.54**	0.47	**3130**	1303	**0.154**	0.077
AUDd	**41.59**	1.53	**6522**	577	**0.259**	0.009	**41.90**	1.86	**7272**	702	**0.250**	0.009	**42.06**	0.67	**7377**	1057	**0.247**	0.005
AUDp	**41.33**	2.32	**6259**	587	**0.255**	0.014	**42.08**	1.99	**6883**	841	**0.254**	0.007	**42.09**	0.44	**6956**	771	**0.249**	0.004
AUDv	**41.20**	1.89	**5991**	613	**0.257**	0.013	**41.85**	2.06	**6648**	886	**0.256**	0.007	**42.17**	0.46	**6630**	653	**0.251**	0.005
BLAa	**40.25**	3.78	**5217**	956	**0.273**	0.008	**42.23**	2.54	**5880**	509	**0.272**	0.007	**38.71**	4.46	**5335**	984	**0.265**	0.010
BLAp	**39.09**	2.28	**5401**	921	**0.268**	0.009	**39.79**	0.99	**6099**	580	**0.266**	0.004	**39.74**	2.88	**6012**	1268	**0.267**	0.005
BLAv	**39.37**	5.81	**4780**	794	**0.270**	0.007	**42.94**	2.01	**5699**	736	**0.265**	0.005	**38.84**	6.47	**5301**	1236	**0.264**	0.012
BMAp	**38.79**	8.43	**4826**	950	**0.275**	0.010	**45.09**	2.21	**5406**	513	**0.278**	0.013	**38.34**	10.73	**5067**	1091	**0.270**	0.012
CA1O	**45.33**	6.08	**3872**	1211	**0.242**	0.015	**48.51**	1.80	**5340**	931	**0.236**	0.012	**39.29**	7.23	**4729**	429	**0.222**	0.016
CA1R	**44.31**	2.51	**3947**	1228	**0.229**	0.009	**46.97**	1.66	**5533**	899	**0.220**	0.010	**41.44**	3.72	**4903**	421	**0.213**	0.009
CA1SLM	**47.62**	13.10	**3514**	1032	**0.270**	0.022	**51.46**	13.07	**4558**	869	**0.263**	0.023	**25.62**	12.46	**4189**	314	**0.234**	0.025
CA1sp	**24.01**	7.27	**5073**	814	**0.295**	0.016	**34.62**	7.04	**5409**	937	**0.291**	0.009	**19.38**	6.65	**4953**	171	**0.275**	0.009
CA2O	**34.40**	13.29	**4033**	448	**0.284**	0.010	**48.44**	5.00	**4612**	873	**0.282**	0.008	**22.09**	12.79	**4332**	424	**0.272**	0.013
CA2R	**22.79**	12.67	**3940**	317	**0.275**	0.023	**40.59**	13.91	**4472**	905	**0.277**	0.018	**9.72**	4.77	**4394**	284	**0.248**	0.018
CA2SLM	**34.57**	26.23	**3909**	581	**0.284**	0.016	**48.71**	16.82	**4435**	1155	**0.284**	0.013	**15.71**	7.86	**4085**	338	**0.266**	0.012
CA2sp	**29.14**	5.88	**7471**	2966	**0.315**	0.008	**34.27**	6.25	**7409**	2529	**0.309**	0.004	**29.50**	4.59	**5256**	394	**0.304**	0.010
CA3O	**20.50**	7.00	**4069**	344	**0.246**	0.020	**35.73**	8.52	**4361**	500	**0.252**	0.016	**14.23**	9.45	**4570**	383	**0.218**	0.023
CA3R	**18.87**	5.88	**4182**	445	**0.232**	0.017	**34.93**	9.55	**4635**	625	**0.242**	0.021	**14.26**	4.43	**4740**	398	**0.210**	0.010
CA3SLM	**28.52**	16.40	**3888**	373	**0.261**	0.024	**45.62**	17.79	**4338**	989	**0.264**	0.028	**11.15**	4.18	**4264**	308	**0.225**	0.012
CA3SLU	**15.99**	7.28	**4010**	380	**0.254**	0.027	**33.36**	9.59	**4506**	630	**0.261**	0.019	**10.99**	5.52	**4484**	365	**0.231**	0.006
CA3sp	**14.08**	7.09	**6179**	1561	**0.297**	0.021	**26.50**	8.13	**5517**	998	**0.283**	0.013	**10.07**	3.28	**5605**	389	**0.273**	0.019
CC	**1.68**	1.29	**3889**	311	**0.235**	0.024	**3.96**	0.47	**3697**	268	**0.247**	0.010	**0.54**	0.34	**4201**	297	**0.192**	0.024
CEA	**31.95**	9.38	**4614**	504	**0.278**	0.015	**41.98**	3.24	**5040**	484	**0.284**	0.009	**32.74**	9.43	**4982**	368	**0.273**	0.005
cing	**7.34**	6.87	**3584**	1028	**0.247**	0.017	**20.63**	5.81	**3800**	258	**0.261**	0.007	**3.14**	1.59	**4489**	274	**0.224**	0.015
COApl1	**50.78**	3.80	**5052**	1155	**0.274**	0.002	**52.89**	2.98	**5815**	811	**0.274**	0.014	**48.05**	6.73	**5657**	1916	**0.269**	0.008
COApl2	**42.13**	3.14	**5044**	1107	**0.278**	0.004	**45.91**	2.66	**5503**	626	**0.279**	0.013	**38.52**	8.89	**5411**	1562	**0.270**	0.004

COApl3	**43.06**	3.49	**4848**	892	**0.277**	0.007	**45.86**	2.41	**5682**	469	**0.271**	0.005	**38.24**	8.52	**5612**	1856	**0.268**	0.007
CP	**36.30**	2.42	**5065**	558	**0.263**	0.017	**38.54**	1.57	**5871**	544	**0.260**	0.006	**34.52**	3.15	**5442**	749	**0.249**	0.010
cpd	**0.89**	0.55	**2795**	1880	**0.208**	0.116	**2.19**	0.36	**3636**	53	**0.257**	0.011	**0.28**	0.30	**2124**	2346	**0.131**	0.121
df	**0.61**	0.51	**2943**	1296	**0.169**	0.098	**1.54**	0.43	**3616**	286	**0.236**	0.018	**0.10**	0.10	**1194**	1772	**0.044**	0.044
DGgrInf	**7.65**	4.73	**4790**	1987	**0.298**	0.008	**15.92**	10.29	**4956**	702	**0.292**	0.018	**3.20**	0.92	**5822**	402	**0.282**	0.011
DGgrSup	**8.88**	5.17	**4963**	2068	**0.304**	0.009	**19.21**	10.59	**5060**	805	**0.291**	0.020	**3.23**	1.20	**5713**	444	**0.287**	0.014
DGmolinf	**11.49**	8.94	**3303**	1085	**0.226**	0.029	**29.71**	17.36	**3996**	599	**0.242**	0.028	**8.45**	5.97	**4413**	318	**0.207**	0.022
DGmolsup	**16.46**	8.09	**3480**	1027	**0.238**	0.023	**37.64**	16.96	**4137**	771	**0.252**	0.030	**8.85**	4.60	**4416**	296	**0.208**	0.010
ECT	**41.04**	1.81	**5949**	684	**0.257**	0.013	**42.15**	1.87	**6371**	739	**0.257**	0.007	**41.79**	0.81	**6323**	1104	**0.253**	0.006
ENTl	**42.13**	2.14	**5514**	569	**0.262**	0.012	**43.66**	1.86	**6129**	788	**0.263**	0.007	**42.96**	1.81	**5552**	1092	**0.259**	0.004
EPd	**36.22**	11.13	**4618**	751	**0.267**	0.018	**44.80**	2.50	**5027**	402	**0.272**	0.007	**36.44**	10.54	**4904**	773	**0.259**	0.016
fi	**0.43**	0.42	**2886**	1930	**0.162**	0.119	**0.89**	0.40	**3525**	280	**0.237**	0.020	**0.05**	0.06	**961**	1115	**0.026**	0.030
Hypothalamus	**41.16**	6.03	**4108**	1853	**0.295**	0.003	**44.25**	4.22	**4642**	209	**0.293**	0.008	**23.55**	15.21	**4554**	488	**0.280**	0.014
int	**0.65**	0.77	**2874**	1921	**0.160**	0.112	**2.11**	0.71	**3571**	291	**0.250**	0.020	**0.13**	0.18	**1998**	2194	**0.069**	0.095
LA	**36.85**	6.64	**4828**	917	**0.273**	0.015	**42.67**	2.77	**5358**	500	**0.274**	0.005	**38.52**	7.45	**5240**	920	**0.269**	0.007
LH	**29.70**	13.33	**3627**	1420	**0.289**	0.015	**46.42**	5.09	**4191**	706	**0.291**	0.007	**12.65**	9.45	**4318**	302	**0.265**	0.012
MEA	**35.58**	12.54	**4614**	762	**0.283**	0.009	**46.22**	3.01	**5003**	402	**0.289**	0.008	**32.22**	11.20	**4838**	750	**0.277**	0.013
MH	**43.25**	3.62	**4354**	2070	**0.308**	0.006	**47.29**	3.76	**5334**	892	**0.303**	0.008	**33.03**	7.63	**4813**	935	**0.293**	0.013
MOp	**42.39**	2.13	**5851**	1903	**0.256**	0.014	**42.99**	1.31	**7302**	582	**0.253**	0.008	**42.51**	2.10	**6595**	706	**0.250**	0.007
MOs	**42.13**	2.68	**6372**	2241	**0.257**	0.012	**42.50**	1.72	**7629**	838	**0.255**	0.006	**41.74**	2.00	**6827**	747	**0.253**	0.008
opt	**0.04**	0.10	**382**	855	**0.026**	0.059	**0.24**	0.14	**2614**	869	**0.169**	0.092	**0.00**	0.00	**N/A**	N/A	**N/A**	N/A
PAA1	**48.15**	3.59	**5591**	1127	**0.275**	0.005	**49.08**	2.19	**5376**	1118	**0.278**	0.018	**46.56**	1.38	**5695**	1649	**0.265**	0.010
PAA2	**33.49**	9.83	**5057**	1549	**0.277**	0.011	**41.72**	4.42	**5111**	803	**0.282**	0.011	**35.79**	9.66	**5268**	1271	**0.270**	0.006
PAA3	**40.54**	3.13	**4779**	974	**0.272**	0.006	**43.26**	1.99	**5396**	754	**0.274**	0.015	**41.04**	3.61	**5433**	1279	**0.266**	0.005
PERI	**41.93**	1.57	**5542**	659	**0.261**	0.012	**43.12**	2.05	**6279**	721	**0.260**	0.007	**43.20**	1.42	**6245**	1007	**0.258**	0.006
PIR1	**45.82**	2.85	**4982**	676	**0.263**	0.012	**47.43**	2.42	**5755**	630	**0.267**	0.011	**44.90**	4.39	**6037**	1615	**0.257**	0.007
PIR2	**32.74**	3.81	**5189**	1134	**0.275**	0.014	**40.05**	3.22	**5413**	402	**0.280**	0.010	**36.57**	7.23	**5730**	1329	**0.271**	0.006
PIR3	**40.68**	3.13	**4815**	646	**0.263**	0.010	**43.58**	1.92	**5625**	614	**0.265**	0.010	**40.83**	3.09	**5615**	1303	**0.259**	0.008
PML	**7.03**	3.60	**3454**	1201	**0.251**	0.017	**25.78**	13.23	**4143**	592	**0.262**	0.025	**5.49**	2.01	**4491**	318	**0.227**	0.008
RSPd	**42.45**	2.32	**6450**	2199	**0.261**	0.011	**42.44**	2.03	**7727**	1037	**0.259**	0.007	**42.53**	1.97	**6649**	736	**0.260**	0.007
RSPv	**43.17**	2.18	**5629**	1878	**0.271**	0.009	**43.54**	1.94	**7247**	1106	**0.267**	0.007	**42.84**	2.49	**5854**	829	**0.267**	0.006
SSp-bfd	**42.53**	1.37	**6892**	331	**0.258**	0.010	**42.41**	2.06	**7747**	925	**0.248**	0.010	**42.11**	1.61	**7377**	1277	**0.243**	0.008
SSp-tr	**42.52**	1.76	**6856**	210	**0.251**	0.017	**42.82**	1.34	**7605**	523	**0.246**	0.009	**42.99**	2.24	**7173**	1033	**0.243**	0.009
stn	**39.15**	4.67	**4524**	1562	**0.297**	0.002	**41.17**	4.12	**5672**	210	**0.289**	0.006	**36.71**	6.80	**4749**	549	**0.290**	0.004
stSup	**0.36**	0.12	**3783**	145	**0.196**	0.057	**0.73**	0.55	**3082**	1008	**0.192**	0.070	**0.07**	0.12	**1227**	2126	**0.060**	0.105
TEa	**41.14**	1.99	**5928**	639	**0.258**	0.012	**41.98**	1.97	**6433**	877	**0.257**	0.008	**41.63**	0.51	**6396**	885	**0.253**	0.006
Thalamus	**14.30**	11.44	**3459**	1296	**0.281**	0.012	**33.22**	11.98	**3967**	774	**0.284**	0.012	**5.41**	6.35	**4275**	373	**0.263**	0.005

<u>Appendix 16:</u> Tables of raw numbers from ketamine PSD95 synaptome mapping

	24H POST-ADMINISTRATION																	
	SALINE CONTROL						**LOW DOSE KETAMINE (10mg/kg)**						**HIGH DOSE KETAMINE (100mg/kg)**					
BREGMA	DENSITY		INTENSITY		SIZE		DENSITY		INTENSITY		SIZE		DENSITY		INTENSITY		SIZE	
2.10	**MEAN**	SD	**MEAN**	SD	**MEAN**	SD	**MEAN**	SD	**MEAN**	SD	**MEAN**	SD	**MEAN**	SD	**MEAN**	SD	**MEAN**	SD
ACAd	**107.19**	9.99	**14462**	170	**0.083**	0.001	**101.95**	7.35	**13619**	1962	**0.084**	0.002	**101.41**	4.69	**13616**	1976	**0.084**	0.002
aco	**9.50**	1.94	**9170**	19	**0.088**	0.000	**7.33**	2.58	**8653**	924	**0.089**	0.002	**6.24**	2.04	**8745**	757	**0.090**	0.000
Ald	**107.32**	1.97	**15312**	814	**0.083**	0.001	**97.59**	4.51	**13659**	1669	**0.083**	0.002	**103.28**	4.23	**15165**	907	**0.083**	0.001
Alv	**100.60**	1.15	**15167**	615	**0.084**	0.001	**91.63**	3.13	**13407**	1865	**0.084**	0.001	**93.72**	4.73	**14497**	905	**0.084**	0.001
AONm	**96.96**	3.24	**9594**	172	**0.078**	0.000	**91.81**	10.48	**8992**	1480	**0.079**	0.002	**88.36**	2.03	**8817**	327	**0.080**	0.001
AONpv	**87.24**	6.91	**10917**	607	**0.083**	0.001	**84.72**	3.97	**10542**	995	**0.082**	0.001	**67.33**	10.82	**9732**	466	**0.086**	0.001
CTX1	**124.39**	3.88	**16791**	570	**0.084**	0.001	**116.25**	8.07	**16078**	1773	**0.084**	0.001	**120.76**	10.68	**16894**	1884	**0.084**	0.001
CTX5	**91.08**	4.33	**13742**	205	**0.083**	0.001	**88.80**	3.65	**12884**	1989	**0.084**	0.001	**89.64**	1.93	**13139**	1640	**0.084**	0.001
CTX6a	**82.90**	5.32	**11419**	355	**0.083**	0.000	**82.03**	3.80	**11038**	1844	**0.083**	0.002	**82.04**	5.02	**11011**	1593	**0.084**	0.002
DP	**96.18**	9.32	**13592**	927	**0.083**	0.001	**96.91**	7.56	**12845**	2423	**0.084**	0.001	**92.60**	4.35	**12829**	862	**0.085**	0.002
EPd	**61.42**	7.19	**9733**	293	**0.086**	0.001	**58.47**	7.76	**9618**	699	**0.085**	0.001	**54.73**	5.57	**8982**	614	**0.087**	0.001
ILA	**96.72**	5.79	**12710**	128	**0.081**	0.000	**97.05**	4.19	**12022**	1969	**0.082**	0.001	**92.99**	3.08	**11702**	1596	**0.083**	0.002
lot	**1.12**	0.06	**8322**	296	**0.091**	0.001	**0.89**	0.33	**7961**	1057	**0.089**	0.001	**0.76**	0.29	**7779**	572	**0.088**	0.005
MOp	**98.94**	3.47	**15481**	643	**0.084**	0.000	**95.98**	6.19	**14696**	1893	**0.084**	0.001	**98.75**	3.26	**15182**	1217	**0.084**	0.001
MOs	**103.52**	9.44	**15141**	1298	**0.084**	0.001	**102.05**	8.95	**14600**	2135	**0.084**	0.001	**102.43**	9.36	**14652**	2518	**0.085**	0.002
ORBl	**95.70**	6.12	**15004**	144	**0.084**	0.001	**92.37**	2.90	**13694**	2015	**0.084**	0.001	**90.60**	4.38	**13935**	961	**0.085**	0.001
ORBm	**103.54**	7.59	**13193**	437	**0.081**	0.001	**100.24**	5.50	**12361**	1838	**0.082**	0.002	**98.78**	5.65	**12291**	2056	**0.083**	0.003
ORBvl	**95.28**	8.88	**13934**	261	**0.082**	0.000	**95.09**	6.35	**12948**	2237	**0.083**	0.002	**91.99**	3.30	**12992**	1173	**0.084**	0.001
OT	**N/A**	N/A	**N/A**	N/A	**N/A**	N/A	**66.61**	12.82	**10723**	700	**0.085**	0.002	**61.67**	11.61	**9917**	698	**0.085**	0.001
PIR1	**89.66**	2.17	**11973**	291	**0.084**	0.001	**84.23**	5.64	**10992**	1632	**0.084**	0.002	**84.54**	1.98	**11281**	136	**0.084**	0.000
PIR2	**75.84**	7.33	**10986**	50	**0.084**	0.000	**70.58**	8.53	**10187**	1419	**0.084**	0.001	**68.19**	2.41	**10549**	362	**0.085**	0.000
PIR3	**73.82**	2.33	**10327**	461	**0.086**	0.000	**69.83**	7.87	**10083**	827	**0.085**	0.001	**66.68**	3.73	**9747**	497	**0.087**	0.001
PL	**106.91**	7.14	**13836**	406	**0.082**	0.000	**102.53**	6.93	**13035**	1873	**0.083**	0.002	**101.48**	4.55	**13193**	2218	**0.084**	0.003
SEZ	**25.41**	2.72	**8838**	262	**0.083**	0.001	**20.57**	9.24	**8253**	907	**0.083**	0.002	**21.84**	0.94	**8053**	460	**0.084**	0.001

TTd1	**109.23**	5.38	**12749**	180	**0.081**	0.001	**104.70**	10.20	**11540**	2214	**0.082**	0.002	**102.78**	8.18	**12324**	1079	**0.082**	0.001
TTd2	**89.30**	5.16	**11212**	382	**0.081**	0.000	**83.64**	9.77	**10250**	1872	**0.082**	0.002	**87.50**	8.12	**10946**	747	**0.083**	0.001
TTd3	**95.41**	0.47	**11011**	418	**0.081**	0.001	**92.77**	5.91	**10040**	1749	**0.081**	0.002	**89.60**	2.03	**10328**	476	**0.083**	0.001
TTv1	**96.07**	5.21	**11417**	582	**0.082**	0.001	**91.67**	11.68	**10396**	1599	**0.082**	0.002	**97.12**	3.19	**11526**	684	**0.081**	0.001
TTv2	**72.99**	9.73	**9917**	245	**0.083**	0.001	**64.71**	11.62	**9094**	1101	**0.083**	0.002	**74.43**	11.90	**10343**	1194	**0.083**	0.002
TTv3	**96.16**	3.70	**10984**	32	**0.081**	0.000	**91.28**	4.77	**9807**	1389	**0.082**	0.002	**93.16**	6.42	**10331**	764	**0.081**	0.002

	24H POST-ADMINISTRATION																	
	SALINE CONTROL						**LOW DOSE KETAMINE (10mg/kg)**						**HIGH DOSE KETAMINE (100mg/kg)**					
BREGMA	DENSITY		INTENSITY		SIZE		DENSITY		INTENSITY		SIZE		DENSITY		INTENSITY		SIZE	
-1.70	**MEAN**	SD	**MEAN**	SD	**MEAN**	SD	**MEAN**	SD	**MEAN**	SD	**MEAN**	SD	**MEAN**	SD	**MEAN**	SD	**MEAN**	SD
alv	**1.41**	1.35	**6002**	763	**0.094**	0.003	**2.50**	1.49	**7036**	580	**0.093**	0.002	**1.55**	1.16	**6472**	1783	**0.088**	0.009
AUDd	**89.97**	4.44	**14659**	1674	**0.090**	0.001	**94.90**	9.27	**16308**	2788	**0.087**	0.002	**95.73**	6.62	**18309**	3275	**0.088**	0.003
AUDp	**93.66**	4.84	**15442**	1316	**0.089**	0.001	**97.37**	7.76	**16707**	2370	**0.087**	0.002	**N/A**	N/A	**N/A**	N/A	**N/A**	N/A
AUDv	**95.97**	7.46	**15580**	1099	**0.089**	0.001	**98.87**	9.01	**16364**	2285	**0.087**	0.002	**N/A**	N/A	**N/A**	N/A	**N/A**	N/A
BLAa	**88.91**	2.43	**13898**	2004	**0.090**	0.003	**93.71**	7.03	**14224**	1556	**0.087**	0.003	**92.74**	3.14	**14502**	282	**0.088**	0.002
BMAp	**75.56**	4.66	**11355**	1875	**0.089**	0.002	**82.33**	11.83	**12330**	2292	**0.087**	0.002	**86.79**	7.86	**12468**	81	**0.087**	0.001
CA1O	**109.79**	52.29	**12805**	2284	**0.086**	0.003	**121.00**	50.16	**14081**	3097	**0.085**	0.003	**132.42**	23.80	**14582**	3264	**0.086**	0.007
CA1R	**136.21**	11.34	**15514**	849	**0.087**	0.002	**142.04**	14.02	**16376**	1733	**0.085**	0.004	**131.45**	23.71	**16011**	3509	**0.088**	0.006
CA1SLM	**113.86**	22.31	**12314**	3791	**0.088**	0.001	**118.21**	20.27	**13702**	2827	**0.086**	0.003	**96.03**	17.85	**11169**	3106	**0.090**	0.006
CA1sp	**49.55**	43.58	**9083**	1826	**0.090**	0.002	**50.44**	41.29	**10295**	2239	**0.088**	0.003	**25.54**	16.11	**9309**	3143	**0.091**	0.005
CA2O	**90.30**	51.76	**8049**	1367	**0.086**	0.008	**107.41**	26.33	**9837**	1474	**0.083**	0.004	**106.79**	18.02	**9295**	2119	**0.085**	0.005
CA2R	**106.92**	16.29	**8615**	958	**0.085**	0.002	**111.60**	8.31	**9445**	835	**0.083**	0.001	**94.67**	18.95	**8769**	2112	**0.087**	0.006
CA2SLM	**109.02**	12.91	**8598**	1031	**0.085**	0.002	**113.13**	5.68	**9479**	740	**0.083**	0.002	**96.47**	18.31	**8185**	1767	**0.086**	0.006
CA2sp	**34.09**	50.88	**6718**	1457	**0.098**	0.010	**25.15**	25.27	**7051**	635	**0.097**	0.006	**7.61**	4.70	**6405**	936	**0.105**	0.002
CA3O	**76.22**	25.70	**8571**	825	**0.094**	0.008	**85.33**	30.41	**9391**	670	**0.091**	0.008	**76.67**	22.36	**8403**	1546	**0.092**	0.007
CA3R	**97.82**	6.36	**9334**	556	**0.092**	0.002	**104.76**	7.89	**10001**	1009	**0.089**	0.002	**91.24**	23.19	**9667**	1875	**0.093**	0.007
CA3SLM	**111.43**	8.81	**8867**	1429	**0.088**	0.004	**119.11**	9.52	**9569**	953	**0.085**	0.002	**99.99**	24.14	**8326**	1481	**0.088**	0.007
CA3SLU	**71.61**	32.12	**10223**	662	**0.100**	0.009	**73.10**	28.67	**11242**	1707	**0.098**	0.009	**53.66**	9.85	**10883**	2718	**0.106**	0.005
CA3sp	**36.44**	19.33	**8836**	1544	**0.107**	0.003	**37.04**	18.28	**9583**	1735	**0.104**	0.003	**24.47**	9.31	**8692**	2439	**0.108**	0.006
CC	**0.65**	0.09	**6650**	764	**0.089**	0.001	**0.97**	0.39	**7906**	1108	**0.088**	0.001	**0.49**	0.41	**6366**	2138	**0.080**	0.015
CEA	**66.16**	8.06	**10478**	924	**0.089**	0.001	**69.34**	11.82	**10921**	1212	**0.087**	0.002	**69.49**	13.40	**11007**	1638	**0.088**	0.003
cing	**6.39**	1.75	**7256**	1044	**0.093**	0.003	**8.67**	2.32	**8686**	1216	**0.091**	0.001	**4.00**	3.56	**5911**	4587	**0.071**	0.047
COApl1	**82.04**	5.95	**13404**	2412	**0.087**	0.001	**82.21**	8.47	**12302**	2147	**0.087**	0.002	**86.65**	6.91	**12659**	2123	**0.087**	0.001
COApl2	**72.30**	3.92	**11825**	2107	**0.090**	0.001	**75.18**	8.65	**11716**	1778	**0.088**	0.002	**82.90**	5.62	**11927**	1487	**0.088**	0.002
CP	**82.07**	5.03	**12404**	802	**0.089**	0.001	**83.28**	6.59	**13407**	1918	**0.087**	0.002	**80.50**	3.34	**12385**	2088	**0.088**	0.003
df	**0.00**	0.00	**N/A**	N/A	**N/A**	N/A	**0.01**	0.02	**230**	514	**0.002**	0.006	**0.05**	0.11	**1175**	2349	**0.019**	0.039
DGgrInf	**6.83**	2.85	**6273**	167	**0.094**	0.002	**9.29**	3.63	**6906**	676	**0.094**	0.001	**7.35**	7.31	**6641**	1477	**0.095**	0.003
DGgrSup	**7.96**	2.82	**6347**	150	**0.095**	0.001	**11.50**	5.44	**6966**	566	**0.094**	0.002	**7.68**	6.37	**6449**	1356	**0.095**	0.004
DGmolinf	**128.95**	8.22	**11664**	1060	**0.086**	0.002	**133.78**	15.34	**12306**	1691	**0.084**	0.004	**121.09**	24.43	**11799**	2691	**0.088**	0.007
DGmolsup	**129.58**	5.93	**12215**	1099	**0.087**	0.002	**134.45**	16.65	**12835**	1670	**0.085**	0.004	**123.95**	27.62	**12025**	2728	**0.088**	0.007
ECT	**103.83**	5.55	**16523**	1264	**0.086**	0.001	**100.55**	2.27	**15706**	1678	**0.085**	0.002	**N/A**	N/A	**N/A**	N/A	**N/A**	N/A
ENTl	**103.16**	7.44	**16104**	1728	**0.085**	0.002	**99.40**	4.67	**15091**	1529	**0.085**	0.002	**100.89**	3.63	**15152**	2809	**0.086**	0.003
EPd	**86.15**	4.61	**11244**	1110	**0.085**	0.001	**89.52**	6.18	**12106**	1673	**0.083**	0.002	**82.25**	8.03	**10861**	1997	**0.085**	0.003
FC	**65.80**	15.08	**6345**	389	**0.084**	0.001	**74.23**	8.46	**6868**	236	**0.083**	0.002	**45.59**	30.05	**6758**	2209	**0.085**	0.005
fi	**0.00**	0.00	**N/A**	N/A	**N/A**	N/A	**0.00**	0.00	**N/A**	N/A	**N/A**	N/A	**0.00**	0.00	**N/A**	N/A	**N/A**	N/A
GPe	**7.43**	1.31	**7119**	318	**0.103**	0.002	**9.74**	1.88	**7826**	708	**0.102**	0.001	**7.34**	2.66	**7319**	1216	**0.105**	0.002
GPi	**4.70**	1.62	**7006**	717	**0.098**	0.001	**5.01**	1.29	**7101**	450	**0.098**	0.001	**3.03**	3.27	**6360**	1340	**0.098**	0.005
Hypothalamus	**22.82**	1.20	**8861**	1847	**0.099**	0.001	**25.09**	2.08	**9008**	1047	**0.097**	0.001	**22.92**	1.32	**8516**	1172	**0.099**	0.001
int	**0.08**	0.10	**1824**	2322	**0.029**	0.037	**0.06**	0.10	**1480**	2263	**0.019**	0.029	**0.03**	0.05	**654**	1307	**0.011**	0.021
LA	**92.99**	5.67	**15191**	1425	**0.090**	0.001	**92.68**	7.61	**15679**	1894	**0.087**	0.002	**90.90**	4.49	**14850**	1133	**0.088**	0.003
LH	**13.26**	2.55	**7557**	438	**0.096**	0.002	**13.70**	2.61	**7911**	756	**0.095**	0.001	**8.43**	6.29	**7580**	1940	**0.097**	0.003
MEA	**64.93**	4.23	**10724**	1201	**0.091**	0.001	**68.50**	7.13	**10712**	1083	**0.089**	0.002	**66.83**	5.64	**10582**	854	**0.090**	0.001
MH	**12.68**	3.77	**7304**	566	**0.089**	0.002	**15.11**	2.37	**8003**	988	**0.087**	0.001	**9.03**	5.68	**7169**	2196	**0.088**	0.003
MOp	**86.75**	2.58	**14132**	675	**0.090**	0.001	**94.15**	7.47	**17554**	3091	**0.087**	0.002	**91.08**	5.57	**15633**	4645	**0.089**	0.003
MOs	**75.89**	2.33	**13485**	682	**0.093**	0.001	**78.53**	2.14	**17015**	3224	**0.090**	0.001	**76.77**	2.19	**14940**	5091	**0.092**	0.002
opt	**0.00**	0.00	**N/A**	N/A	**N/A**	N/A	**0.00**	0.00	**N/A**	N/A	**N/A**	N/A	**0.00**	0.00	**N/A**	N/A	**N/A**	N/A
PAA1	**82.63**	9.66	**11966**	670	**0.087**	0.001	**92.48**	14.89	**12979**	2028	**0.086**	0.003	**88.70**	7.83	**12503**	1464	**0.086**	0.002
PAA2	**81.15**	4.68	**12718**	2504	**0.088**	0.002	**83.48**	7.90	**12135**	2226	**0.087**	0.003	**84.61**	2.79	**12226**	2234	**0.086**	0.001
PAA3	**81.57**	11.08	**13086**	2751	**0.088**	0.002	**88.45**	12.19	**13113**	2263	**0.087**	0.002	**91.59**	6.86	**12944**	483	**0.086**	0.001
PERI	**105.67**	4.82	**16554**	1341	**0.086**	0.001	**101.51**	3.27	**15529**	1510	**0.085**	0.002	**106.91**	7.59	**15969**	2875	**0.086**	0.003
PIR1	**97.83**	5.28	**14630**	819	**0.085**	0.001	**96.21**	6.72	**13500**	1883	**0.085**	0.002	**95.55**	1.00	**12970**	1798	**0.087**	0.001
PIR2	**66.01**	1.58	**11920**	1272	**0.087**	0.000	**65.11**	7.72	**10941**	1596	**0.086**	0.001	**68.70**	2.50	**10840**	1158	**0.087**	0.001
PIR3	**96.83**	10.37	**14505**	2253	**0.086**	0.001	**98.89**	8.35	**14182**	1989	**0.085**	0.002	**94.24**	2.36	**13086**	1818	**0.087**	0.002
PML	**49.46**	7.83	**8523**	415	**0.103**	0.001	**52.05**	7.88	**9141**	926	**0.102**	0.004	**44.62**	12.47	**8603**	1945	**0.106**	0.007
RSPd	**74.22**	3.47	**12864**	523	**0.093**	0.001	**74.45**	1.27	**15337**	2991	**0.091**	0.002	**74.83**	2.97	**14577**	5105	**0.092**	0.002
RSPv	**64.73**	4.09	**10939**	910	**0.093**	0.001	**65.59**	2.19	**12629**	2591	**0.091**	0.002	**63.40**	9.06	**12117**	5017	**0.092**	0.003

SI	**18.14**	4.11	**8064**	1009	**0.099**	0.001	**16.20**	1.98	**8233**	643	**0.098**	0.002	**9.93**	7.94	**8139**	1288	**0.098**	0.004
SSp-bfd	**88.45**	5.59	**14259**	1934	**0.089**	0.002	**91.34**	6.79	**17131**	3287	**0.087**	0.001	**90.59**	2.63	**15427**	2947	**0.089**	0.003
SSp-tr	**96.56**	4.52	**15303**	949	**0.088**	0.001	**102.77**	6.11	**18784**	3166	**0.085**	0.002	**99.21**	2.95	**16252**	3231	**0.088**	0.002
stSup	**0.07**	0.06	**1660**	1449	**0.026**	0.023	**0.14**	0.05	**3398**	1575	**0.048**	0.024	**0.04**	0.06	**785**	1360	**0.013**	0.022
TEa	**99.29**	6.53	**16199**	987	**0.087**	0.001	**101.74**	4.52	**16256**	1955	**0.086**	0.002	**N/A**	N/A	**N/A**	N/A	**N/A**	N/A
Thalamus	**60.55**	3.25	**8021**	652	**0.084**	0.001	**65.94**	4.62	**8554**	654	**0.082**	0.001	**46.75**	21.44	**7663**	2423	**0.086**	0.005

<u>Appendix 17:</u> Example spread of data points for different Cohen's d effect sizes

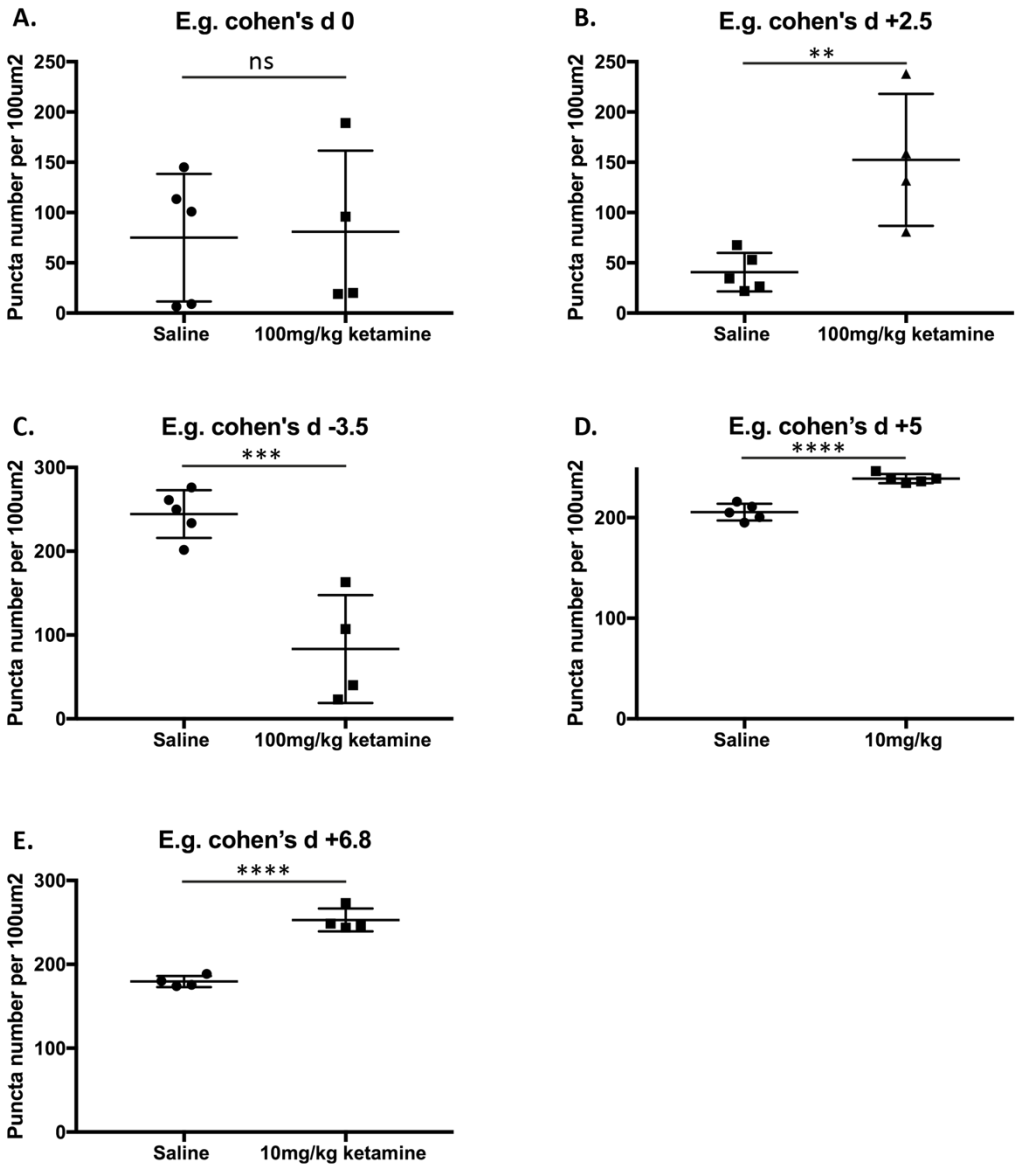

Appendix.figure 8 – Example plots of individual data points underlying different Cohen's d effect size values. *Data points = individual mice, line = mean, error bars = SD.* ***A.*** *Cohen's d = 0, p = 0.903, data from the thalamus at 1h post-administration.* ***B.*** *Cohen's d = +2.5, p = 0.008, data from DGmolsup at 1h post-administration.* ***C.*** *Cohen's d = -3.5, p = 0.001, data from CA1slm 6h post-administration.* ***D.*** *Cohen's d = +5, p < 0.0001, data from RSPv at 6h post-administration.* ***E.*** *Cohen's d +6.8, p < 0.0001, data from stn at 6h post-administration.*